LATE-STAGE EXHUMATION OF METAMORPHIC CORE COMPLEXES AND LANDSCAPE DEVELOPMENT DURING OROGENIC COLLAPSE OF THE NORTH AMERICAN CORDILLERA

A DISSERTATION

SUBMITTED TO THE FACULTY OF GRADUATE SCHOOL

OF THE UNIVERSITY OF MINNESOTA

BY

ERKAN TORAMAN

IN PARTIAL FULFILLMENT OF THE REQUIREMENTS

FOR THE DEGREE OF

DOCTOR OF PHILOSOPHY

CHRISTIAN TEYSSIER, DONNA L. WHITNEY, ADVISORS

FEBRUARY 2014

Acknowledgements

First and foremost, I would like to thank my advisors, Christian Teyssier and Donna L. Whitney, for their continuous support throughout the years. Without your guidance, patience, and constant encouragement this work would not be possible. You have provided me freedom to pursue many aspects of this research, even though at times when I wasn't sure if that particular approach would work. Thank you for long discussions that broadened my understanding of science and academic life in general. I can't express my gratitude for involving me with many other projects you work on, especially the ones in central Turkey, which allowed me to explore different perspectives on Anatolian tectonics and use new research tools. I hope and look forward to work with you in future projects!

Many thanks to members of my written, oral, and final exam committee members Martin O. Saar, Karen Kleinspehn, Joshua Feinberg, and Annia Fayon for taking the time to read my work. I am indebted to Annia Fayon for introducing me to the wonders of fission-track analysis and for long, enlightening discussions on diffusional processes in thermochronology. I thank Martin Saar for his encouragement for modeling of thermochronometric data, even though that work has not made into this thesis but still "in progress". I would like to also thank to Peter Hudleston for our inspiring and joyful conversations on different topics ranging from Alpine tectonics to folding. I thank both Peter Reiners and Stuart Thomson for their help in U-Th/He analysis and interpretations. I greatly appreciate Ray Donelick and Paul O'Sullivan for their help in Cf irradiation of my apatite samples. Thank you to Olivier Vanderhaeghe and Luc Seibenaller who

introduced me to the spectacular scenery and geology of the Thor-Odin dome and shared an unforgettable adventure with me in my first field season.

Many thanks to past and present members of the STAMP group whose support, friendship, and encouragement kept me sane during my time in Minnesota. I am thankful to Val Morgan-Stanley, Elisa-Fitz Diaz, Raphael Gottardi, Matt Carter, William Nachlas, Jen Wright, Roxanne Renedo, and Katherine Fornash for sharing their ideas and laughter throughout the years. I also thank Ravi Appana, Laura Vietti, Brian Bagley, Nick Seaton, Ben Stanley, Ioan and Ioanna Lascu, Sharon Kressler and all my other friends in the department for everything they have done.

I acknowledge funding from the National Science Foundation and the University of Minnesota, Department of Earth Sciences.

Finally and most importantly, I would like to thank my family in Turkey and Minneapolis. I wouldn't have done this without their endless support and love!

Abstract

Exogenic and endogenic processes control the exhumation of partially molten crust in extending orogens. Their relative contribution to total denudation is critical to evaluate different tectonic models. Therefore, assessing the timing, rates, style, and conditions of events from melt crystallization to cooling at near-surface temperatures is significantly important for understanding the thermo-mechanical evolution of orogenic crust and linking deep-to-shallow processes. Metamorphic core complexes (MCC) and gneiss domes located within the hinterland of orogenic belts expose a significant quantity of former partially-molten mid-to-lower crust in the form of migmatites. The Thor-Odin, Frenchman's Cap, and Okanogan domes are exposed in the biggest Cordilleran-style metamorphic core complex, the Shuswap MCC, where a series of migmatitic gneiss domes formed during collapse of the thickened crust in the Cenozoic. The Thor-Odin and Frenchman's Cap domes form the Shuswap MCC's narrow northern end where the present day topographic relief reaches up to 2.5 km with deeply incised valleys and ubiquitous glacial features. The Okanogan dome, on the other hand, represents the wider, lower-relief (≤ 1km) southern termination.

In the Thor-Odin and Frenchman's Cap domes, zircon U-Th/He ages range from 45 to 37 Ma. Apatite fission track ages range between 48 to 14 Ma and increase with increasing sample elevation. Thermal modeling of samples from higher altitudes (~2100 to 1800 m) verify only rapid Eocene cooling, whereas the lower-elevation samples (~1800 to 500 m) reveal an additional Plio-Quaternary cooling event. The presence of the top of a fossil Eocene partial annealing zone at ~1800 m indicates that the migmatite

dome reached near-surface depths (1-2 km) during its initial exhumation mainly by detachment tectonics. Apatite U-Th/He chronometry of these samples yields Miocene (26-5 Ma) ages. A number of low elevation (~500 m) samples collected from valleys reveal intra-sample single grain U-Th/He ages. Combined with the results of thermal modeling, these age variations indicate a rapid exhumation pulse at ca. 3 Ma, possibly related to continental glaciation.

In the Okanogan dome, zircon U-Th/He ages range from 51 to 41 Ma and decrease towards the detachment fault zone, emphasizing up to 3.7 km/myr slip rate on the detachment zone. Apatite fission track and U-Th/He ages vary from 51 to 23 Ma, recording a very slow phase of erosional exhumation of the dome that removed ~ 2 km of rocks subsequently after its initial rapid ascent facilitated by detachment tectonics in the Eocene. Low-temperature data also document different cooling paths of rocks depending on their structural level; rocks closer to the detachment zone display rapid cooling rates (≥ 100 °C/myr), whereas deeper structural levels cool slowly (10-30 °C/myr).

As in the North American Cordilleran hinterland, a series of migmatite-cored metamorphic core complexes is exposed in the Hellenides, where the geodynamic context of migmatitic dome formation is well known from previous research. Multiple low-temperature thermochronologic techniques combined with existing structural, geo- and thermochronologic, and petrologic data from Cordilleran and central Aegean migmatitic gneiss domes document rapid ascent of partially molten mid-to-lower crustal rocks, facilitating significant mass and heat advection to the shallow crust. Heat advection results in a high-geothermal gradient in shallow crust and shifts the brittle-

ductile transition zone close to the surface. Percolation of surface-derived fluids through fault and fracture zones enables rapid cooling of rocks and enhances the brittle rheology.

Table of Contents

List of Figures

Chapter 2: Low-temperature thermochronologic record of Eocene migmatite dome emplacement and late Cenozoic landscape development, Shuswap core complex, British Columbia

Chapter 3: Low-temperature thermochronometric record of shallow emplacement of migmatite beneath a detachment shear zone

Chapter 4: Thermal and rheological evolution of mid-crustal rocks during formation of migmatite-cored metamorphic core complexes

List of Tables

Chapter 1: Introduction

Orogenic belts formed at convergent boundaries are a locus of juvenile crust production and recycling. During the growth of an orogen, continental crust gets thicker owing to tectonic shortening and mantle-derived melts. Eventually these belts reach a critical point where the system cannot continue to grow vertically and horizontally and start to collapse under its own weight. Numerical models and geological and geophysical observations suggest that partial melting in deep crust leads to a rheological layering in which rigid upper crust overlies less viscous mid-to-lower crustal layers (Block and Royden, 1990; Bird, 1991; Clark and Royden, 2000; Rey et al., 2001). Furthermore, the presence of melt at middle to lower crustal levels can drive collapse of large hot orogens during the last stages of orogeny and can cause development of localized domal uplifts where rapidly exhumed high-pressure and high- temperature metamorphic rocks crops out owing to horizontal and vertical ductile extrusion of mid to lower crustal rocks (McKenzie et al., 2000; Beaumont et al, 2001; Vanderheaghe and Teyssier, 2001; Teyssier and Whitney, 2002). Although both exogenic and endogenic processes control the ascent of partially-molten deep crust, and facilitates mass and heat transfer within the crust and affect Moho and surface topography (Teyssier et al., 2005; Rey et al., 2011; Schenker et al., 2012), their relative contribution to total denudation history is not easy to differentiate. Evaluating the timing, conditions and tempo of events from melt crystallization to cooling at surface temperatures has therefore fundamental importance for understanding the link between shallow-to-deep processes, and the thermo-mechanical evolution of orogenic crust.

The main goal of this study is to reconstruct the thermal history of different levels of partially-molten orogenic crust during and after its exhumation to the Earth's surface. This approach allows unraveling spatial and temporal variations in exhumation, documenting relative roles of tectonic and erosional processes, and understanding topographic evolution.

In this study, I focused on three migmatite-cored gneiss domes from the North American Cordillera: the Thor-Odin and Frenchman's Cap domes (British Columbia, Canada); and the Okanogan dome (Washington State, USA). All domes are located in the Shuswap metamorphic core complex (MCC). The Thor-Odin and Frenchman's Cap domes form the Shuswap MCC's narrow, high-relief northern end, whereas the Okanogan dome represents its wider, lower-relief southern termination. Timing of melt formation/crystallization and metamorphic conditions in both regions are well-established and display similar results.

Each chapter following this introduction is presented as separate manuscripts for publication. The second chapter, *Low-temperature thermochronologic record of Eocene migmatite dome emplacement and late Cenozoic landscape development, Shuswap core complex, British Columbia*, has been submitted to Tectonics. This study focuses on the Thor-Odin and Frenchman's Cap domes and uses multiple low-temperature thermochronometic ages to understand detailed cooling paths at different structural levels of these gneiss domes. Results of this work document that these domes experienced rapid Eocene cooling (≥60 °C/my) related to initial exhumation via detachment tectonics. Preservation of the Eocene apatite partial annealing zone suggests that the dome rocks reached the near-surface (1-2 km) mostly via tectonic exhumation,

and little erosion of the Eocene surface has occurred since that time. This study also documents a younger cooling event that resulted in dissection of the Eocene surface and the formation of deeply incised valleys, possibly related to continental glaciations at ~3 Ma.

The third chapter, *Low-temperature thermochronometric record of shallow emplacement of migmatite beneath a detachment shear zone*, addresses cooling of the Okanogan dome from ~190 to 40 °C using apatite and zircon fission track and U-Th/He methods. Using samples collected from a transect covering various lithologies parallel to the shear direction, this work indicates that exhumation of the dome was achieved mainly by detachment tectonics in the Eocene and that slip rate on the detachment fault might be as high as 3.7km/my. This work further documents ~2 km of erosional exhumation of the dome shortly after the cessation of detachment faulting. Results from a second transect that covers different structural depths from the detachment fault zone to migmatitic core indicate spatial differences in cooling as rocks closer to the detachment fault zone experienced rapid cooling (≥ 100 °C/my), whereas deeper structural levels recorded much lower cooling rates (10-30 °C/my).

The fourth chapter, *Thermal and rheological evolution of mid-crustal rocks during formation of migmatite-cored metamorphic core complexes*, focuses on the role of partially-molten crust during lithospheric extension. Using geological data from well-explored migmatite-cored metamorphic complexes exposed in the central Aegean and North American Cordillera, this chapter highlights the first-order similarities in both regions and uses this information to better understand the thermal and mechanical processes occurring within partially molten crust during and after exhumation. Results

indicate these migmatite-cored metamorphic core complexes record a temporal and kinematic continuum during exhumation. Rapid exhumation leads to perturbation of the thermal structure in the shallow crust and results in migration of the brittle-ductile transition zone to shallow depths, which significantly affect the stress state, rheology, and hydrology of the crust.

The fifth and final chapter "Conclusions" highlights the main results of this work.

References

Beaumont, C., Jamieson, R.A., Nguyen, M.H., and Lee, B., 2001. Himalayan tectonics explained by extrusion of a low-viscosity crustal channel coupled to focused surface denudation: Nature (London), v. 414, p. 738-742.

Bird, P., 1991. Lateral extrusion of lower crust from under high topography, in the isostatic limit. Journal of Geophysical Research, **96**, 10275-10286.

Block, L. & Royden, L.H., 1990. Core complex geometries and regional scale flow in the lower crust. Tectonics, **9,** 557-567.

Clark, M.K. & Royden, L.H., 2000. Topographic ooze: Building the eastern margin of Tibet by lower crustal flow. Geology, **28**, 703-706.

McKenzie, D., Nimmo, F., Jackson, J.A., Gans, P.B., and Miller, E.L., 2000. Characteristics and consequences of flow in the lower crust: Journal of Geophysical Research, B, Solid Earth and Planets, v. 105, p. 11029-11046.

Rey, P., Vanderhaeghe, O. & Teyssier, C., 2001. Gravitational collapse of the continental crust: definition, regimes and modes. Tectonophysics, **342**, 435-449.

Rey, P.F., Teyssier, C., Kruckenberg, S.C., Whitney, D.L., 2011. Viscous collision in channel explains double domes in metamorphic core complexes. Geology, 39, 4, 387-390

Schenker, F. L., Gerya, T., Burg, J. P., 2012. Bimodal behavior of extended continental lithosphere: Modeling insight and application to thermal history of migmatitic core complexes. Tectonophysics, 579, 88-103.

Teyssier, C., and Whitney, D.L., 2002. Gneiss domes and orogeny: Geology, v. 30, p. 1139- 1142.

Teyssier, C., Ferré, E.C., Whitney, D.L., Norlander, B., Vanderhaeghe, O., Parkinson, D., 2005. Flow of partially molten crust and origin of detachments during collapse of the Cordilleran orogen, in Bruhn, D., Burlini, L., eds., High-strain zones: Structure and physical properties: London. Geological Society of London Special Publications, vol. 245pp. 39-64,.

Vanderhaeghe, O., Teyssier, C., 2001.Partial melting and flow of orogens: Tectonophysics, v. 342, p. 451-472.

Chapter 2: Low-temperature thermochronologic record of Eocene migmatite dome emplacement and late Cenozoic landscape development, Shuswap core complex, British Columbia

Erkan Toraman[1], Christian Teyssier[1], Donna L. Whitney[1], Annia K. Fayon[1], Stuart N. Thomson[2], Peter W. Reiners[2]

[1] *University of Minnesota, Department of Earth Sciences, 310 Pillsbury Drive SE Minneapolis, MN 55455-0231*

[2] *University of Arizona, Department of Geosciences, Gould-Simpson Building, 1040 E. 4th St., Tucson, AZ 85721-0077*

Submitted to Tectonics

Exhumed mid-to-lower crustal rocks offer an opportunity to elucidate deep-to-shallow crustal processes and therefore heat and mass transport during orogeny. We present low-T thermochronology data (zircon and apatite (U-Th)/He, apatite fission track) that inform the timing and rates of Cenozoic cooling and exhumation as well as recent incision of a migmatite dome in the Shuswap metamorphic core complex, British Columbia (Canada). Samples collected at high altitude (> 1800 m) in the migmatite dome document rapid Eocene cooling (≥60 °C/my) related to initial exhumation via detachment tectonics. Samples collected below 1800 m display a wide range of apatite fission-track ages (43-15 Ma). Track-length distributions indicate that 1800 m corresponds to the upper boundary of the Eocene apatite partial annealing zone. These age-elevation relations imply that the dome rocks reached the near-surface (1-2 km) during initial tectonic exhumation in the Eocene and that little erosion of the Eocene surface has occurred since that time. Thermal modeling of the lowest elevation samples (≤ ~600 m) reveals a young cooling event that possibly related to dissection of the

Eocene surface and the formation of deeply incised valleys. These data, when integrated with intra-sample apatite (U-Th)/He age variations observed in valley-bottom samples, indicate enhanced glacial erosion and relief production at the onset of continental glaciations at ~3 Ma.

2.1. Introduction

Orogenic belts expose lower-to-mid crustal rocks that were at least partially exhumed along low-angle normal faults in metamorphic core complexes (MCC). These core complexes commonly contain migmatite domes that represent former partially molten crust [*Vanderhaeghe and Teyssier*, 2001; *Teyssier and Whitney,* 2002; *Whitney et al.,* 2004; 2013; *Denèle et al.,* 2007; *Kruckenberg et al.,* 2008; 2011]. Many field-based investigations and numerical modeling studies have documented pressure-temperature-time and strain history of dome rocks to understand the relationship between partial melting and crustal dynamics [*McKenzie et al.,* 2000; *Beaumont et al,* 2001; *Tirel et al.,* 2004; *Fayon et al.,* 2004b; *Hinchey et al.,* 2006; *Thiede et al.,* 2006; *Rey et al.,* 2009a; 2010; 2011; *McFadden et al.,* 2010; *Brown et al.,* 2012; *Little et al.,* 2011]. A key finding of these investigations is that the presence of partially molten crust enables crustal flow that, when vertical, transports hot rocks rapidly from deep (> 20 km) to shallow (< 3 km) crustal levels [e.g., *Tirel et al.,* 2004; *Rey at al.,* 2009b, 2011]. Near-isothermal decompression is commonly interpreted from reaction textures in dome migmatites and associated rocks [*Kruckenberg and Whitney,* 2011; *Goergen and Whitney,* 2012a,b]. The tight range of ages recorded by high-to-medium temperature chronometers (zircon U-Pb to mica $^{40}Ar/^{39}Ar$) in migmatite domes [*Norlander et al.,* 2002; *Vanderhaeghe et al.,* 2003; *Robinson et al.,* 2007; *Kruckenberg et al.,* 2008;

Gordon et al., 2008, 2012; *Spalla et al.,* 2011, *Little et al.,* 2011; *Stübner et al.,* in press] has been interpreted to indicate rapid cooling (≥50 °C/km), in good agreement with numerical models [e.g., *Rey et al.,* 2009a, 2009b].

Low-temperature thermochronology has been applied to metamorphic core complexes to understand the timing and rate of tectonic and erosional processes, to document detachment fault geometry and total slip along the fault, and to determine the thermal structure of the crust prior to extensional faulting [*Foster and John,* 1999; *Wells et al.,* 2000; *Fayon et al.*, 2000; *Carter et al.,* 2004, 2006; *Stockli,* 2005; *Thomson and Ring,* 2006, *Thomson et al.*, 2009; *Foster et al.,* 2010]. In this paper, we show how the results of low-temperature thermochronology can be used to track tectonic processes in a migmatite-cored metamorphic core complex from high- to low-temperature – that is, from dome emplacement to the latest stages of landscape development. We present new results from zircon and apatite (U-Th)/He, and apatite fission-track analyses from the Thor-Odin and Frenchman's Cap domes in the Shuswap MCC. Deep valleys have incised the domes, providing structural relief and therefore access to study the pressure-temperature-time evolution of different structural levels of the core complex. Relief production can also be evaluated using age-elevation profiles as well as regionally distributed samples. We integrate results from multiple low-temperature thermochronometers with previous structural, metamorphic, and geo/thermochronological data, and evaluate the relative roles of erosion and tectonic processes that are control the exhumation of deep crust and the reorganization of topography at the surface.

2.2. Geologic Setting

The tectonic evolution of the Canadian Cordillera involved crustal thickening and heating by terrane accretion and magmatism during the Late Jurassic to early Eocene, followed by rapid exhumation of mid to lower crustal rocks in metamorphic core complexes. Eocene exhumation of high-grade metamorphic rocks was coeval with extensional basin development, widespread basaltic volcanism, and the end of thrusting in the Rocky Mountain foreland [*Coney et al.,* 1980; *Armstrong,* 1982; *Parrish et al.,* 1988; *Brown et al.,* 1986; *Carr,* 1992; *Vanderhaeghe and Teyssier,* 1997; *Crowley et al.,* 2001; *Vanderhaeghe et al.,* 2003; *DeCelles,* 2004; *Teyssier et al.,* 2005; *Kruckenberg et al.,* 2008; *Gordon et al.,* 2008]. Exhumation was concentrated in the Omineca crystalline belt, which represents the exhumed hinterland of the Rocky Mountain foreland fold and thrust belt and has been interpreted as a discrete welt of thickened crust [*Brown,* 1980] or as the eastern margin of a collapsed orogenic plateau that extended to the Coast Mountains in the west [*Whitney et al.,* 2004]. In the Omineca belt, high-grade metamorphic rocks (including migmatite) and granitic intrusions are exposed within a ~400 km long belt that includes several gneiss domes (Frenchman's Cap, Thor-Odin, Pinnacles, Valhalla, Passmore, Priest River, Okanogan-Kettle). Taken together, these rocks form the largest metamorphic core complex (the Shuswap MCC) in the North American Cordillera (Figure 2.1).

2.2.1. The Thor-Odin Dome

At the latitude of the Thor-Odin dome, the Shuswap MCC exposes a 15 km thick crustal section bounded by detachment faults on the east (Columbia River fault) and west (Eagle River-Okanagan fault) (Figure 2.2). The MCC in this region can be divided

into three tectonic units [*Vanderhaeghe and Teyssier,* 1997]. The upper unit consists of Mesozoic plutonic rocks and low-grade to unmetamorphosed early Cenozoic sedimentary and volcanic rocks in the hanging walls of the detachment faults [*Mathews,* 1981; *Colpron et al.,* 1996]. Below the detachment faults, the middle unit comprises high-grade (amphibolite to upper amphibolite facies) metapelitic schist, calc-silicate, marble, amphibolite, and quartzite; these are intruded by leucogranite. The lower unit forms the core of the Thor-Odin dome and consists of migmatitic para- and orthogneiss and amphibolite. North-south trending normal/oblique brittle faults cut all units and affect the present-day topography of the dome. The highest peaks of the region are in the dome and are bordered on the east by the high-angle Columbia River normal fault, which cuts the low-angle Columbia River detachment fault zone, and on the west by the high-angle Victor Lake Fault (Figure 2.2). Local relief in this part of the dome is ~ 2 km and the structurally deepest rocks (the lower unit) are exposed in the highest peaks.

Thermobarometric data and reaction textures in high-grade rocks of the lower unit have been interpreted to indicate near-isothermal decompression of the dome rocks from metamorphic conditions of ~800 °C, and ≥10 kbar [*Duncan,* 1984; *Norlander et al.,* 2002; *Hinchey and Carr,* 2007; *Spalla et al.,* 2011; *Goergen and Whitney,* 2012a, b]. Furthermore, the reaction textures observed in these rocks suggest metamorphism under melt-present conditions and interaction of melt and minerals during decompression [*Norlander et al.,* 2002; *Hinchey and Carr,* 2007]. Similar textures have been reported from other domes in the Shuswap MCC, including the Okanogan dome [*Kruckenberg and Whitney,* 2011] and the Passmore dome [*Marshall and Simandl,* 2006]. The middle unit experienced maximum metamorphic conditions of ~650-800 °C at 7-9 kbar [*Ghent*

et al., 1977; *Nyman et al.,* 1995; *Norlander et al.,* 2002] throughout the entire unit [*Teyssier et al.,* 2005].

Previous geochronometric investigations of the Thor-Odin dome have focused on dating the crystallization and cooling of orthogneiss and migmatite in the core of the lower unit (dome), leucogranite in the middle unit, and various rocks in the upper unit. U-Pb zircon and monazite analysis of the upper unit documented ages between 174-161 Ma, interpreted as the mid-Jurassic emplacement of calc-alkaline plutonic rocks in an island arc setting [*Parrish and Wheeler,* 1983; *Carr,* 1991]. Cooling of these plutonic rocks was determined by K-Ar and Ar/Ar methods, indicating very slow cooling (1-3 °C/Ma) until the Eocene [*Colpron et al.,* 1996]. The K-Ar method was also used to date rhyolitic to basaltic volcanic rocks in the extensional basins; these yield ages between 49 and 47 Ma [*Matthews,* 1981]. Sedimentary units intercalated with these volcanic rocks contain pebbles from nearby calc-alkaline plutonic rocks, as well as gneiss and leucogranite from the footwall rocks, suggesting that exhumation of the high-grade metamorphic rocks was achieved before ~ 49 Ma [*Matthews,* 1981].

U-Pb zircon and Rb-Sr mineral-whole rock ages from the lower unit of the Thor-Odin dome range from Late Archean to Tertiary. The oldest ages have been documented from migmatitic gneiss (~2.7 Ga) that are intruded by orthogneiss, yielding ages from 1.9 to 1.8 Ga, and have been interpreted to indicate an affinity with the North American basement [*Duncan,* 1984; *Armstrong and Ward,* 1991; *Parkinson,* 1991, 1992; *Parrish,* 1995; *Crowley,* 1997; *Vanderhaeghe et al.,* 1999; *Hinchey et al.,* 2006]. Some of the youngest crystallization ages come from syntectonic granites (Ladybird leucogranite) that intruded the middle unit and form laccoliths in the detachment zone. U-Pb zircon

and monazite ages range between ~100 to 50 Ma; the majority of ages cluster around 60-55 Ma [*Carr,* 1991, 1992; *Parkinson,* 1992; *Vanderhaeghe et al.,* 1999; *Johnston et al.,* 2000]. These ages, combined with geochemical analysis, have been interpreted to indicate a crustal source for the leucogranite [*Sevigny et al.,* 1989; *Carr,* 1992]. Monazite and zircon U-Pb ages from granitic leucosomes in Thor-Odin dome migmatite yield even younger rim ages of ~56-51 Ma [*Vanderhaeghe et al.,* 1999; *Teyssier et al.,* 2005; *Hinchey et al.,* 2006]. The similarity in crystallization ages of the leucogranite and migmatite has been interpreted to indicate Paleocene-Eocene high-grade metamorphism and partial melting of continental crust [*Vanderhaeghe et al.,* 1999; *Johnston et al.,* 2000; *Teyssier et al.,* 2005; *Hinchey et al.,* 2006]. Therefore, although there are indications of inherited zircons (primarily in zircon cores), there is evidence for major reworking (metamorphism, partial melting) of the crust during the Cordilleran orogeny, including dome formation and emplacement of leucogranite sheets beneath the detachment fault zones.

$^{40}Ar/^{39}Ar$ thermochronology yields hornblende ages of ~59-54 Ma and biotite and muscovite ages of ~49-47 Ma, consistent throughout all structural units of the Shuswap MCC in the vicinity of the Thor-Odin dome [*Vanderhaeghe et al.,* 2003; *Mulch et al.,* 2006]. Modeling of K-feldspar $^{40}Ar/^{39}Ar$ data indicates cooling below ~ 150 °C at 45 Ma, except in samples collected directly beneath the footwall of the Columbia River Fault; in these footwall rocks, results are consistent with rapid cooling at ~33 Ma [*Vanderhaeghe et al.,* 2003]. Zircon fission-track (ZFT; cooling below 250 °C) and apatite fission-track (AFT; cooling below 60 °C) ages from higher elevations are ca. 54 and 40 Ma, respectively [*Lorencak et al.,* 2001], whereas samples from lower

elevations yielded younger ages ZFT and AFT ages of 38 to 20 Ma, respectively [*Lorencak et al.,* 2001; *Fayon et al.,* 2004a]. These data combined with $^{40}Ar/^{39}Ar$ ages indicate rapid cooling of deep crustal rocks in the Eocene.

2.2.2 The Frenchman's Cap Dome

The Frenchman's Cap Dome (Figure 2.3), located north of the Thor-Odin dome (Figure 2.1), exposes ~12 km of crustal section. The core of the dome consists of migmatitic para- and orthogneiss that record peak P-T conditions of 750-860 °C and ~12 kbar at ~64-49 Ma, depending on the structural level of the dome [*Crowley and Parrish,* 1999; *Crowley et al.,* 2001; *Gervais et al.,* 2011]. U-Pb zircon and titanite results document crystallization between 52 and 49 Ma [*Gervais et al.,* 2010]. These and other data have suggested that the effects of early Tertiary Cordilleran deformation diminished toward the deeper levels of the dome [*Crowley et al.,* 2008; *Gervais et al.,* 2010; *Gervais and Brown*, 2011]. Upper amphibolite-facies paragneiss and quartzite mantle the core of the dome, and U-Pb monazite analysis yields ages ranging between 60 and 50 Ma [*Parrish,* 1995; *Crowley and Parrish,* 1999; *Crowley et al.,* 2001; *Foster et al.,* 2004]. Biotite and hornblende $^{40}Ar/^{39}Ar$ thermochronology for the mantling units indicate cooling between 58 and 48 Ma. No previous low-temperature thermochronology data (fission-track, (U-Th)/He) have been reported from the Frenchman's Cap dome.

2.3. Low-Temperature Thermochronology

Apatite fission-track (AFT) thermochronology is a well-established method that relies on the preservation of damage zones or tracks that form by spontaneous decay of ^{238}U in minerals and glasses [*Fleischer et al.,* 1975]. Fission tracks in apatite instantaneously anneal at temperatures over ~120 °C, but remain relatively stable below

~60 °C [*Gleadow et al.,* 1986; *Donelick et al.,* 1999; *Ketcham et al.,* 1999]. Within the temperature range between ~120°C and 60°C - the apatite partial annealing zone (APAZ) - track lengths are systematically reduced over time. Therefore, the combination of fission-track age and track-length distribution can reveal how long a rock spent in the APAZ, and therefore how fast it cooled [e.g. *Gallagher,* 1995; *Ketcham,* 2005]. The magnitude of track length reduction depends on time and temperature a sample has resided within the APAZ [*Gleadow et al.,* 1986]. In general, rapidly cooled samples retain long confined tracks and have unimodal track-length distributions with a mean confined track-length (MTL) ≥ 14 μm [e.g., *Gleadow et al.,* 1986]. Samples that have resided in the APAZ for extended periods or experienced complex thermal histories retain shorter confined tracks (≤ 14 μm) and negatively skewed or bimodal track-length distributions.

Along with time and temperature, the crystallographic orientation and chemical composition of apatite grains influence the annealing processes [*Ketcham,* 2003]. In order to assess the kinetic properties of an apatite grain, its chlorine content or the arithmetic mean fission track etch pit diameter parallel to the c-axis (Dpar) are commonly measured [*Donelick et al.,* 2005] and incorporated into quantitative thermal models [e.g. *Ketcham,* 2005].

(U-Th)/He thermochronology uses accumulation in a crystal of ^{4}He resulting from decay of U, Th, and Sm via α-particle emission. Both laboratory experiments and measurements from borehole data indicate that He is released from apatite structure at temperatures around 80°C and is retained below ~40°C, a temperature range called the helium partial retention zone (HePRZ) by analogy with the APAZ [*Farley,* 2002]. For

cooling rates ~10 °C/my and grain sizes ~60±20 μm the closure temperature of He in apatite is ~70 °C [*Farley,* 2000]. Zircon has a higher closure temperature than apatite, ranging between ~170 and 190°C, although these estimates vary with grain size, radiation damage, and cooling rate [*Reiners et al.,* 2004, *Guenthner et al.,* 2013].

2.3.1. Analytical Methods

AFT samples were separated using standard magnetic and heavy mineral techniques. Apatite grains were placed into epoxy resin, polished to exhibit maximum surface exposure, and etched for 20 s in 5 M HNO_3 at room temperature. Grain mounts were covered with low-U mica external detector and irradiated at Oregon State University Radiation Center with a neutron dose of $1x10^{16}$ neutrons/cm^2. Mica detectors were etched in 50% HF for ~20 minutes at room temperature to reveal induced tracks. A Nikon Optiphot microscope with 100x dry objective attached to a drawing tube and digitizing table was used to count fission track densities and horizontal confined tracks. For track length measurements additional sets of grain mounts were prepared and irradiated using ^{252}Cf in order to enhance etchable horizontal confined tracks.

For ZHe and AHe analysis individual zircon and apatite grains were handpicked based on their shape and size. Special care was taken to avoid grains with inclusions and fractures. Alpha ejection factors were calculated after *Farley* [2002]. Single apatite or zircon grains were packed in Nb tubes and heated in order to liberate ^4He using a Nd-YAG laser cell connected to the He extraction and measurement line. He isotopic ratio was determined using a known volume of ^3He spike in a quadrupole mass spectrometer following the procedures outlined by *Reiners et al*. [2003] and *Reiners* [2005].

2.3.2. Results of Thermochronogical Analysis

A suite of 57 samples was collected from various lithologies including orthogneiss, paragneiss, granitic leucosome, quartzite, and amphibolite. Although this study primarily focuses on the Thor-Odin dome, six samples were collected from a traverse through the Frenchman's Cap dome in order to compare its low temperature thermal evolution with the Thor-Odin dome.

Summary of all ages are listed in Table 2.1. Details of thermochronometric data are provided in Tables 2.2, 2.3, and 2.4.

2.3.2.1. North Thor-Odin

Samples were collected along Highway 1 at a fairly constant elevation of 500-600 m and also on a steep transect (Mt Revelstoke) in the hanging wall of the high-angle Columbia River fault (Figure 2.2). Some samples were dated by multiple chronometric techniques; out of 19 samples in this traverse, 3 were analyzed using ZHe, AFT, and AHe thermochronometers, and 4 using two thermochronometers (Table 2.1). Ages are presented below in order of highest (ZHe) to lowest (AHe) closure temperature.

ZHe. Nine samples collected along Highway 1 are from a 5.5 km-wide block bounded by two high-angle normal faults, the Three-Valley Gap and Victor Lake faults. Ages range from 45.1 ± 1.9 to 37.4 ± 1.2 Ma, with no particular trend in either the horizontal (map distance) or vertical (elevation) directions (Figure 2.2, Tables 2.1 and 2.2).

AFT. Eleven AFT ages from the Highway 1 and Mt Revelstoke traverses range from 32.4 ± 6.3 to 14.0 ± 4.0 Ma, with no regional trend (Figure 2.2). All samples except one (BC-10-35) pass the Chi-square test (Table 2.3). MTL measurements vary from 12.3 ± 0.2 to 10.7 ± 0.2 μm, with standard deviations of 1.7 to 2.0 μm. All samples show bimodal mean track-length distribution and Dpar values range from 3.8 to 2.1 μm.

AHe. Along Highway 1 and between the Three-Valley Gap and Victor Lake high-angle normal faults, AHe ages range from 12.6 ± 0.3 to 7.6 ± 0.4 Ma, with most ages around 7-8 Ma. No trend in age is discernible with respect to the position of samples relative to the faults (Figure 2.2, Table 2.4). On the Mt Revelstoke transect, the five samples analyzed range between 26.4 ± 1.0 and 15.7 ± 1.4 Ma. Ages vary slightly with elevation: the sample showing the youngest age is located at 600 m elevation, and the sample that records the oldest age is located at 1600 m (Figure 2.2, Table 2.4).

2.3.2.2. South Thor-Odin

Samples were collected along a broad region in the southern part of the Thor-Odin dome, from the Columbia River in the east to Sugar Lake in the west (Figure 2.2). Owing to high relief and relatively easy access on forest roads, two sample transects were collected in the south Thor-Odin region: The Mt Symonds transect goes from the Columbia River (elevation ~ 500 m) to the flank of Mt Odin (2600 m); the near-vertical Sugar Mountain transect is located on the western flank of Sugar Mountain between 1370 and 2182 m elevation. We also obtained four samples from the hanging-wall of the Columbia River detachment fault, on the bank of the Columbia River (Figure 2.2).

In addition, seven isolated samples were collected throughout the southern Thor-Odin region, and one sample is from a granite boulder collected in the Enderby basin; this group of samples will be referred to as “isolated samples”.

ZHe. Two samples were analyzed for ZHe; the sample from the hanging-wall (01-73) yields an age of 30.9 ± 0.7 Ma, whereas the footwall sample (01-77) is 44.3 ± 0.9 Ma in age (Figure 2.2).

AFT. Nineteen AFT dates from the Mt Symonds transect range from 44.8 ± 8.8 to 18.0 ± 4.0 Ma (Figure 2.2). Ages strongly correlate with elevation: younger ages are from samples collected at the lower altitudes (~500m). All but one sample (99-142) pass the Chi-square test, indicating that these samples represent single age populations (Table 2.3). Mean track lengths from ten samples vary from 14.5 ± 0.1 to 9.9 ± 0.3, with standard deviations from 1.1 to 2.6 μm. Samples with long MTL (>14 μm) have unimodal track-length distribution, whereas samples with shorter MTL (< 14 μm) display bimodal track-length distribution. Dpar values range from 3.5 to 1.9 μm, suggesting relatively slow annealing of apatite grains (Table 2.3).

The four samples from the Sugar Mountain transect range between 47.9 ± 7.8 and 34.6 ± 5.6 Ma and show a strong correlation between age and elevation, with higher altitude (~2100m) samples revealing older ages (Figure 2.4). All samples pass the Chi-square test, and mean track length values from two samples for which track lengths were measured range between 13.5 ± 0.1 and 11.9 ± 0.2 μm, with standard deviations 2.2 to 1.2 μm. Dpar values are 2.4 and 1.9 μm (Table 2.3).

In order to increase regional coverage, we collected seven additional samples ("isolated samples") (Figure 2.2). Apatite fission-track ages are between 37.0 ± 5.4 and 16.5 ± 2.8 Ma, and all samples pass the chi-squared test (Table 2.1). Mean track length measurements are between 13.0 ± 0.2 and 12.5 ± 0.2 μm, with standard deviations of 1.5 to 1.9 μm, respectively. Dpar values range between 3.3 and 1.8 μm.

AHe. Five samples from this part of the Thor-Odin dome region were analyzed for AHe; all samples are close to the Columbia River with similar altitudes and three of them are located in the hanging wall of the Columbia River detachment fault (Figure 2.2).

Hanging-wall samples (01-72, 01-79, 01-80) yield ages between 11.9 ± 0.3 and 4.9 ± 0.3 Ma and two footwall samples (01-77, 01-78) give ages of 4.6 ± 0.2 and 12.6 ± 0.4 Ma (Figure 2.2, Table 2.1). Importantly, three of these samples (01-72, 01-77, 01-78) show wide range of intra-sample grain ages, which we discuss in detail later in section 5.2.

2.3.2.3. Frenchman's Cap

Six samples were collected from the Frenchman's Cap area (Figures 2.3-2.4) on a transect with altitudes ranging from ~800 to 1700 m. AFT ages range from 42.9 ± 14.2 to 21.1 ± 3.2 Ma (Table 2.1). Only three samples yielded sufficient apatite fractions for track length analysis. MTL measurements are between 13.0 ± 0.2 and 10.3 ± 0.2 μm, with standard deviations ranging from 2.3 to 1.8 μm. High Dpar values between 2.8 and 1.9 μm indicate that these samples are characterized by relatively slow fission track annealing (Table 2.3).

2.4. Thermal Modeling

Thermochronometric data from this study were modeled using the HeFTy software, which utilizes a number of forward and inverse models in order to find optimum temperature-time (T-t) paths using fission-track annealing and He diffusion parameters for apatite and zircon [*Ketcham,* 2005]. Measured AFT length distributions and ages were modeled using the multicompositional annealing model of *Ketcham et al.* [2007b] and c-axis projected track lengths of observed data [*Ketcham et al.,* 2007a]. Dpar values were used as a kinetic parameter to calculate initial track lengths.

The present-day surface temperature was set at 15±5 °C for samples collected at < 1700 m altitude, and 10±10 °C for those from >1700 m altitude. $^{40}Ar/^{39}Ar$ white mica ages were used to define the starting time-temperature condition for when the sample

was at 325±25 °C. Samples were assumed to have entered the APAZ (~120-60 °C) ~10 Ma before and after their corresponding central ages if the MTL's of samples are relatively long (>14 μm). In the case of mixed or bimodal track-length distributions with relatively short MTL (implying that those samples resided within the partial annealing zone for some time), the samples were allowed to enter the partial annealing zone sometime between ~20 m.y. before and after their measured central ages.

Mean ZHe and AHe ages, where available, were included as additional T-t constraints in the models based on He partial retention zone of ~190-170 °C for zircon [*Reiners et al.,* 2004] and ~40-80 °C for apatite [*Wolf et al.,* 1998]. Helium diffusion in zircon and apatite was modeled after *Reiners et al.* [2004] and *Flowers et al.* [2009], respectively.

Random sub-segment spacing and Monte Carlo inversion were used to find viable thermal histories. Monotonic cooling was assumed for all samples. HeFTy uses goodness-of-fit statistics to evaluate the fit between the predicted and observed age and track length data for each randomly generated thermal path. We used goodness-of-fit values of 0.5 and 0.05 for "good" and "acceptable" paths. Models were run until 100 randomly generated "good" solutions were found.

2.4.1. North Thor-Odin

Modeling results of samples from the nearly constant-elevation (500-600 m) along Highway 1 suggest three episodes of cooling (Figure 2.5). All models require high cooling rates (~ 20-30 °C/my) prior to temperatures <120 °C, followed by very slow cooling rates (<1 °C/my) within the APAZ. Starting sometime between 10 and 1 Ma, a

sharp increase in cooling rate, up to ~15 °C/my, is observed in all modeled samples except one (BC-10-33) (Figure 2.5).

2.4.2. South Thor-Odin

2.4.2.1. Thor-Odin transect

Modeled thermal histories from the Thor-Odin section indicate that all rocks experienced high cooling rates up to 50 °C/my before they reached APAZ temperatures; then cooling patterns start to differ (Figures 2.6-2.7). Samples collected from low altitudes (01-80, 01-78, and 01-79), between 450 and 700 m, show relatively long residence time (45 to 5 Ma) within the APAZ while cooling was slow (< 1 °C/my). Modeling predicts that cooling accelerated (up to 20 °C/my) at a time that is bracketed between ~10 and 2 Ma (Figure 2.6).

Model results for rocks collected from altitudes of ~700-1800 m show a decrease in cooling rates at sometime between ~42 and 30 Ma, following the initial high values (Figures 2.6, 2.7). For four samples (99-141, BC-10-12, BC-10-14, BC-10-18), this phase of cooling is as slow as 2 °C/my, although the first three samples record much lower values of cooling rates (<1 °C/my) within the last portion of their modeled temperature-time paths. Sample BC-10-07 was collected from the local valley bottom at 1326 m. Modeling results for this sample show an increase in cooling rates up to ~7 °C/my since ~6 Ma, similar to the samples collected from low altitudes (< 700 m).

Modeled thermal histories of rocks from altitudes between 1800 and 2700 m (99-142, E-2F, BC-10-08, BC-10-09) indicate that all these samples cooled rapidly from high temperatures through the apatite partial annealing zone, at rates ranging from 10 to

40 °C/my between ~48 and 35 Ma (Figure 2.7). A sharp decrease of cooling rates around 32 Ma (<1 °C/my) followed this phase of rapid cooling.

2.4.2.2. Sugar Mountain

Modeling results for Sugar Mountain samples suggest that the rocks experienced very high cooling rates (up to 60 °C/my) prior to entering the APAZ (~60-120 °C) between ~49 and 35 Ma (Figure 2.7). Modeled cooling rates decelerated drastically (< 5 °C/my) through the APAZ. Results for sample BC-10-42, which was collected at a lower altitude (1369 m), indicate that the rock spent more time within the APAZ and experienced a slight increase in cooling rate (> 3°C/my) starting at ~20 Ma. In contrast, model results predict that cooling rates for sample BC-10-41 (1681 m) consistently decreased to very low values (<1°C/my) starting ~ 20 Ma.

2.4.2.3. Isolated samples

All five modeled rock samples suggest initial high cooling rates (~20-60 °C/my) from high-temperature to the APAZ (~60-120 °C) (Figure 2.8). A significant drop in cooling rates (< 5 °C/my) within the APAZ is characteristic for all samples, although samples LC-12 and LC-15 display longer residence in the APAZ. Samples BC-10-40 and BC-10-51 show accelerated cooling up to 10 °C/my starting between ~8 and 2 Ma.

2.4.3. Frenchman's Cap

Modeled cooling histories from the Frenchman's Cap rock samples show that all three localities initially experienced high cooling rates (~20-80 °C/my) down to temperatures of ~120 °C (Figure 2.9). All samples display a decrease in modeled cooling rates within the AFT partial annealing zone. Sample BC-08-40 was collected from a

higher altitude (1342 m) relative to the other two samples and records more or less constant cooling rate of ~ 5 °C/my after ca. 25 Ma. In contrast, modeling results for lower elevation samples BC-08-44 and BC-08-45 suggest that these rocks resided within the APAZ much longer than BC-10-40, where they experienced maximum temperatures ~ 90-80 °C and cooling rates < 1 °C/my. Additionally, both of these rocks record a late Miocene to Pliocene cooling event, sometime between ~10 and 1 Ma (Figure 2.9).

2.5. Discussion

The low-temperature thermochronologic data presented here, combined with previously documented thermobarometry and geo/thermochronology from the region, provide new insight into the timing of dome formation and landscape development in the northern Shuswap MCC. Results indicate that the high-grade metamorphic dome rocks (migmatite) reached shallow crustal levels, where they acquired Eocene AFT ages that are only slightly younger than the age of high-T crystallization and cooling, consistent with previously published data [*Lorencak et al.,* 2001]. The new AFT ages from the Frenchman's Cap and Thor-Odin domes reveal the top of a fossil APAZ which formed during Eocene time and was exhumed as a result of a younger cooling event.

The Mount Symonds profile, which covers ~2 km of relief, shows that samples from >1800 m elevation are characterized by long, unimodal track-length distribution (>14 μm) and small standard deviations (<1.2 μm). In contrast, samples collected below 1800 m show AFT ages that decrease with decreasing elevation and reveal shorter mean track length (<14 μm), larger standard deviations (>1.2 μm), and bimodal track-length distributions. Rocks that are currently at lower elevation have experienced more annealing than the rocks from the upper part of the profile (Figure 2.4). Such a pattern of

lower ages with shorter track lengths is diagnostic of the upper portion of an exhumed APAZ; at elevations >1800 m, rocks have preserved fast cooling through the APAZ, and these rocks have been at temperatures < 60 °C since ~45 Ma (Figure 2.10). The preserved APAZ formed under relatively stable thermal conditions, resulting in a very shallow slope of age versus elevation in which the slope does not correspond to an apparent exhumation rate [e.g. *Gleadow and Fitzgerald,* 1987]. Consequently, the change in the slope at around 45 Ma indicates cessation of a major cooling event that we interpret as the end of exhumation of the gneiss dome after detachment tectonics and associated brittle faulting.

A "boomerang plot" of mean track lengths vs AFT central ages can be used to illustrate a two-stage (or more) thermal history of rocks that have experienced different maximum paleo-temperatures during a later cooling phase [e.g. *Gallagher et al.,* 1998]. If the curve is fully formed, this later cooling event is represented by relatively younger ages with long mean track lengths (>14 μm). The older ages with long mean track lengths are recorded in samples that were exhumed to near-surface temperatures during an earlier cooling event and therefore record no information about the younger cooling event. Samples collected in the APAZ and associated with the younger cooling event are represented by an intermediate age range with shorter mean track lengths.

A mean track length vs AFT central age plot of our data reveals a partially developed "boomerang" curve (Figure 2.11). Eocene exhumation is marked by long mean track lengths (>14 μm). As the AFT central ages decrease, the mean track lengths from the corresponding samples also diminish, implying significant post-Eocene annealing during residence in the APAZ. These samples represent a "mixed" age

population and, as a consequence, they cannot be interpreted as simple cooling ages. Although the ascending portion of the curve is not documented within our dataset, this thermal event should be younger than the youngest AFT age (~14 Ma). Thus, the Shuswap MCC experienced two episodes of cooling: the first cooling event is related to dome exhumation in the Eocene, and a second post-middle Miocene cooling event (Figure 2.12).

2.5.1 Eocene Cooling and Exhumation of the Thor-Odin region of the Shuswap MCC

The cooling and exhumation history of the Shuswap MCC can be reconstructed by combining previously published P-T-t estimates and geochronologic data as well as new ages from this study. Eocene U-Pb zircon ages as young as 56-51 Ma [*Vanderhaeghe et al.,* 1999; *Hinchey et al.,* 2006] and U-Pb monazite ages as young as ca. 53 Ma [*Teyssier et al.,* 2005] have been obtained from migmatite and syntectonic granitoids that form the lower unit of the Thor-Odin dome. The overlying middle unit between the lower unit and the core-complex detachments contains extensive granite sheets and laccoliths of the 60-55 Ma Ladybird leucogranite suite [*Carr, 1991, 1992; Johnston et al., 2000*]. Lower-unit migmatites record decompression at high T (750°C) from ~ 8-10 kbar to ~ 4-5 kbar [*Norlander et al.*, 1999; *Hinchey et al.*, 2006; *Goergen and Whitney*, 2012a, b]; this decompression and crystallization of partial melt (56-51 Ma) was followed by rapid cooling. Therefore, post-decompression cooling of the dome rocks began in a high geothermal gradient of ~40-50 °C/km that may have been established by 51 Ma.

Based on structural and metamorphic studies, the Thor-Odin dome can be viewed as the locus of substantial vertical flow of partially molten crust beneath an extensional system in a manner similar to that proposed by *Rey et al.* [2009a, b; 2011]. In this system, upward flow through the middle crust was fed by lateral flow of low-viscosity (partially molten) lower crust beneath the dome [*Teyssier et al.,* 2005; *Rey et al*., 2009b], resulting in the decompression textures (e.g. coronas of cordierite + spinel on kyanite) that are preserved in the deepest exposed levels of the dome.

The final stages of deformation occurred in the solid-state and are recorded in the detachment shear zones that bound the core complex. Based on $^{40}Ar/^{39}Ar$ geochronology of synkinematic muscovite, *Mulch et al.* [2007] proposed that muscovite grains, dated at 49-48 Ma, record the age of deformation-recrystallization of the quartzite mylonite that bounds the Thor-Odin dome to the east. $^{40}Ar/^{39}Ar$ cooling ages of 49-47 Ma, obtained from the footwall of the eastern and western detachments of the Shuswap core complex in the Thor-Odin dome region [*Vanderhaeghe et al.*, 2003], are identical to the age of mylonitization, suggesting coeval deformation in detachments and cooling below ~400°C of the core-complex rocks of all structural levels [*Mulch et al.,* 2007]. Argon multi-domain diffusion modeling of K-feldspar [*Vanderhaeghe et al.,* 2003] and ZFT data from previous studies [*Lorencak et al.,* 2001] document the distribution of low-temperature cooling ages across the core complex. The ZFT ages show a broad distribution between 53 and 38 Ma, although the majority of ages cluster around 50-45 Ma [*Lorencak et al.,* 2001], similar to the $^{40}Ar/^{39}Ar$ ages.

The cooling history of the dome rocks below ~ 190°C is captured by ZHe, AFT, and AHe ages. ZHe ages from this study are restricted to low elevations (~500 m) in the

valley that parallels Highway 1; ages range from 45 to 37 Ma. Regional AFT ages display a significant difference between the western and eastern parts of the core complex. Near the western detachment (Sicamous, Enderby; Figure 2.2) ages are clustered around 45 Ma, whereas in the eastern portion of the core complex, including the Thor-Odin dome region, ages vary between 48 and 20 Ma [*Lorencak et al.,* 2001; *Fayon et al.*, 2004a], similar to ages that were obtained in this study.

AFT ages point to an asymmetry in the development of the core complex; the rocks that are at ~500-1100 m present-day elevation in the western part of the complex reached temperatures ≤ 60 °C by ~45 Ma [*Lorencak et al.,* 2001]; these rocks most likely represent the top of the APAZ or the region above it. In the eastern part of the complex, where the migmatite dome is located, this relation is only true for rocks on the high mountain peaks (> ~1800 m elevation). Rocks above that elevation retain Eocene ages (48-42 Ma), and the MTL distributions in these samples document rapid cooling through the APAZ (Figures 2.4-2.7; Table 2.1). The difference in APAZ elevation between the eastern and western parts of the core complex reaches ~1300 m.

This elevation difference of the top boundary of the APAZ can be explained by at least three different scenarios. In one interpretation, relief of the APAZ is associated with a difference in Eocene topography, with the eastern region having been more elevated than the western region. Given that first-order topography affects shallow isotherms [e.g. *Stüwe et al.,* 1994], the topographic elevation difference would have exceeded 1300 m. Geomorphic observations from British Columbia show that the Eocene relief of the region could have been ~1000 m, similar to what it is today [*Tribe*,

2005]. Therefore, topographic effects alone do not provide an adequate explanation for the lateral variation in thermal structure.

Alternatively, the bending of isotherms may have been controlled by a lateral gradient in the geotherm. In this scenario, Eocene isotherms would have been more compressed in the eastern region than in the west, owing to heat advection from dome emplacement, to produce the observed APAZ relief regardless of surface topography. In the east, near-synchroneity of high-to-low temperature geochronology suggests the existence of a high geothermal gradient (~40-60 °C/km) during exhumation of lower-to-mid orogenic crust. In order to maintain ~1300 m of relief in the ~60 °C isotherm, the geothermal gradient in the western part of the core complex must have been only ~20-26 °C/km. Besides the fact that such a lateral gradient in the geotherm is unlikely, vitrinite reflectance studies of early Cenozoic basins (Enderby and Trinity Hills) preserved in the western hanging wall reveal a geothermal gradient of >50 °C/km during or slightly after basin formation at ~50 Ma [*Mathews*, 1981], similar to the high geothermal gradient documented in the eastern region. Although the geothermal gradient was likely higher in the dome region, the difference between eastern and western domains of the core complex cannot be as profound as to explain the 1300 m relief in the isotherm that bounds the APAZ.

Finally, the observed offset of the ~60 °C isotherm may be a consequence of late-stage deformation of that surface. In the vicinity of the dome several well-defined brittle faults, such as the Victor Lake, Three-Valley Gap, and Columbia River normal faults (Figure 2.1), cut across the ductile structures and form topographic lineaments that control first-order fluvial networks [*Lorencak et al.,* 2001; *Kruse and Williams,* 2005].

The timing of these faults is poorly known; it is generally accepted that these faults were formed during Eocene exhumation, however, whether they were active at ~55 to 51 Ma [e.g. *Kruse and Williams,* 2005] or after ~45 Ma [*Lorencak et al.,* 2001] is not clear. Additionally, the total offset along these faults is poorly documented. Based on displacement of km-scale regional fold hinges, it has been proposed that the Victor Lake fault has accommodated ~2000 m of normal fault displacement [*Kruse and Williams,* 2005]. According to this estimate, brittle faulting might have juxtaposed different levels of shallow crust and produced the observed offset of the top of the APAZ. However, it is difficult to assess this scenario as the regional coverage of low-T chronometers is insufficient across the core complex. It is likely that the APAZ relief has multiple causes, including the three processes mentioned above. The region of the lower unit that has exposed the migmatite dome likely registered a slightly elevated geotherm, produced higher elevation, and continued to move upward as a horst during the final stages of Eocene exhumation.

Regardless of the origin of APAZ relief, ZHe, AFT, and AHe ages (Table 2.1) as well as T-t histories obtained from HeFTy models (Figure 2.7) suggest that the final emplacement depth of the high-grade, lower unit rocks was close to the surface (~1-2 km). Therefore, exhumation from ductile to brittle-ductile conditions and cooling to ≤ 60 °C was achieved during a single event in the Eocene.

2.5.2 Post Middle-Miocene Cooling and Exhumation

The AFT data for the Thor-Odin dome show a partially developed boomerang curve, indicating that a second cooling event affected the region sometime after ca. 14 Ma (Figure 2.11). The exact timing of this event cannot be assessed from fission-track

data alone. Track-length modeling of these data, particularly the low elevation samples collected from valley floors (~500 m), indicates that these rocks experienced slow cooling through the APAZ, requiring a cooling event between ~10 and 2 Ma (Figures 2.5, 2.6, 2.11). Furthermore, AHe ages suggest this cooling event should be at or younger than 5 Ma. In addition, AHe results from three samples collected on the shore of the Columbia River show a wide range of single grain ages: ~21-4 Ma for sample 01-78; 27-2.6 Ma for 01-77, and 10-3 Ma for 01-72 (Table 2.4).

Many factors may cause age variations in single grain AHe analysis. For example, the presence of U-rich fluid inclusions or solid phases within dated apatite can lead to age variations in single grain ages, since excess ^{4}He causes older ages [*Farley,* 2002]. No fluid or solid inclusions were observed during grain selection for these samples and we do not consider this the best explanation for the scatter in ages. Close proximity of apatite grains to high-U bearing phases has also been suggested to produce significant single-age variations, because implantation of α-particles from neighboring grains may cause older ages [e.g. *Speigel et al.,* 2009]. It is possible that the variations in single grain ages are related to this implantation but we cannot evaluate this effect. Another factor creating dispersion in age data is the zoning of parent isotopes that induces incorrect α-ejection correction. This process is enhanced if a sample experiences slow cooling through the partial retention zone [*Meesters and Dunai,* 2002]. Although our fission-track mount-mica pairs do not show any zoning patterns, we cannot rule out zoning as a potential source for single-grain age dispersions in our samples.

Helium retentivity in an apatite crystal can be modified by radiation damage as it affects the closure temperature of AHe system [*Shuster et al.,* 2006; *Flowers et al.,*

2009; *Gautheron et al.,* 2009]. In their radiation damage accumulation and annealing model (RDAAM) *Flowers et al.* [2009] demonstrated that if rocks slowly cool through the PRZ or are reheated after long residence at near-surface temperatures, apatite grains with high eU (effective U concentration) give older ages relative to those with lower eU values. In our dataset, samples 01-78 and 01-77 show correlation between eU and age (Table 2.4), suggesting that radiation damage might play a significant role in the observed age scatter. Similar to the radiation damage, varying grain size can modify He retentivity in apatite [*Reiners and Farley,* 2001]. For example, a rock cooling relatively quickly through the PRZ shows no age-size correlation, whereas rocks that experience prolonged residence within the PRZ exhibit age-size correlation. Only one of our samples, 01-78, shows such age-size correlation so this factor unlikely contributes significantly to the observed age scatter.

In summary, despite the fact that AHe ages alone do not provide a clear signal of a young (<3 Ma) cooling event, intra-sample AHe variations of several samples as well as fission-track modeling strongly suggest a significant increase of cooling rates in samples collected from valley floors (Figures 2.5-2.6). The large variation of intra-sample AHe ages has been shown to inform exhumation and relief histories. For instance, *Hansen and Reiners* [2006] reported wide intra-sample single grain AHe ages from the southern coast of East Greenland, where ages range between ~250 to 20 Ma, and young ages (~20 Ma) are only observed from low-elevation samples. They interpreted these young ages to reflect a glacial incision event resulting in ~1.5 km of local valley erosion. Similarly, we propose that young intra-sample ages (~3 Ma) record the timing of the second cooling event in the northern Shuswap MCC. We further

propose that this cooling event is linked to the onset of the north hemisphere glaciations at 3.5-2.7 Ma [*Haug et al.,* 2005; *Lisiecki and Raymo,* 2005; *Mudelsee and Raymo,* 2005], causing accelerated erosion below the current 1800 m elevation that resulted in widening and deepening of valleys by glacial incision. Preservation of older ages (Eocene) in high elevation samples (>1800 m) further supports the idea of localized incision in valleys, rather than a regional erosional event. Large topographic changes and relief modification has been previously shown in western British Columbia during late Neogene glaciation [*Farley et al.,* 2001; *Ehlers et al.,* 2006; *Shuster et al.,* 2006; *Densmore et al.,* 2007; *Olen et al.,* 2012]. Our results indicate that the effects of continental glaciations can be traced into continental interiors.

2.6. Conclusions

New zircon (U-Th)/He (ZHe), apatite fission-track (AFT), and apatite (U-Th)/He (AHe) cooling ages from the Shuswap metamorphic core complex range from 45 to 30 Ma, 48 to 14 Ma, and 26 to 5 Ma, respectively. Apatite fission track ages generally increase with elevation, with a break in slope at ~1800 m and ca. 45 Ma in age-elevation profiles. Using track-length distribution patterns, we interpreted this profile as the upper portion of an exhumed partial annealing zone. Both fission-track ages and track-length modeling results of samples collected above 1800 m elevation show similar thermal histories, involving rapid cooling (40-60 °C/my) from higher temperatures through the apatite partial annealing zone between ~45 Ma. Exhumation essentially ceased at this time and cooling rates decreased sharply to ≤1 °C/my, suggesting that exhumation of the dome rocks to shallow depths (≤ 3 km) was achieved in Eocene time.

Although the lack of a complete apatite partial annealing zone profile inhibits determining the exact timing of the second cooling episode, AFT central age versus mean track-length distribution indicates this event must be younger than ~14 Ma. Multiple thermochronologic ages and track-length modeling from low-elevation samples (<600 m) at valley bottoms, as well as intra-sample AHe age variations in some of these samples reveal a more recent rapid cooling event sometime after the late Miocene. Because this recent cooling episode is only recorded in samples from the valley bottoms, we interpret this young cooling as acceleration of erosion below ~1800 m associated with the localized incision of valleys owing to the onset of northern hemisphere glaciations at ~3 Ma. By combining multiple thermochronometers from age-elevation profiles along with spatially distributed and valley bottom samples, we show that low-temperature thermochronology can be used to extract information about the emplacement of high-grade rocks, such as migmatite-cored metamorphic core complexes, as these rocks are transferred rapidly from the mid-crust to ≤3 km from the Earth's surface in a single exhumation event.

References

Armstrong, R.L. (1982), Cordilleran metamorphic core complexes; from Arizona to southern Canada, *Annual Review of Earth and Planetary Sciences*, v. 10, p. 129-154.

Armstrong, R.L., and P.L. Ward (1991), Evolving geographic patterns of Cenozoic magmatism in the North American Cordillera; the temporal and spatial association of magmatism and metamorphic core complexes, *J. Geophys. Res.*, 96(B8), 13201–13224, doi:10.1029/91JB00412 .

Beaumont, C., R.A. Jamieson, M.H. Nguyen, and B. Lee (2001), Himalayan tectonics explained by extrusion of a low-viscosity crustal channel coupled to focused surface denudation, *Nature*, v. 414, p. 738-742.

Brown, R.L. (1980), Frenchman Cap dome, Shuswap complex, British Columbia: a progress report, in *Current Research*, Part A, Geological Survey of Canada, Paper 80-1A, 47–51.

Brown, R.L., J.M. Journeay, L.S. Lane, D.C. Murphy, and C.J. Rees (1986), Obduction, backfolding and piggyback thrusting in the metamorphic hinterland of the southeastern Canadian Cordillera, *J. Struct. Geol.*, 8, 255-268.

Brown, S.R., H.D. Gibson, G.D.M. Andrews, D.J. Thorkelson, D.D. Marshall, J.D. Vervoot, and N. Rayner (2012), New constrains on Eocene extension within the Canadian Cordillera and identification of Phanerozoic protoliths for footwall gneisses of the Okanagan Valley shear zone, *Lithosphere*, 4, 4, 354-377.

Carr, S.D (1992), Tectonic setting and U-Pb geochronology of the early Tertiary Ladybird leucogranite suite, Thor-Odin-Pinnacles area, southern Omineca belt, British Colombia, *Tectonics*, 11, 258-278.

Carr, S.D. (1991), U-Pb zircon and titanite ages of three Mesozoic igneous rocks south of the Thor-Odin-Pinnacles area, southern Omineca Belt, British Columbia, *Can. J. Earth Sci.*, 28, 1877-1882.

Carter, T.J., B.P. Kohn, D.A. Foster, and A.J.W. Gleadow, (2004), How the Harcuvar Mountains metamorphic core complex became cool: Evidence from apatite (U-Th)/He thermochronometry, *Geology*, v. 32, p. 985–988, doi: 10.1130/G20936.1.

Carter, T.J., B.P. Kohn, D.A. Foster, A.J.W. Gleadow, and J.D. Woodhead (2006), Late-stage evolution of the Chemehuevi and Sacramento detachment faults from apatite (U-Th)/He thermochronometry-Evidence for mid-Miocene accelerated slip, *Geological Society of America Bulletin,* v. 118, p. 689–709.

Colpron, M., R.A. Price, D.A. Archibald, and D.M. Carmichael (1996), Middle Jurassic exhumation along the western flank of the Selkirk fan structure: thermobarometric and thermochronometric constrains from the Illecillewaet synclinorium, Southeastern British Columbia, *Geological Society of America Bulletin*, 108, 1372–1392.

Coney, P.J., M.D., Jr. Crittenden, P.J. Coney, and G.H. Davis (1980), Cordilleran metamorphic core complexes; an overview, in *Cordilleran metamorphic core complexes*, Memoir, Geological Society of America, p. 7-31.

Crowley, J. (1997), U-Pb geochronologic constraints on the cover sequence of the Monashee Complex, Canadian Cordillera: Paleoproterozoic deposition on basement, *Can. J. Earth Sci.*,34, 1008-1022.

Crowley, J.L., R.L. Brown, F. Gervais, and H.D. Gibson (2008), Assessing inheritance of zircon and monazite in granitic rocks: an example from the Monashee Complex, Canadian Cordillera, *Journal of Petrology*, 49, 1915-1929.

Crowley, J.L., R.L. Brown, and R.R. Parrish (2001), Diachronous deformation and a strain gradient beneath the Selkirk allochthon, northern Monashee complex, southeastern Canadian Cordillera, *Journal of Structural Geology* 23, 1103-1121.

Crowley, J.L., and R.R. Parrish (1999), U-Pb isotopic constraints on diachronous metamorphism in the northern Monashee complex, southern Canadian Cordillera, *Journal of Metamorphic Geology*, 17, 483-502.

DeCelles, P.G. (2004), Late Jurassic to Eocene evolution of the Cordilleran thrust belt and foreland basin system, western U.S.A., *American Journal of Science*, 304, 105–168.

Denèle, Y., P. Olivier, G. Gleizes, and P. Barbey (2007), The Hospitalet gneiss dome (Pyrenees) revèisited, Lateral flow during Variscan transpression in the middle crust, *Terra Nova*, v. 19, p. 419–453, doi:10.1111/j.1365-3121 .2007.00770.x.

Densmore, M. S., T. A. Ehlers, and G.J. Woodsworth (2007), Effect of Alpine glaciation on thermochronometer age-elevation profiles, *Geophysical Research Letters*, 34, L02502, doi:10.1029/2006GL028371.

Donelick, R. A., R. A. Ketcham, and W. D. Carlson (1999), Variability of apatite fission-track annealing kinetics: II. Crystallographic orientation effects, *American Mineralogist*, 84, 1224-1234.

Donelick, R.A., P.B. O'Sullivan, and R.A. Ketcham (2005), Apatite fission track analysis, *Reviews in Mineralogy and Geochemistry*, vol. 58, 49-94.

Duncan, I.J. (1984), Structural evolution of the Thor-Odin gneiss dome, *Tectonophysics*, 101, 87-130.

Dunkl, I. (2002), TRACKKEY: a Windows program for calculation and graphical presentation of fission track data, *Computers & Geosciences*, 28(1), 3-12.

Ehlers, T. A., K. A. Farley, M. E. Rusmore, G. J. Woodsworth (2006), Apatite (U-Th)/He signal of large-magnitude accelerated glacial erosion, southwest British Columbia, *Geology*, 34(9), 765-768.

Farley, K. A., L. T. Wolf, and L. T. Silver (1996), The effects of long alpha-stopping distances on (U-Th)/He ages, *Geochimica et Cosmochimica Acta*, *60*, 4223-4229.

Farley, K.A. (2000), Helium diffusion in apatite: General behavior as illustrated by Durango fluorapatite, *Journal of Geophysical Research*, 105, 2903-2914.

Farley, K.A., M.E. Rushmore, and S.W. Bouge (2001), Post-10 Ma uplift and exhumation of the northern Coast Mountains, British Columbia, *Geology*, 29, 99-102.

Farley, K.A. (2002), (U-Th)/He dating: Techniques, calibrations, and applications, *Reviews in Mineralogy and Geochemistry*, vol. 47, 819-844.

Fayon, A. K., S. M. Peacock, E. Stump, and S. J. Reynolds (2000), Fission track analysis of the footwall of the Catalina detachment fault, Arizona: Tectonic denudation, magmatism, and erosion. *Journal of Geophysical Research: Solid Earth*, *105*(B5), 11047-11062.

Fayon, A.K., A. Mulch, C. Teyssier, M. Person, and O. Vanderhaeghe (2004a), Fluid flow and heat transfer during exhumation of metamorphic core complexes, *GSA Annual meeting*, paper no 237-13.

Fayon, A.K., D.L. Whitney, and C. Teyssier (2004b), Exhumation of orogenic crust: diapiric ascent vs. low-angle normal faulting. in *Gneiss Domes and Orogeny,* edited by D.L.Whitney, C. Teyssier, and C.S. Siddoway, pp. 129-139, Geological Society of America Special Paper, 380.

Fleischer, R. L., P. B. Price, and R. M. Walker (1975), *Nuclear Tracks in Solids*, University of California Press.

Flowers, R. M., D. L. Shuster, B. P. Wernicke, and K. A. Farley (2007), Radiation damage control on apatite (U-Th)/He dates from the Grand Canyon region, Colorado Plateau, *Geology*, *35*(5), 447-450.

Flowers, R. M., R. A. Ketcham, D. L. Shuster, and K. A. Farley (2009), Apatite (U-Th)/He thermochronometry using a radiation damage accumulation and annealing model, *Geochimica et. Cosmochimica Acta*, 73(8), 2347–2365, doi:10.1016/j.gca.2009.01.015.

Foster, D. A., and B. E. John (1999), Quantifying tectonic exhumation in an extensional orogen with thermochronology: Examples from the southern Basin and Range province escape, in *Exhumation Processes: Normal Faulting, Ductile Flow and Erosion*, edited by U. Ring et al., pp. 87-107, Geological Society of London Special Publications, 154.

Foster, G., R.R. Parrish, M.S.A. Horstwood, S. Chenery, J. Pyle, and H.D. Gibson (2004), The generation of prograde *P-T-t* points and paths; a textural, compositional, and chronological study of metamorphic monazite, *Earth and Planetary Science Letters*, v. 228, p. 125–142, doi:10.1016/j.epsl.2004.09.024.

Foster, D.A., W.C., Jr. Grice, and T.J. Kalakay (2010), Extension of the Anaconda metamorphic core complex: 40Ar/39Ar thermochronology and implications for Eocene tectonics of the northern Rocky Mountains and the Boulder batholith, *Lithosphere*, v. 2, p. 232–246,doi:10.1130/L94.1.

Gallagher, K. (1995), Evolving temperature histories from apatite fission-track data, *Earth and Planetary Science Letters*, 136(3), 421-435.

Gallagher, K., R. Brown, and C. Johnson (1998), Fission track analysis and its applications to geological problems, *Annual Review of Earth and Planetary Sciences*, 26(1), 519-572.

Galbraith, R. F., and G. M. Laslett (1993), Statistical models for mixed fission track ages, *Nuclear Tracks and Radiation Measurements*, *21*(4), 459-470.

Gautheron, C., L. Tassan-Got, J. Barbarand, and M. Pagel (2009), Effect of alpha-damage annealing on apatite (U–Th)/He thermochronology, *Chemical Geology*, 266(3), 157-170.

Gervais, F., R. L. Brown, and J. L. Crowley (2010), Tectonic implications for a Cordilleran orogenic base in the Frenchman Cap dome, southeastern Canadian Cordillera, *Journal of Structural Geology*, 32(7), 941-959.

Gervais, F., and R. L. Brown (2011), Testing modes of exhumation in collisional orogens: Synconvergent channel flow in the southeastern Canadian Cordillera, *Lithosphere*, 3(1), 55-75.

Ghent, E.D., J. Nicholls, M.Z. Stout, and B. Rottenfusser (1977), Clinopyroxene amphibolite boudins from Three Valley Gap, British Columbia, *The Canadian Mineralogist*, 15, 269– 282.

Gleadow, A. J. W., I. R. Duddy, P. F. Green, and J. F. Lovering (1986), Confined track lengths in apatite: A diagnostic tool for thermal history analysis, *Contributions to Mineralogy and Petrology*, 94 (4), 405-415.

Gleadow, A. J. W., and P.G. Fitzgerald (1987), Uplift history and structure of the Transantarctic Mountains: New evidence from fission track dating of basement apatites in the Dry Valleys area, southern Victoria Land, *Earth and Planetary Science Letters*, 82(1), 1-14.

Goergen, E. T., and D. L. Whitney (2012a), Long length scales of element transport during reaction texture development in orthoamphibole-cordierite gneiss: Thor-Odin dome, British Columbia, Canada, *Contributions to Mineralogy and Petrology*, 163(2), 337-352.

Goergen, E. T., and D.L. Whitney (2012b), Corona networks as three-dimensional records of transport scale and pathways during metamorphism, *Geology*, 40(2), 183-186.

Gordon, S. M., D. L. Whitney, C. Teyssier, M. Grove, and W. J. Dunlap (2008), Timescales of migmatization, melt crystallization, and cooling in a Cordilleran gneiss dome: Valhalla complex, southeastern British Columbia, *Tectonics*, 27, TC4010, doi:10.1029/2007TC002103.

Gordon, S. M., T. A. Little, B. R. Hacker, S. A. Bowring, M. Korchinski, S. L. Baldwin, A. R. C. Kylander-Clark, and M.-A. Millet (2012), Multi-stage exhumation of young UHP–HP rocks: timescales of melt crystallization in the D'Entrecasteaux Islands, southeastern Papua New Guinea, *Earth and Planetary Science Letters*, 351–352, 237–246.

Gottardi, R., C. Teyssier, A. Mulch, T.W. Vennemann, and M.L. Wells (2011), Preservation of an extreme transient geotherm in the Raft River detachment shear zone, *Geology*, 39, 8, 759-762.

Green, P. F. (1981), A new look at statistics in fission-track dating. *Nuclear tracks*, *5*(1), 77-86.

Guenthner, W. R., P. W. Reiners, R. A. Ketcham, L. Nasdala, and G. Giester (2013), Helium diffusion in natural zircon: Radiation damage, anisotropy, and the interpretation of zircon (U-Th)/He thermochronology, *American Journal of Science*, 313(3), 145–198. doi:10.2475/03.2013.01.

Hansen, K., and P. W. Reiners (2006), Low temperature thermochronology of the southern East Greenland continental margin: evidence from apatite (U–Th)/He and fission track analysis and implications for intermethod calibratios, *Lithos*, 92(1), 117-136.

Haug, G. H., A. Ganopolski, D. M. Sigman, A. Rosell-Mele, G. E. Swann, R. Tiedemann, S.L. Jaccard, J. Bollmann, M.A. Maslin, M.J. Leng, and G. Eglinton (2005), North Pacific seasonality and the glaciation of North America 2.7 million years ago, *Nature*, 433(7028), 821-825.

Hinchey, A.M., S.D. Carr, P.D. McNeill, and N. Rayner (2006), Paleocene-Eocene high-grade metamorphism, anatexis, and deformation in the Thor-Odin dome, Monashee complex, southeastern British Columbia, *Canadian Journal of Earth Sciences*, 43, 1341-1365.

Hinchey, A. M., and S. D. Carr (2007), Protolith composition of cordierite-gedrite basement rocks and garnet amphibolite of the Bearpaw lake area of the Thor-Odin dome, Monashee Complex, British Columbia, Canada, *The Canadian Mineralogist*, 45(3), 607-629.

Hurford, A. J., and P. F. Green (1983), The zeta age calibration of fission-track dating, *Chemical Geology*, 41, 285-317.

Johnston, D.H., P.F. Williams, R.L. Brown, J.L. Crowley, and S.D. Carr (2000), Northeastward extrusion and extensional exhumation of crystalline rocks of the Monashee Complex, southeastern Canadian Cordillera, *Journal of Structural Geology*, 22, 603–625.

Ketcham, R. A. (1996), Thermal models of core-complex evolution in Arizona and New Guinea: Implications for ancient cooling paths and present-day heat flow, *Tectonics*, 15(5), 933-951

Ketcham, R. A., R. A. Donelick, and W. D. Carlson (1999), Variability of apatite fission-track annealing kinetics: III. Extrapolation to geological time scales, *American Mineralogist*, 84, 1235-1255.

Ketcham, R. A. (2003), Observations on the relationship between crystallographic orientation and biasing in apatite fission-track measurements, *American Mineralogist*, 88 (5-6), 817-829.

Ketcham, R. A. (2005), Forward and inverse modeling of low-temperature thermochronometry data, *Reviews in Mineralogy and Geochemistry*, 58 (1), 275-314.

Ketcham, R. A., A. Carter, R. A. Donelick, J. Barbarand, and A. J. Hurford (2007a), Improved measurement of fission-track annealing in apatite using c-axis projection, *American Mineralogist*, 92 (5-6), 789-798.

Ketcham, R. A., A. Carter, R. A. Donelick, J. Barbarand, and A. J. Hurford (2007b), Improved modeling of fission-track annealing in apatite, *American Mineralogist*, 92(5-6), 799-810.

Kruckenberg, S. C., and D.L. Whitney (2011), Metamorphic evolution of sapphirine-and orthoamphibole-cordierite-bearing gneiss, Okanogan dome, Washington, USA, *Journal of Metamorphic Geology*, 29(4), 425-449.

Kruckenberg, S.C., D.L. Whitney, C. Teyssier, M. Fanning, and W.J. Dunlap (2008), Paleocene-Eocene migmatite crystallization, extension, and exhumation in the hinterland of the northern Cordillera: Okanogan dome, Washington USA, *Geological Society of America Bulletin*, 120(7-8), 912-929.

Kruse, S., and P. F. Williams (2005), Brittle faulting in the Thor Odin culmination, Monashee complex, southern Canadian Cordillera: constraints on geometry and kinematics. *Canadian Journal of Earth Sciences*, 42(12), 2141-2160.

Lisiecki, L. E., and M. E. Raymo (2005), A Pliocene-Pleistocene stack of 57 globally distributed benthic d18O records, *Paleoceanography*, 20, PA1003, doi:10.1029/2004PA001071.

Little, T. A., B. R. Hacker, S. M. Gordon, S. L. Baldwin, P. G. Fitzgerald, S. Ellis, M. Korchinski (2011), Diapiric exhumation of Earth's youngest (UHP) eclogites in the gneiss domes of the D'Entrecasteaux Islands, Papua New Guinea, *Tectonophysics*, 510(1), 39-68.

Lorencak, M., D. Seward, O. Vanderhaeghe, C. Teyssier, and J.P. Burg (2001), Low-temperature cooling history of the Shuswap metamorphic core complex, British Columbia: Constraints from apatite and zircon fission-track ages, *Canadian Journal of Earth Sciences*, 38, 1615-1625.

Marshall, D., and G. Simandl (2006), Phase relations and metamorphism in the sapphirine bearing granulites of the Valhalla complex, Slocan Valley, BC, *GAC/MAC Annual Meeting*, 31, 96.

Mathews, W.H. (1981), Early Cenozoic resetting of potassium-argon dates and geothermal history of north Okanagan area, British Columbia, *Canadian Journal of Earth Sciences*, v. 18, p. 1310–1319.

McFadden, R. R., C. Teyssier, C. S. Siddoway, D. L. Whitney, and C. M. Fanning (2010), Oblique dilation, melt transfer, and gneiss dome emplacement, Geology, 38(4), 375-378.

McKenzie, D., F. Nimmo, J.A. Jackson, P.B. Gans, and E.L. Miller (2000), Characteristics and consequences of flow in the lower crust, *Journal of Geophysical Research*, B, Solid Earth and Planets, v. 105, p. 11029-11046.

Meesters, A. G. C. A., and T. J. Dunai (2002), Solving the production–diffusion equation for finite diffusion domains of various shapes: Part I. Implications for low-temperature (U-Th)/He thermochronology, *Chemical Geology*, 186(3), 333-344.

Mudelsee, M., and M. E. Raymo (2005), Slow dynamics of the Northern Hemisphere glaciation, *Paleoceanography*, 20(4).

Mulch, A., C. Teyssier, M. A. Cosca, T. W. Vennemann (2006), Thermomechanical analysis of strain localization in a ductile detachment zone, *Journal of Geophysical Research: Solid Earth*, (1978–2012), 111(B12).

Norlander, B.H., D.L. Whitney, C. Teyssier, O. Vanderhaeghe, and R.A. Wiebe (2002), Partial melting and decompression of the Thor-Odin Dome, Shuswap metamorphic core complex, Canadian Cordillera, *Lithos*, v. 61, p. 103-125.

Nyman, M.W., D.R.M. Pattison, and E.D. Ghent (1995), Melt extraction during formation of K-feldspar-sillimanite migmatites, west of Revelstoke, British Columbia, *Journal of Petrology*, 36, 351-372.

Olen, S. M., T. A. Ehlers, and M. S. Densmore (2012), Limits to reconstructing paleotopography from thermochronometer data, *Journal of Geophysical Research: Earth Surface*, (2003–2012), 117(F1).

Parkinson, D.L. (1991), Age and isotopic character of Early Proterozoic basement gneisses in the southern Monashee Complex, southeastern British Columbia, *Canadian Journal of Earth Sciences*, 28, 1159-1168.

Parkinson, D.L. (1992), Age and tectonic evolution of the southern Monashee complex, southeastern British Columbia: A window into the deep crust, *Ph.D. thesis*, Univ. of California, Santa Barbara.

Parrish, R.R. (1995), Thermal evolution of the southeastern Canadian Cordillera, *Canadian Journal of Earth Sciences*, 32, 1618-1642.

Parrish, R.R., and J.O.Wheeler (1983), An U-Pb zircon age for the Kuskanax batholith, southeast British Columbia, *Canadian Journal of Earth Sciences*, 20, 1751-1756.

Parrish, R.R., S.D. Carr, and D.L. Parkinson (1988), Eocene extensional tectonics and geochronology of the southern Omineca belt, British Colombia and Washington, *Tectonics*, v. 7, p. 181-212.

Reiners, P. W., and K. A. Farley (2001), Influence of crystal size on apatite (U–Th)/He thermochronology: an example from the Bighorn Mountains, Wyoming, *Earth and Planetary Science Letters*, 188(3), 413-420.

Reiners, P. W., Z. Zhou, T. A. Ehlers, C. Xu, M. T. Brandon, R. A. Donelick, and S. Nicolescu (2003), Post-orogenic evolution of the Dabie Shan, eastern China, from (U-Th)/He and fission-track dating, *American Journal of Science*, 303, 489 – 518.

Reiners, P.W., T.L. Spell, S. Nicolescu, and K.A. Zanetti (2004), Zircon (U-Th)/He thermochronometry: He diffusion and comparison with Ar/Ar dating, *Geochimica et Cosmochimica Acta*, 68, 1857-1887.

Reiners, P.W. (2005), Zircon (U-Th)/He thermochronometry, *Reviews in Mineralogy and Geochemistry*, v. 58, 151-179.

Rey, P., C. Teyssier, and D.L. Whitney (2009a), Extension rates, crustal melting and core complex dynamics, *Geology*, 37, 391– 394.

Rey, P.F., C. Teyssier, and D.L. Whitney (2009b), The Role of Partial Melting and Extensional Strain Rates in the Development of Metamorphic Core Complexes, *Tectonophysics*, v. 477, p. 135–144.

Rey, P. F., C. Teyssier, and D. L. Whitney (2010), Limit of channel flow in orogenic plateaux. *Lithosphere*, 2(5), 328-332.

Rey, P.F., C. Teyssier, S.C. Kruckenberg, and D.L. Whitney (2011), Viscous collision in channel explains double domes in metamorphic core complexes, *Geology*, 39, 4, 387-390

Robinson, A. C., A. Yin, C. E. Manning, T. M. Harrison, S. H. Zhang, and X. F. Wang (2007), Cenozoic evolution of the eastern Pamir: Implications for strain-accommodation mechanisms at the western end of the Himalayan-Tibetan orogen, *Geological Society of America Bulletin*, 119(7–8), 882–896.

Sevigny, J.H., R.R. Parrish, and E.D. Ghent (1989), Petrogenesis of peraluminous granites, Monashee Mountains, southeastern Canadian Cordillera, *Journal of Petrology*, 30, 557- 581.

Shuster, D. L., R. M. Flowers, and K. A. Farley (2006), The influence of natural radiation damage on helium diffusion kinetics in apatite, *Earth and Planetary Science Letters*, 249(3), 148-161.

Spalla, M. I., D. Zanoni, P. F. Williams, G. Gosso (2011), Deciphering cryptic P–Td–t histories in the western Thor-Odin dome, Monashee Mountains, Canadian Cordillera: A key to unravelling pre-Cordilleran tectonic signatures, *Journal of Structural Geology*, 33(3), 399-421.

Spiegel, C., B. Kohn, D. Belton, Z. Berner, and A. Gleadow (2009), Apatite (U–Th–Sm)/He thermochronology of rapidly cooled samples: the effect of He implantation, *Earth and Planetary Science Letters*, 285(1), 105-114.

Stockli, D.F. (2005), Application of low-temperature thermochronometry to extensional tectonic settings, *Reviews in Mineralogy and Geochemistry*, vol. 58, p. 420-461.

Stübner, K., L. Ratschbacher, C. Weise, J. Chow, J. Hoffman, J. Khan, D. Rutte, B. Sperner, J.A. Pfander, B.R. Hacker, I. Dunkl, M. Tichomirowa, M.A. Stearns, I. Bahram, M. Gadoev, R. Gloaguen, R. Jonckheere, E. Kanaev, V. Minaev, I. Oimahmadoc, N. Rajabov, K.P. Stanek (2013), The giant Shakhdara migmatitic gneiss dome, Pamir, India–Asia collision zone, II: Timing of dome formation, *Tectonics*, DOI: 10.1002/tect.20059, in press

Stüwe, K., L. White & R. Brown, (1994), The influence of eroding topography on steady-state isotherms. Application to fission track analysis, *Earth and Planetary Science Letters*, 124(1), 63-74.

Teyssier, C., and D.L. Whitney (2002), Gneiss domes and orogeny, *Geology*, v. 30, p. 1139- 1142.

Teyssier, C., E.C. Ferré, D.L. Whitney, B. Norlander, O. Vanderhaeghe, and D. Parkinson (2005), Flow of partially molten crust and origin of detachments during collapse of the Cordilleran orogen, in *High-strain zones: Structure and physical properties*, edited by D. Bruhn and L. Burlini, pp. 39-64, Geological Society of London Special Publications, vol. 245.

Thiede, R. C., J. R. Arrowsmith, B. Bookhagen, M. McWilliams, E. R. Sobel, and M. R. Strecker (2006), Dome formation and extension in the Tethyan Himalaya, Leo Pargil, northwest India, *Geological Society of America Bulletin*, 118(5-6), 635-650.

Thomson, S.N., and U. Ring (2006), Thermochronologic evaluation of post-collision extension in the Anatolide orogen, western Turkey, *Tectonics*, 25, TC3005, doi:10.1029/2005TC001833

Thomson, S.N., U. Ring, S. Brichau, J. Glodny, and T.M. Will (2009), Timing and nature of formation of the Ios metamorphic core complex, southern Cyclades, Greece, in *Extending a Continent: Architecture, Rheology and Heat Budget*, edited by U. Ring, and B. Wernicke, p. 139–167, Geological Society of London Special Publication, 321.

Tirel, C., J.P. Brun, and E. Burov (2004), Thermomechanical modeling of extensional gneiss domes, in *Gneiss domes in orogeny,* edited by D.L. Whitney et al., p. 67–78, Geological Society of America Special Paper, 380.

Vanderhaeghe, O., and C. Teyssier (1997), Formation of the Shuswap metamorphic complex during late-orogenic collapse of the Canadian Cordillera: role of ductile thinning and partial melting of the mid- to lower crust, *Geodinamica Acta*, 10, 41-58.

Vanderhaeghe, O., C. Teyssier, and R. Wysoczanski (1999), Structural and geochronological constraints on the role of partial melting during the formation of the Shuswap metamorphic core complex at the latitude of the Thor-Odin Dome, British Columbia, *Canadian Journal of Earth Sciences*, v. 36, p. 917-943.

Vanderhaeghe, O., and C. Teyssier (2001), Crustal scale rheological transitions during late-orogenic collapse, *Tectonophysics*, 335, 211-228.

Vanderhaeghe, O., C. Teyssier, I. McDougall and, and W.J Dunlap (2003), Cooling and exhumation of the Shuswap metamorphic core complex constrained by Ar/Ar thermochronology, *Geological Society of America Bulletin*, v 115, p. 200-216.

Wells, M.L., L.W. Snee, and A.E. Blythe (2000), Dating of major normal fault systems using thermochronology: An example from the Raft River detachment, Basin and Range, western United States, *Journal of Geophysical Research*, 105, 16303-16327.

Whitney, D.L., S.R. Paterson, K.L. Schmidt, A.F. Glazner, and C.F. Kopf (2004), Growth and demise of continental arcs and orogenic plateaux in the North American Cordillera: from Baja to British Columbia, in *Vertical Coupling and Decoupling in*

the Lithosphere, edited by J. Grocott, K.J.W. McCaffrey, G. Taylor and B. Tikoff, pp. 167-176, Geological Society of London Special Publications, vol. 227.

Whitney, D. L., C. Teyssier, P. Rey, and W. R. Buck (2013), Continental and oceanic core complexes, *Geological Society of America Bulletin*, 125(3-4), 273-298.

Wolf, R. A., K. A. Farley, and D. M. Kass (1998), Modeling of the temperature sensitivity of the apatite (U–Th)/He thermochronometer, *Chemical Geology*, 148(1), 105-114.

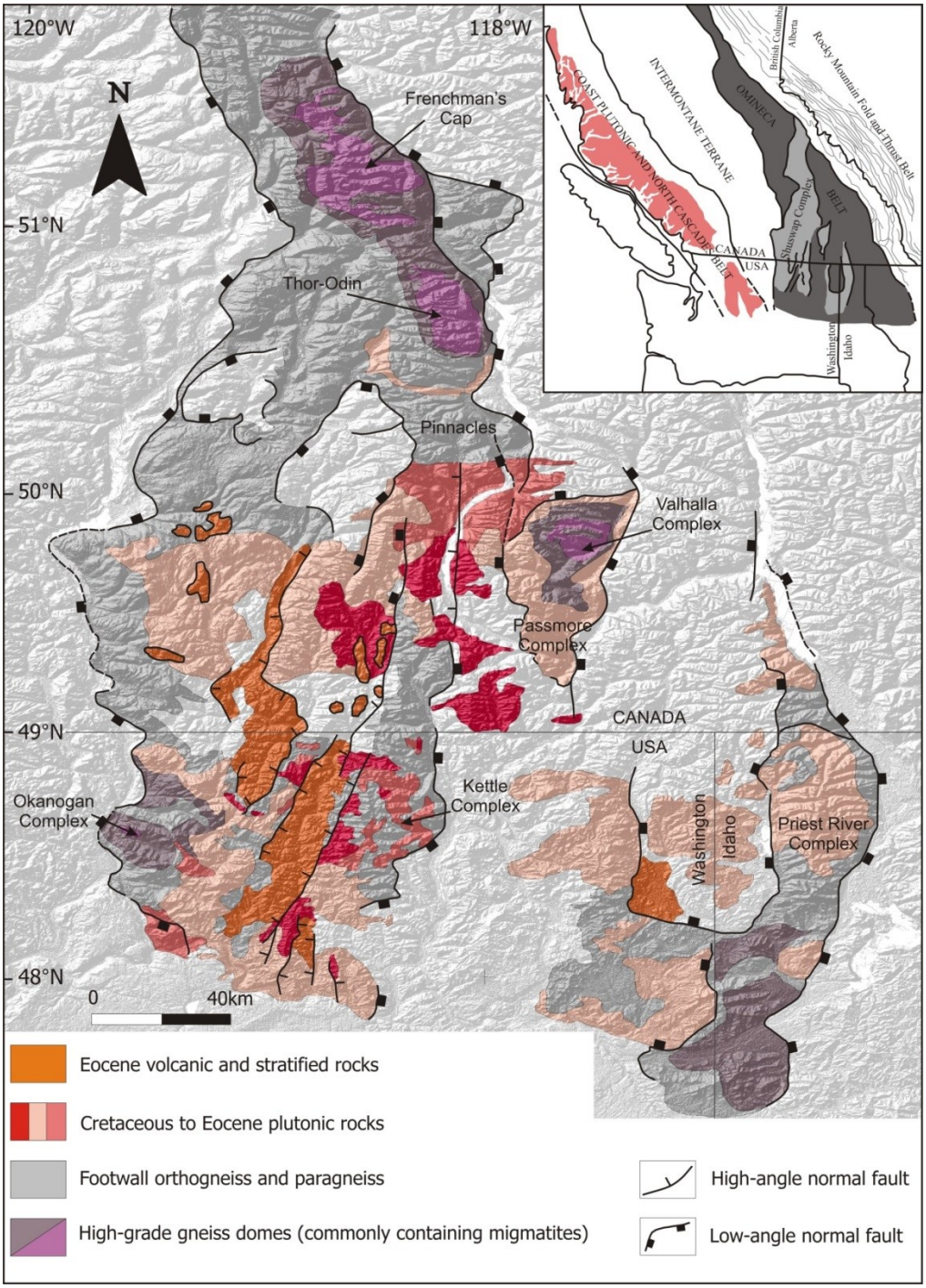

Figure 2.1 Simplified geologic map of the Omineca Belt [after Kruckenberg et al., 2008]. Inset shows the location of the Omineca Belt and major tectonic belts of the northern North American Cordillera.

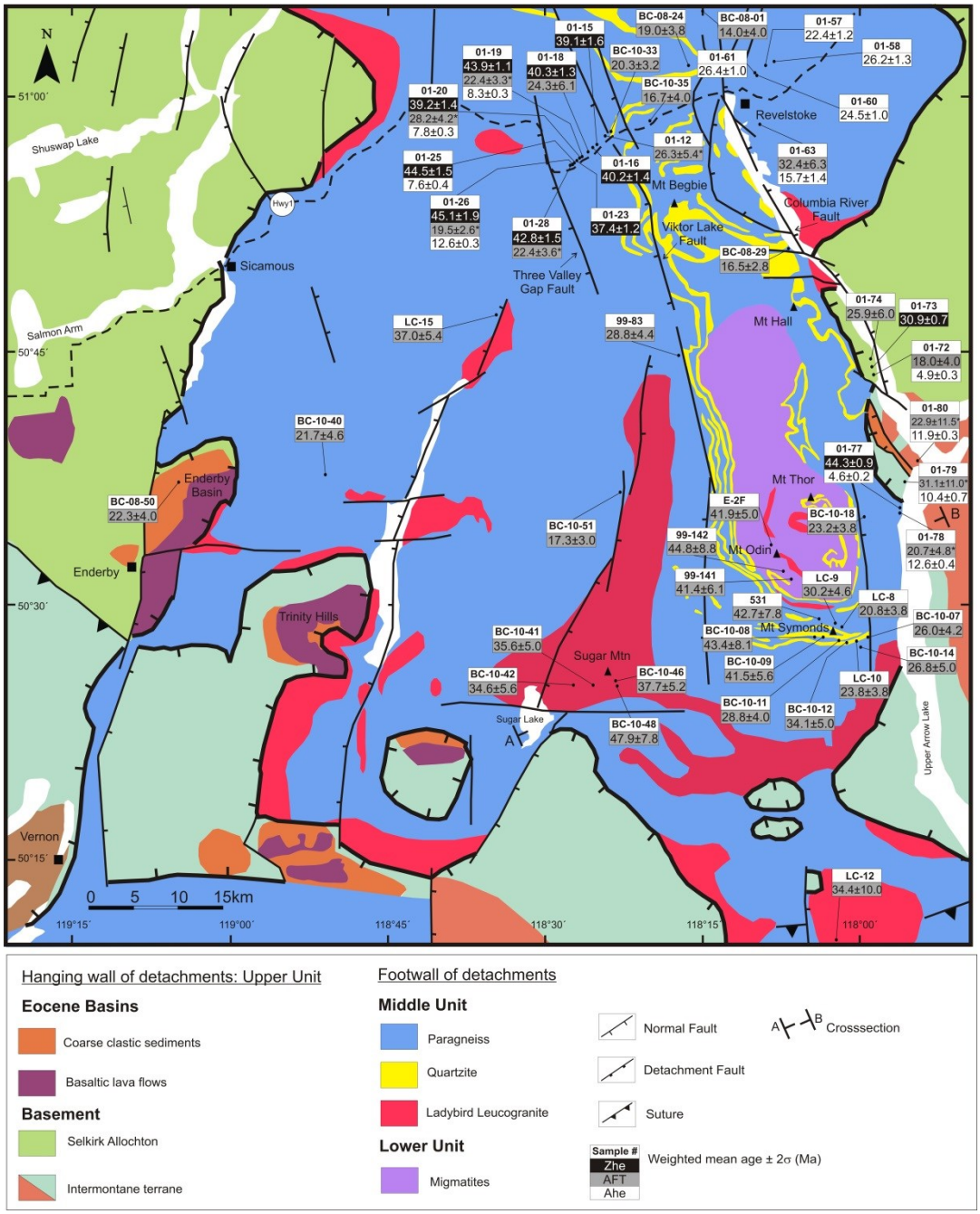

Figure 2.2 Simplified geologic map of the Thor-Odin dome [modified after Vanderhaeghe et al., 2003] showing main lithological units, structures, sample locations, and apatite fission track and apatite/zircon (U-Th)/He results. AFT ages with asterisks (*) are after Fayon et al. [2004a].

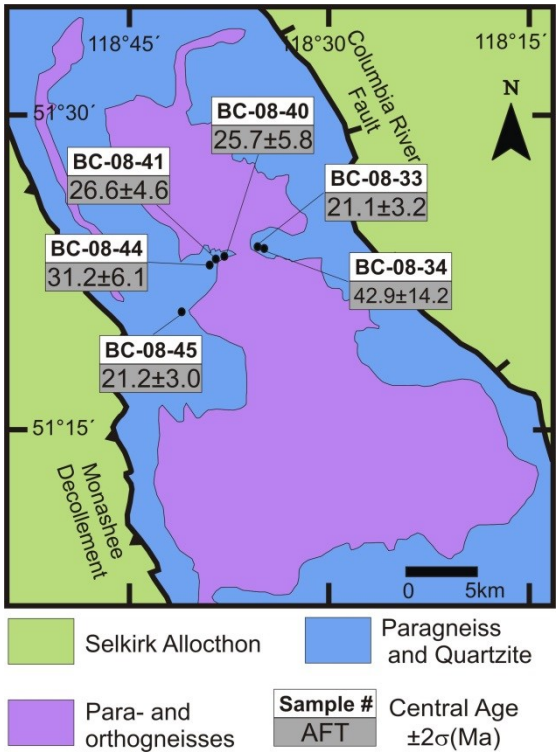

Figure 2.3 Simplified geologic map of the Frenchman's Cap Dome [modified after Gervais et al., 2010]. Map shows main lithological units and structures, sample locations, and apatite fission track results.

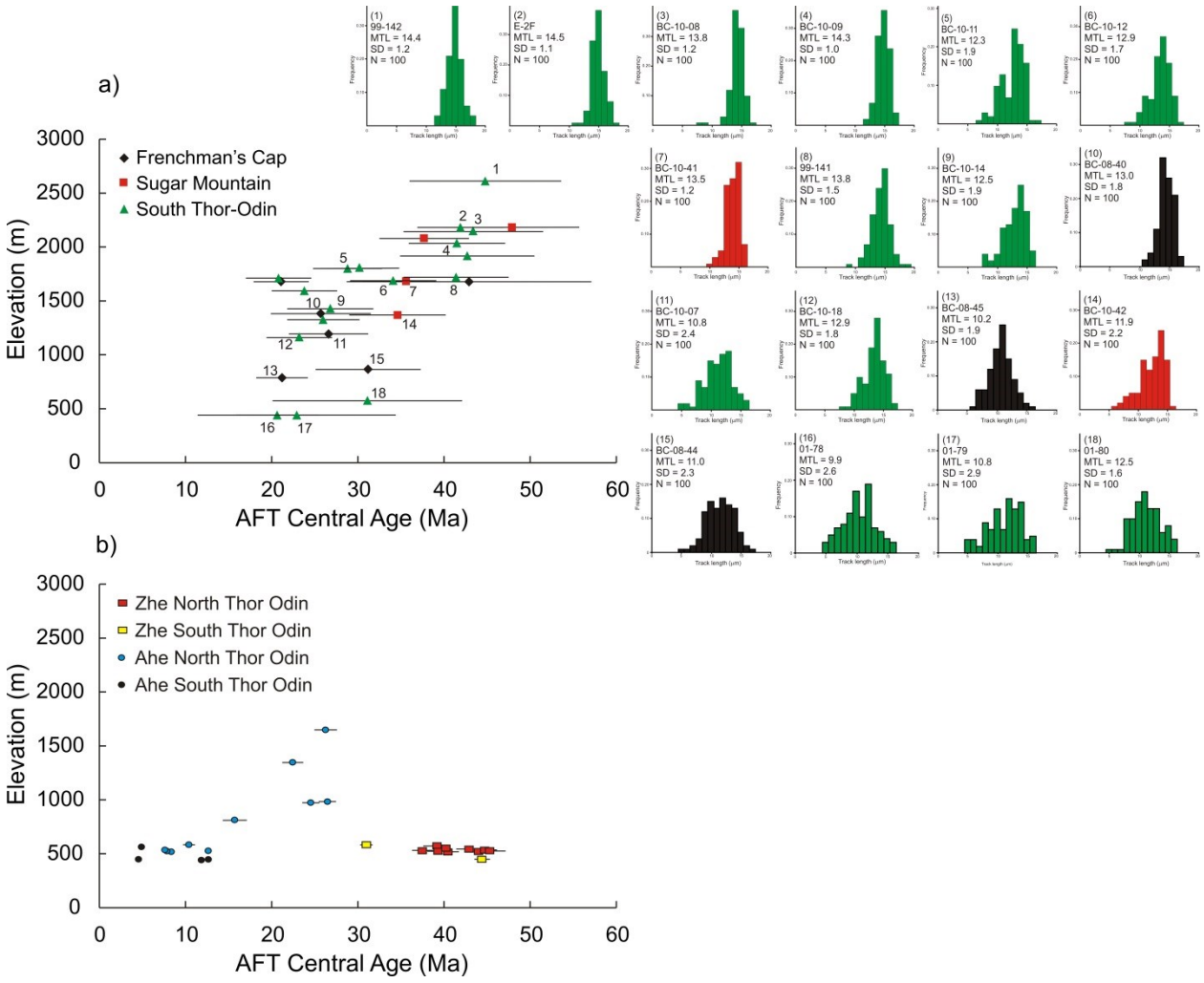

Figure 2.4 a) AFT Central Age-elevation profiles for the northern Shuswap MCC, including the confined track-length distributions. Samples from the Frenchman's Cap dome labeled as diamonds, whereas squares (Sugar Mountain) and triangles (Thor-Odin) represent the Thor-Odin dome samples. Numbers refer to corresponding track-length distribution of that sample. MTL, Mean track length; SD, standard deviation; N, number of tracks. b) AHe and ZHe age-elevation profiles for the Thor-Odin dome.

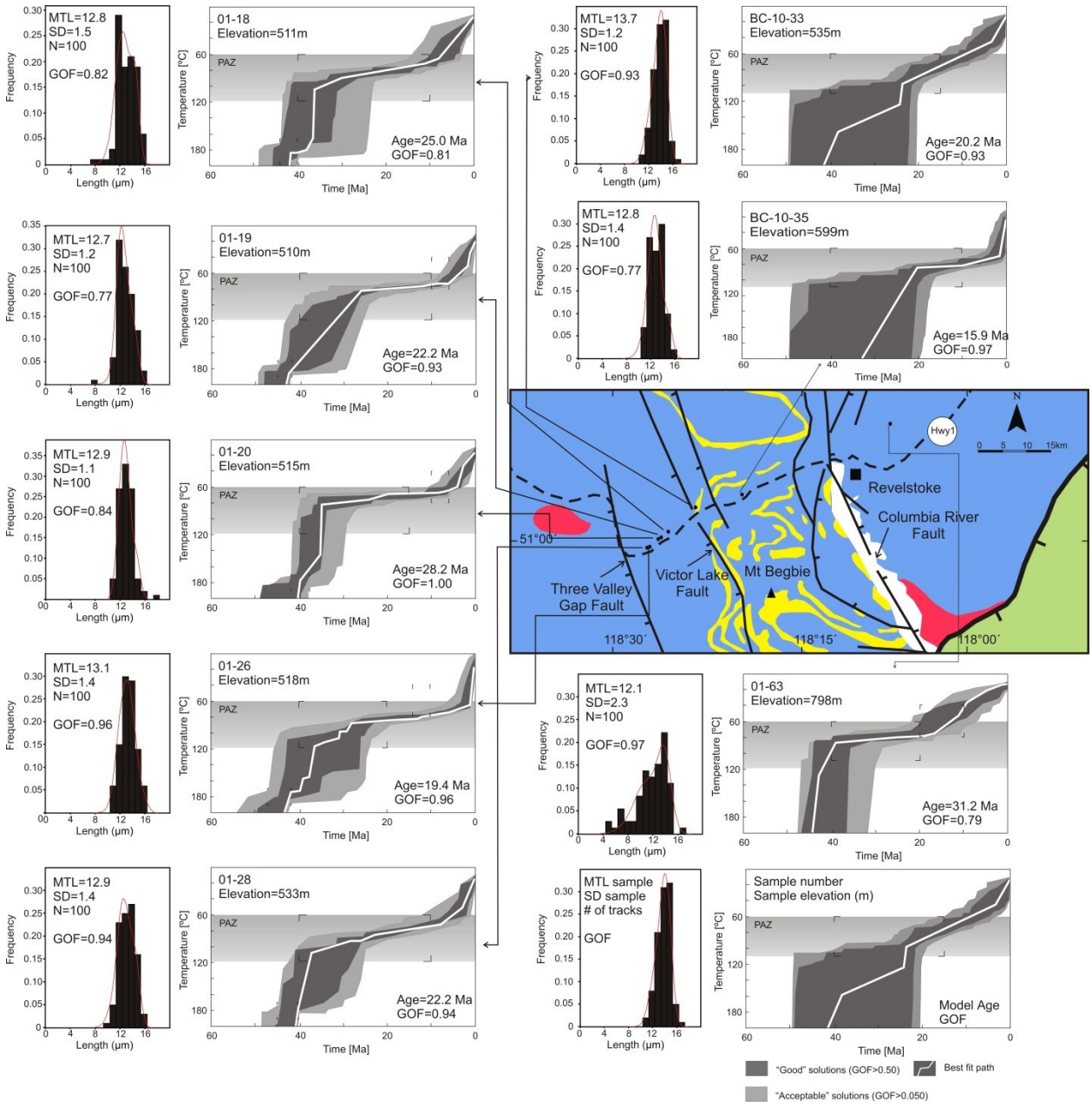

Figure 2.5 Results of HeFTy modeling for samples collected in the Revelstoke area and along Highway 1. Legend for modeling is shown in lower right. Note that length measurements reported in Figures 2.5-2.9 are projected parallel to the c-axis and differ from the mean track-lengths and standard deviations reported in text and Tables 2.1 and 2.3. GOF, goodness of fit; MTL, Mean track length; SD, standard deviation.

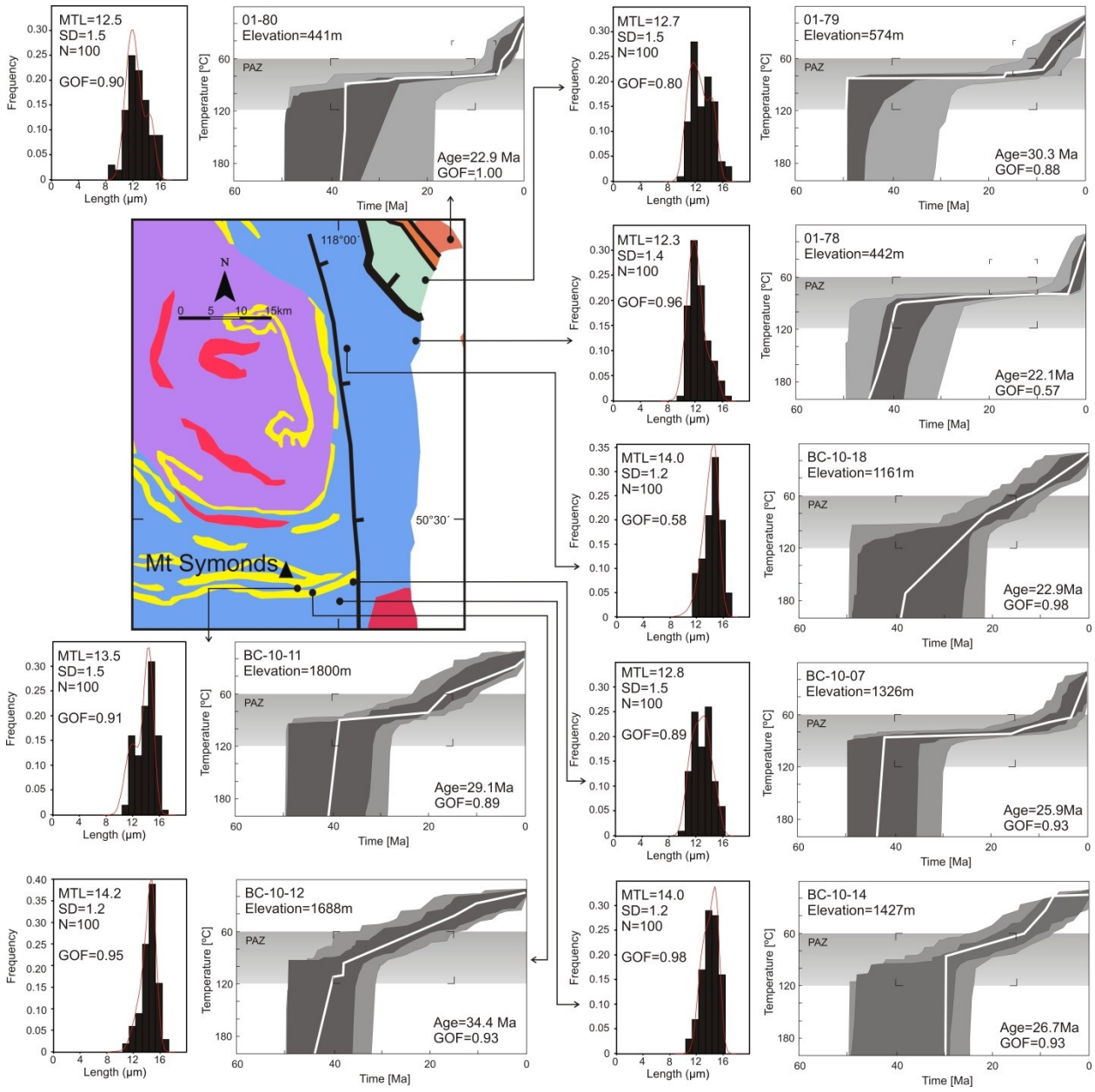

Figure 2.6 HeFTy modeling results with corresponding c-axis corrected track length distributions for the Thor-Odin dome. (Same legend as Figure 2.5)

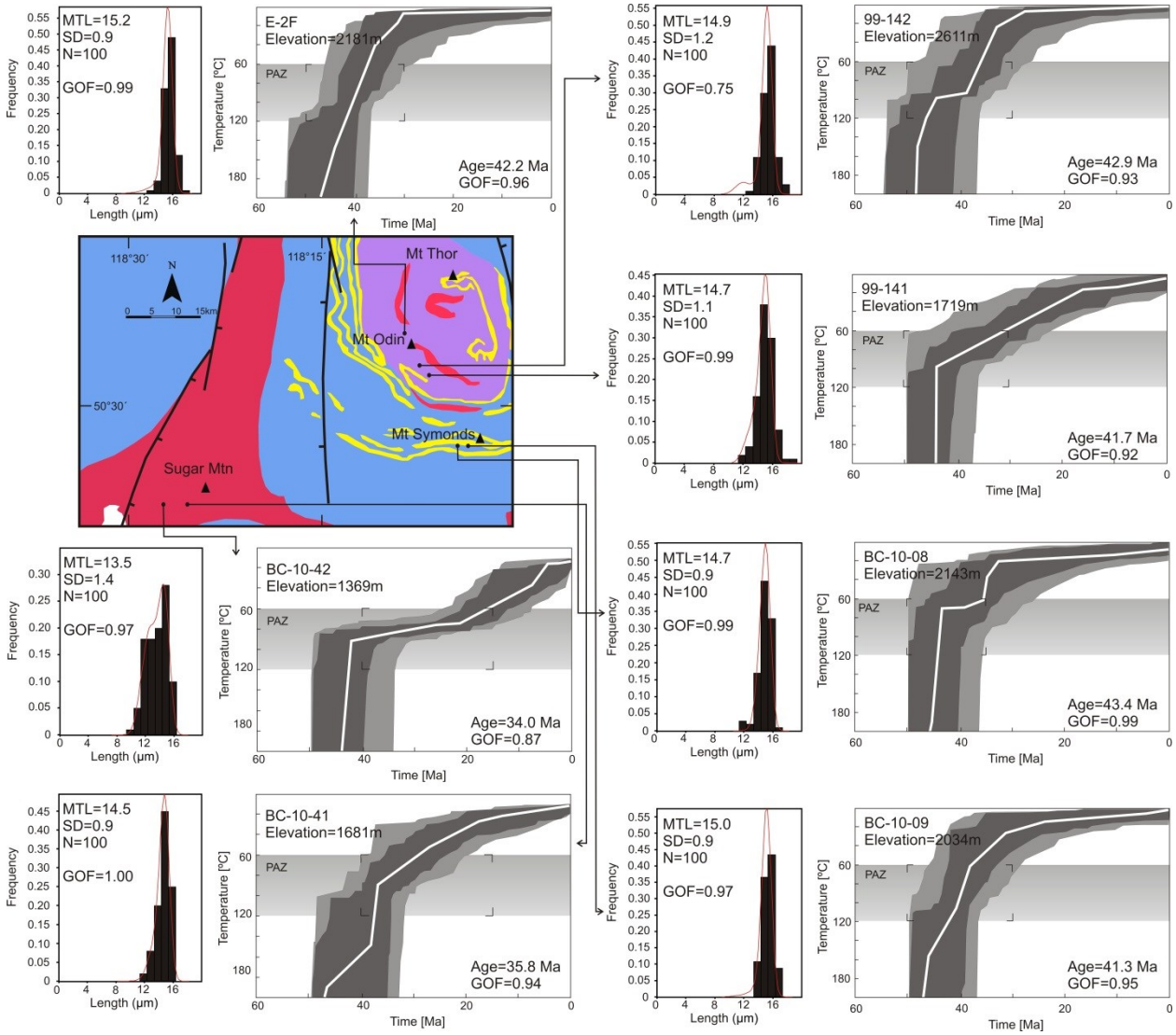

Figure 2.7 HeFTy modeling results with corresponding c-axis corrected track length distributions for the Mt Symonds and Sugar Mountain. (Same legend as Figure 2.5)

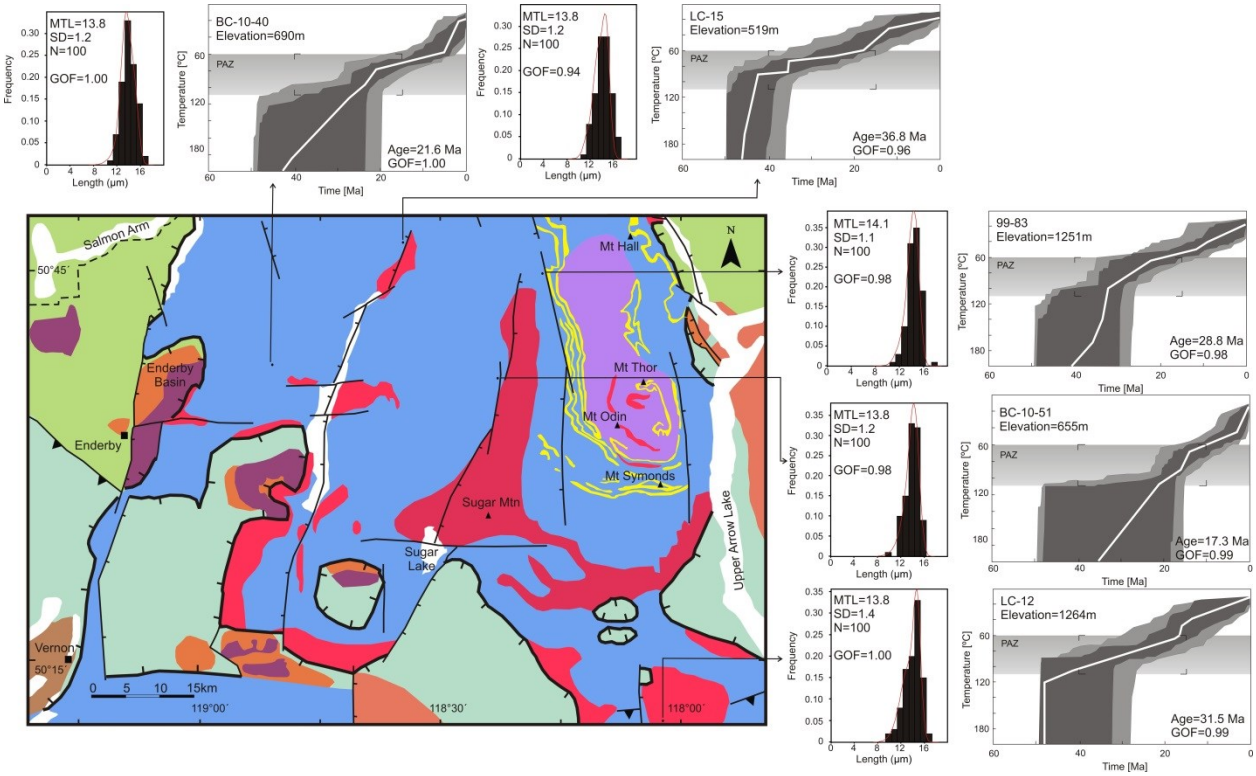

Figure 2.8 HeFTy modeling results with corresponding c-axis corrected track length distributions for the isolated samples from the Thor-Odin dome. (Same legend as Figure 2.5)

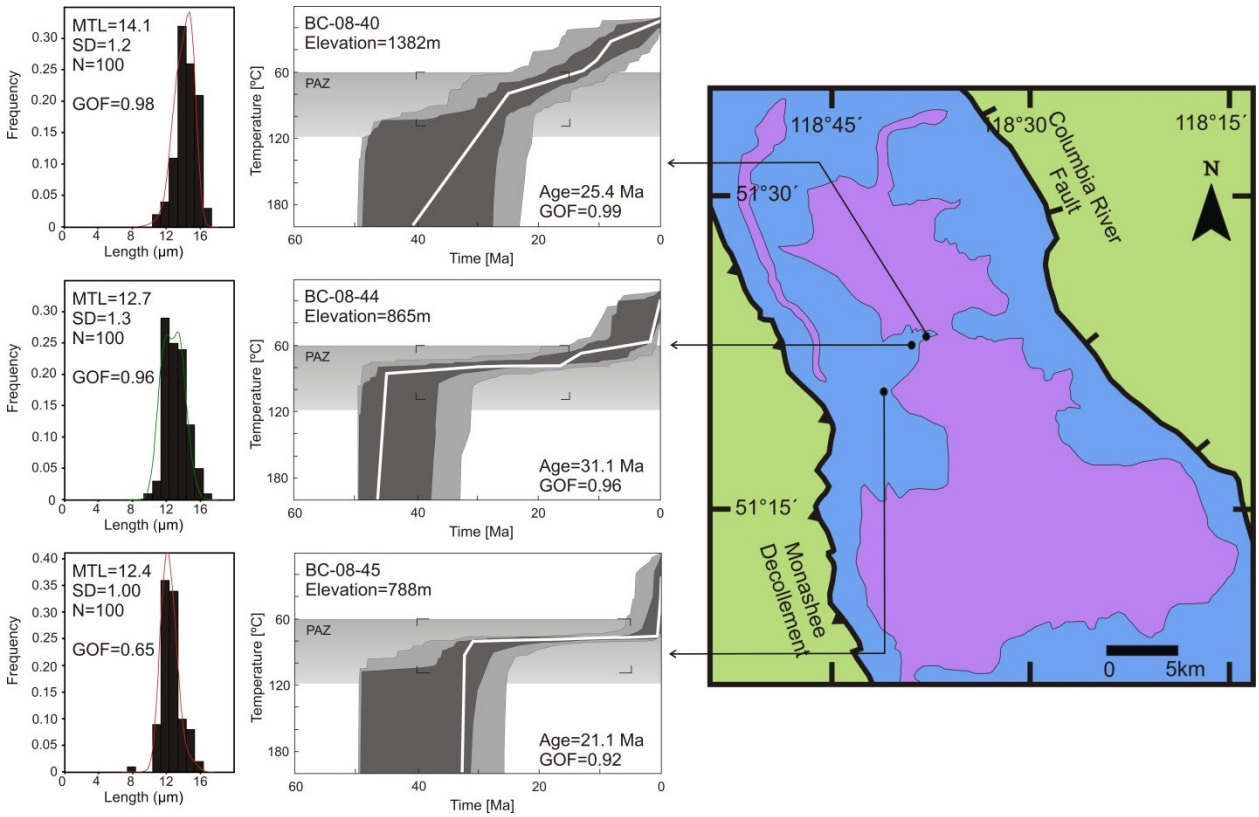

Figure 2.9 HeFTy modeling results with corresponding c-axis corrected track length distributions for the Frenchman's Cap dome. (Same legend as Figure 2.5)

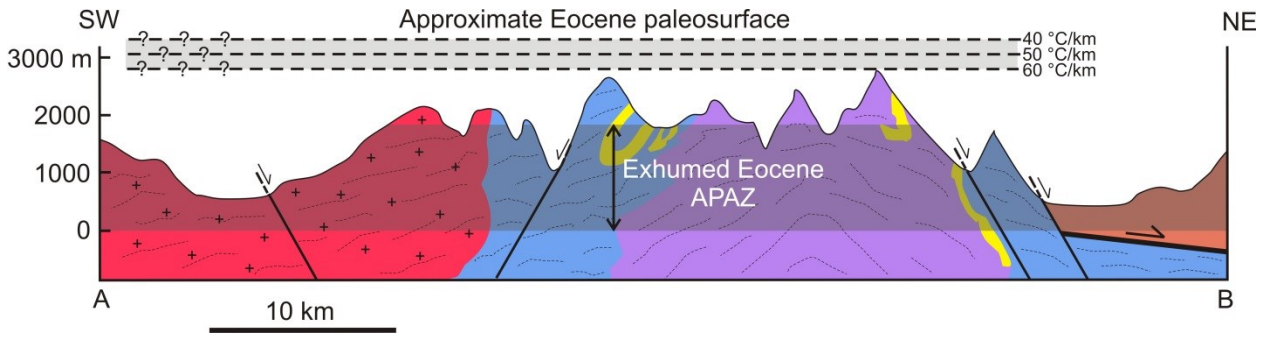

Figure 2.10 Simplified geological cross-section across the Shuswap MCC at the latitude of the Thor-Odin done, showing exhumed Eocene APAZ, and approximate location of Eocene paleosurface for different paleo-geothermal gradient estimations. Although the bottom of the APAZ is not represented in our data, its location should be lower than the lowest elevation sample (441 m) collected.

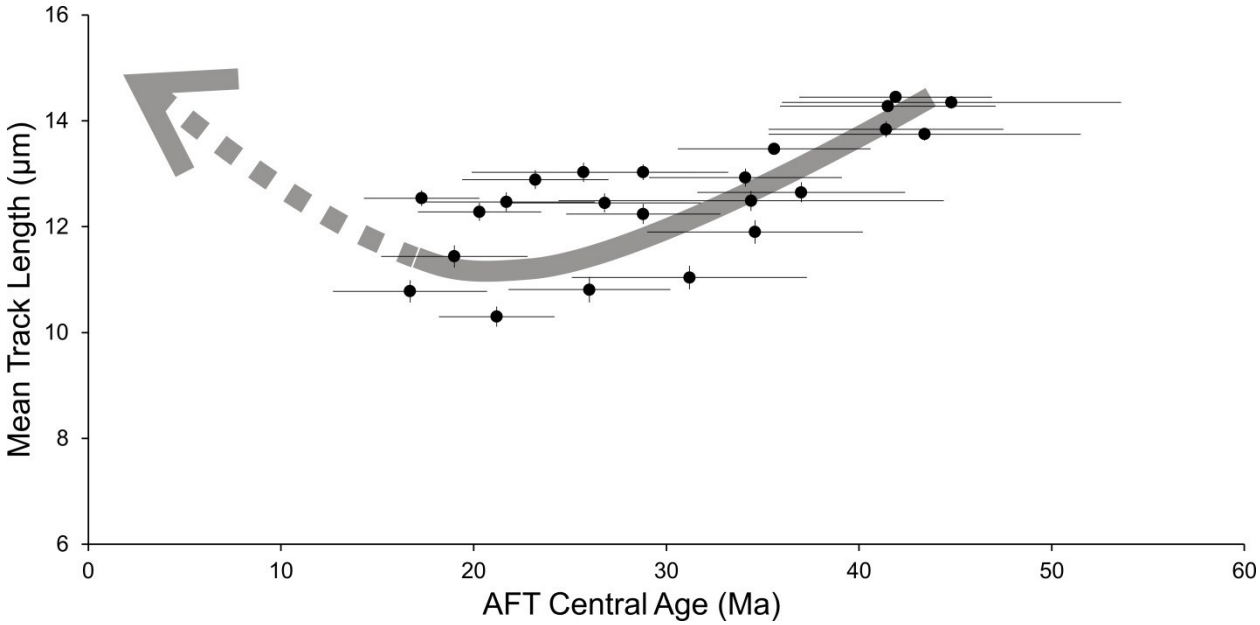

Figure 2.11 Plot of mean track lengths versus AFT central age (boomerang plot) for the northern Shuswap MCC. This partially-developed boomerang plot indicates an Eocene cooling event, recorded by long (≥14 µm) tracks, and a second cooling event, which is younger than ca. 14 Ma. See text for detailed discussion.

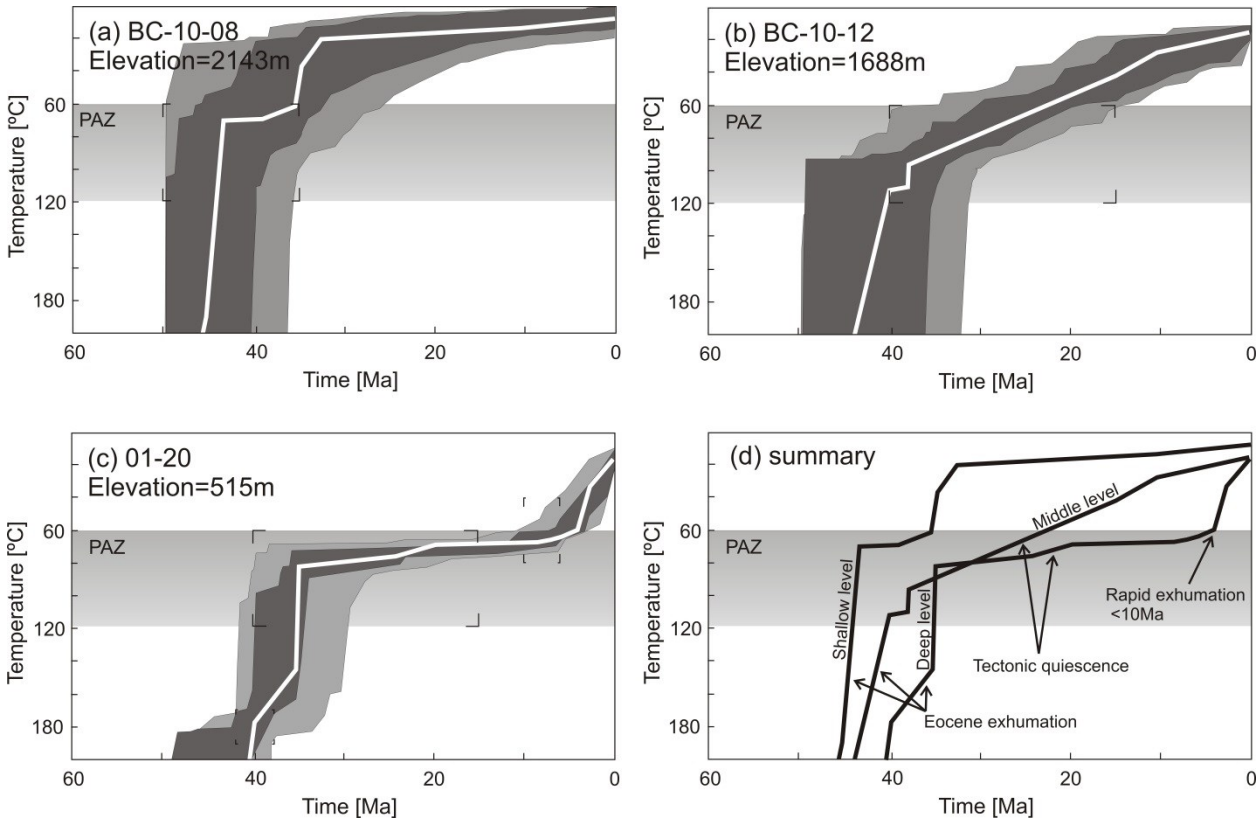

Figure 2.12 Apatite fission track modeling results from representative samples from different structural depths showing multistage cooling and exhumation history of the northern Shuswap MCC. (a) Model results indicate that higher elevation rocks only record rapid Eocene cooling that followed emplacement of the dome. (b) Modeling results of samples from intermediate elevation document that these rocks spend significant time within the partial annealing zone. (c) Modeling of the lowest elevation samples indicates post-Miocene cooling. (d) Summary diagram showing a simplified illustration of thermal history of different structural levels of this part of the Shuswap MCC.

Table 2.1 Summary of low-temperature thermochronology results. AFT ages with asterisks (*) are after Fayon et al. [2004].

Sample Name	AHe Age ± 2σ (Ma)	AFT Age ± 2σ (Ma)	ZHe Age ± 2σ (Ma)	AFT Track Length±SD (µm)
01-12		26.3±5.4*		
01-15			39.1±1.6	
01-16			40.2±1.4	
01-18		24.3±6.1	40.3±1.3	10.95±2.43
01-19	8.3±0.3	22.4±3.3*	43.9±1.1	10.69±2.04
01-20	7.8±0.3	28.2±4.2*	39.2±1.4	10.74±2.05
01-23			37.4±1.2	
01-25	7.6±0.4		44.5±1.5	
01-26	12.6±0.3	19.5±2.6*	45.1±1.9	11.24±2.00
01-28		22.4±3.6*	42.8±1.5	11.34±1.89
01-57	22.4±1.2			
01-58	26.2±1.3			
01-60	24.5±1.0			
01-61	26.4±1.0			
01-63	15.7±1.4	32.4±6.3		11.51±2.63
01-72	4.9±0.3	18.0±4.0		
01-73			30.9±0.7	
01-74		25.9±6.0		
01-77	4.6±0.2		44.3±0.9	
01-78	12.6±0.4	20.7±4.8*		9.97±2.62
01-79	10.4±0.7	31.1±11.0*		10.76±2.85
01-80	11.9±0.3	22.9±11.5*		10.80±2.32
99-141		41.4±6.1		13.84±1.52
99-142		44.8±8.8		14.35±1.23
99-83		28.8±4.4		13.03±1.50
531		42.7±7.8		
E-2F		41.9±5.0		14.45±1.11
LC-10		23.8±3.8		
LC-12		34.4±10.0		12.49±1.98
LC-15		37.0±5.4		12.65±1.91
LC-8		20.8±3.8		
LC-9		30.2±4.6		
BC-08-01		14.0±4.0		
BC-08-24		19.0±3.8		11.44±2.05
BC-08-29		16.5±2.8		

Table 2.1. (continued)

Sample Name	AHe Age ± 2σ (Ma)	AFT Age ± 2σ (Ma)	ZHe Age ± 2σ (Ma)	AFT Track Length±SD (µm)
BC-08-33		21.1±3.2		
BC-08-34		42.9±14.2		
BC-08-40		25.7±5.8		13.03±1.81
BC-08-41		26.6±4.6		
BC-08-44		31.2±6.1		11.04±2.25
BC-08-45		21.2±3.0		10.30±1.95
BC-08-50		22.3±4.0		
BC-10-07		26.0±4.2		10.81±2.36
BC-10-08		43.4±8.1		13.75±1.24
BC-10-09		41.5±5.6		14.28±1.04
BC-10-11		28.8±4.0		12.24±1.99
BC-10-12		34.1±5.0		12.93±1.72
BC-10-14		26.8±5.0		12.45±1.89
BC-10-18		23.2±3.8		12.89±1.83
BC-10-33		20.3±3.2		12.28±1.72
BC-10-35		16.7±4.0		10.78±2.07
BC-10-40		21.7±4.6		12.47±1.85
BC-10-41		35.6±5.0		13.47±1.18
BC-10-42		34.6±5.6		11.90±2.17
BC-10-46		37.7±5.2		
BC-10-48		47.9±7.8		
BC-10-51		17.3±3.0		12.54±1.55

Table 2.2. Single grain zircon (U-Th)/He replicate data. Mwar, the mass-weighted average radius; Ft, geometrical correction for alpha ejection; eU, effective uranium [*Flowers et al*, 2007].

Sample Number	Mass (μg)	mwar (μm)	U (ppm)	Th (ppm)	He (nmol/g)	Raw Age (Ma)	Error (±1σ)	Corrected Age (Ma)	Error (±1σ)	HAC (Ft)	eU (ppm)
01-15Zr-1	2.49	34.8	700	134	118	30.1	0.9	42.2	1.2	0.71	732
01-15Zr-2	1.91	31.3	260	112	39.3	25.3	0.7	36.8	1.1	0.69	287
01-16Zr-1	5.03	42.3	319	53.1	54.1	30.2	0.9	39.4	1.2	0.77	331
01-16Zr-2	3.72	40.5	558	19.9	92.1	30.3	0.9	40.3	1.2	0.75	563
01-16Zr-3	4.02	51.3	1470	60.8	258	32.2	0.9	40.9	1.2	0.79	1484
01-18Zr-1	5.13	39.5	1282	473	241	31.9	0.9	42.2	1.2	0.76	1394
01-18Zr-2	6.64	44.0	424	276	84.6	32.0	0.9	41.2	0.8	0.78	489
01-18Zr-3	11.1	57.3	223	115	42.1	31.2	0.8	38.0	1.0	0.82	250
01-19Zr-1	24.5	87.0	214	614	73.2	37.7	0.8	43.4	0.9	0.87	358
01-19Zr-2	9.28	68.3	167	500	55.6	35.9	0.8	43.4	0.9	0.83	285
01-19Zr-3	13.3	75.8	157	406	52.1	37.9	0.8	44.8	1.0	0.85	253
01-20Zr-1	2.46	38.8	226	534	55.6	29.1	0.6	40.2	0.9	0.72	351
01-20Zr-2	0.31	16.0	552	94.0	53.9	17.4	0.5	37.5	1.1	0.46	574
01-23Zr-1	0.49	20.5	736	141	85.6	20.6	0.6	37.9	1.1	0.54	770
01-23Zr-2	1.13	32.3	499	101	69.4	24.6	0.7	36.2	1.0	0.68	523
01-23Zr-3	1.38	37.8	579	54.4	86.5	27.1	0.8	38.2	1.1	0.71	592
01-25Zr-1	1.55	30.0	1809	61.0	266	27.0	0.9	40.1	1.4	0.67	1823
01-25Zr-2	4.45	48.8	530	436	124	36.3	0.9	46.5	1.2	0.78	633
01-25Zr-3	3.30	54.0	3703	244	726	35.7	1.1	45.9	1.4	0.78	3760
01-26Zr-1	7.73	57.0	1220	101	23	34.4	1.0	42.1	1.2	0.82	1244
01-26Zr-2	4.98	56.5	3313	67.3	714	39.7	1.2	49.5	1.5	0.80	3329
01-28Zr-1	29.9	69.3	548	63.2	130	42.7	1.3	49.7	1.4	0.86	563
01-28Zr-2	6.80	49.8	444	68.1	79.2	31.8	0.9	40.1	1.2	0.79	460
01-28Zr-3	6.51	43.8	438	25.0	75.9	31.7	0.9	40.6	1.2	0.78	443
01-73Zr-1	2.27	36.0	459	57.9	64.6	25.3	0.5	35.7	0.7	0.71	473
01-73Zr-2	2.75	36.5	575	21.3	85.2	27.2	0.6	37.6	0.8	0.72	580
01-73Zr-3	1.92	32.5	318	21.7	31.3	17.9	0.4	25.7	0.5	0.70	323
01-77Zr-1	35.6	82.0	476	98.8	111	41.1	0.7	47.1	0.8	0.87	499
01-77Zr-2	139	141	482	60.0	104	39.0	0.7	42.3	0.8	0.92	496
01-77Zr-3	81.2	103	393	65.5	87.5	39.6	0.8	43.9	0.8	0.90	408

Table 2.3. Apatite fission track data. AFT ages with asterisks (*) are after Fayon et al. [2004]. AFT ages are calculated using a zeta of 289 ± 11 for SRM 612 standard glass [Hurford and Green, 1983]; zeta value was calculated using a weighted mean average of 4 Fish Canyon tuff and 3 Durango age standards. ρ_d, density of induced tracks in the standard glass micas; N_d, total number of tracks in the standard glass; ρ_s, density of spontaneous tracks; N_s, number of spontaneous tracks; ρ_i, density of induced tracks; N_i, number of induced tracks; U, uranium content; P(χ2), chi-square probability [Green, 1981]; SE, standard error of mean track length; SD, standard deviation of mean track length measurements; DPAR, arithmetic mean fission track etch pit diameter parallel to the c-axis [Donelick et al., 2005]. Central ages [Galbraith and Laslett, 1993] were calculated using the Trackkey program [Dunkl, 2002].

Sample Number	Lat/Long	Elevation (m)	Number of Grains	Dosimeter Track Density (10^{-6} cm^{-2})			U (ppm)	P(χ^2) (%)	Central Age (Ma±2σ)	Mean Track Length, µm±SE (number of tracks)	SD (µm)	DPAR (µm)
				ρ_d (N_d)	ρ_s (N_s)	ρ_i (N_i)						
01-12*	50°57.360' -118°24.357'	572	8	2.092 (13215)	0.285 (106)	3.511 (1305)	16.6	45	26.3±5.4			
01-18	50°56.171' -118°26.193'	511	16	1.380 (8365)	0.098 (78)	0.832 (666)	20.8	63.1	24.3±6.1	10.95±0.24 (100)	2.43	2.2
01-19*	50°56.522' -118°26.280'	510	10	1.800 (12003)	0.807 (218)	9.520 (2571)	52.4	49.7	22.4±3.3	10.69±0.20 (100)	2.04	
01-20*	50°56.490' -118°27.359'	515	10	2.074 (13215)	0.940 (209)	10.150 (2257)	48.4	66.0	28.2±4.2	10.74±0.20 (100)	2.05	
01-26*	50°56.345' -118°27.660'	518	10	1.846 (12003)	0.795 (265)	11.640 (3882)	62.4	26.2	19.5±2.6	11.24±0.20 (100)	2.00	
01-28*	50°56.171' -118°26.193'	533	10	1.869 (12003)	0.545 (173)	7.040 (2237)	37.3	15.8	22.4±3.6	11.34±0.19 (100)	1.89	
01-63	50°55.798' -118°27.959'	798	20	1.320 (8365)	0.255 (138)	1.577 (853)	42.3	47.5	32.4±6.3	11.51±0.31 (100)	2.63	2.3
01-72	50°43.255' -118°0.475'	553	20	1.290 (8365)	0.095 (100)	1.023 (1079)	29.4	19.7	18.0±4.0			
01-74	50°43.255' -118°0.475'	510	21	1.270 (8365)	0.366 (233)	2.894 (1838)	86.2	52.5	25.9±6.0			
01-78*	50°34.558' -118°56.990'	441	7	1.892 (12003)	0.336 (80)	4.570 (1132)	24.9	53.4	20.7±4.8	9.97±0.26 (100)	2.62	
01-79*	50°36.539' -117°57.183'	574	8	2.007 (12003)	0.103 (37)	1.030 (369)	5.1	32.1	31.1±11.0	10.76±0.29 (100)	2.85	
01-80*	50°38.586' -117°56.384'	441	6	2.115 (9278)	0.107 (17)	1.530 (243)	7.2	95.6	22.9±11.5	10.80±0.23 (100)	2.32	
99-141	50°31.417 -118°09.249'	1719	13	1.480 (8145)	1.065 (305)	5.485 (1571)	125.3	43.1	41.4±6.1	13.84±0.15 (100)	1.52	2.6
99-142	50°32.640' -118°09.250'	2611	20	1.510 (4061)	0.546 (316)	2.685 (1555)	68.1	0.2	44.8±8.8	14.35±0.12 (100)	1.23	3.5
99-83	50°42.996' -118°18.001'	1251	20	1.460 (8145)	0.439 (254)	3.207 (1857)	80.2	64.4	28.8±4.4	13.03±0.15 (100)	1.50	2.7

Table 2.3. (continued)

Sample Number	Lat/Long	Elevation (m)	Number of Grains	Dosimeter Track Density (10^{-6} cm^{-2})			U (ppm)	P(χ^2) (%)	Central Age (Ma±2σ)	Mean Track Length, µm±SE (number of tracks)	SD (µm)	DPAR (µm)
				ρ_d (N_d)	ρ_s (N_s)	ρ_i (N_i)						
531	50°28.998' -118°05.832'	1916	11	1.570 (4061)	0.490 (183)	2.598 (970)	64.1	94.3	42.7±7.8			
E-2F	50°33.563' -118°09.618'	2181	20	1.390 (8145)	2.178 (664)	1.042 (3176)	271.3	66.4	41.9±5.0	14.45±0.11 (100)	1.11	2.74
LC-10	50°27.633' -118°02.635'	1594	20	1.410 (8145)	0.374 (248)	3.199 (2121)	69.3	3.8	23.8±3.8			
LC-12	50°00.633' -118°02.328'	1264	22	1.430 (8145)	0.092 (22)	0.603 (77)	14.4	10.2	34.4±10.0	12.49±0.19 (100)	1.98	1.80
LC-15	50°47.196' -118°34.362'	519	20	1.480 (4061)	0.573 (332)	3.307 (1915)	84.9	68.2	37.0±5.4	12.65±0.19 (100)	1.91	2.03
LC-8	50°28.165' -118°03.360'	1711	19	1.200 (8145)	0.185 (176)	1.540 (1463)	49.6	72.1	20.8±3.8			
LC-9	50°28.283' -118°03.616'	1803	20	1.170 (8145)	0.370 (300)	2.069 (1677)	55.6	79.2	30.2±4.6			
BC-08-01	51°13.245' -118°13.583	611	20	1.260 (8145)	0.067 (61)	0.866 (790)	24.6	81.8	14.0±4.0			
BC-08-24	51°01.166' -118°16.193'	966	20	1.500 (8145)	0.139 (122)	1.583 (1391)	37.6	72.5	19.0±3.8	11.44±0.21 (100)	2.05	3.8
BC-08-29	50°50.771' -118°06.762'	575	21	1.220 (8145)	0.234 (183)	2.556 (2000)	77.1	18.9	16.5±2.8			
BC-08-33	51°24.887' -118°34.624'	1678	21	1.370 (8145)	0.301 (279)	2.817 (2612)	85.1	79.2	21.1±3.2			
BC-08-34	51°24.887' -118°34.625'	1678	13	1.370 (8145)	0.124 (69)	0.589 (328)	9.9	14.5	42.9±14.2			
BC-08-40	51°23.761' -118°39.684'	1382	20	1.280 (8145)	0.168 (100)	1.201 (717)	34.9	91.5	25.7±5.8	13.03±0.18 (100)	1.81	2.61
BC-08-41	51°23.645' -118°40.291'	1193	20	1.090 (8145)	0.192 (202)	1.134 (1195)	37.4	99.5	26.6±4.6			
BC-08-44	51°23.448' -118°40.916'	865	20	1.330 (8145)	0.183 (146)	1.123 (896)	35.8	96.2	31.2±6.1	11.04±0.22 (100)	2.25	1.93
BC-08-45	51°22.181' -118°42.407'	788	20	1.300 (8145)	0.353 (305)	3.122 (2696)	92.1	75.2	21.2±3.0	10.30±0.19 (100)	1.95	2.75

Table 2.3.(continued)

Sample Number	Lat/Long	Elevation (m)	Number of Grains	Dosimeter Track Density (10^{-6} cm^{-2})			U (ppm)	P(χ^2) (%)	Central Age (Ma±2σ)	Mean Track Length, µm±SE (number of tracks)	SD (µm)	DPAR (µm)
				ρ_d (N_d)	ρ_s (N_s)	ρ_i (N_i)						
BC-08-50	50°38.248' -119°02.378'	1169	21	1.130 (8145)	0.184 (218)	1.384 (1620)	43.7	18.1	22.3±4.0			
BC-10-07	50°27.722' -118°01.829'	1326	20	1.230 (4383)	0.256 (231)	1.744 (1574)	54.2	79.3	26.0±4.2	10.81±0.24 (100)	2.36	3.22
BC-10-08	50°27.803' -118°05.543'	2143	20	1.250 (4383)	0.419 (167)	1.735 (692)	51.01	93.3	43.4±8.1	13.75±0.12 (100)	1.24	2.38
BC-10-09	50°27.781' -118°05.377'	2034	20	1.270 (4383)	1.322 (440)	5.824 (1938)	181.1	85.3	41.5±5.6	14.28±0.1 (100)	1.04	3.46
BC-10-11	50°27.715' -118°03.518'	1800	20	1.310 (4383)	0.965 (385)	6.329 (2524)	178.3	54	28.8±4.0	12.24±0.19 (100)	1.99	1.9
BC-10-12	50°27.750' -118°03.076'	1688	20	1.340 (4383)	0.437 (321)	2.474 (1816)	80.6	95.2	34.1±5.0	12.93±0.17 (100)	1.72	2.81
BC-10-14	50°27.052' -118°02.014'	1427	16	1.360 (4383)	0.306 (169)	2.236 (1235)	63	36.2	26.8±5.0	12.45±0.18 (100)	1.89	2.2
BC-10-18	50°34.656' -118°01.927'	1161	20	0.913 (3314)	0.401 (282)	2.304 (1621)	90.7	24.3	23.2±3.8	12.89±0.18 (100)	1.83	2.74
BC-10-33	50°57.432' -118°24.027'	535	20	1.400 (4383)	0.409 (365)	4.095 (3651)	107.8	9.4	20.3±3.2	12.28±0.17 (100)	1.72	2.42
BC-10-35	50°59.739' -118°21.031'	599	20	1.420 (4383)	0.212 (209)	2.734 (2695)	71.3	0	16.7±4.0	10.78±0.21 (100)	2.07	2.34
BC-10-40	50°38.128' -118°50.577'	690	20	1.440 (4383)	0.176 (143)	1.694 (1374)	46.1	27.7	21.7±4.6	12.47±0.18 (100)	1.85	3.34
BC-10-41	50°26.564' -118°26.130'	1681	20	1.470 (4383)	0.340 (345)	2.027 (2054)	49.7	75	35.6±5.0	13.47±0.11 (100)	1.18	2.41
BC-10-42	50°26.386' -118°27.600'	1369	20	1.490 (4383)	0.280 (277)	1.750 (1729)	49.6	32	34.6±5.6	11.90±0.22 (100)	2.17	1.87
BC-10-46	50°26.640' -118°23.372'	2080	20	1.510 (4383)	0.805 (460)	4.661 (2664)	108.6	26.6	37.7±5.2			
BC-10-48	50°26.553' -118°23.374'	2182	22	1.530 (4383)	0.531 (255)	2.447 (1175)	58.8	70	47.9±7.8			
BC-10-51	50°35.562' -118°24.062'	655	20	0.937 (3314)	0.184 (187)	1.442 (1461)	54.9	72.5	17.3±3.0	12.54±0.15	1.55	2.23

Table 2.4. Single grain apatite (U-Th)/He replicate data. Mwar, the mass-weighted average radius; HAC (Ft), geometric correction for alpha ejection [*Farley et al.*, 1996]; eU, effective uranium [*Flowers et al*, 2007].

Sample Number	Mass (μg)	mwar (μm)	U (ppm)	Th (ppm)	Sm (ppm)	He (nmol/g)	Raw Age (Ma)	Error (±1σ)	Corrected Age (Ma)	Error (±1σ)	HAC (Ft)	eU (ppm)
01-19-1	4.58	56.5	33.6	12.3	178	0.95	4.82	0.2	4.83	0.2	0.75	36.4
01-19-2	3.65	49.5	83.3	16.6	324	3.24	6.86	0.2	9.48	0.2	0.72	87.2
01-20-1	7.77	66.0	24.4	0.74	348	0.69	5.16	0.2	6.57	0.2	0.79	24.6
01-20-2	7.06	68.0	78.7	88.3	108	3.49	6.49	0.1	8.34	0.2	0.78	99.4
01-25-1	3.20	47.8	50.0	24.9	89.5	1.59	5.27	0.2	7.40	0.3	0.71	55.9
01-25-2	1.85	38.8	59.8	38.8	104	1.96	5.27	0.3	8.04	0.4	0.66	68.8
01-26-1	3.80	43.3	87.4	10.8	277	4.44	9.12	0.2	12.9	0.3	0.71	89.9
01-26-2	4.74	56.8	32.5	9.04	173	1.67	8.90	0.3	11.9	0.3	0.75	34.6
01-26-3	2.99	46.3	75.8	1.99	214	3.71	8.99	0.2	12.7	0.3	0.71	76.3
01-57-1	5.96	63.5	7.54	1.37	243	0.85	19.4	0.7	24.4	0.9	0.80	7.86
01-57-2	2.86	48.8	18.1	8.60	452	1.70	15.2	0.6	20.9	0.8	0.73	20.1
01-58-1	3.43	51.8	16.6	0.94	227	1.53	16.6	0.6	22.3	0.8	0.75	16.8
01-58-2	3.21	52.0	12.9	0.94	153	1.83	25.3	0.8	34.1	1.1	0.74	13.2
01-60-1	6.49	62.8	17.5	1.30	155	1.77	18.3	0.4	23.6	0.6	0.77	17.8
01-60-2	2.19	48.0	18.6	2.44	198	2.08	19.9	0.8	27.8	1.1	0.72	19.2
01-61-1	2.05	56.8	10.6	1.69	132	1.18	19.6	0.8	26.4	1.1	0.74	11.0
01-63-1	0.95	32.0	16.0	0.92	75.2	0.80	9.11	0.6	14.5	1.0	0.63	16.2
01-63-2	1.02	32.8	15.5	0.51	75.5	0.92	10.8	0.6	17.1	1.0	0.64	15.6
01-72-1	6.74	58.3	10.4	1.22	165	0.16	2.71	0.1	3.47	0.2	0.16	10.6
01-72-2	3.97	53.0	10.9	0.41	147	0.49	8.05	0.2	10.9	0.3	0.74	11.0
01-77-1	2.29	43.3	57.2	28.7	30.1	6.67	19.3	0.4	27.5	0.5	0.70	63.9
01-77-2	2.29	44.8	36.4	13.6	23.8	1.85	8.67	0.2	12.3	0.3	0.71	39.6
01-77-3	2.76	53.0	45.1	21.0	29.3	0.52	1.93	0.1	2.62	0.1	0.74	49.9
01-78-1	3.41	51.3	26.2	8.34	22.0	1.50	9.87	0.2	13.3	0.3	0.74	28.1
01-78-2	4.80	55.5	54.4	33.1	26.9	5.38	16.0	0.3	21.1	0.4	0.76	62.1
01-78-3	1.12	31.8	29.0	8.14	20.2	0.42	2.54	0.2	4.24	0.3	0.60	30.9
01-79-1	2.98	56.0	3.62	0.27	41.6	0.15	7.38	0.6	9.72	0.8	0.76	3.68
01-79-2	1.47	36.8	6.92	1.09	27.8	0.26	6.80	0.5	10.3	0.8	0.66	7.18
01-79-3	3.56	50.5	7.59	0.85	74.4	0.33	7.70	0.3	10.6	0.4	0.73	7.80
01-80-1	6.26	71.3	21.0	34.5	280	1.40	8.83	0.1	11.1	0.2	0.80	29.1
01-80-2	8.86	69.0	12.0	5.21	171	0.83	11.5	0.2	14.5	0.3	0.79	13.2

Chapter 3: Low-temperature thermochronometric record of shallow emplacement of migmatite beneath a detachment shear zone

Erkan Toraman[1], Christian Teyssier[1], Donna L. Whitney[1], Annia K. Fayon[1], Stuart N. Thomson[2], Peter W. Reiners[2], and Seth C. Kruckenberg[3]

[1] *University of Minnesota, Department of Earth Sciences, 310 Pillsbury Drive SE Minneapolis, MN 55455-0231*

[2] *University of Arizona, Department of Geosciences, Gould-Simpson Building, 1040 E. 4th St., Tucson, AZ 85721-0077*

[2] *Boston College, Department of Earth and Environmental Sciences, Devlin Hall 213, 140 Commonwealth Avenue, Chestnut Hill, Massachusetts, 02647*

Metamorphic core complexes containing high-grade metamorphic rocks, including migmatite, are major sites for mass and heat transfer in orogens. The Okanogan gneiss dome is the southernmost member of a series of gneiss domes exposed in core complexes in the hinterland of the northern North American Cordillera. Previous petrologic and geochronologic studies have shown that the footwall rocks of the detachment fault that bounds the Okanogan core complex were partially molten during near-isothermal decompression, were fully crystallized by ~ 51 Ma, and experienced cooling from ~700°C to ~300°C within a few million years. New low-temperature thermochronology results (apatite fission track, zircon and apatite (U-Th)/He) from from the Okanogan dome document the overlap between high-to-low temperature ages, indicating emplacement of partially molten crust at near-surface depths (≤ 2 km). Zircon (U-Th)/He ages range from 50.9 ± 1.5 to 41.2 ± 1.0 Ma, are older in the east and decrease westward toward the detachment fault. They record rapid footwall cooling and exhumation between ~51 to ~45 Ma at a maximum slip rate up to 3.7 km/my. AFT ages

range between 50.5 ± 8.6 to 22.8 ± 4.2 Ma and are spatially invariant over 18 km across the dome in the shear direction. Together with AHe ages, which are between 48.0±1.1 to 28.2±1.7 Ma, these AFT ages reflect erosional unroofing that removed ~2 km of overburden shortly after the cessation of detachment faulting. Our results indicate that rocks closer to the detachment fault zone experienced rapid cooling (≥ 100 °C/my) whereas deeper structural levels recorded much lower cooling rates (10-30 °C/my). We conclude that the rapid exhumation and cooling of the Okanogan dome ca. 51-45 Ma reflect stabilization and isostatic equilibrium of the orogenic crust at the end of Cordilleran orogenesis.

3.1. Introduction

Crustal extension leads to the exhumation of deep, hot rocks to shallow levels. The resulting structure is a core complex, which consists of high-grade metamorphic rocks and granitic bodies bounded by a low-angle normal fault (e.g., Crittenden et al., 1980; Lister et al., 1984; Dewey, 1988). Many core complexes contain domal structures comprised of migmatite that was partially molten during extension and that crystallized during the final stages of dome emplacement (Whitney et al., 2004; 2013). Exhumation of these migmatite-cored metamorphic core complexes (Rey et al., 2009a) results in significant mass and heat transfer and the likely reorganization of surface and Moho topography.

Numerical models predict that extension in the upper crust sets the low viscosity (partially molten) lower crust in motion, resulting in rapid upward flow of deep crust in domes that form directly beneath upper crustal normal faults (Wdowinski and Axen, 1992; Rey et al., 2011; Whitney et al., 2013). The high-temperature history of rocks in

the footwall of these normal faults has been documented by pressure-temperature (*P-T*) and geochronological investigations (primarily U-Pb zircon and monazite dating). For example, the Shuswap metamorphic core complex of the northern North American Cordillera contains high-grade rocks in the core of migmatite domes that experienced near-isothermal decompression at T > 750°C from > 0.8 GPa to ~ 0.3 GPa during Eocene extension (Norlander et al., 2002; Hinchey et al., 2006; Kruckenberg et al., 2008; Gordon et al., 2008).

Because rocks in rising migmatite domes experience little or no cooling during exhumation, rapid advection of heat promotes a high thermal gradient and closely - spaced isotherms in the roof of the domes. In this transient thermal regime, when rock ascent decreases or ceases, isotherms move away from the Earth's surface. Rocks experience high cooling rates and lock their isotopic ages for different thermochronometers. Therefore, understanding the high-T to low-T cooling history of dome rocks provides insight into the mechanisms and rate of ascent, and the depth at which migmatite dome rocks crystallize and cool. These quantities relate directly to the rate of extension and the viscosity distribution of the deep crust, including the presence of partial melt, as shown in dynamic models of dome emplacement (Rey et al., 2009a,b; 2011).

In this paper we focus on the low-T cooling history of the Okanogan migmatite dome (Washington, USA), from melt crystallization to final exhumation. We present new zircon and apatite (U-Th)/He as well as apatite fission-track analyses from the footwall rocks of the Okanogan detachment and evaluate the mechanisms of exhumation of this migmatite-cored metamorphic core complex. More generally we reflect on the

thermal consequences of the shallow emplacement depths of partially molten crust in metamorphic core complexes.

3.2. Regional and Geological Setting

Core complexes containing migmatite (gneiss) domes occur in the northern North American Cordillera, where crust thickened during Mesozoic convergence and accretion of terranes, before undergoing orogenic collapse and/or extension in Eocene time. Locally, extension resulted in rapid exhumation of mid- to lower crustal rocks (metamorphic core complexes) beneath extensional detachment shear zones, coeval development of supra-detachment basins, and widespread magmatism (Armstrong 1982; Monger et al, 1982; Coney and Harms, 1984; Okulitch, 1984; Parrish et al., 1988; Suydam and Gaylord, 1997; Vanderhaeghe et al., 2003; DeCelles, 2004; Teyssier et al., 2005; Kruckenberg et al., 2008; Brown et al., 2012). The Omineca Belt separates allochthonous terranes to the west from the North American craton to the east (Coney, 1980) and exposes the northernmost Cordilleran metamorphic core complexes. The core complexes include a series of north-south trending gneiss/migmatite domes from British Columbia (Canada) to Washington-Idaho (USA): Frenchman's Cap, Thor-Odin, Valhalla-Passmore, and Okanogan-Kettle-Priest River (Fig. 3.1). The western margin of the Omineca belt is defined by the Okanogan-Eagle River detachment system (Fig. 3.2A), which can be traced fairly continuously for ~500 km. This study focuses on the Okanogan dome that forms the footwall of the Okanogan detachment system south of the Canada-USA border (Fig. 3.1).

The hanging wall of the Okanogan dome consists of greenschist or subgreenschist facies Paleozoic to lower Jurassic metavolcanic and metasedimentary units that are commonly intruded by pre-Triassic to Eocene igneous rocks (Church, 1973; Fox et al., 1977; Mathews, 1981; Parkinson, 1985) and several high-angle normal fault-bounded basins that were filled with Eocene sedimentary and volcanic strata. Three NE-SW oriented en-échelon graben (Toroda Creek, Republic, and Keller) cut the Okanogan and Kettle domes and preserve thick sequences of interbedded sedimentary and volcanic rocks (Fig. 3.2A, Fox et al, 1977; Parkinson, 1985; Holder and Holder, 1988; Stoffel et al., 1991). The Toroda Creek graben contains ~4 km of homoclinally east-dipping volcano-sedimentary strata. K-Ar dating of volcanics in the basins yields ages of ca. 53-48 Ma (Pearson and Obradovic, 1977). Clasts of high-grade schist, gneiss, and deformed plutonic rocks observed in higher stratigraphic units indicate that the dome rocks were exhumed to the Earth surface during basin formation (Suydam and Gaylord, 1997).

The White Lake basin is located on the hanging-wall of the Okanogan detachment in south-central British Columbia and contains ~2.5 km of intercalated volcanic and sedimentary fill interpreted as an evolving supra-detachment basin (McClaughry and Gaylord, 2005). In this basin basaltic to rhyolithic volcanic rocks yield cooling ages of ca. 53-48 Ma (Church, 1985). Similar to the Toroda Creek Basin, clasts of mylonite and deformed metamorphic rocks commonly occur within the basin, implying that exhumation of footwall rocks and basin formation were synchronous (McClaughry and Gaylord, 2005).

In the studied region the Okanogan detachment fault and underlying shear zone are exposed in a ~ 1-2 km thick section. The sheared rocks are characterized by

amphibolite-facies ductile fabrics that grade upward into a greenschist-facies mylonitic fabric overprinted by brittle structures. This structural sequence likely developed during progressive exhumation of the dome (Goodge and Hansen, 1983; Kruckenberg et al., 2008). In the section from high-grade tectonite to mylonite, shallowly west-dipping corrugated foliation surfaces and a prominent NW-SE trending mineral lineation indicate top-to-northwest shear. Kinematic analysis of shear bands, asymmetric mica fish and porphyroclasts, and vergence of folds also indicate dominant top-to-northwest shear during ductile deformation of footwall rocks (Hansen and Goodge, 1988; Kruckenberg et al., 2008). The common occurrence of striations along foliation planes has been interpreted as reactivation of these surfaces under brittle conditions, recording the same stress regime obtained from ductile structures (Eyal et al., 2006).

The footwall of the Okanogan detachment shear zone consists of orthogneiss and upper amphibolite-facies Tonasket paragneiss (Snook, 1965; Fox et al., 1976). The high melt-fraction migmatitic Tonasket gneiss is exposed in the structurally deepest regions as two NW-SE trending domes (Stowe Mountain and Burge Mountain domes, Kruckenberg et al., 2008; Fig. 3.2B). The Tonasket gneiss is locally interlayered with amphibolite and calc-silicate and overlain by augen orthogneiss and amphibolite-facies quartzite, marble, and schist (Cheney, 1980). Between the high melt-fraction migmatite core and the overlying lower melt-fraction units is a km-scale layer of gedrite-cordierite gneiss that locally contains kyanite, spinel, staurolite, anorthite, and sapphirine (Kruckenberg and Whitney, 2011); this unit resembles Mg-Al-rich gneiss lenses in other migmatite domes of the Shuswap Complex (Duncan, 1984; Norlander et al., 2002; Hinchey et al, 2006; Goergen and Whitney, 2012a, b). P-T path reconstruction and the

presence of symplectitic textures around kyanite and staurolite in gedrite-cordierite adjacent to the high melt-fraction Stowe Mtn migmatite have been interpreted to indicate near-isothermal decompression of the dome rocks from the mid-crust at ~720-750 °C and ~8 kbar (~28 km for crustal density of 2.8 g/cm^3) to shallower crust (<3 kbar, or <~10 km, Kruckenberg and Whitney, 2011).

All these units were intruded by granitic gneiss and granodioritic plutons of the Colville Batholith (Fig. 3.2, Fox et al, 1976; Carlson and Moye, 1990). The similarity of the trend of intrusive contacts of the Colville Batholith and associated dikes and the graben-bounding high-angle faults, the occurrence of penetrative mylonitic deformation in the intrusive suites of the batholith, and inferences about the source rocks of metamorphic and plutonic clasts in sedimentary rocks in the graben collectively suggest that gneiss dome formation, graben development, and batholith emplacement were contemporaneous (Goodge and Hansen, 1988; Holder and Holder, 1988; McClaughry and Gaylord, 2005; Kruckenberg et al., 2008). This is consistent with geochronologic data that document coeval migmatite crystallization, detachment faulting, and basin development over a wide region in Paleocene to Eocene time (Kruckenberg et al., 2008; Brown et al., 2012).

Previous geochronological studies of the Okanogan dome have mainly focused on the timing of migmatite and pluton crystallization (Fox et al., 1976; Kruckenberg et al., 2008). U-Pb SHRIMP analysis of zircon rims in migmatite and associated pegmatite bodies collected from migmatite to mylonite (section from Stowe Mountain to detachment fault, Fig. 3.2B) yielded crystallization ages ranging from 59.8 ± 0.5 to 48.8 ± 0.6 Ma (Kruckenberg et al., 2008). Zircon cores from the same samples have ages

ranging from ca. 85-70 Ma. In the same Stowe Mountain to detachment fault section a titanite U-Pb age yields 47.1 ± 0.5 Ma, and biotite Ar/Ar ages are 48.0 ± 0.1 to 47.1 ± 0.2 Ma (Kruckenberg et al., 2008).

The low-temperature history of the Okanogan complex high-grade core has not been explored in detail. Two apatite fission track ages, 51 ± 5 and 53 ± 5 Ma, have been previously reported from granitic gneisses exposed in the northern Okanogan dome, ~30 km north of our sampling site (Naeser et al., 1970; Fox et al., 1976). Similarly, two ZHe and two AHe ages has been reported from the footwall units exposed further north in Canada (near US-Canada border). ZHe chronometry yielded ages of 48.5 ± 3.7 and 40.1 ± 7.0 Ma, whereas AHe analysis yielded ages of 54.1 ± 12.0 and 40.0 ± 22.0 (Callahan, 2007). ZHe and AHe ages from the hanging-wall units, on the other hand, show a broad distribution of ages; ZHe ages range between ca. 96 and 42 Ma, and AHe ages range between 90 and 21 Ma (Callahan, 2007).

3.3. Analytical and Sampling Methods

Samples analyzed in this study were collected from the Okanogan dome, including samples from the same traverse analyzed by Kruckenberg et al. (2008). Sample lithologies include high melt-fraction migmatite, orthogneiss, and mylonitic orthogneiss deformed in the detachment zone. Twenty samples were collected on two traverses from the detachment fault to the interior part of the dome. These samples were studied using apatite fission-track (AFT) and zircon and apatite U-Th/He (ZHe, AHe) thermochronology.

3.3.1. Apatite Fission-Track Thermochronology

AFT thermochronology is based on the damage zones (tracks) formed by spontaneous fission of ^{238}U (Fleischer et al., 1975; Wagener and Van der haute, 1992). Once formed, fission tracks partially or entirely anneal, with the extent of annealing depending primarily on the temperature field they experienced. Tracks are effectively stable below ~60 $^{\circ}C$ owing to very slow annealing rates, but instantaneous annealing occurs above ~120 $^{\circ}C$ (Gleadow and Duddy, 1981; Gleadow et al., 1986). In the temperature range ~ 60-120 $^{\circ}C$ (Partial Annealing Zone, PAZ), track density and track lengths systematically reduce as a function of time and temperature (e.g. Gleadow et al., 1986). The annealing process is also influenced by the chemical composition and the crystallographic orientation of apatite grains (Donelick et al., 1990; Ketcham, 2003). Because annealing kinetics can vary among apatite grains within a sample, measuring kinetic parameters is routinely used in AFT analysis. Among several kinetic parameters, chlorine content and Dpar, the arithmetic mean fission-track etch pit diameter parallel to the c-axis, are commonly measured (Donelick et al., 2005).

Apatite crystals were separated using standard magnetic and heavy mineral techniques. Grain mounts were prepared using epoxy resin, polished to 0.25 μm, and etched for 20 s in 5 M HNO_3 at room temperature. All grain mounts were covered with low-U mica external detector. SRM612 uranium-dosed glasses were placed at the top and bottom of the package in order to monitor neutron fluence. Samples were irradiated at Oregon State University Radiation Center with a neutron dose of 1×10^{16} neutrons/cm^2. External mica detectors were etched in 50% HF for ~20 minutes at room temperatures. Fission track densities were counted using a Nikon Optiphot microscope with 100x dry objective and total magnification of 1250x. Horizontal confined tracks

were measured using an attached drawing tube and digitizing table calibrated with a stage micrometer. Zeta calibration factor was calculated using three Durango and four Fish Canyon Tuff age standards. Central ages (Galbraith and Laslett, 1993) were calculated using the Trackkey program (Dunkl, 2002) with zeta value of 289±11. The Binomfit program (Brandon et al, 1998) was used to identify single age components of a sample if the sample fails the chi-square test.

An additional set of grain mounts was prepared for ^{252}Cf irradiation from samples yielding enough apatite crystals in order to enhance etchable horizontal confined tracks (Donelick and Miller, 1991). Track length distributions were determined by measuring a statistically significant number of horizontal confined tracks with corresponding angles to the crystallographic c-axis (Laslett et al., 1982). Radiply cooled samples have long mean tracks (>14 μm) showing a symmetric distribution; conversely, slowly cooled samples or complex cooling histories typically produce short track lengths (<14 μm) and negatively skewed track-length distributions. The magnitude of track length reduction depends on the time a sample resides within the partial annealing zone (Gleadow et al., 1986).

3.3.2. Zircon and Apatite (U-Th)/He Thermochronology

(U-Th)/He thermochronology is based on the accumulation of ^{4}He as a result of the decay of U, Th, and Sm by α-particle emission (Zeitler et al., 1987; Farley, 2002). Diffusion experiments on apatite and empirical observations from borehole data and exhumed crustal blocks show that He is expelled from the crystal structure at temperatures of ~80 $^{\circ}C$ and is retained below ~40 $^{\circ}C$ (Farley, 2002; Stockli et al., 2000). The temperature range of ~40-80 $^{\circ}C$ is called the Helium Partial Retention Zone

(HePRZ). For typical cooling rates (~10 °C/Myr) and grain sizes (~60±20 μm) the closure temperature for He in apatite is ~70 °C (Farley, 2000). He in zircon has a much higher closure temperature range relative to apatite, ranging between ~170 °C -190 °C, depending on cooling rate and crystal size (Reiners et al., 2003).

Apatite and zircon crystals were handpicked under high-powered magnification based on their shape, size, and internal structures (e.g., fractures, inclusions). Their sizes were then measured in two orientations for an alpha ejection factor calculation (Farley, 2002). Single apatite or zircon grains were packed and heated in order to liberate ^{4}He using a Nd-YAG laser cell connected to the He extraction and measurement line. He isotopic ratio was determined using a known volume of ^{3}He spike in a quadrupole mass spectrometer following the procedures outlined by Reiners et al. (2003) and Reiners (2005).

3.3.3. Modeling Methods

The temperature-time (T-t) history of individual samples was calculated using the HeFTy program, which can implement forward and inverse models based on FT annealing and He diffusion parameters of apatite and zircon (version 1.7.5, Ketcham, 2005). Modeling of AFT ages and track-lengths used the multicompositional annealing model of Ketcham et al. (2007b) and c-axis projected track lengths of observed data (Ketcham et al., 2007a). Initial track lengths were calculated using measured D_{par} values as a kinetic parameter. Diffusion properties of He in apatite and zircon were modeled following Flowers et al. (2009, RDAAM model) and Reiners et al. (2004), respectively. We applied ^{40}Ar/^{39}Ar biotite ages of the Okanogan gneiss (Kruckenberg et al., 2008) as "high-temperature" input between ~350 and 300 °C. Additional input was placed

between 300 °C and surface temperature, which was set to 20±20 °C for all samples, in order to seek all possible T-t paths. HeFTy classifies randomly generated T-t paths based on goodness of fit statistics, which is an estimate of the fit between the predicted and observed age and track-length data (Ketcham, 2005). Good and acceptable fit paths have goodness of fit values of 0.5 to 0.05, respectively, for our models. We ran models until 100 randomly generated "good" paths were found, except one sample (OK-324) in which only "acceptable" solutions were achieved.

3.4. Results

3.4.1. Thermochronology

We present nine zircon (U-Th)/He (ZHe), and fifteen apatite (U-Th)/He (AHe) and apatite fission track (AFT) ages, for which eight fission-track length distributions were determined (Table 3.1). All AFT ages are reported as central ages with associated 2σ error. ZHe and AHe ages are reported as weighted mean ages of multiple replicates. Details of the AHe and ZHe analyses and fission-track measurements are in Tables 3.2-3.4.

3.4.1.1. Traverse 1

Eleven samples were collected along traverse 1, which extends from the detachment fault trace in the west to the interior section of the dome along a regional synformal structure over a linear distance of 18.5 km (Fig. 3.2B). At the detachment zone, samples were collected from an ultramylonitic orthogneiss (OK-329) and a cataclastically deformed augen gneiss (OK-328). To the east, samples OK-327 and OK-326 were collected from a biotite-rich quartzofeldspathic orthogneiss and augen gneiss, respectively. Two biotite-rich quartzofeldspathic gneisses (OK-325, OK-322) and two

granodioritic augen gneisses (OK-324, OK-323) were sampled in the middle of the traverse. Three samples from granodioritic gneiss (OK-321, OK-320, OK-319) were collected at the eastern end of the traverse.

ZHe ages from eight samples range from 50.9 to 41.2 Ma, with younger ages close to the detachment fault. The three samples at the eastern end of the traverse (13-18.5 km from contact) yielded an average age of ca 48 Ma, while samples at the western end of the traverse and within ~4 km from the contact averaged ca 44 Ma.

AFT analysis from six samples reveals ages ranging between 50.5 and 39.8 Ma, with no systematic pattern of ages relative to proximity to the detachment fault. Three samples (OK-327, OK-325, OK-319) show low age-dispersion and passed the chi-square test, indicating that these ages represent single populations (Fig. 3.2B). Three other samples collected from the middle to eastern end of the traverse (OK-320, OK-323, OK-324) failed the test, implying that multiple age populations may be present. Decomposition of the central ages to determine possible single age components of samples failing the chi-square test showed that sample OK-320 has two age groups of 52.2 Ma and 23.5, the former being 83% of the whole population. Similarly, OK-324 has two age components of 17.2 (8.7%) and 45.1 Ma (91%). Three age populations, 25.0 (24%), 45.0 (21%), and 80.1 Ma (26%) were calculated for OK-323.

Only two samples (OK-324, OK-327) yielded sufficient apatite grains for track length analysis; mean track lengths are slightly shorter (<14 μm) and have low standard deviation (<1.4 μm). Both samples have a unimodal track-length distribution, indicating that these samples spent a relatively short time within the apatite PAZ and might represent the higher segment (close to the top) of the apatite PAZ. Dpar values are high

(>1.75 μm), suggesting relatively slow annealing of apatite grains (Carlson et al., 1999; Donelick et al., 2005).

Weighted mean AHe ages of nine samples covering the entire traverse vary between 48 and 32.2 Ma. In contrast to AFT data, AHe ages decrease with proximity to the detachment. Mean ages were calculated using three replicate analyses of each sample, except OK-322 and OK-319. Two out of three aliquots of sample OK-319 yielded considerably older ages (older than migmatite crystallization ages of ~50 Ma) and were excluded from further data analysis and interpretation. Sample OK-322 yielded only two suitable apatite grains and gave an age of 48 ± 1.3 Ma. In the eastern part of the traverse (13-18.5 km), ages vary between 49 and 40 Ma (average ca. 45 Ma), while samples within 4 km of the present trace of the detachment fault yielded AHe ages from 41.2 to 32.2 Ma (average ca. 38 Ma). All ages are younger or within 2σ error of AFT ages from the same samples.

3.4.1.2. Traverse 2

Traverse 2 is located in the Stowe Mountain area and extends from the detachment fault to the high melt-fraction migmatite in a section over 6 km long, exposing approximately 1.5 km of structural thickness (Fig. 3.2B). Nine samples were collected from various types of gneissic rocks including quartzofeldspathic orthogneiss (OK-305, OK-317, OK-337, OK-339), banded gneiss (OK-315), amphibolite-rich gneiss (OK-306), migmatitic gneiss (OK-307, OK-311), and a leucocratic granodiorite diatexite (03-OK-80).

We obtained only one ZHe analysis from this traverse, from a sample that was collected from the detachment fault zone (OK-339). This sample yields an age of 47.4

Ma, similar to some ZHe ages obtained from Traverse 1 at the same structural level. Seven samples were analyzed for AFT; ages range from 49.5 to 22.8 Ma. The youngest ages come from the samples collected near the detachment fault zone (OK-339) and from the migmatitic core (O3-OK-80), 22.8±4.2 and 22.8±4.4 Ma, respectively. Two samples, OK-311 and OK-315, failed the chi-square test, suggesting the presence of mixed ages. OK-315 has two age components; 35.6 Ma (75.8%) and 54.2 Ma (24.2%). Sample OK-311 has a dominant Eocene age component (44.4 Ma, 89%) and a small fraction of Cretaceous ages (80 Ma, 11%).

Track-length distributions were obtained from six samples, and the track-length means are between 12.43 to 14.48 μm. Long mean track lengths show symmetric distribution, while shorter confined tracks are negatively skewed (Fig. 3.2B, Table 3.1). Like Traverse 1, Traverse 2 is characterized by high Dpar values (>1.75 μm).

Four samples from Traverse 2 were dated using apatite (U-Th)/He analysis. Weighted mean AHe cooling ages vary from 29.3 to 42.9 Ma. After rejection of one obvious outlier, two aliquots of sample OK-338 provided the youngest mean AHe age of the Okanogan dome (28.2 ± 1.7 Ma).

3.4.2. Thermal Modeling

Thermal modeling results for Traverse 1 indicate that all samples cooled rapidly from initial high-temperatures through the apatite PAZ (~60-120 °C) (Fig. 3.3). T-t modeling of samples collected from the structurally lowest levels of Traverse 1 (13-18.5 km distance to detachment) indicates that the rocks continued to cool rapidly (≥60 °C /my) through the AHe closure temperature, at which point the rocks reached T < 50°C. This rapid cooling was followed by extremely slow cooling of ~3 °C/My (Fig. 3.5;

samples OK-319 to 321). Samples collected closest to the detachment fault (OK-328,329) show a very similar cooling history. However, samples OK-324 to OK-327, which are located at slightly deeper structural levels, display prolonged residence time at temperatures ~80-40°C.

Thermal modeling of Traverse 2, covering a section from the detachment zone to the top of the migmatitic core, reveals a distinct cooling pattern as a function of structural depth. Samples collected near the detachment fault zone (OK- 337, 338) display high cooling rates (≥100 °C/my) through PAZ, followed by significant decrease of cooling rates to <5 °C/my at ca. 45 Ma (Fig. 3.4). Samples OK-317 and 315, representing the deeper levels of the section, show some residence in the PAZ after their initial rapid cooling and record a more gradual cooling after ca. 35 Ma. Modeling results of sample OK-311 reveal similar cooling history of rocks near the detachment fault, even though this sample is structurally deeper. The structurally deepest samples (OK-305 and 307, and 03-OK-80) might have experienced high cooling rates initially, similar to what is observed in other samples from this traverse. However, these deepest samples record more or less constant and very low cooling rate (~3°C/my) starting after ca. 40 Ma (Fig. 3.4).

3.5. Interpreatiton of Thermochronology Data

Cooling histories determined from multiple low-temperature thermochronometric systems from footwall units reveal parameters of extensional faulting in many metamorphic core complexes (Foster and John, 1999; Fayon et al., 2000; Axen et al., 2001; Lorencak et al., 2001; Stockli, 2005; Thomson and Ring, 2006; Foster et al., 2010). As each thermochronologic system is sensitive to different

temperature ranges, the combination of cooling histories from different chronometers can be used to construct a complete T-t path of individual samples.

Low-temperature ages from samples collected parallel to the slip direction of detachment faults have been used to quantify the timing of slip, slip rate, and fault dip angle change (Foster and John, 1999; Stockli, 2005; Brichau et al., 2008; Stübner et al., 2013). In Traverse 1, although complications exist, ZHe ages generally decrease from east to west, parallel to the hanging-wall slip direction over 18 km of map distance (Fig. 3.5). At the eastern end of Transect 1, structurally lower samples give older ages (~51 Ma for OK-321) relative to samples that are close to the detachment fault zone to the west (~41 Ma for OK-328). We interpret changes of ZHe ages as a function of distance as a record of slip on the low-angle detachment fault. Therefore, the regression of all ZHe age data in age-distance plot implies a slip rate of 3.7 km/my. This slip rate calculation, however, assumes that thermal steady-state was achieved (Ketcham et al., 2006) and that erosion was negligible. If regional erosion was effective during footwall slip, then the calculated slip would be lower. Assuming the approximate slip rate of 3.7 km/my during detachment fault activity between ~51 and ~45 Ma implies ~22 km of total horizontal offset. Depending on the fault geometry this horizontal offset can be translated into vertical exhumation. Assuming a fault dip angle between 30° and 10° yields vertical exhumation of ~13 to ~4 km, respectively.

In contrast to the ZHe trend, AFT ages are concordant throughout Transect 1, ranging between 50 to 39 Ma, with a weighted mean age of 45 ± 6.4 Ma (Fig. 3.5). Furthermore, samples that were analyzed by both ZHe and AFT methods yield similar ages for each thermochronometer. We calculated time-averaged cooling rates from

samples in which ZHe and AFT age pairs were obtained. Dividing respective closure temperatures by differences in age from these samples yields average cooling rates of ~10-30 °C/my in this traverse. It has been shown that near concordant ages of different chronometers and rapid cooling rates (~40-100 °C/my) are common in areas where exhumation was facilitated by detachment faulting (e.g. Foster and John, 1999, Thomson and Ring, 2006; Brichau et al., 2008). Because the cooling rates obtained from ZHe-AFT pairs in the Okanogan dome are much lower than unroofing caused by tectonic denudation, we interpreted them as a result of dominant erosional denudation.

Three AFT ages from the Traverse 1 (OK-320, OK-0323, OK-324) failed the chi-square test, suggesting multiple single age components may exist in those samples. This can be caused by several processes. For instance, single grain AFT age distribution in samples from the PAZ tend to have a wide range in single grain ages, whereas samples below or above the PAZ have a narrower distribution of ages (e.g. O'Sullivan and Parrish, 1995). Therefore, the non-Poisson age distributions of three samples that failed the chi-square test can be explained by the position of samples relative to the PAZ. Alternatively, the differences in the annealing kinetics owing to variations in apatite composition can result in mixed ages (e.g. Gleadow and Duddy, 1981). Out of the three samples, only one (OK-324) has both track length (13.74±1.39) and Dpar (2.47 μm) measurements; these values support a difference in annealing kinetics to explain the observed mixed ages.

In Traverse 1, AHe ages are younger towards the detachment fault (Figs. 3.2B, 3.5). Ages close to the eastern end of the traverse are as old as 49 Ma, whereas younger ages (32 Ma) are observed close to the detachment fault. Thermal modeling of these

samples indicates that they spent prolonged residence (over 30 m.y.) at near-surface conditions (Fig. 3.3), and may have spent various time within the apatite PRZ (e.g. OK-321, 325, 326). Therefore we interpret the variations of AHe ages as being associated with exposure of different depths within the apatite PRZ related to later erosional exhumation of the Okanogan dome. Taken all together, results from Traverse 1 document rapid exhumation and cooling of the Okanogan dome via mainly tectonic unroofing (low-angle detachment faulting and high-angle normal faults) until ca. 45 Ma, followed by slow regional erosional exhumation.

Traverse 2 provides an opportunity to sample different structural levels of the Okanogan dome from the detachment fault to the migmatitic core. Compared to Traverse 1, results of AFT analysis show more complex age patterns in the slip direction (Fig. 3.6). Here, AFT ages generally increase from the detachment fault in the west to the interior of the dome to the east (i.e. deeper structural levels) in the first 4 km of the transect. Samples from the structurally deepest levels of the transect (03-OK- 80, OK-305, OK-307) revealed considerably younger (~22 to 26 Ma) AFT ages. Track-length measurements documented that all samples except one (OK-311) have relatively short mean track-length (<14 μm), indicating that these samples experienced prolonged residence within the PAZ. Detailed field mapping of Stowe Mountain indicates that several high-angle fault zones exist in the region closer to the detachment fault (Fig. 3.6, Kruckenberg et al., 2008), and this could affect the thermal structure of the shallow crust recorded by low-temperature chronometers.

The sample with longer mean-track-length (14.48±0.94); OK-311) was collected near a brittle fault zone. When considered with the track-length data, the age of this

sample (47.5 ± 7.4 Ma) might be interpreted in two ways. First, observed AFT data might reflect the timing of high-angle faulting ca. 47 Ma. Although easily seen in the field as steep, planar surfaces, the faults don't show any significant vertical displacement. This suggests that vertical displacement might have been insufficient to affect AFT ages across these faults. Alternatively, AFT data might reflect a more localized thermal event, such as hydrothermal activity along these fault zones. The second hypothesis can be supported by the common occurrence of chlorite and epidote in these rocks, particularly along fault planes (Kruckenberg et al., 2008).

Two AFT samples from this traverse failed the chi-square test (OK-315 and OK-311). Sample OK-315 has short mean track length (12.98 ± 0.18 μm). This suggests that this sample had prolonged residence time in the PAZ, and this lead to preservation of multiple age populations recorded by the AFT chronometer. OK-311, on the other hand, has long mean track-length (14.48±0.94) and a high Dpar value (2.38). This suggests that the annealing of apatite grains is relatively slow and therefore the older single age fractions could be results from partially reset apatite grains.

Apatite He ages from four samples collected from higher-to-middle structural levels from Traverse 2 yielded slightly older ages in structurally deeper samples, similar to the AFT age trend of corresponding samples (Fig. 3.6). As for the Traverse 1, we interpreted this AHe age pattern as a result of erosional processes that affected the core of the dome.

We calculated the mean cooling rates for one million year intervals to explore spatial differences across the dome using "good" T-t path solutions (goodness of fitness

> 0.5) from HeFTy models (Fig. 3.7). This analysis shows that samples closer to the detachment fault zone (shallow structural levels) cooled rapidly and reached near-surface depths, whereas samples at deeper structural levels cooled more gradually as they experienced longer residence time at higher temperatures after the cessation of detachment faulting. This is in good agreement with numerical models that show relatively slow cooling of deep portions of footwall rocks owing to rapid advection of isotherms during detachment faulting (Fayon et al., 2004; Robinson et al., 2010).

3.6. Discussion

3.6.1. Tectonic vs Erosional exhumation of the Okanogan dome

Collectively, geo/thermochronologic and thermobarometric data from footwall rocks of the Okanogan dome indicate that they have experienced decompression at constant high temperature followed by rapid cooling near the surface. Contrasting cooling ages (Eocene vs Paleozoic to Eocene) and cooling histories during Eocene (2-5 °C/my vs ≥ 100 °C/my) between footwall and hanging-wall units, along with structural data, show that the Okanogan detachment fault accommodated the exhumation of partially molten crust from depths of ~28 km to shallow levels of the crust (≤2 km) in Eocene (Fox et al., 1977; Goodge and Hansen, 1988; Stoffel et al., 1991; Callahan, 2007; Kruckenberg et al., 2008; Kruckenberg and Whitney, 2011; this work). While the detachment fault system controls the spatio-temporal evolution of deep-seated rocks, sedimentary strata deposited in the hanging wall basins keep record of the progressive exhumation of the core complex; thus provide a link between surface and deep Earth processes. In the Okanagon dome these sedimentary and volcanic deposits accumulated

in a supradetachment basin (White Lake) and en-echelon grabens (Toroda Creek, Republic, Keller) (Suydam and Gaylord, 1997; Gaylord et al., 2001; McClaughry and Gaylord, 2005). Previous studies provided detailed stratigraphy and sedimentology of these basins and identified clasts of high-grade gneiss and migmatitic rocks in these sediments. For instance, in the Torada Creek graben sedimentary units containing mylonitic granodiorite and quartz-mica schist clasts overlies ca. 51-50 Ma of age volcanic rocks and is overlain by another volcanic layer that yielded ca. 49-48 Ma of K-Ar ages (Pearson and Obradovic, 1977; Suydam and Gaylord, 1997). This suggests that exhumation and surface exposure of the footwall rocks had achieved no later than ca. 48 Ma. The oldest K-Ar age of ca. 53 Ma (Pearson and Obradovic, 1977) from volcanic layers indicate that extensional structures in the upper crust had already formed while crystallization of melt was taken place in partially-molten deep crustal rocks. The onset of the detachment faulting ca. 52-50 Ma led the footwall rocks rapidly exhume and cool as the fault-bounded basins were filling with sediments from highlands exposed in the footwall (Suydam and Gaylord, 1997). Predominant ca. 50 Ma of ZHe ages document that footwall rocks rapidly exhumed and cooled through ~170 °C. Moreover, samples yielding ca. 50 Ma AFT ages (e.g.OK-319, OK-327, OK-338) indicate that some sections of the dome had achieved temperatures less than ~60 °C. Although some portions of the basin might have been eroded, younger K-Ar ages indicate that it was filled ca. 48 Ma. and dissected and rotated by normal and strike-slip faults (Suydam and Gaylord, 1997). Sample OK-311 was probably recorded this high-angle brittle faulting in the footwall (AFT age of 47.5 Ma). Based on low-thermochronology results of the footwall rocks, especially ZHe ages, we suggest that tectonic deformation ended ca. 45

Ma. Therefore, the Okanogan dome rocks essentially behaved as a single unit as they rapidly cooled and exhumed to very shallow depths (~1-2 km) beneath a detachment system. Tectonic denudation was the dominant exhumation mechanism and is recorded by $^{40}Ar/^{39}Ar$, ZHe, and possibly a small portion of AFT ages. We interpreted spatially invariant AFT ages across the dome (Fig. 3.5) and low time-averaged cooling rates from ZHe-AFT pairs as a reflection of erosional exhumation of the dome that is recorded by most of the AFT ages and AHe ages. Although we cannot constrain erosion rates due to lack of vertical profiles in the footwall, cooling from ~60 °C implies removal of ≤ 1.5 km crustal material since then (assuming the geothermal gradient was ≥ 50 °C/km), suggesting very low erosion post-orogenic rates (~0.03 mm/yr). Zircon and apatite (U-Th)/He ages from vertical and horizontal profiles from the hanging-wall units in the western Okanogan Range suggest very slow (0.01-0.06 mm/yr) erosion rates in this region between 60-30 Ma (Callahan, 2007). We suggest that this erosion rate estimates reflects background regional exhumation and, therefore, both footwall and hanging-wall shared the same erosional history after cessation of detachment tectonics.

3.6.2. Cooling and exhumation of the Okanogan Dome and its implications for regional geodynamics

The synthesis of new low-temperature thermochronologic data presented in this study together with previously published geo/thermochronology, structural, metamorphic, and thermobarometry results elucidate the dynamic link between deep and shallow crust during continental extension in northern North American Cordillera. These data show that partial melting, high-grade metamorphism and associated deformation occurred during Paleocene-Eocene time in the Okanogan dome. The structures and P-T-t

paths obtained from the Okanogan gneiss dome are correlative with other gneiss domes exposed in the Shuswap MCC. All these gneiss domes record near-isothermal decompression from metamorphic conditions of ~800 °C and ≥ 10 kbar to ≤ 5 kbar followed by rapid cooling and exhumation via detachment tectonics around 50-45 Ma, synchronous with upper crustal extension (Thor-Odin dome; Lorencak et al., 2001; Norlander et al., 2002; Vanderhaeghe et al., 2003; Hinchey et al., 2006; Frenchman's Cap; Crowley et al., 2001; Gervais et al, 2010, 2011; Valhalla and Passmore domes; Gordon et al., 2008; Aberdeen complex; Glombick et al., 2006 a,b; Grand Forks complex; Cubley et al., 2012, 2013).

The timing of crystallization of migmatites and crosscutting pegmatite bodies has been determined from ca. 59-49 Ma U-Pb zircon rim and monazite ages sampled at Stowe Mountain (Fig. 3.2; Kruckenberg et al., 2008). The ca. 47 Ma titanite U-Pb age and biotite $^{40}Ar/^{39}Ar$ ages ranging between 48-47 Ma indicate the onset of rapid cooling of the footwall rocks from crystallization of migmatite through the Ar closure temperature in biotite (~325 °C). Therefore, the emplacement of dome rocks beneath the detachment faults from ductile (melt-present) to brittle-ductile conditions was achieved within a few million years, with initial cooling rates in excess of 100 °C/my.

The low-temperature thermochronology data from the Okanogan dome document the temporal continuity from melt crystallization temperatures to near-surface conditions. ZHe thermochronometry yielded ages ranging between 51 to 41 Ma; these overlap with $^{40}Ar/^{39}Ar$ ages. ZHe ages systematically vary along the detachment fault, indicating that motion along the detachment fault was recorded by this chronometer. Such age progression corresponds to a slip rate of 3.7 km/my, which implies ~22 km of

horizontal offset and maximum 13 km vertical exhumation. Previous estimations of horizontal extension across the Okanogan detachment fault zone vary between 12 to 90 km based on geothermobarometric and geochronologic constraints (Parkinson, 1985; Glombick et al., 2006b; Brown et al., 2012). This wide range results from different assumptions regarding the thermal state of the crust, geometry of the fault zone, and the amount of vertical thinning and vertical flow of migmatites.

Results of AFT chronometry show a broad age distribution, ranging between 50 and 23 Ma, across the dome. Even though it is not clear, owing to large analytical errors, whether AFT ages record tectonic exhumation, the overlap between AFT and ZHe ages in Traverse 1 (Fig. 3.5) and the relatively low (~10-30 °C/my) cooling rates recorded by ZHe -AFT age pairs suggests that AFT ages, at least in part, reflect rapid erosional exhumation likely linked to the isostatic rebound of footwall rocks.

AHe chronometry yielded ages ranging from 48 to 28 Ma, although the majority of ages are ≥ 40 Ma. The concordance of AHe ages with higher temperature chronometers in some samples (e.g. OK-319, OK-320; Table 3.1) and the decrease in ages in a direction parallel to tectonic transport across the dome (Fig. 3.5) could be interpreted as cooling below the AHe closure temperature as a result of tectonic exhumation. However, the ca. 40-20 Ma AHe ages obtained from the hanging-wall of the Okanogan dome (Callahan, 2007), a range similar to those in the footwall, suggest that AHe chronometry does not reflect tectonic exhumation. Instead, we interpret AHe ages from the footwall units to record cooling related to regional erosion after the exhumation of deep crustal rocks at ca. 45 Ma. Therefore, both AFT and AHe ages are likely related to erosional exhumation and not tectonic denudation.

In summary, all geo-and thermochronological, thermobarometric data, and field observations from the Okanogan dome indicate that thinning and necking of the brittle upper crust was isostatically compensated by the flow of partially molten lower crust. Rapid exhumation and cooling of the crust was chiefly achieved by detachment faulting between ca. 51-45 Ma with a minor contribution from erosional denudation.

Numerical models that address the P-T-strain history of partially molten mid-crustal rocks during exhumation beneath a detachment fault predict rapid vertical flow of material to shallow depths under extended regions in the upper crust (Fig. 3.9, Rey et al., 2009 a, b; 2011; Whitney et al., 2013). Sensitive to thermal and kinematic conditions, these models predict different T-t, P-T, and cooling rate-t paths for exhumed mid-crustal rocks under fast (few cm/yr) and slow (mm/yr) extension rates (Fig. 3.9). If subjected to fast extension rates, migmatites record near-isothermal decompression followed by rapid cool along a high geothermal gradient (35 to 65 °C/km) over a few million years, and yield narrow range of ages from high-to-low temperature, similar to what has been documented at Shuswap MCC (Fig. 3.9; Rey et al., 2009b). In detail, however, each rock unit experiences a different cooling path depending on its structural position: rocks closer to the detachment fault zone cool rapidly earlier in their exhumation path, whereas rocks located in deeper levels of the crust cool more slowly (Fig. 3.9). Therefore, the combined results of this study and previous work are consistent with the presence of large volumes of partially molten middle crust in the Cordilleran hinterland, which rapidly exhumed and cooled at the boundary between cold foreland (Rocky Mountains) and melt rich hinterland (Omineca Belt) in Paleocene-Eocene (Teyssier et al., 2005).

Low-temperature thermochronometers can be used to document the timing of creation and/or modification of surface morphology as lithospheric-scale deformation profoundly affects the construction of topography and relief development. In the North American Cordillera, stable isotope paleoaltimetric data from detachment faults and syntectonic basins have been interpreted to document migration of a topographic wave from north to south, beginning in the southern Canadian Cordillera in the early Eocene (~50 Ma) and reaching southern Nevada by the Oligocene (~23 Ma) (e.g., Chamberlain et al., 2012). Hydrogen isotope data from white mica and quartz in quartzite in the fault that bounds the Shuswap MCC on its eastern edge suggest mean paleoelevation estimates of ≥ 4 km at British Columbia (Fig 3.1, Thor-Odin dome) and ≥ 3 km in Washington (Kettle dome), indicating ~1 km of orogen-parallel variations in topography (Mulch et al., 2007). Paleoaltimetry analysis from the syntectonic basins, on the other hand, indicates lower paleoelevations (~2.5-2.9 km, Wolfe et al., 1998). This suggests 0.5-1 km of relief between basins and neighboring highlands, similar to sedimentological observations in these basins (McClaughry and Gaylord, 2005). Therefore, preservation of Eocene ages (50-45 Ma) in low-T thermochronometers, especially in AFT and AHe ages, from the Okanogan and Thor-Odin domes (Toraman et al., 2012), document that exhumation of mid-crustal rocks led to production of local relief between the hanging-wall (relatively low-standing sedimentary basins) and footwall regions (fault-bounded igneous and metamorphic rocks). These results further suggest that extensional exhumation and thermal reorganization of the orogenic crust during Paleocene-Eocene in the northern Cordillera was temporally and kinematically linked from the deep crust to the Earth's surface.

References

Armstrong, R.L., 1982, Cordilleran metamorphic core complexes; from Arizona to southern Canada: Annual Review of Earth and Planetary Sciences, v. 10, p. 129-154.

Axen, G. J., Lam, P. S., Grove, M., Stockli, D. F., & Hassanzadeh, J., 2001, Exhumation of the west-central Alborz Mountains, Iran, Caspian subsidence, and collision-related tectonics: Geology, 29(6), 559-562.

Brandon, M. T., Roden-Tice, M. K., & Garver, J. I., 1998, Late Cenozoic exhumation of the Cascadia accretionary wedge in the Olympic Mountains, northwest Washington State: Geological Society of America Bulletin, 110(8), 985-1009.

Brichau, S., Ring, U., Carter, A., Bolhar, R., Monié, P., Stockli, D., & Brunel, M., 2008, Timing, slip rate, displacement and cooling history of the Mykonos detachment footwall, Cyclades, Greece, and implications for the opening of the Aegean Sea basin: Journal of the Geological Society, 165(1), 263-277.

Brown, S.R., Gibson, H.D., Andrews, G.D.M., Thorkelson, D.J., Marshall, D.D., Vervoot, J.D., and Rayner, N., 2012, New constrains on Eocene extension within the Canadian Cordillera and identification of Phanerozoic protoliths for footwall gneisses of the Okanagan Valley shear zone: Lithosphere, 4, 4, 354-377.

Callahan, O.A., 2007, Exhumation and topographic development of the Okanogan Range, northeast North Cascades [Master Thesis]: Bellingham, Western Washington University, 207 p.

Carlson, D.H., and Moye, F.J., 1990, The Colville igneous complex: Paleogene volcanism, plutonism, and extension in northeastern Washington, *in* Anderson, J.L., ed., The nature and origin of Cordilleran magmatism: Boulder, Colorado, Geological Society of America Memoir, v. 174, p. 375–394.

Carlson, W.D., Donelick, R.A., and Ketcham, R.A., 1999, Variability of apatite fission-track annealing kinetics I: Experimental results: American Mineralogist, 9, 1213–1223.

Chamberlain, C. P., Mix, H. T., Mulch, A., Hren, M. T., Kent-Corson, M. L., Davis, S. J., Horton, T.W., & Graham, S. A., 2012, The Cenozoic climatic and topographic evolution of the western North American Cordillera: American Journal of Science, 312(2), 213-262.

Cheney, E.S., 1980, Kettle dome and related structures of northeastern Washington, *in* Crittenden, M.D., Coney, P.J., Davis, G.H., eds., Cordilleran Metamorphic Complexes: Boulder, Colorado, Geological Society of America Memoir, v. 153, p. 463-483.

Church, N. B., 1973, Geology of the White Lake basin: British Columbia Dept. of Mines Petroleum Resources Bull., v. 61, p. 120

Coney, P.J., and Harms, T.A., 1984, Cordilleran metamorphic core complexes:Cenozoic extensional relics of Mesozoic compression: Geology, v. 12, p. 550-554.

Coney, P.J., 1980, Cordilleran metamorphic core complexes; an overview, *in* Crittenden, M.D., Coney, P.J., Davis, G.H., eds., Cordilleran metamorphic core complexes: Boulder, Colorado, Geological Society of America Memoir, p. 7-31.

Crittenden, M.D., Coney, P.J., and Davis, G.H., 1980, Cordilleran metamorphic core

complexes: Geological Society of America Memoir, v. 153, 490 p.

Crowley, J.L., Brown, R.L., and Parrish, R.R., 2001, Diachronous deformation and a strain gradient beneath the Selkirk allochthon, northern Monashee complex, southeastern Canadian Cordillera: Journal of Structural Geology 23, 1103-1121.

Cubley, J. F., Pattison, D. R. M., Archibald, D. A., & Jolivet, M., 2013, Thermochronological constraints on the Eocene exhumation of the Grand Forks complex, British Columbia, based on 40Ar/39Ar and apatite fission track geochronology: Canadian Journal of Earth Sciences, 50(5), 576-598.

Cubley, J. F., Pattison, D. R. M., Tinkham, D. K., & Fanning, C. M., 2012, U-Pb geochronological constraints on the timing of episodic regional metamorphism and rapid high-T exhumation of the Grand Forks complex, British Columbia: Lithos, v. 156, p. 241-267

DeCelles, P.G., 2004, Late Jurassic to Eocene evolution of the Cordilleran thrust belt and foreland basin system, western U.S.A.: American Journal of Science, 304, 105–168.

Dewey, J. F., 1998, Extensional collapse of orogens: Tectonics, 7(6), 1123-1139.

Donelick, R. A., & Miller, D. S., 1991, Enhanced tint fission track densities in low spontaneous track density apatites using ^{252}Cf-derived fission fragment tracks: A model and experimental observations: International Journal of Radiation Applications and Instrumentation. Part D. Nuclear Tracks and Radiation Measurements, 18(3), 301-307.

Donelick, R. A., Ketcham, R. A., and Carlson, W. D., 1999, Variability of apatite fission-track annealing kinetics: II. Crystallographic orientation effects: American Mineralogist, 84, 1224-1234.

Donelick, R.A., O'Sullivan, P.B., and Ketcham, R.A., 2005, Apatite fission track analysis: Reviews in Mineralogy and Geochemistry, vol. 58, 49-94.

Duncan, I.J., 1984, Structural evolution of the Thor-Odin gneiss dome: Tectonophysics, 101, 87-130.

Dunkl, I., 2002, TRACKKEY: a Windows program for calculation and graphical presentation of fission track data: Computers & Geosciences, 28(1), 3-12.

Eyal, Y., Osadetz, K. G., & Feinstein, S., 2006, Evidence for reactivation of Eocene joints and pre-Eocene foliation planes in the Okanagan core-complex, British Columbia, Canada: Journal of Structural Geology, 28(11), 2109-2120.

Farley, K.A., 2000, Helium diffusion in apatite: General behavior as illustrated by Durango fluorapatite: Journal of Geophysical Research, 105, 2903-2914.

Farley, K.A., 2002, (U-Th)/He dating: Techniques, calibrations, and applications: Reviews in Mineralogy and Geochemistry, vol. 47, 819-844.

Fayon, A. K., Peacock, S. M., Stump, E., & Reynolds, S. J., 2000, Fission track analysis of the footwall of the Catalina detachment fault, Arizona: Tectonic denudation, magmatism, and erosion: Journal of Geophysical Research Solid Earth, 105(B5), 11047-11062.

Fayon, A.K., D.L. Whitney, and Teyssier, C., 2004, Exhumation of orogenic crust: diapiric ascent vs. low-angle normal faulting, *in* Whitney, D.L., Teyssier, C.,

Siddoway, C.S., eds. Gneiss Domes and Orogeny: Boulder, Colorado, Geological Society of America Special Paper 380, pp. 129-139.

Fleischer, R. L., P. B. Price, and Walker, R. M., 1975, Nuclear Tracks in Solids: Berkeley, California, University of California Press, 605 p.

Flowers, R. M., Ketcham, R. A., Shuster, D. L., and Farley, K. A., 2009, Apatite (U-Th)/He thermochronometry using a radiation damage accumulation and annealing model: Geochimica et. Cosmochimica Acta, 73(8), 2347–2365, doi:10.1016/j.gca.2009.01.015.

Foster, D. A., and John, B. E., 1999, Quantifying tectonic exhumation in an extensional orogen with thermochronology: Examples from the southern Basin and Range province escape, *in* Ring, U., Brandon, M.T., Lister, G., S., Willett, S.D., eds., Exhumation Processes: Normal Faulting, Ductile Flow and Erosion: London, Geological Society of London Special Publications 154, pp. 87-107.

Foster, D.A., Grice, W.C.Jr., and Kalakay, T.J., 2010, Extension of the Anaconda metamorphic core complex: 40Ar/39Ar thermochronology and implications for Eocene tectonics of the northern Rocky Mountains and the Boulder batholith: Lithosphere, v. 2, p. 232–246,doi:10.1130/L94.1.

Fox, K.F., Jr., Rinehart, C.D., Engels, J.C., and Stern, T.W., 1976, Age of emplacement of the Okanogan gneiss dome, North-central Washington: Geological Society of America Bulletin, v. 87, p. 1217-1224.

Fox, K.F., Jr., Rinehart, C.D., and Engels, J.C., 1977, Plutonism and orogeny in North-central Washington; timing and regional context: Alexandria, Virginia, U.S. Geological Survey Professional Paper 989, 32 p.

Galbraith, R. F., & Laslett, G. M., 1993, Statistical models for mixed fission track ages: Nuclear Tracks and Radiation Measurements, 21(4), 459-470.

Gébelin, A., Mulch, A., Teyssier, C., Heizler, M., Vennemann, T., Seaton, N. C. A., 2011, Oligo-Miocene extensional tectonics and fluid flow across the Northern Snake Range detachment system, Nevada: Tectonics, 30, TC5010, doi:10.1029/2010TC002797.

Gervais, F., and Brown, R. L., 2011, Testing modes of exhumation in collisional orogens: Synconvergent channel flow in the southeastern Canadian Cordillera: Lithosphere, 3(1), 55-75.

Gervais, F., Brown, R. L., and Crowley, J. L., 2010, Tectonic implications for a Cordilleran orogenic base in the Frenchman Cap dome, southeastern Canadian Cordillera: Journal of Structural Geology, 32(7), 941-959.

Gleadow, A. J. W., & Duddy, I. R., 1981, A natural long-term track annealing experiment for apatite: Nuclear Tracks, 5(1), 169-174.

Gleadow, A. J. W., Duddy, I. R., Green, P. F., and Lovering, J. F., 1986, Confined track lengths in apatite: A diagnostic tool for thermal history analysis: Contributions to Mineralogy and Petrology, 94 (4), 405-415.

Glombick, P., R.I. Thompson, P. Erdmer, L. Heaman, R.M. Friedman, M. Villeneuve, and Daughtry, K.L., 2006a, U-Pb constraints on the thermotectonic evolution of the Vernon antiform and the age of the Aberdeen gneiss complex, southeastern Canadian Cordillera: Canadian Journal of Earth Science, 43, 213-244.

Glombick, P., Thompson, R. I., Erdmer, P., & Daughtry, K. L., 2006b, A reappraisal of the tectonic significance of early Tertiary low-angle shear zones exposed in the

Vernon map area (82 L), Shuswap metamorphic complex, southeastern Canadian Cordillera: Canadian Journal of Earth Sciences, 43(2), 245-268.

Goergen, E. T., and Whitney, D. L., 2012a, Long length scales of element transport during reaction texture development in orthoamphibole-cordierite gneiss: Thor-Odin dome, British Columbia, Canada: Contributions to Mineralogy and Petrology, 163(2), 337-352.

Goergen, E. T., and Whitney, D.L., 2012, Corona networks as three-dimensional records of transport scale and pathways during metamorphism: Geology, 40(2), 183-186.

Goodge, J.W., and Hansen, V.L., 1983, Petrology and structure of rocks in the southwest portion of Okanogan Dome, north-central Washington: Northwest Geology, 12, 13-24.

Gordon, S. M., Whitney, D. L., Teyssier, C., Grove, M., and Dunlap, W. J., 2008, Timescales of migmatization, melt crystallization, and cooling in a Cordilleran gneiss dome: Valhalla complex, southeastern British Columbia: Tectonics, 27, TC4010, doi:10.1029/2007TC002103.

Gottardi, R., Kao, P. H., Saar, M. O., & Teyssier, C., 2013, Effects of permeability fields on fluid, heat, and oxygen isotope transport in extensional detachment systems: Geochemistry, Geophysics, Geosystems, p. 1-30.

Gottardi, R., Teyssier, C., Mulch, A., Vennemann, T.W., and Wells, M.L., 2011, Preservation of an extreme transient geotherm in the Raft River detachment shear zone: Geology, 39, 8, 759-762.

Hansen, V. L., & Goodge, J. W., 1988, Metamorphism, structural petrology, and regional evolution of the Okanogan complex, northeastern Washington, *in* Ernst,

W.G., ed., Metamorphism and Crustal Evolution of the Western United States, Rubey Colloq. Series vol. 7: Englewood Cliffs, N.J., Prentice-Hall, pp. 233-270.

Hinchey, A.M., Carr, S.D., McNeill, P.D., and Rayner, N., 2006, Paleocene-Eocene high-grade metamorphism, anatexis, and deformation in the Thor-Odin dome, Monashee complex, southeastern British Columbia: Canadian Journal of Earth Sciences, 43, 1341-1365.

Holder, R.W., and Holder, G.A., 1988, The Colville Batholith; Tertiary plutonism in Northeast Washington associated with graben and core-complex (gneiss dome) formation: Geological Society of America Bulletin, 100, 1971-1980.

Holder, G. A. M., Holder, R. W., & Carlson, D. H., 1990, Middle Eocene dike swarms and their relation to contemporaneous plutonism, volcanism, core-complex mylonitization, and graben subsidence, Okanogan Highlands, Washington: Geology, 18(11), 1082-1085.

Ketcham, R. A., Carter, A., Donelick, R. A., Barbarand, J., and Hurford, A. J., 2007a, Improved measurement of fission-track annealing in apatite using c-axis projection: American Mineralogist, 92 (5-6), 789-798.

Ketcham, R. A., Carter, A., Donelick, R. A., Barbarand, J., and Hurford, A. J., 2007b, Improved modeling of fission-track annealing in apatite: American Mineralogist, 92(5-6), 799-810.

Ketcham, R. A., 1996, Thermal models of core-complex evolution in Arizona and New Guinea: Implications for ancient cooling paths and present-day heat flow: Tectonics, 15(5), 933-951.

Ketcham, R. A., 2003, Observations on the relationship between crystallographic orientation and biasing in apatite fission-track measurements: American Mineralogist, 88 (5-6), 817-829.

Ketcham, R. A. (2005), Forward and inverse modeling of low-temperature thermochronometry data: Reviews in Mineralogy and Geochemistry, 58 (1), 275-314.

Kruckenberg, S.C., Whitney, D.L., Teyssier, C., Fanning, M., and Dunlap, W.J., 2008, Paleocene-Eocene migmatite crystallization, extension, and exhumation in the hinterland of the northern Cordillera: Okanogan dome, Washington USA: Geological Society of America Bulletin, 120(7-8), 912-929.

Kruckenberg, S. C., and Whitney, D.L., 2011, Metamorphic evolution of sapphirine-and orthoamphibole-cordierite-bearing gneiss, Okanogan dome, Washington, USA: Journal of Metamorphic Geology, 29(4), 425-449.

Laslett, G. M., Kendall, W. S., Gleadow, A. J. W., & Duddy, I. R., 1982, Bias in measurement of fission-track length distributions: Nuclear Tracks and Radiation Measurements, 6(2), 79-85.

Lister, G.S., Banga, G., and Feenstra, A., 1984, Metamorphic core complexes of Cordilleran type in the Cyclades, Aegean Sea, Greece: Geology, 12, 221-225.

Lorencak, M., Seward, D., Vanderhaeghe, O., Teyssier, C., and Burg, J.P., 2001, Low-temperature cooling history of the Shuswap metamorphic core complex, British Columbia: Constraints from apatite and zircon fission-track ages: Canadian Journal of Earth Sciences, 38, 1615-1625.

Mathews, W.H., 1981, Early Cenozoic resetting of potassium-argon dates and geothermal history of north Okanagan area, British Columbia: Canadian Journal of Earth Sciences, v. 18, p. 1310–1319.

McClaughry, J. D., & Gaylord, D. R., 2005, Middle Eocene sedimentary and volcanic infilling of an evolving supradetachment basin: White Lake Basin, south-central British Columbia: Canadian Journal of Earth Sciences, 42(1), 49-66.

Monger, J.W.H., Price, R.A., and Tempelman-Kluit, D.J., 1982, Tectonic accretion and the origin of the two major metamorphic and plutonic welts in the Canadian Cordillera: Geology, 10, 70-75.

Morrison, J., and Anderson, J. L., 1998, Footwall refrigeration along a detachment fault: implications for thermal evolution of core complexes: Science, v. 279, p. 63-66

Mulch, A., Teyssier, C., Cosca, M. A., and Chamberlain, C. P., 2007, Stable isotope paleoaltimetry of Eocene core complexes in the North American Cordillera: Tectonics, v. 26., TC4001, doi:10.1029/2006TC001995.

Mulch, A., Teyssier, C., Cosca, M. A., Vanderhaeghe, O., and Vennemann, T. W., 2004, Reconstructing paleoelevation in eroded orogens: Geology, v. 32, p. 525-528.

Naeser C. W., Engels J. C. & Dodge F. C. W., 1970, Fission track annealing and age determinations of epidote minerals: Journal of Geophysical Research, 75, 1579 1584.

Norlander, B.H., Whitney, D.L., Teyssier, C., Vanderhaeghe, O., and Wiebe, R.A., 2002, Partial melting and decompression of the Thor-Odin Dome, Shuswap metamorphic core complex, Canadian Cordillera: Lithos, v. 61, p. 103-125.

O'Sullivan, P. B., & Parrish, R. R., 1995, The importance of apatite composition and single-grain ages when interpreting fission track data from plutonic rocks: a case

study from the Coast Ranges, British Columbia: Earth and Planetary Science Letters, 132(1), 213-224.

Okulitch, A.V., 1984, The role of the Shuswap metamorphic complex in Cordilleran tectonism; a review: Canadian Journal of Earth Sciences, 21, 1171-1193.

Parkinson, D., 1985, Geochronology of the western side of the Okanogan metamorphic core complex, southern B.C.: Geological Society of America Abstracts with Programs, 17, 399.

Parrish, R.R., S.D. Carr, and Parkinson, D.L., 1988, Eocene extensional tectonics and geochronology of the southern Omineca belt, British Colombia and Washington: Tectonics, v. 7, p. 181-212.

Pearson, R.C., and Obradovich, J.D., 1977, Eocene rocks in Northeast Washington; radiometric ages and correlation: Washington, U.S. Geological Survey Bulletin, 50 p.

Person, M. P., Mulch, A., Teyssier, C., Gao, Y., 2007, Isotope Transport and Exchange During Detachment Tectonics, Shuswap Metamorphic Core Complex, British Columbia: American Journal of Science, v. 307, p. 555-589.

Reiners, P.W., 2005, Zircon (U-Th)/He thermochronometry: Reviews in Mineralogy and Geochemistry, v. 58, 151-179.

Reiners, P.W., Spell, T.L., Nicolescu, S., and Zanetti, K.A., 2004, Zircon (U-Th)/He thermochronometry: He diffusion and comparison with Ar/Ar dating: Geochimica et Cosmochimica Acta, 68, 1857-1887.

Reiners, P. W., Zhou, Z., Ehlers, T. A., Xu, C., Brandon, M. T., Donelick, R. A., and Nicolescu, S. (2003), Post-orogenic evolution of the Dabie Shan, eastern China,

from (U-Th)/He and fission-track dating: American Journal of Science, 303, 489 – 518.

Rey, P., Teyssier, C., and Whitney, D.L., 2009a, Extension rates, crustal melting and core complex dynamics: Geology, 37, 391– 394.

Rey, P.F., Teyssier, C., and Whitney, D.L., 2009b, The Role of Partial Melting and Extensional Strain Rates in the Development of Metamorphic Core Complexes: Tectonophysics, v. 477, p. 135–144.

Rey, P.F., Teyssier, C., Kruckenberg, S.C., and Whitney, D.L., 2011, Viscous collision in channel explains double domes in metamorphic core complexes: Geology, 39, 4, 387-390

Robinson, A. C., Yin, A., Lovera, O.M., 2007, The role of footwall deformation and denudation in controlling cooling age patterns of detachment systems: An application to the Kongur Shan extensional system in the Eastern Pamir: Tectonophysics, 496, 28-43.

Snook, J.R., 1965, Metamorphic and structural history of "Colville batholith" gneisses, north central Washington: Geological Society of America Bulletin, 76, 759-776.

Stockli, D. F., Farley, K. A., & Dumitru, T. A., 2000, Calibration of the apatite (U-Th)/He thermochronometer on an exhumed fault block, White Mountains, California: Geology, 28(11), 983-986.

Stockli, D.F., 2005, Application of low-temperature thermochronometry to extensional tectonic settings: Reviews in Mineralogy and Geochemistry, vol. 58, p. 420-461.

Stoffel, K.L., Joseph, N.L., Waggoner, S.Z., Gulick, C.W., Korosec, M.A., and Bunning, B.B., 1991, Geologic map of Washington Northeast Quadrant: Washington Division

of Geology and Earth Resources, Geologic Map GM-39, 1:250 000, 1 sheet, 44 p. text.

Stübner, K., Ratschbacher, L., Weise, C., Chow, J., Hoffman, J., Khan, J., Rutte, D., Sperner, B., Pfander, J.A., Hacker, B.R., Dunkl, I., Tichomirowa, M., Stearns, M.A., Bahram, I., Gadoev, M., Gloaguen, R., Jonckheere, R., Kanaev, E., Minaev, V., Oimahmadoc, I., Rajabov, N., Stanek, K.P., 2013, The giant Shakhdara migmatitic gneiss dome, Pamir, India–Asia collision zone, II: Timing of dome formation: Tectonics, (in press), DOI:10.1002/tect.20059.

Suydam, J.D., and Gaylord, D.R., 1997, Toroda Creek half graben, northeast Washington: Late-stage sedimentary infilling of a syn-extensional basin: Geological Society of America Bulletin, 109, 1333-1348.

Teyssier, C., Ferré, E.C., Whitney, D.L., Norlander, B., Vanderhaeghe, O., and Parkinson, D., 2005, Flow of partially molten crust and origin of detachments during collapse of the Cordilleran orogen, *in* Bruhn, D., Burlini, L., eds., High-strain zones: Structure and physical properties: London, Geological Society of London Special Publications, vol. 245pp. 39-64,.

Thomson, S.N., and Ring, U., 2006, Thermochronologic evaluation of post-collision extension in the Anatolide orogen, western Turkey: Tectonics, 25, TC3005, doi:10.1029/2005TC001833

Tirel, C., Brun, J.P., and Burov, E., 2004, Thermomechanical modeling of extensional gneiss domes, *in* Whitney, D.W., Teyssier, C., Siddoway, C.S., eds., Gneiss domes in orogeny: Boulder, Colorado, Geological Society of America Special Paper, 380, p. 67–78.

Toraman, E., Whitney, D.L., Teyssier, C., Fayon, A.K., Thomson, S.K., Reiners, P.W., 2012, Low-temperature thermochronology record of tectonic and erosional exhumation of gneiss domes in the northern North American Cordillera: Geological Society of America Abstract with Programs, vol. 44, no. 7, p.128

Vanderhaeghe, O., Teyssier, C., McDougall, I., and Dunlap, W.J, 2003, Cooling and exhumation of the Shuswap metamorphic core complex constrained by Ar/Ar thermochronology: Geological Society of America Bulletin, v 115, p. 200-216.

Wagner, G., and Van den Haute, P., 1992, Fission track dating: Dordrecht, Kluwer Academic Publishers, 285 p.

Wdowinski, S., and Axen, G.J., 1992, Isostatic rebound due to tectonic denudation: A viscous flow model of a layered lithosphere: Tectonics, 11, 303-315.

Whitney, D.L., Paterson, S.R., Schmidt, K.L., Glazner, A.F., and Kopf, C.F., 2004, Growth and demise of continental arcs and orogenic plateaux in the North American Cordillera: from Baja to British Columbia, *in* Grocott, J., McCaffrey, K.J.W., Taylor, G. and Tikoff, B., eds., Vertical Coupling and Decoupling in the Lithosphere: London, Geological Society of London Special Publications, vol. 227, pp. 167-176.

Whitney, D. L., Teyssier, C., Rey, P., and Buck, W. R., 2013, Continental and oceanic core complexes: Geological Society of America Bulletin, 125(3-4), 273-298.

Wolfe, J. A., Forest, C. E., and Molnar, P., 1998, Paleobotanical evidence of Eocene and Oligocene paleoaltitudes in midlatitude western North America: Geological Society of America Bulletin, v. 110, n. 5, p. 664–678.

Zeitler, P. K., Herczeg, A. L., McDougall, I., & Honda, M., 1987, U-Th-He dating of apatite: A potential thermochronometer: Geochimica et Cosmochimica Acta, 51(10), 2865-2868.

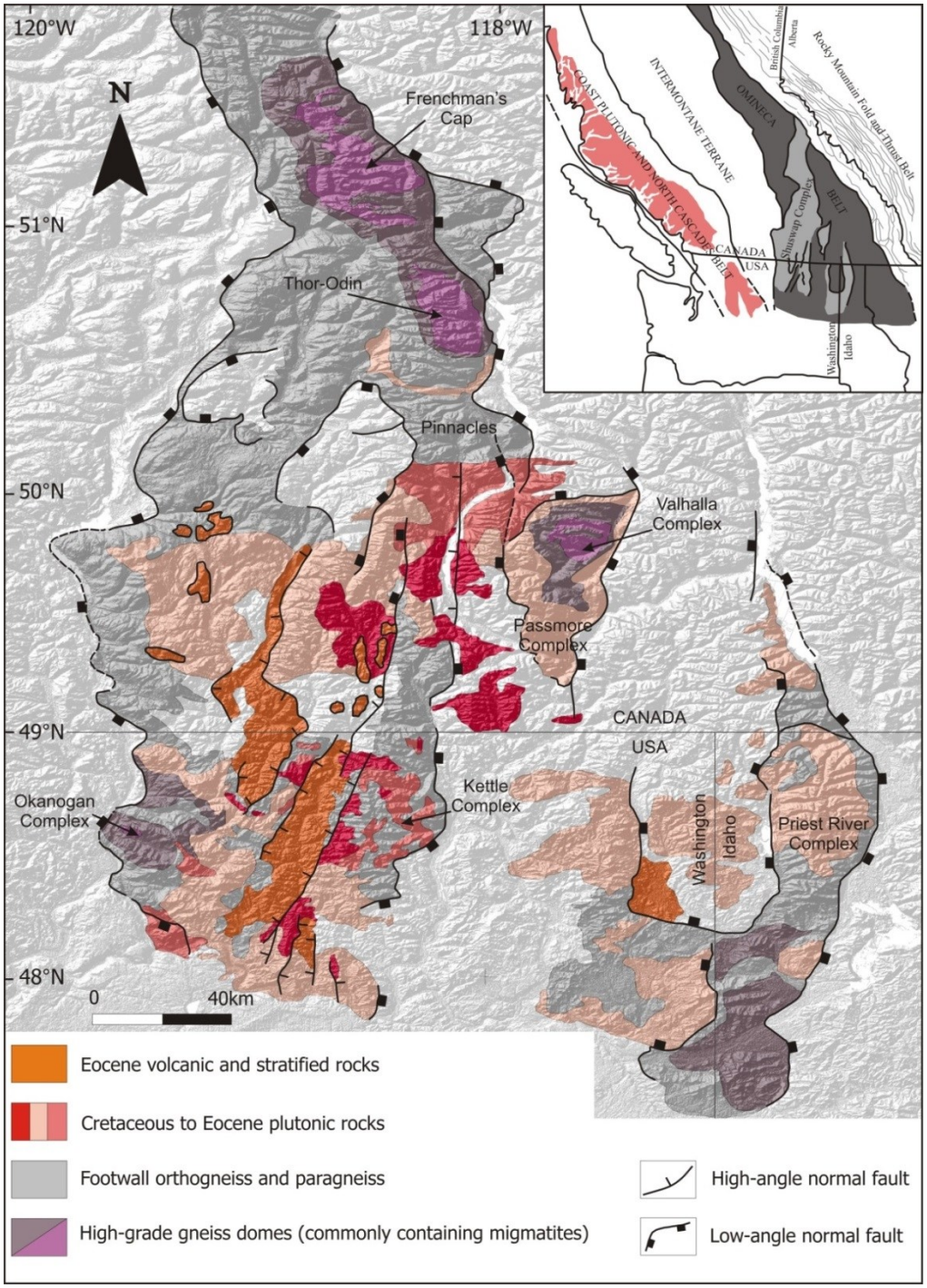

Figure 3.1. Simplified geologic map of the Omineca Belt (after Kruckenberg et al., 2008). Inset shows the location of the Omineca Belt and tectonic belts of the northern Cordillera.

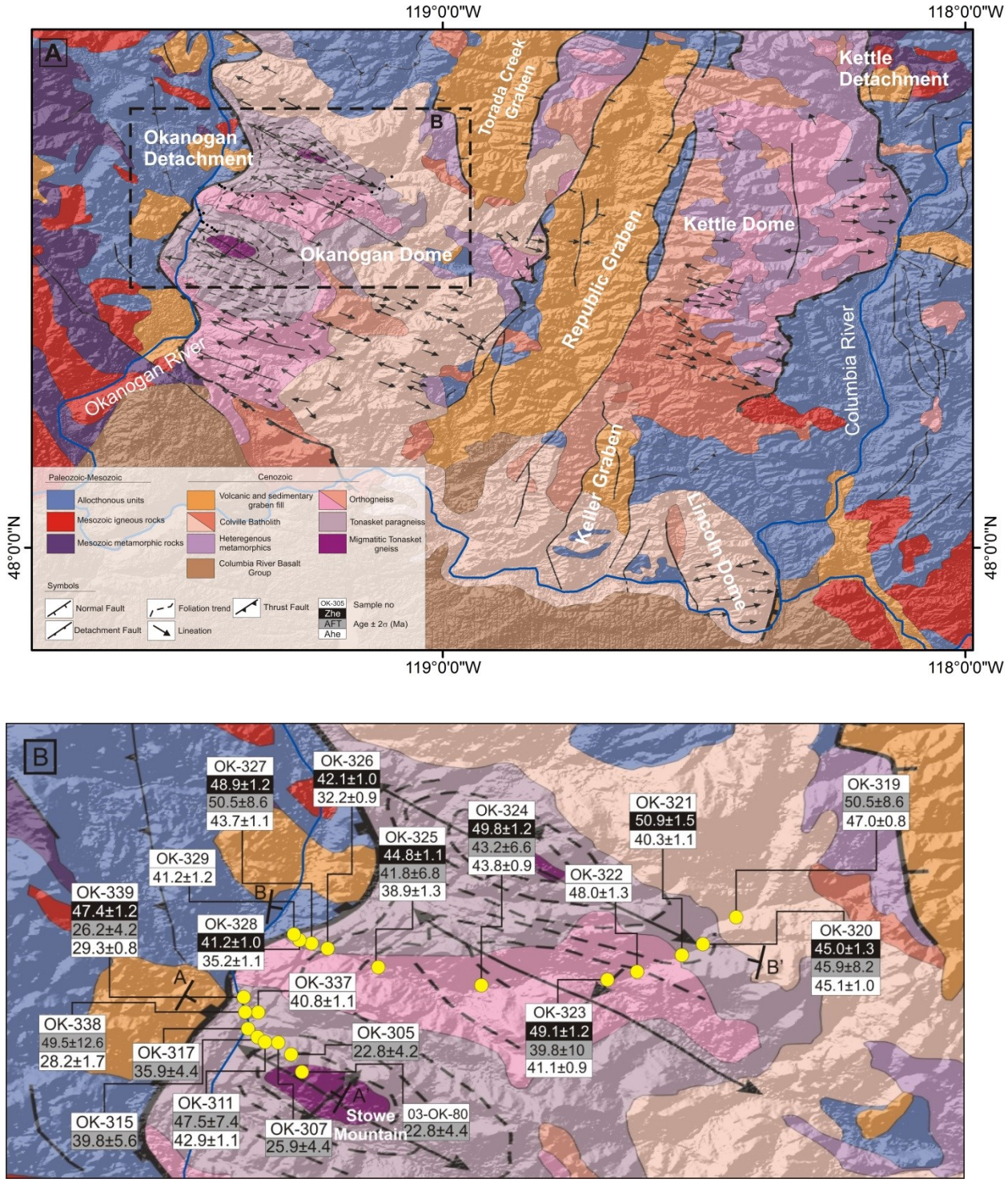

Figure 3.2. (A) Simplified geological map of the Okanogan Dome (after Stoffel et al., 1991 and Kruckenberg et al., 2008) (B) Enlargement of geological map showing sample locations, apatite/zircon (U-Th)/He and apatite fission track ages.

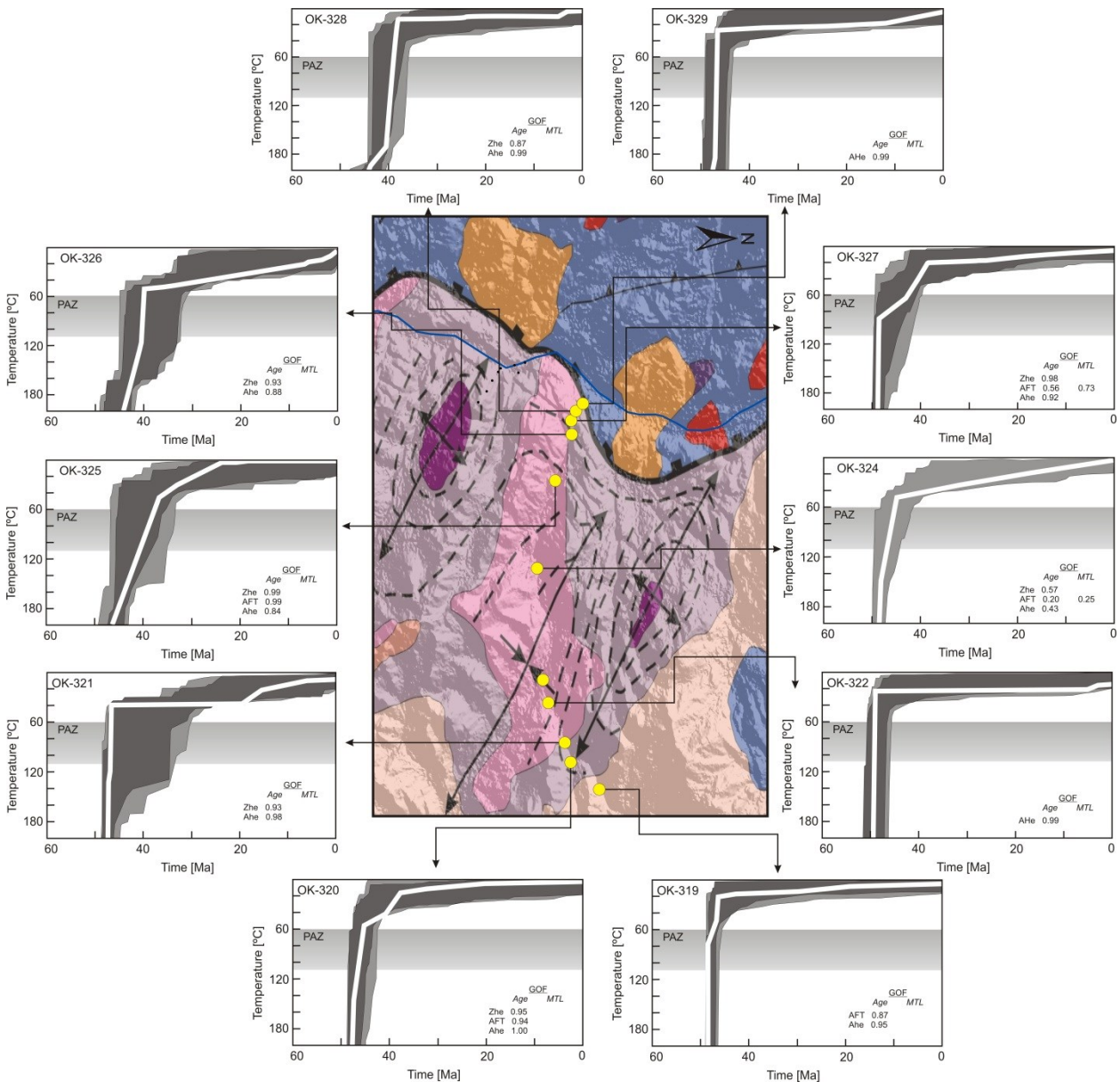

Figure 3.3. Thermal modeling results of the Traverse 1.Randomly generated good and acceptable solutions are shown in dark and light gray envelops. The best-fit solution is shown in white line. Light gray box represents apatite partial annealing zone. GOF; goodness of fit, MTL; mean track length.

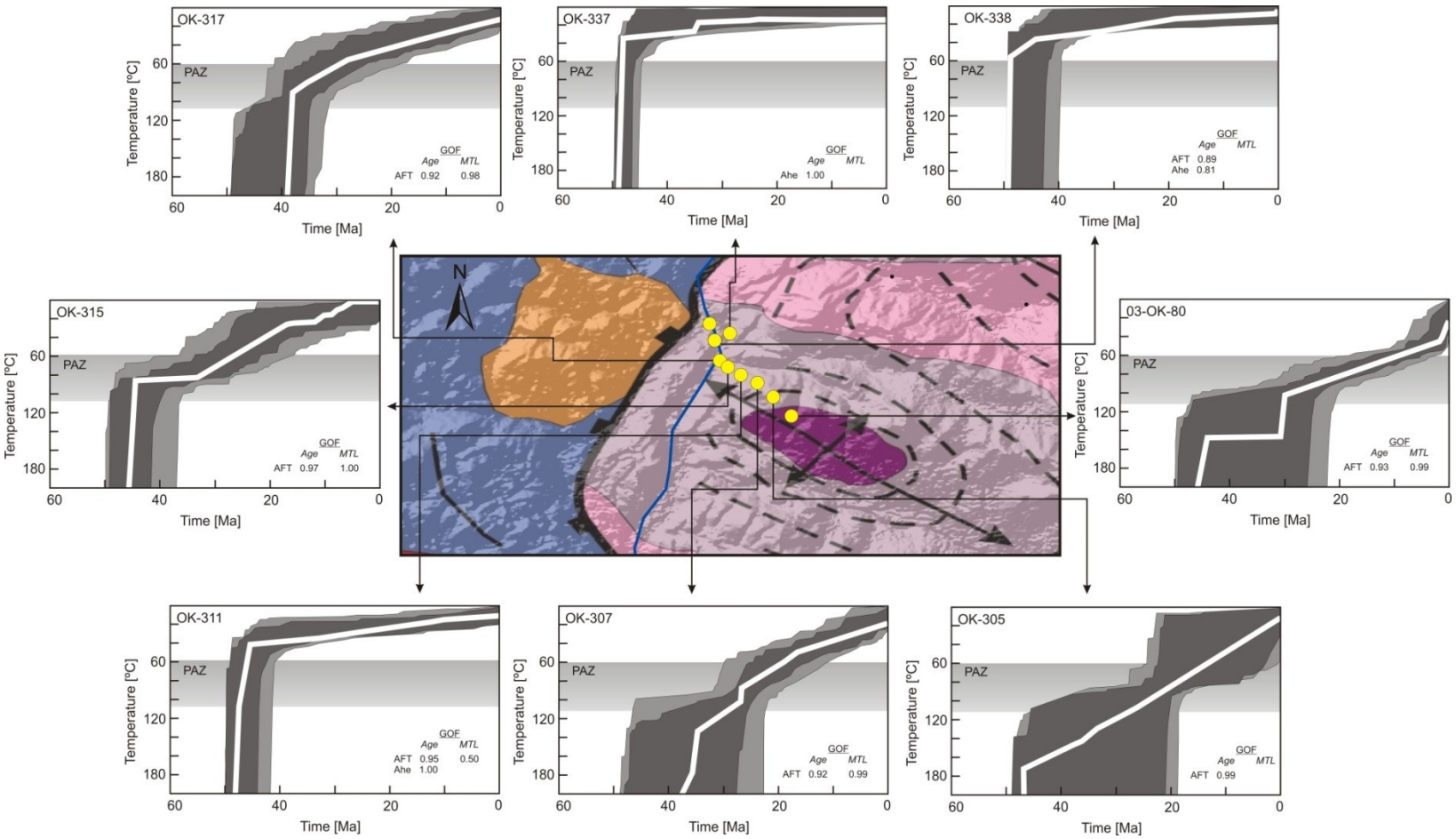

Figure 3.4. Results of thermal modeling of samples from the Traverse 2. Light and dark gray envelops correspond "acceptable" and "good" fit solutions, the best-fit temperature-time path is shown as a thick white line. Additionally apatite partial annealing zone (PAZ) is marked in each model. GOF; goodness of fit, MTL; mean track length.

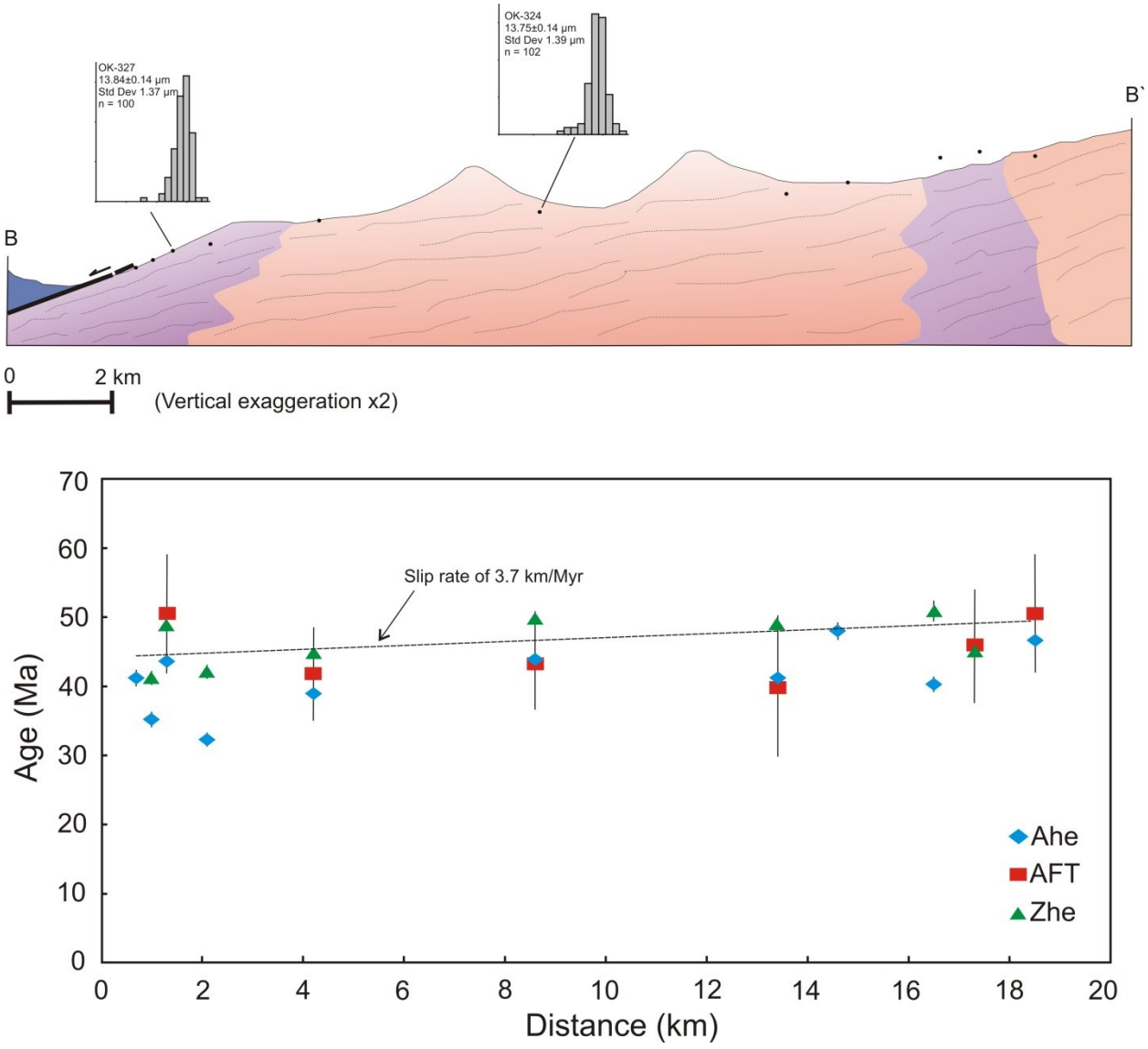

Figure 3.5. Simplified WNW-ESE geologic cross-section of the Traverse 1 along B-B' line, showing apatite track-length data. Some samples are projected on to profile plane. The lower panel shows age vs distance plot of all chronometers. The dashed-line represents the best-fit regression line (R^2=0.28) to zircon (U-Th)/He data, implying a slip rate of 3.7 km/my.

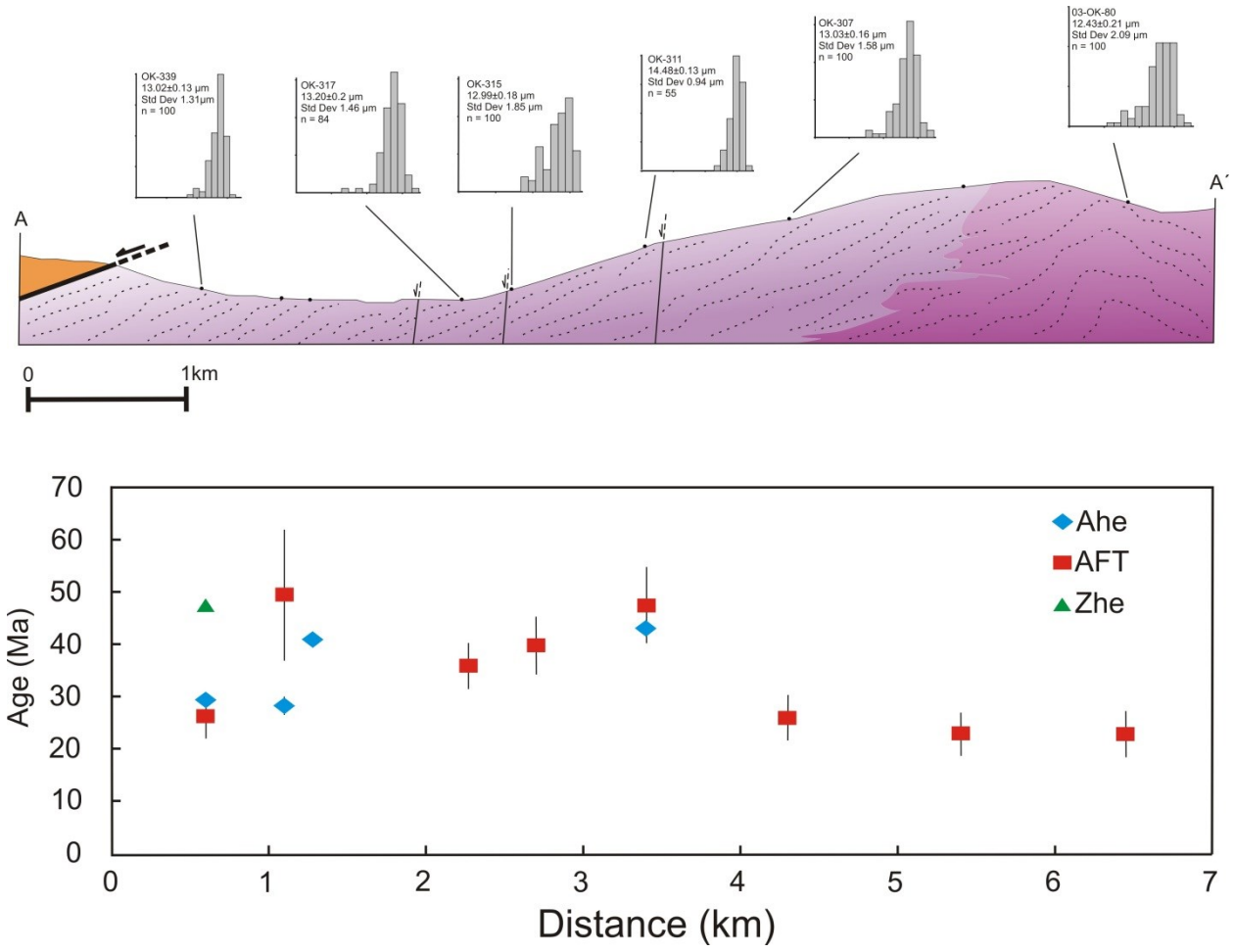

Figure 3.6. WNW-ESE geologic crossection of the Traverse 2 with track-length measurements. The lower panel shows age vs distance plot of all chronometers.

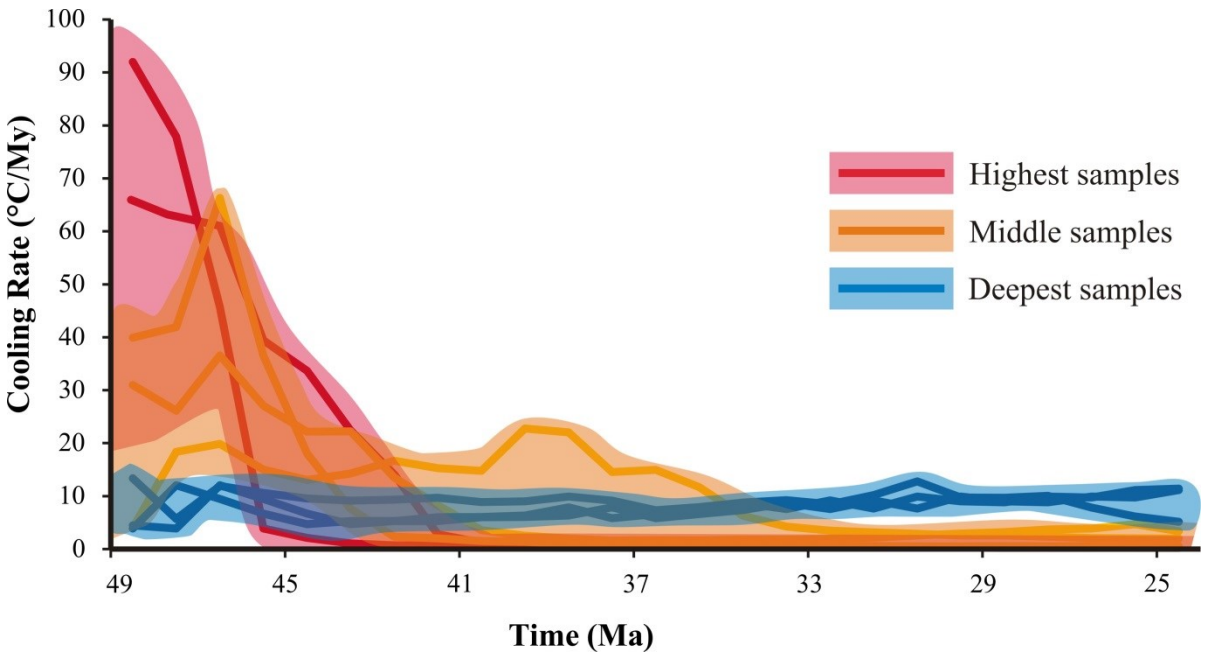

Figure 3.7. Plot of cooling rates calculated from "good" solutions from the HEFTY modeling in 1 million years interval from the Traverse 2. Samples are color-coded depending on their structural position; structurally deeper samples are blue, the middle samples are orange, and the highest samples are red.

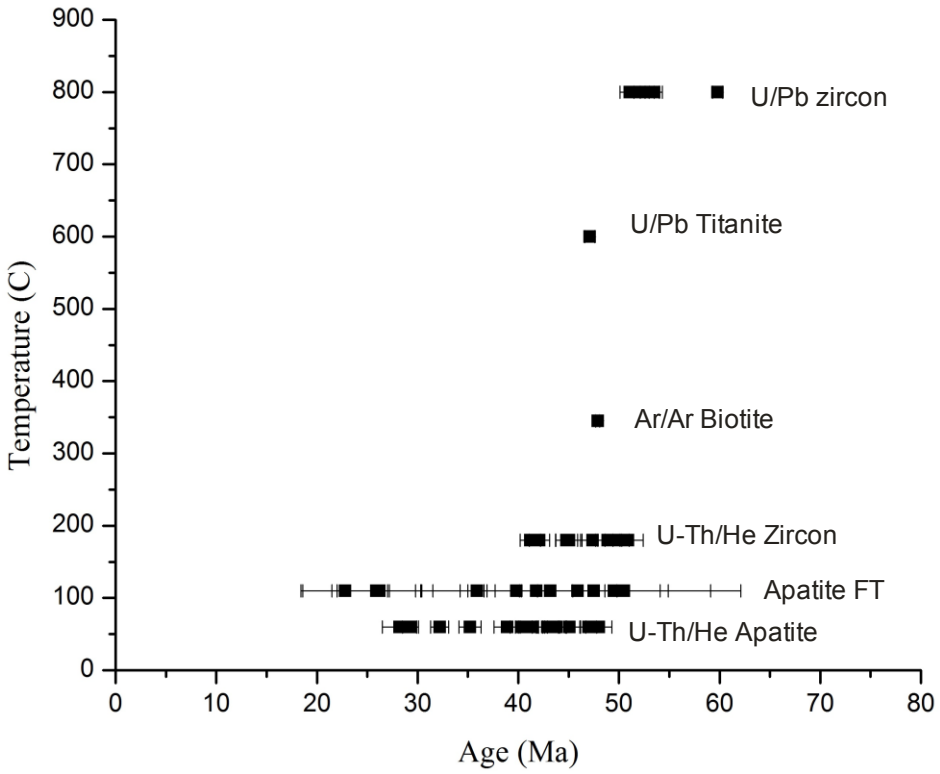

Figure 3.8. Temperature-time plot of geo/thermochronological data from the Okanogan dome. High-to-medium temperature age data (U-Pb and Ar/Ar) are from Kruckenberg et al. (2008).

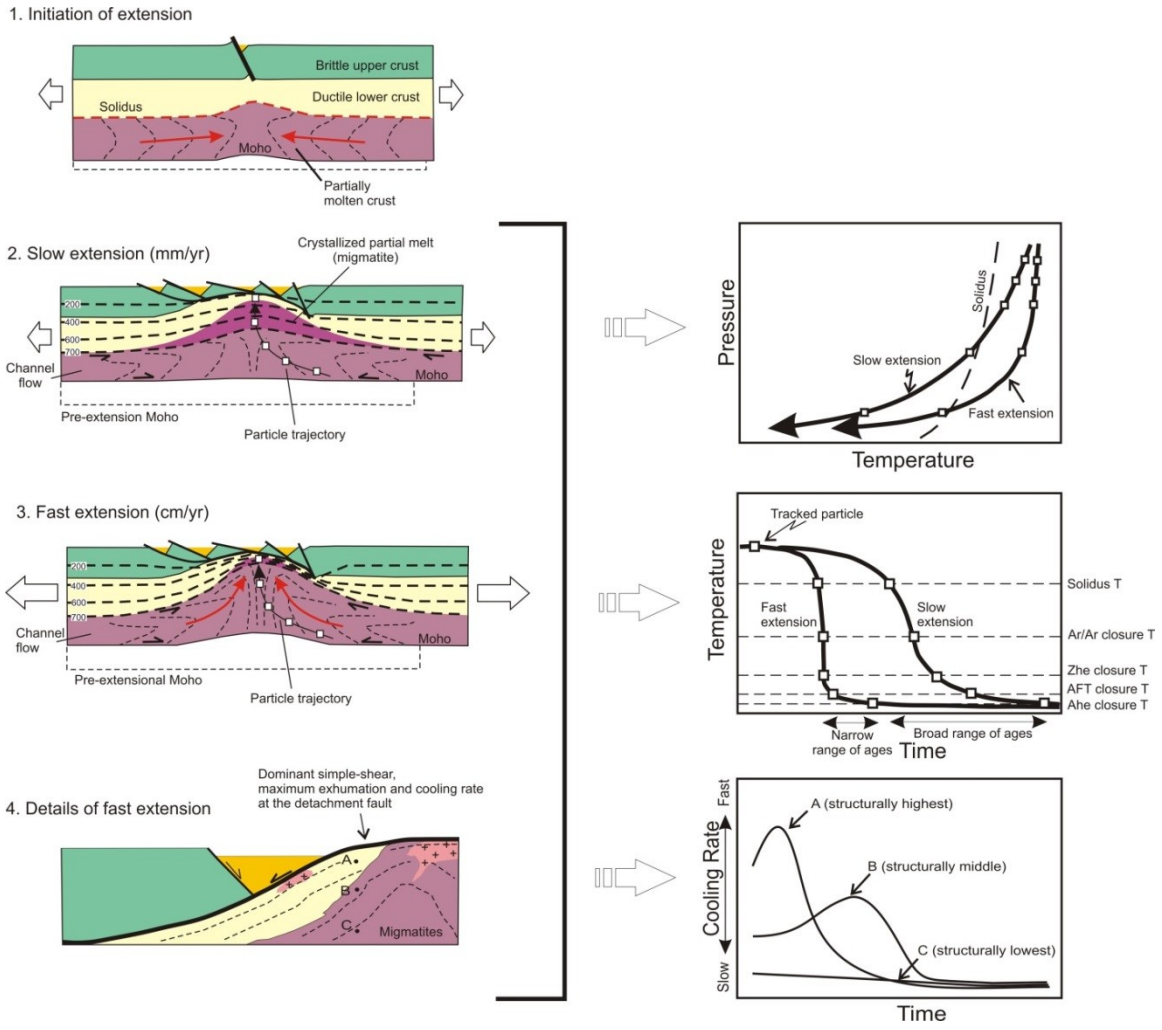

Figure 3.9. Conceptual figure showing different modes of crustal extension and expected P-T, T-t and cooling rate-t histories for fast and slow extension rate. Crustal extension models are after Whitney et al. (2013).

Table 3.1 Summary of Low-Temperature thermochronometric ages.

Sample Name	AHe Age ± 2σ (Ma)	AFT Age ± 2σ (Ma)	ZHe Age ± 2σ (Ma)	AFT Track Length ± SD (μm)
OK-305		22.8 ± 4.2		
OK-307		25.9 ± 4.4		13.03 ± 1.58
OK-311	42.9 ± 1.1	47.5 ± 7.4		14.48 ± 0.94
OK-315		39.8 ± 5.6		12.98 ± 1.85
OK-317		35.9 ± 4.4		13.20 ± 1.46
OK-319	47.0 ± 0.8	50.5 ± 8.6		
OK-320	45.1 ± 1.0	45.9 ± 8.2	45.0 ± 1.3	
OK-321	40.3 ± 1.1		50.9 ± 1.5	
OK-322	48.0 ± 1.3			
OK-323	41.1 ± 0.9	39.8 ± 10.0	49.1 ± 1.2	
OK-324	43.8 ± 0.9	43.2 ± 6.6	49.8 ± 1.2	13.75 ± 1.39
OK-325	38.9 ± 1.3	41.8 ± 6.8	44.8 ± 1.1	
OK-326	32.2 ± 0.9		42.1 ± 1.0	
OK-327	43.7 ± 1.1	50.5 ± 8.6	48.9 ± 1.2	13.84 ± 1.37
OK-328	35.2 ± 1.1		41.2 ± 1.0	
OK-329	41.2 ±1.2			
OK-337	40.8 ± 1.1			
OK-338	28.2 ± 1.7	49.5 ± 12.6		
OK-339	29.3 ± 0.8	26.2 ± 4.2	47.4 ± 1.2	13.02 ± 1.31
03-OK-80		22.8 ± 4.4		12.43 ± 2.09

Table 3.2. Single grain apatite (U-Th)/He replicate data.

Sample Number	Mass (μg)	mwar (μm)	U (ppm)	Th (ppm)	Sm (ppm)	He (nmol/g)	Raw Age (Ma)	Error (±1σ)	Corrected Age (Ma)	Error (±1σ)	HAC (Ft)	Eu (ppm)
OK-311-1	6.74	70.5	9.04	0.82	711	1.89	34.7	0.8	43.3	1.0	0.80	9.23
OK-311-2	6.68	78.0	4.41	0.40	286	0.93	35.5	0.9	44.0	1.1	0.81	4.50
OK-311-3	6.40	70.5	6.84	0.61	359	1.33	33.2	0.7	41.6	0.9	0.80	6.99
OK-319-1	12.9	81.3	7.75	3.50	298	1.89	39.1	0.6	47.0	0.8	0.83	8.57
OK-320-1	3.50	50.3	25.9	4.14	203	4.72	32.3	0.6	43.5	0.8	0.74	26.8
OK-320-2	2.73	42.5	28.8	5.25	237	5.51	33.6	0.7	47.5	0.9	0.71	30.1
OK-320-3	3.42	46.5	33.2	4.17	239	6.10	32.8	0.6	44.9	0.8	0.73	34.1
OK-321-1	1.06	37.8	3.22	1.53	38.5	0.39	19.9	0.9	31.0	1.4	0.64	3.58
OK-321-2	3.84	58.3	11.8	2.13	70.3	2.31	34.6	0.7	45.4	0.9	0.76	12.3
OK-321-3	1.35	37.3	20.9	6.09	75.8	3.14	25.9	0.5	39.4	0.8	0.66	22.4
OK-322-1	4.22	49.0	25.9	8.85	229	5.35	35.0	0.6	47.2	0.9	0.74	28.0
OK-322-2	3.99	61.0	20.4	9.37	216	4.64	37.5	0.7	49.0	0.9	0.77	22.6
OK-323-1	3.25	51.3	16.3	14.8	417	3.12	28.5	0.5	38.7	0.6	0.74	19.8
OK-323-2	1.55	41.3	14.8	37.4	291	3.57	27.6	0.6	41.4	0.8	0.67	23.6
OK-323-3	1.01	34.5	10.4	22.3	317	2.53	29.1	0.7	47.1	1.1	0.62	15.7
OK-324-1	7.60	68.3	26.3	3.83	132	5.04	34.2	0.6	42.6	0.8	0.80	27.2
OK-324-2	4.84	53.3	27.9	4.05	139	5.11	32.5	0.6	42.8	0.8	0.76	28.9
OK-324-3	2.85	48.0	24.7	6.30	162	4.82	33.9	0.7	46.6	0.9	0.73	26.1
OK-325-1	2.22	39.0	5.90	1.37	106	0.92	26.9	0.7	39.3	1.1	0.68	6.22
OK-325-2	1.42	37.0	6.40	4.47	148	0.96	23.3	1.1	35.6	1.7	0.65	7.44
OK-325-3	2.12	41.0	7.88	1.90	173	1.26	27.4	0.7	39.6	0.9	0.69	8.33
OK-326-1	4.88	60.5	8.98	2.04	71.4	1.29	24.9	0.5	32.2	0.7	0.77	9.46
OK-326-2	5.51	55.0	14.8	3.41	116	2.59	30.5	0.6	39.8	0.8	0.77	15.6
OK-326-3	2.09	38.0	7.78	7.36	83.7	0.67	12.9	0.7	19.2	1.0	0.67	9.51
OK-327-1	4.12	47.0	14.5	2.94	108	2.72	32.8	0.7	44.6	0.9	0.74	15.2
OK-327-2	5.98	61.3	11.3	3.24	79.7	2.29	34.9	0.7	44.6	0.9	0.78	12.0
OK-327-3	3.54	48.5	11.8	3.60	94.4	2.11	30.5	0.7	41.5	1.0	0.74	12.7
OK-328-1	1.78	39.5	10.7	11.5	72.1	1.86	25.5	0.8	37.9	1.2	0.67	13.4
OK-328-2	2.09	36.0	25.2	10.4	74.1	3.79	25.3	0.5	38.1	0.8	0.67	27.7
OK-328-3	1.06	33.5	21.8	6.91	115	2.33	18.4	0.6	29.3	1.0	0.63	23.4
OK-329-1	2.60	45.8	14.7	1.87	44.4	2.23	27.1	0.6	37.8	0.9	0.72	15.2
OK-329-2	3.02	43.8	32.7	2.11	53.5	5.77	32.1	0.6	44.9	0.9	0.72	33.2
OK-337-1	1.74	34.5	12.5	2.50	213	1.83	25.4	0.8	38.9	1.2	0.65	13.1
OK-337-2	3.48	56.5	12.4	2.22	261	1.98	27.8	0.6	36.8	0.8	0.75	12.9
OK-337-3	5.46	71.0	10.9	2.78	320	2.42	37.4	0.7	46.5	0.9	0.80	11.6
OK-338-1	1.13	27.8	15.5	10.9	146	2.34	23.8	0.8	40.8	1.3	0.58	18.1

Table 3.2 (continued)

Sample Number	Mass (μg)	mwar (μm)	U (ppm)	Th (ppm)	Sm (ppm)	He (nmol/g)	Raw Age (Ma)	Error (±1σ)	Corrected Age (Ma)	Error (±1σ)	HAC (Ft)	Eu (ppm)
OK-338-2	2.15	42.8	7.47	2.80	77.9	0.62	13.9	0.8	20.0	1.1	0.70	8.13
OK-339-1	3.54	54.8	9.47	2.32	79.3	1.19	21.9	0.6	29.1	0.8	0.75	10.0
OK-339-2	4.11	51.3	10.3	2.07	87.9	1.06	18.1	0.5	24.2	0.6	0.75	10.8
OK-339-3	6.80	77.0	17.7	1.67	118	3.02	30.6	0.6	37.9	0.8	0.81	18.1

Table 3.3. Single grain zircon (U-Th)/He replicate data.

Sample Number	Mass (μg)	mwar (μm)	U (ppm)	Th (ppm)	He (nmol/g)	Raw Age (Ma)	Error (±1σ)	Corrected Age (Ma)	Error (±1σ)	HAC (Ft)	Eu (ppm)
OK-320Zr-1	21.5	74.5	799	202	187	40.9	1.2	47.8	1.4	0.86	847
OK-320Zr-2	9.85	53.0	888	180	186	37.1	0.9	45.7	1.1	0.81	930
OK-320Zr-3	16.2	56.5	1078	218	218	35.7	0.8	43.0	1.0	0.83	1129
OK-321Zr-1	13.6	57.8	1557	68.6	380	44.7	1.1	54.2	1.3	0.82	1573
OK-321Zr-2	8.97	54.3	441	170	99.4	38.2	0.9	47.3	1.1	0.81	481
OK-321Zr-3	6.54	46.3	555	182	134	41.5	1.1	52.9	1.4	0.78	598
OK-323Zr-1	2.77	34.5	2170	615	437	34.9	0.7	49.0	1.0	0.71	2315
OK-323Zr-2	3.54	36.0	3216	413	547	30.6	0.8	41.7	1.1	0.73	3313
OK-323Zr-3	9.00	45.8	693	273	189	46.2	0.9	58.3	1.2	0.79	757
OK-324Zr-1	6.48	42.0	394	101	85.7	37.9	0.8	48.9	1.0	0.77	418
OK-324Zr-2	7.48	45.3	566	264	135	39.9	0.8	50.9	1.0	0.78	628
OK-324Zr-3	7.18	46.0	443	211	103	38.9	0.8	49.6	1.1	0.79	493
OK-325Zr-1	2.70	36.5	752	451	132	28.4	0.6	39.4	0.9	0.72	858
OK-325Zr-2	1.54	30.3	297	175	64.1	34.9	0.7	52.2	1.0	0.67	339
OK-325Zr-3	1.39	29.5	671	227	116	29.8	0.7	45.1	1.0	0.66	725
OK-326Zr-1	4.27	36.3	374	93.9	69.4	32.4	0.7	43.6	0.9	0.74	396
OK-326Zr-2	4.49	42.3	645	200	123	33.1	0.7	43.5	0.9	0.76	692
OK-326Zr-3	3.17	34.8	100	41.6	17.2	28.9	0.6	39.9	0.8	0.72	110
OK-327Zr-1	4.34	40.0	1078	213	224	36.7	0.8	48.7	1.1	0.75	1128
OK-327Zr-2	1.55	27.8	893	143	170	33.9	0.7	51.6	1.1	0.66	927
OK-327Zr-3	0.95	25.8	503	211	88.2	29.5	0.6	47.1	0.9	0.63	553
OK-328Zr-1	6.24	51.2	233	49.0	42.1	31.8	0.7	40.2	0.9	0.79	244
OK-328Zr-2	6.59	52.3	789	142	151	33.9	0.7	42.7	0.9	0.80	822
OK-328Zr-3	6.49	46.8	618	88.7	110	31.8	0.7	40.5	0.9	0.79	639
OK-339Zr-1	3.05	35.0	314	201	66.5	33.9	0.7	47.1	1.0	0.72	361
OK-339Zr-2	1.95	30.3	905	105	157	31.3	0.8	45.6	1.1	0.69	930
OK-339Zr-3	1.45	29.5	545	103	102	33.1	0.8	49.7	1.1	0.67	570

Table 3.4 Apatite Fission Track Data.

Sample Number	Lat/Long	Elevation (m)	Number of Grains	Dosimeter Track Density (10^{-6} cm^{-2})			U (ppm)	P(χ^2) (%)	Central Age (Ma±2σ)	Mean Track Length, µm±SE (number of tracks)	SD (µm)	DPAR (µm)
				ρ_d (N_d)	ρ_s (N_s)	ρ_i (N_i)						
OK-305	48.605/-119.431	1001	13	1.728 (1917)	0.247 (166)	2.71 (1823)	58.1	34.4	22.8 ± 4.2			
OK-307	48.612/-119.450	750	13	1.665 (1917)	0.283 (207)	2.62 (1917)	56.1	21.3	25.9 ± 4.4	13.03 ± 0.16 (100)	1.58	3.19
OK-311	48.617/-119.450	616	20	1.634 (1917)	0.35 (445)	1.75 (2223)	37.8	3.4	47.5 ± 7.4	14.48 ± 0.13 (55)	0.94	2.38
OK-315	48.622/-119.458	399	21	1.603 (1917)	0.446 (595)	2.59 (3455)	57.1	1.2	39.8 ± 5.6	12.98 ± 0.18 (100)	1.85	2.46
OK-317	48.624/-119.461	343	20	1.571 (1917)	0.442 (561)	2.78 (3535)	62.6	36	35.9 ± 4.4	13.20 ± 0.2 (84)	1.46	2.01
OK-319	48.709/-119.097	988	22	1.259 (1917)	0.208 (262)	0.753 (951)	21.3	24.1	50.5 ± 8.6			
OK-320	48.686/-119.120	962	19	1.54 (1917)	0.537 (596)	2.52 (2798)	57.2	0	45.9 ± 8.2			
OK-323	48.661/-119.193	725	16	1.509 (1917)	0.487 (480)	2.95 (2903)	67.8	0	39.8 ± 10			
OK-324	48.657/-119.287	654	19	1.478 (1917)	0.547 (652)	2.69 (3208)	65.9	0.1	43.2 ± 6.6	13.75 ± 0.14 (102)	1.39	2.47
OK-325	48.673/-119.364	585	21	1.228 (1917)	0.202 (252)	0.857 (1066)	26.3	61	41.8 ± 6.8			
OK-327	48.688/-119.416	404	22	1.259 (1917)	0.208 (262)	0.753 (951)	21.3	24.1	50.5 ± 8.6	13.84 ± 0.14 (100)	1.37	3.18
OK-338	48.636/-119.463	273	20	1.196 (1917)	0.0715 (89)	0.245 (310)	7.3	62	49.5 ± 12.6			
OK-339	48.645/-119.466	275	20	1.321 (1917)	0.228 (253)	1.67 (1846)	44.2	20.6	26.2 ± 4.2	13.02 ± 0.13 (100)	1.31	3.04
03-OK-80	48.596/ -119.419	886	19	1.08 (3314)	0.118 (143)	0.811 (978)	26.5	92.3	22.8 ± 4.4	12.43 ± 0.21 (100)	2.09	

Chapter 4: Thermal and rheological evolution of mid-crustal rocks during formation of migmatite-cored metamorphic core complexes

Migmatite-cored metamorphic core complexes exposed in the North American Cordillera and central Aegean islands allow the assessment of the thermo-mechanical evolution of partially-molten mid-to-lower crustal rocks in extensional domains. These complexes display similar P-T-t paths involving a near-isothermal decompression followed by a subsequent rapid cooling, and record a temporal and kinematic continuum during their exhumation to the Earth's surface. Perturbation of the thermal structure at shallow depths (≤ 5km) owing to heat advection causes the brittle-ductile transition (BDT) zone to migrate towards the surface, and therefore influences the state of stress, hydrology, and rheology of the crust. Regional extensional strain is accommodated by kinematically compatible ductile and brittle structures, although the style of faulting may alternate between dip-slip to strike-slip owing to changes in the configuration of principle stress axes. Using brittle faults and pervasive fracture sets developed above the BDT zone, percolation of surface-derived fluids removes heat effectively and leads to high geothermal gradients in the shallow crust. This convective fluid flow leads to brittle behavior of rocks and therefore develops a feedback mechanism with the BDT zone and fluid circulation.

4.1. Introduction

Migmatite-cored metamorphic core complexes (McMMC) occur in many orogenic belts (Rey et al., 2009a,b) including the Alpine-Himalayan Belt (Lister et al., 1984; Jolivet et al., 1994, 2010; Grasemann et al, 2012; Vanderhaeghe, 2004; Kruckenberg et al., 2011; Robinson et al., 2007; Stübner et al., 2013), Hercynian (Burg et al., 1994; Vanderhaeghe et al., 1999), Caledonian (Andersen et al., 1991), and North American Cordillera (Parrish et al., 1988; Norlander et al., 2002; Vanderhaeghe et al., 2003; Teyssier et al., 2005; Hinchey et al., 2006; Gordon et al., 2008; Kruckenberg et al., 2008; Brown et al., 2012). These McMMC's preserve the pressure-temperature-time and deformation history of deep orogenic crust during its exhumation to the surface as a result of lithospheric extension. Both numerical and field-based studies have demonstrated that the ascent of partially-molten deep crust facilitate heat and mass transfer within orogens, and affect surface and Moho topography (Teyssier and Whitney, 2002; Whitney et al., 2004; Teyssier et al., 2005; Rey et al., 2009a, b, 2011; Schenker et al., 2012; Stübner et al., 2013).Unraveling the timing, conditions and tempo of events recorded in these rocks is important to understand factors and mechanisms controlling the thermo-mechanical evolution of orogenic crust, such as the effect of boundary conditions and strain rates; internal dynamics and flow pattern of anatectic deep crust; style of extension experienced within different crustal depths (i.e. coupling vs decoupling of shallow and deep crust and its consequences); and initiation and evolution of strain localization of detachment faults (Block and Royden, 1990, Tirel et al., 2004, Vanderhaeghe, 2004; Rey et al. 2009a, 2009b, 2011; Kruckenberg et al., 2011).

Numerical models exploring lithospheric extension predict a specific P-T-t paths for the migmatite-cored metamorphic core complexes in which the migmatitic core is characterized by a phase of isothermal decompression, followed by rapid cooling of rocks as they come very close to the surface (e.g. Tirel et al., 2004; Rey et al., 2009a, 2009b, 2011; Schenker et al., 2012). Field-based studies focusing on the timing and metamorphic conditions of migmatization and McMCC formation document P-T paths compatible with first-order predictions of these numerical models, especially from migmatite crystallization to medium-range temperatures (~750-350 °C) (Vanderhaeghe et al., 2003; Gordon et al., 2008; Kruckenberg et al., 2008, 2011; Rey et al., 2009a, 2009b; Brown et al., 2012). However, how these rocks continue to cool below ~350°C to surface temperature is critical to understand the complete exhumation history of the partially molten crust, including the possible role of detachment tectonics in the ultimate stages of exhumation.

One of most important outcomes of McMCC studies is the formation of a thermal perturbation in shallow crustal depths owing to denudation related heat advection. Because rapidly exhuming anatectic crust keeps its temperature profile as it ascends to shallow levels, the emplacement of migmatitic rocks results in a high geothermal gradient in shallow crustal depths (e.g. Whitney et al., 2013). More importantly, the rapid denudation of partially molten crust raises the depth of transition from crystal-plastic to cataclastic flow (BDT) near the surface. The brittle-ductile transition zone commonly acts as a weak zone form localized deformation, fluid circulation, and pluton emplacement (e.g. Regenauer-Lieb and Yuen, 2004). Therefore, this thermal disturbance ultimately affects the mechanical behavior of crust by affecting

distribution of strain and stress within the system. As a result, rocks may continue to deform under hydrostatic pressure rather than lithostatic pressures (e.g. Siebenaller et al., 2013). Such changes in pressure field also modify the style of faulting as confining pressure has significant effects on the mechanical behavior of rocks.

The depth of the BDT can also influence crustal-scale fluid circulation in extensional domains. Numerical models investigating thermo-mechanical effects of fluids percolating through the crust documented that these fault zones can serve as conduits in which meteoric surface waters can travel into significant depths and change permeability, composition, and thermal regime of rocks (e.g. Person et al., 2007; Gottardi et al., 2013). Field-based stable isotope studies in metamorphic core complexes show that meteoric-fluid signatures are preserved in metamorphic minerals incorporated into crystal structure of recrystallized white mica, emphasizing very high paleo-geothermal gradients within the detachment fault zone during exhumation (Morrison and Anderson, 1998; Mulch et al., 2004, 2006, 2007; Gebelin et al., 2011; Gottardi et al, 2011). Furthermore, the BDT can act as a barrier between two distinct hydrologic domains through which surface-derived fluids and magmatic and metamorphic fluids percolate (Famin et al., 2004, 2005). Consequently, the presence of fluids leads to drastic rheologic and thermal changes across the BDT (e.g. Siebenaller et al., 2013).

In this paper, we focus on the thermal and rheological effects of McMCC exhumation. Using a wealth of existing structural, geochemical, petrological, geo-and thermochronological data, we review P-T-t and deformation histories of McMCC's exposed in the northern North American Cordillera and central Aegean domain. These McMCC's display temporal continuity from melt crystallization to near-surface

conditions accompanied with a continuum of kinematics between ductile shearing and late brittle slip, thus provide a unique opportunity to understand thermo-mechanical evolution of extending crust during the last stages of the orogeny.

4.2. Characteristics of migmatite-cored metamorphic core complexes

In this section we will first review the geodynamic history of the northern North American Cordillera and central Agean domain, and then focus on geological evolution of specific McMCC's exposed in these regions. Our aim is to show that these complexes share common first-order features, even though variations exist in details. Both regions experienced collision and subduction related crustal thickening and partial melting in middle and lower-crust that exhumed and formed McMCC's during subsequent extensional collapse of the orogenic belt.

4.2.1. Central Aegean domain

4.2.1.1. Aegean Geodynamics

The Cenozoic tectonic history of the eastern Mediterranean is shaped by convergence between the African and Eurasian plates and subduction of the Hellenic slab. The southward retreat of the Hellenic trench resulted in collapse of the central part of the Hellenic belt and lithospheric extension leading widespread plutonism, volcanism, and metamorphic core complex formation in the Aegean domain during the late Oligocene to late Miocene (Dewey and Şengör, 1979; Lister et al., 1984; Jolivet et al., 1994; Jolivet and Brun, 2010). In the northern Cyclades islands (Andros, Tinos, Mykonos, Ikaria) these MCC's are bounded and exhumed by the North Cycladic Detachment System (NCDS) with a consistent top-to-NNE sense of shear whereas the

islands in western Cyclades (Kea, Kythnos, Serifos, Sifnos) were exposed by the West Cycladic Detachment System (WCDS) with a top-to-S kinematics (Jolivet et al., 2010; Grasemann et al., 2012) (Figure 4.1). Seismic studies show that Moho is flat in the central Agean at 25-28 km and lower crust shows strong seismic anisotropy that is parallel to Miocene extension, indicating persuasive viscous flow of the crust during core complex formation (Endrun et al., 2011).

Most of these islands display well-preserved structural cross-sections from footwall to detachment fault to hanging-wall. The footwall units of the Attic-Cycladic massifs record two distinct metamorphic events; an early blueschist facies metamorphism (M1) related with exhumation during the Eocene within the subduction channel (Jolivet et al., 2003; Ring et al., 2010; Jolivet and Brun, 2010), and a second upper greenschist to amphibolite facies metamorphism locally reaching partial melting (M2) in the late Oligocene-early Miocene (Altherr et al, 1982; Ring et al., 2007; Brun and Faccena, 2008). This second metamorphic phase was followed by near-isothermal decompression, involving rapid exhumation and cooling, and formation of migmatites and syntectonic plutons in the Miocene (Lister et al., 1984; Keay et al., 2001; Vanderhaeghe, 2004; Duchêne et al., 2006; Martin et al., 2006, 2008). The hanging-wall units are mainly comprised of fault-bounded sedimentary basins (Jansen, 1973; Sánchez-Gómez et al., 2002; Bargnesi et al., 2013).

4.2.1.2. Naxos

The most complete structural section of the Attic-Cycladic massifs is exposed in the island of Naxos and exhibits three distinct tectono-stratigraphic units (Vanderhaeghe, 2004). The upper unit is composed of low-grade marble, schist, and ophiolitic mélange

unconformably overlain by Cenozioc sedimentary rocks (Jansen, 1973). The middle and lower units are exposed below over 1 km thick detachment fault zone, which is well exposed in the western part of the island. The middle unit includes alternating marble and schist layers containing mafic and ultramafic boudins (Jensen and Schuiling, 1976). An elongate dome containing migmatite (mostly diatexite with some metatexite), leucogneiss, and marbles forms the lower unit. Together with the middle unit, this migmatitic dome constitutes the core of a Barrovian metamorphic sequence that is approximately concentric to the dome core (Buick and Holland, 1989; Vanderhaeghe, 2004; Kruckenberg et al., 2011). A granodiorite pluton is exposed along the western coast of the Naxos, displaying intrusive contact with metamorphic rocks (middle and lower units) and tectonic contact with upper units (Figure 4.2).

Previous petrological, geochronological, and structural data documented that lithologies exposed in the middle and lower units preserve both M1 and M2 metamorphism and related deformation. Relics of Eocene blueschist facies metamorphism (M1) is best preserved in rocks at the southern Naxos, indicating metamorphic conditions of ~350 °C at 10 kbar (Avigad, 1998; Duchêne et al., 2006). These rocks yield U-Pb zircon rim ages of 57 to 41 Ma and phengite $^{40}Ar/^{39}Ar$ data ages of 45 ± 5 Ma (Wijbrans and McDougall, 1988; Martin et al., 2006, 2008). This high-temperature low-pressure metamorphism is largely overprinted by greenschist-to-amphibolite facies M2 metamorphism that resulted in formation of migmatite domes. Mineral assemblages and textures in the migmatitic core record near-isothermal decompression from peak metamorphic conditions of 8 kbar and 800 °C (Jansen and Schuiling, 1976; Buick and Holland, 1989; Duchêne et al., 2006). Zircon rim

overgrowths from these migmatites yield U-Pb ages of ca. 17 Ma and cooling below ~300 °C was achieved by ~10 Ma based on amphibole, biotite and white mica $^{40}Ar/^{39}Ar$, and Rb/Sr mineral-whole rock ages (Wijbrans and McDougall, 1988; Keay et al., 2001; Martin et al., 2006, 2008; Duchêne et al., 2006). These metamorphic units were intruded by a granodioritic pluton ca. 11 Ma (Wijbrans and McDougall, 1988; Keay et al., 2001). The cooling history of the dome rocks below ~250 °C to 60 °C is captured by zircon/apatite fission track and U-Th/He ages that mainly cluster around 12 to 9 Ma (Figure 4.3, Brichau et al., 2006; Seward et al., 2009). These ages indicate that the Naxos McMCC experienced rapid cooling (~100 to 50 °C/myr) and exhumation rates (6-8 km/Ma).

Rocks exposed in the footwall of the Naxos detachment display an excellent record of fabrics from upper amphibolite facies ductile deformation to greenschist facies cataclastic deformation, therefore provide a window into processes and conditions during ductile-to-brittle transition. Mineral and stretching lineations in the middle and lower units and kinematic indicators show consistently top-to-NNE sense of shear, parallel to the long axis of the migmatitic dome (Vanderhaeghe, 2004; Kruckenberg et al., 2011). Gneissic and mylonitic foliation in regional scale form overall domal shape and these ductile fabrics are cut by E-W oriented brittle transtensional faults that control the first-order surface morphology of the island. Metamorphic conditions and processes acting during exhumation through the brittle-ductile transition were recorded by fluid inclusions in three different generations of quartz veins in the lower unit (Siebenaller et al., 2013). The earliest formed quartz veins are parallel to mylonitic folition and formed in ductile regime. Inclusions within these veins were characterized by immiscible CO_2-

rich and high-salinity fluids, probably formed at peak metamorphic conditions during M2 metamorphism, and trapped under metamorphic conditions of ~625 °C and ~380 MPa (Siebenaller et al., 2013). The second set of quartz veins are mostly discordant to foliation but in places transposed into the foliation plane. They host fluid inclusions that were trapped at brittle-ductile transition zone and yield ~410-280 °C and ~180-50 MPa. The most abundant quartz veins are E-W oriented and cross-cut all previous ductile and brittle structures. They record conditions in brittle field under conditions from ~210-280 °C and 40-50 MPa. Aqueous fluids with low δD values become increasingly dominant in these quartz veins, indicating indisputable presence of meteoric fluids percolating within the brittle crust (Figure 4.4, Siebenaller et al., 2013).

4.2.1.3. Mykonos

On Mykonos island extensional structures are related to M2 metamorphism and the activity of the NCSD zone (Menant et al., 2013). These structures are best recorded by the middle unit, which is a granitic intrusion forming most of the island. This km-scale laccolith intruded into migmatitic gneiss, micaschist, and marble (the lower unit), which constitutes the core of the dome (Faure et al., 1991). The lower unit is best exposed on the western tip of the island and neighboring island Rhinia (Figure 4.5). The upper unit comprises fault-bounded sedimentary basins filled with early (?) to late Miocene sediments synchronous with detachment activity (Sánchez-Gómez et al., 2002). Timing of laccolith emplacement was ca. 13 Ma based on U-Pb zircon ages (Brichau et al., 2008). $^{40}Ar/^{39}Ar$ hornblende and biotite ages range between 13 to 11 Ma, whereas zircon fission track and U-Th/He thermochronology yield ages of 13 to 9 Ma. Overlapping within 2-sigma error range, apatite fission track and U-Th/He ages range

from 12.5 to 9 Ma (Figure 4.6). Overall these ages indicate cooling rates of the lower and middle units were as high as 100 °C/myr (Brichau et al., 2008).

Structural data from the middle unit document that magmatic structures progressively evolve into mylonitized fabrics close to the detachment zone, displaying shallowly dipping NW-SE striking foliation and NE-trending mineral or stretching lineation. Together with kinematic indicators, these structures indicate top-to-NE sense of ductile shear (Denéle et al., 2011). Two detachment fault zone have been identified in Mykonos: the Livada and Mykonos faults. The Livada detachment fault zone was formed due to reactivation of intrusive contact of the laccolith as a ductile low-angle normal fault shear zone. The slip in the brittle domain, on the other hand, was accommodated by the Mykonos detachment zone (Lecomte et al., 2010). Field observations on these detachment faults and mineral veins suggest that top-to-NE extensional shearing was continuous when rocks were passing through ductile to brittle deformation regimes. As a result of this continuation, NW-SE oriented high-angle brittle normal faults and steeply-dipping barite and Fe-hydroxite veins developed in all structural units ca. 11 to 10 Ma (Lecomte et al., 2010; Menant et al., 2013). Shortly after, these normal faults were reactivated as conjugate strike-slip faults, in places dissecting detachment fault zones. The youngest brittle structures are associated with E-W to NW-SE trending compressional structures, causing reactivation of older planar structures in a new stress regime (Menant et al., 2013).

4.2.2. The northern North American Cordillera

4.2.2.1. The Shuswap Metamorphic Core Complex (MCC)

Forming the largest metamorphic core complex in the North American Cordillera, the Shuswap MCC exposes a series of north-south trending migmatite-domes from British Columbia (Canada) to Washington-Idaho (USA) (Figure 4.7). The core complex formed as a result of orogenic extension in the Eocene following subduction, crustal thickening, and terrane accretion during the Mesozoic (Armstrong 1982; Monger et al, 1982; Coney and Harms, 1984; Parrish et al., 1988; Vanderhaeghe et al., 2003; Teyssier et al., 2005; Kruckenberg et al., 2008). Exposed over 400 km long belt, high-grade mid-crustal rocks are bounded by detachment faults, the Columbia River and Eagle River-Okanogan faults on the east and west, respectively (Figure 4.7). Although the relics of earlier metamorphism and accompanied deformation are locally preserved, high-grade rocks in the core of migmatite domes record near-isothermal decompression at >750 °C from > 8 kbar to ~ 3 kbar during Eocene extension (Norlander et al., 2002; Vanderhaeghe et al., 2003; Hinchey et al., 2006; Kruckenberg et al., 2008; Gordon et al., 2008, Brown et al., 2012). The hanging-wall of the detachment faults consist of Paleozoic to Mesozoic plutonic and metamorphic rocks and normal fault-bounded basins that were filled with Eocene sedimentary and volcanic rocks (Church, 1973; Fox et al., 1977; Mathews, 1981). Clasts of mylonites and deformed metamorphic rocks exposed beneath the detachment fault are commonly identified in these basins, indicating synchronous development of basins and footwall denudation (Suydam and Gaylord, 1997; McClaughry and Gaylord, 2005).

In the next section we focus on the Thor-Odin and Okanogan gneiss domes, representing respectively the narrow and high-relief northern end, and the wider and lower-relief southern termination of the Shuswap MCC. Both domes expose high-grade

metamorphic and plutonic rocks that are structurally and temporally correlative to each other.

4.2.2.1 The Thor-Odin dome

In the Thor-Odin dome, lithologies forming the upper unit consist of Mesozoic plutonic rocks and low-grade to unmetamorphosed early Cenozoic sedimentary and volcanic rocks (Mathews, 1981; Colpron et al., 1996). Below the detachment faults, the middle unit comprises amphibolite-to upper amphibolite facies gneisses and a network of leucogranite laccoliths, originated from the underlying migmatite. The lower unit forms the structural core and composed of migmatitic para- and orthogneiss (Figure 4.8, Vanderhaeghe et al., 1999).

Thermobarometric data from the lower unit indicate near-isothermal decompression of the core rocks from 800 °C and ≥10 kbar, whereas the middle unit recorded peak metamorphic conditions of ~650-800 °C at 7-9 kbar (Duncan, 1984; Ghent et al., 1977; Nyman et al., 1995; Norlander et al., 2002; Teyssier et al., 2005; Hinchey and Carr, 2007; Spalla et al., 2011; Goergen and Whitney, 2012a, b). U-Pb ages of monazite and zircon rims from migmatites yield ages of ~56-51 Ma, slightly younger crystallization age of laccoliths that cluster around 60-55 Ma (Carr, 1991, 1992; Parkinson, 1992; Vanderhaeghe et al., 1999; Johnston et al., 2000, Teyssier et al., 2005; Hinchey et al., 2006). $^{40}Ar/^{39}Ar$ thermochronology yields ca. 49-47 Ma biotite and muscovite cooling ages in all structural units (Vanderhaeghe et al., 2003; Mulch et al., 2006). Zircon fission track ages cluster around 50-45 Ma, whereas zircon U-Th/He ages are ca. 45-37 Ma (Lorencak et al., 2001; Toraman et al, 2012). The cooling history of middle and lower units below ~120 °C is captured by apatite fission track and U-Th/He

thermochronology. Apatite fission track and U-Th/He ages ages range between 48 to 14 Ma and 26 to 5 Ma, respectively. AFT ages vary with elevation (Figure 4.9, Toraman et al., 2012). Combined with track-length modeling, these ages document rapid cooling (≥60 °C/my) and exhumation of dome rocks to very shallow depths (1-2 km) ca. 45 Ma and a recent cooling phase related to continental glaciation at ~3 Ma (Chapter 2 of this thesis).

High-grade metamorphic rocks exposed in the middle and lower units have shallowly dipping foliation and well-developed, east-west trending horizontal mineral and stretching lineation, indicating E-W extension (e.g. Vanderhaeghe and Teyssier, 2001). In the detachment fault zones, these amphibolite facies ductile fabrics are overprinted by concordant greenschist facies fabrics, pseudotachylites and cataclasite zones, which indicates transition from ductile to brittle domain (Vanderhaeghe et al., 2003). An array of N-S striking brittle normal and strike-slip faults cut all units and ductile structures, controlling the first-order morphology of the Thor-Odin dome (Johnson and Brown, 1996). Parallel to the regional orientation of an Eocene dyke system the earliest brittle faults were formed as N-S striking dextral faults and overprinted by or reactivated later as NNW-SSE striking conjugate normal faults (Kruse and Williams, 2005).

4.2.2.2. The Okanogan dome

The upper unit of the Okanogan dome consist of Palaeozoic to Mesozoic metamorphic and igneous rocks and NE-SW oriented fault-bounded sedimentary basins that preserve thick (>4 km) sequences of Eocene sedimentary and volcanic rocks (Fox et al, 1977; Parkinson, 1985; Holder and Holder, 1988; Stoffel et al., 1991) (Figure 4.10).

Most of these basins contain clasts of the middle and lower units exposed beneath a detachment fault zone (Suydam and Gaylord, 1997; McClaughry and Gaylord, 2005). The lower unit is exposed in two NW-SE trending sub-domes on the Stowe and Burge Mountains, and dominated by migmatitic para- and orthogneiss (the Tonasket gneiss). Amphibolite facies gneiss, calc-schist, and quartzite with relatively less partial melt form the middle unit (Cheney, 1980; Hansen and Goodge, 1988). Both the middle and lower units were intruded by granodioritic plutons of the Colville Batholith.

P-T estimates of the Okanogan dome come from a kilometers-scale Mg-Al-rich layer that is located between the middle and upper unit, that displays symplectitic textures around kyanite and staurolite. This emphasizes near-isothermal decompression of the dome rocks from peak metamorphic conditions of 750 °C and 8 kbar (Kruckenberg and Whitney, 2011). U-Pb zircon ages indicate crystallization of migmatites and associated pegmatitic dykes were between ca. 60-49 Ma (Kruckenberg et al., 2008). Biotite $^{40}Ar/^{39}Ar$ thermochronology yields ages ca. 47 Ma (Kruckenberg et al., 2008). Overlapping the younger end of migmatite crystallization and cooling through ~325 °C, zircon U-Th/He ages range between 51 to 45 Ma. Apatite fission track and U-Th/He ages are between 51-23 Ma, reflecting ~2km of erosional unroofing of the dome after the cessation of detachment faulting (Figure 4.11).

In most places the Okanogan dome displays well-developed low-dipping gneissic foliation and pervasive lineation with top-to-WNW kinematic sense. Foliation surfaces become steeper closer to NW-trending micro-to-meso scale anti-and synforms (Kruckenberg et al., 2008). Transition from ductile to brittle regime is better preserved in the detachment zone, where amphibolite facies fabric is overprinted by greenschist

facies minerals. Structures within the detachment zones indicate continuity of stress field as rocks passed through the BDT (Hansen and Goodge, 1988). Pervasive, close-spaced NNE-striking fracture zones parallel to major ductile-brittle fault zones and dykes were developed in all structural levels. These structures indicate that WNW-SSE extensional regime was still dominant when rocks were passing through ductile-to-brittle regime (Eyal et al., 2006). Probably synchronous with this fracturing, ductile planar structures in the middle and lower units, such as foliation and shear planes, were reactivated as strike-slip and dip-slip faults. The youngest brittle deformation phase resulted in reactivation of previously formed extensional fractures. These reactivation structures, however, formed under compressional stress regimes, which might indicate a significant change of stress field (Eyal et al., 2006).

4.3. Discussion

4.3.1. Thermal and mechanical consequences of McMCC exhumation

The synthesis of field observations from McMCC's exposed in the northern North American Cordillera and Cycladic islands brings some new insights into the thermo-mechanical evolution of deep orogenic crust. The presence of a significant volume of partial melt in mid-to-lower crustal levels results in variations in viscosity of the crust, and results in a rheologically weak layer. When subjected to extensional stress, synchronous development of brittle extension in the upper crustal levels and viscoplastic flow of ductile deep crust result in formation of migmatite-cored metamorphic core complexes (e.g. Vanderhaeghe et al., 2003; Rey et al., 2009a, b; Kruckenberg et al., 2010; Whitney et al., 2013). Geo- and thermochronologic data indicate very short time window from zircon crystallization to cooling through surface temperatures (~5-8 Ma),

and emphasize very rapid cooling (≥ 100 °C/Ma) and exhumation (~8-10 km/myr) of these migmatites and mantling metamorphic rocks (Figures 4.3, 6, 9, 11). This thermal history suggests that fast exhumation promotes heat advection which leads to high geothermal gradient at shallow depths. The most fundamental consequence of this thermal disturbance is the migration of the brittle-ductile transition zone closer to the surface.

The shallowing of the BDT zone has significant impacts on fault mechanics. Field observations in the Cycladic islands, for instance, indicate that the upward migration of the BDT might have caused the formation of new low-angle normal fault zones that accommodated extensional strain in the brittle domain (e.g. Brichau et al., 2007). In addition to strain localization on new surfaces, some shallow-dipping planar features, such as foliation and shear zones, were overprinted by brittle structures. This suggests later reactivation of these surfaces, and therefore the presence of two discrete slip histories, and/or a continuously evolving shear zone from ductile-to-brittle fields. Discontinuous brittle slip that causes bending or offsetting of foliation planes suggests reactivation of earlier structures. The continuum of kinematics from sub-solidus to post-solidus deformation, on the other hand, can be seen in a range of structures. At the regional scale, the compatibility of ductile and brittle kinematics is expressed by similarity in orientation of dykes, basins bounded by high-angle normal faults, and pervasive fracture systems (Kruse and Williams, 2005; Menant et al., 2013). At the outcrop scale, this continuum is best demonstrated by kinematic consistency between slickensides and calcite steps (brittle), and mineral lineation (ductile) in these rocks (e.g. Eyal et al., 2006; Mehl et al., 2005).

Another effect of the location of the BDT zone is related to the cooling mechanisms of hot mid-crustal rocks. Detailed cooling histories of Cycladic and North American McMCC's necessitates an explanation other than conductive cooling of rocks since that would require more time than is observed in these systems. Studies focusing on the rock-fluid interaction using oxygen and hydrogen stable isotopes have demonstrated the ubiquitous occurrence of meteoric fluid in mylonites and cataclastic rocks in detachment faults, implying fluid convection can effectively cool these rocks (Mulch et al., 2004; Famin et al., 2004). Moreover, the composition of fluid inclusions within metamorphic rocks indicates that the BDT forms a boundary between chemically and thermally two different crustal reservoirs. Fluid inclusions in ductile domain form metamorphic reactions and magmatic crystallization, and equilibrate with their host rocks under lithostatic conditions through a normal geothermal gradient (~30 °C/km). Fluid inclusions in the brittle domain, on the other hand, are characterized by meteoric origin, and indicate hydrostatic pressures with higher (~50 °C/km) geothermal gradient (Siebenaller et al., 2013). Therefore, above the BDT zone fluid-flow through fractures allows a rapid heat dissipation that keeps geothermal gradient high in shallow depths. As the system further cools, its rheology becomes more brittle, and consequently, a feedback mechanism develops between fluid-induced cooling and rheology of the crust.

The low-temperature thermochronology ages (apatite fission track and U-Th/He) from Cycladic and northern North American McMCC's indicate very high cooling rates (>100 °C/myr) as these rocks cooled from ~120 to 40 °C (Brichau et al., 2006, 2008; Seward et al., 2009: Toraman et al., 2012). This increase in cooling rate can be interpreted as an increase in exhumation rate. Alternatively, it might happen as a result

of more efficient cooling of rocks by fluid-induced convection as the rocks approach the surface. Discriminating between these two scenarios is important because they imply significantly different tectonic and erosional histories. Combining P-T-t paths from fluid-inclusions and thermochronologic ages suggests that fluid-induced cooling of rocks in the brittle domain was recorded by those chronometers, without any changes in exhumation rate (Figure 4.4, Siebenaller et al., 2013). This result further suggests that formation of these migmatite-cored metamorphic core complexes was achieved by a single exhumation phase (Brichau et al., 2008; Toraman et al., 2012).

The change of confining pressure from lithostatic to hydrostatic state further affects the configuration of principal stress axes, and therefore, how brittle deformation is accommodated in these rocks. During ductile extensional exhumation the maximum stress axis is (σ_1) vertical, and intermediate (σ_2) and minimum (σ_3) principle stresses are horizontal. After rocks passed through the BDT zone, however, the intermediate and maximum stress axes might switch their positions as the minimum stress axis remains the same. This new stress configuration with vertical σ_2 and horizontal σ_1 and σ_3 results in formation of the strike-slip faults. Paleostress analyses of metamorphic rocks in Mykonos indicate such change in the stress regime and formation of conjugate set of strike-slip faults, although overall regional extension directions remained the same (Menant et al., 2013).

4.4. Conclusions

Several well-exposed migmatite-cored metamorphic core complexes in the central Aegean and northern North American Cordillera unravel the detailed dynamics of partially-molten mid-crustal rocks exhumed in the core of these collapsed orogens. A

combination of field observations with thermobarometry and geo/thermochronology document the rapid ascent of anatectic crustal rocks, which results in the upward migration of isotherms in shallow crustal depths due to heat advection. This rapid exhumation and cooling displays the BDT zone towards the surface and enables these systems to "quench" structures as rocks pass through ductile-to-brittle deformation regimes. The shallowing of BDT zone has several significant effects on rheology, strain localization on new and/or pre-existing surfaces, style of faulting, and cooling mechanisms. Because rocks experience lower pressure environments as they come closer to the surface, permutation of principle stress axes might cause changes in faulting from dip-slip to strike-slip shear. Development of two significantly different hydrologic domains separated by the BDT zone leads convection of meteoric fluids through fractures in the brittle domain. This not only accelerates cooling of rocks, but also leads to further embrittlement of the crust.

References

Altherr, R., H. Kreuzer, I. Wendt, H. Lenz, G. A. Wagner, J. Keller, W. Harre, Hohndorf, A., 1982. A Late Oligocene/Early Miocene high temperature belt in the anti-cycladic crystalline complex (SE Pelagonian, Greece), Geol. Jb. 23, 97–164.

Andersen, T. B., Jamtveit, B., Dewey, J. F., Swensson, E., 1991. Subduction and eduction of continental crust: major mechanisms during continent-continent collision and orogenic extensional collapse, a model based on the south Norwegian Caledonides. Terra Nova, 3(3), 303-310.

Armstrong, R.L., 1982. Cordilleran metamorphic core complexes; from Arizona to southern Canada. Annual Review of Earth and Planetary Sciences, v. 10, p. 129-154.

Avigad, D., Baer, G., Heimann, A., 1998. Block rotations and continental extension in the central Aegean Sea: palaeomagnetic and structural evidence from Tinos and Mykonos (Cyclades, Greece). Earth and Planetary Science Letters, 157(1), 23-40.

Bargnesi, E. A., Stockli, D. F., Mancktelow, N., Soukis, K., 2012. Miocene core complex development and coeval supradetachment basin evolution of Paros, Greece, insights from (U-Th)/He thermochronometry. Tectonophysics, 595–596 (2013) 165–182

Block, L., and Royden, L. H., 1990. Core complex geometries and regional scale flow in the lower crust. Tectonics, 9(4), 557-567.

Brichau, S., Ring, U., Ketcham, R. A., Carter, A., Stockli, D., Brunel, M., 2006. Constraining the long-term evolution of the slip rate for a major extensional fault system in the central Aegean, Greece, using thermochronology. Earth and Planetary Science Letters, 241(1), 293-306.

Brichau, S., Ring, U., Carter, A., Monié, P., Bolhar, R., Stockli, D., Brunel, M., 2007. Extensional faulting on Tinos island, Aegean sea, Greece: How many detachments? Tectonics, 26 (4).

Brichau, S., Ring, U., Carter, A., Bolhar, R., Monié, P., Stockli, D., Brunel, M., 2008. Timing, slip rate, displacement and cooling history of the Mykonos detachment footwall, Cyclades, Greece, and implications for the opening of the Aegean Sea basin. Journal of the Geological Society, 165(1), 263-277.

Brown, S.R., Gibson, H.D., Andrews, G.D.M., Thorkelson, D.J., Marshall, D.D., Vervoot, J.D., Rayner, N., 2012. New constrains on Eocene extension within the Canadian Cordillera and identification of Phanerozoic protoliths for footwall gneisses of the Okanagan Valley shear zone. Lithosphere, 4, 4, 354-377.

Brun, J. P., Faccenna, C., 2008. Exhumation of high-pressure rocks driven by slab rollback. Earth Planetary Science Letters, 272, 1–7, doi:10.1016/ j.epsl.2008.1002.1038

Buick, I. S., and Holland, T. J. B., 1989. The PTt path associated with crustal extension, Naxos, Cyclades, Greece. Geological Society, London, Special Publications, 43(1), 365-369.

Burg, J. P., Van Den Driessche, J., Brun, J. P., 1994. Syn-to post-thickening extension in the Variscan Belt of Western Europe: modes and structural consequences. Géologie de la France, 3, 33-51.

Carr, S.D., 1992. Tectonic setting and U-Pb geochronology of the early Tertiary Ladybird leucogranite suite, Thor-Odin-Pinnacles area, southern Omineca belt, British Colombia. Tectonics, 11, 258-278.

Carr, S.D., 1991. U-Pb zircon and titanite ages of three Mesozoic igneous rocks south of the Thor-Odin-Pinnacles area, southern Omineca Belt, British Columbia. Can. J. Earth Sci., 28, 1877-1882.

Cheney, E.S., 1980. Kettle dome and related structures of northeastern Washington, in Crittenden, M.D., Coney, P.J., Davis, G.H., eds., Cordilleran Metamorphic Complexes: Boulder, Colorado, Geological Society of America Memoir, v. 153, p. 463-483.

Church, N. B., 1973. Geology of the White Lake basin. British Columbia Dept. of Mines Petroleum Resources Bull., v. 61, p. 120

Colpron, M., R.A. Price, D.A. Archibald, Carmichael, D.M., 1996. Middle Jurassic exhumation along the western flank of the Selkirk fan structure: thermobarometric and thermochronometric constrains from the Illecillewaet synclinorium, Southeastern British Columbia. Geological Society of America Bulletin, 108, 1372–1392.

Coney, P.J., Harms, T.A., 1984. Cordilleran metamorphic core complexes: Cenozoic extensional relics of Mesozoic compression. Geology, v. 12, p. 550-554.

Dewey, J. F., Şengör, A.M.C., 1979. Aegean and surrounding regions: Complex multiplate and continuous tectonics in a convergent zone. Geological Society of America Bulletin, 90, 84–92, doi:10.1130/0016-7606(1979) 90<84:AASRCM>2.0.CO;2.

Duchêne, S., Aïssa, R., Vanderhaeghe, O., 2006. Pressure-temperaturetime evolution of metamorphic rocks from Naxos (Cyclades, Greece): Constraints from thermobarometry and Rb/Sr dating. Geodin. Acta, 19, 301–321, doi:10.3166/ga.19.301-321.

Duncan, I.J., 1984. Structural evolution of the Thor-Odin gneiss dome. Tectonophysics, 101, 87-130.

Endrun, B., Lebedev, S., Meier, T., Tirel, C., Friederich, W., 2011. Complex layered deformation within the Aegean crust and mantle revealed by seismic anisotropy. Nature Geoscience, 4(3), 203-207.

Eyal, Y., Osadetz, K. G., Feinstein, S., 2006. Evidence for reactivation of Eocene joints and pre-Eocene foliation planes in the Okanagan core-complex, British Columbia, Canada. Journal of Structural Geology, 28(11), 2109-2120.

Famin, V., Philippot, P., Jolivet, L., Agard, P., 2004. Evolution of hydrothermal regime along a crustal shear zone, Tinos Island, Greece. Tectonics, 23(5), doi:10.1029/2003TC001509.

Famin, V., Hébert, R., Philippot, P., Jolivet, L., 2005. Ion probe and fluid inclusion evidence for co-seismic fluid infiltration in a crustal detachment. Contributions to Mineralogy and Petrology, 150(3), 354-367.

Faure, M., Bonneau, M., Pons, J., 1991. Ductile deformation and syntectonic granite emplacement during the late Miocene extension of the Aegean (Greece). Bulletin de la Société Géologique de France, 162, 3-12.

Fox, K.F., Jr., Rinehart, C.D., Engels, J.C., 1977. Plutonism and orogeny in North-central Washington; timing and regional context: Alexandria, Virginia. U.S. Geological Survey Professional Paper 989, 32 p.

Gébelin, A., Mulch, A., Teyssier, C., Heizler, M., Vennemann, T., Seaton, N. C. A., 2011. Oligo-Miocene extensional tectonics and fluid flow across the Northern Snake Range detachment system, Nevada. Tectonics, 30, TC5010, doi:10.1029/2010TC002797.

Ghent, E.D., J. Nicholls, M.Z. Stout, Rottenfusser, B., 1977. Clinopyroxene amphibolite boudins from Three Valley Gap, British Columbia. The Canadian Mineralogist, 15, 269– 282.

Goergen, E. T., and Whitney, D. L., 2012a. Long length scales of element transport during reaction texture development in orthoamphibole-cordierite gneiss: Thor-Odin dome, British Columbia, Canada. Contributions to Mineralogy and Petrology, 163(2), 337-352.

Goergen, E. T., and Whitney, D.L., 2012b. Corona networks as three-dimensional records of transport scale and pathways during metamorphism. Geology, 40(2), 183-186.

Gordon, S. M., Whitney, D. L., Teyssier, C., Grove, M., Dunlap, W. J., 2008. Timescales of migmatization, melt crystallization, and cooling in a Cordilleran gneiss dome: Valhalla complex, southeastern British Columbia. Tectonics, 27, TC4010, doi:10.1029/2007TC002103.

Gottardi, R., Teyssier, C., Mulch, A., Vennemann, T.W., Wells, M.L., 2011. Preservation of an extreme transient geotherm in the Raft River detachment shear zone. Geology, 39, 8, 759-762.

Gottardi, R., Kao, P. H., Saar, M. O., Teyssier, C., 2013. Effects of permeability fields on fluid, heat, and oxygen isotope transport in extensional detachment systems. Geochemistry, Geophysics, Geosystems, 1-30.

Grasemann, B., Schneider, D. A., Stöckli, D. F., Iglseder, C., 2012. Miocene bivergent crustal extension in the Aegean: Evidence from the western Cyclades (Greece). Lithosphere, 4(1), 23-39.

Hansen, V. L., and Goodge, J. W., 1988. Metamorphism, structural petrology, and regional evolution of the Okanogan complex, northeastern Washington, in Ernst,

W.G., ed., Metamorphism and Crustal Evolution of the Western United States, Rubey Colloq. Series vol. 7: Englewood Cliffs, N.J., Prentice-Hall, pp. 233-270.

Hinchey, A. M., and Carr, S.D., 2007. Protolith composition of cordierite-gedrite basement rocks and garnet amphibolite of the Bearpaw lake area of the Thor-Odin dome, Monashee Complex, British Columbia, Canada. The Canadian Mineralogist, 45(3), 607-629.

Hinchey, A.M., Carr, S.D., McNeill, P.D., Rayner, N., 2006. Paleocene-Eocene high-grade metamorphism, anatexis, and deformation in the Thor-Odin dome, Monashee complex, southeastern British Columbia. Canadian Journal of Earth Sciences, 43, 1341-1365.

Holder, R.W., and Holder, G.A., 1988. The Colville Batholith; Tertiary plutonism in Northeast Washington associated with graben and core-complex (gneiss dome) formation. Geological Society of America Bulletin, 100, 1971-1980.

Jansen, J. B. H., 1973. Geological Map of Greece, Island of Naxos, 341 pp., Inst. for Geol. and Min. Resour., Athens

Jansen, J. B. H., and Schuiling, R. D., 1976. Metamorphism on Naxos; petrology and geothermal gradients. American Journal of Science, 276(10), 1225-1253.

Johnson, B.J., and Brown, R.L., 1996. Crustal structure and early Tertiary extensional tectonics of the Omineca belt at 518N latitude, southern Canadian Cordillera. Canadian Journal of Earth Sciences, v. 33, p. 1596–1611.

Johnston, D.H., P.F. Williams, R.L. Brown, J.L. Crowley, Carr, S.D., 2000. Northeastward extrusion and extensional exhumation of crystalline rocks of the

Monashee Complex, southeastern Canadian Cordillera. Journal of Structural Geology, 22, 603–625.

Jolivet, L., and Brun, J.P., 2010. Cenozoic geodynamic evolution of the Aegean region. Int. J. Earth Sci., 99, 109–138, doi:10.1007/s00531- 00008-00366-00534.

Jolivet, L., Brun, J.P., Gautier, P., Lallemant, S., Patriat, M., 1994. 3D kinematics of extension in the Aegean region from the early Miocene to the present: Insights from the ductile crust. Bull. Soc. Geol. Fr., 165(3), 195–209

Jolivet, L., Faccenna, C., Goffé, B., Burov, E., Agard, P., 2003. Subduction tectonics and exhumation of high-pressure metamorphic rocks in the Mediterranean orogens, Am. J. Sci., 303, 353–409.

Jolivet, L., Lecomte, E., Huet, B., Denèle, Y., Lacombe, O., Labrousse, L., Le Pourhiet, L., Mehl, C., 2010. The North Cycladic detachment system. Earth and Planetary Science Letters, v. 289, p. 87–104, doi:10.1016/j .epsl.2009.10.032.

Keay, S., G. Lister, Buick, I., 2001. The timing of partial melting, Barrovian metamorphism and granite intrusion in the Naxos metamorphic core complex, Cyclades, Aegean Sea, Greece. Tectonophysics, 342, 275–312, doi:10.1016/S0040-1951(01)00168-8.

Kruckenberg, S.C., Whitney, D.L., Teyssier, C., Fanning, M., Dunlap, W.J., 2008. Paleocene-Eocene migmatite crystallization, extension, and exhumation in the hinterland of the northern Cordillera: Okanogan dome, Washington USA. Geological Society of America Bulletin, 120(7-8), 912-929.

Kruckenberg, S. C., and Whitney, D.L., 2011. Metamorphic evolution of sapphirine-and orthoamphibole-cordierite-bearing gneiss, Okanogan dome, Washington, USA. Journal of Metamorphic Geology, 29(4), 425-449.

Kruckenberg, S. C., and Whitney, D.L., 2011. Metamorphic evolution of sapphirine-and orthoamphibole-cordierite-bearing gneiss, Okanogan dome, Washington, USA. Journal of Metamorphic Geology, 29(4), 425-449.

Kruckenberg, S. C., Vanderhaeghe, O., Ferré, E., Teyssier, C., Whitney, D. L., 2011. Flow of partially molten crust and the internal dynamics of a migmatite dome, Naxos, Greece. Tectonics, 30(3).

Kruse, S., and Williams, P. F., 2005. Brittle faulting in the Thor Odin culmination, Monashee complex, southern Canadian Cordillera: constraints on geometry and kinematics. Canadian Journal of Earth Sciences, 42(12), 2141-2160.

Lecomte, E., Jolivet, L., Lacombe, O., Denèle, Y., Labrousse, L., Le Pourhiet, L., 2010. Geometry and kinematics of Mykonos detachment, Cyclades, Greece: Evidence for slip at shallow dip. Tectonics, 29 (5). DOI: 10.1029/2009TC002564

Lister, G. S., Banga, G., Feenstra, A., 1984. Metamorphic core complexes of Cordilleran type in the Cyclades, Aegean Sea, Greece. Geology, 12, 221–225, doi:10.1130/0091-7613(1984)12<221: MCCOCT>2.0.CO;2

Lorencak, M., Seward, D., Vanderhaeghe, O., Teyssier, C., Burg, J.P., 2001. Low-temperature cooling history of the Shuswap metamorphic core complex, British Columbia: Constraints from apatite and zircon fission-track ages. Canadian Journal of Earth Sciences, 38, 1615-1625.

Martin, L., S. Duchêne, E. Deloule, Vanderhaeghe, O., 2006. The isotopic composition of zircon and garnet: A record of the metamorphic history of Naxos, Greece. Lithos, 87, 174–192, doi:10.1016/j. lithos.2005.06.016.

Martin, L. A. J., S. Duchêne, E. Deloule, Vanderhaeghe, O., 2008. Mobility of trace elements and oxygen in zircon during metamorphism: Consequences for geochemical tracing. Earth Planet. Sci. Lett., 267, 161–174, doi:10.1016/j.epsl.2007.11.029.

Mathews, W.H., 1981. Early Cenozoic resetting of potassium-argon dates and geothermal history of north Okanagan area, British Columbia. Canadian Journal of Earth Sciences, v. 18, p. 1310–1319.

McClaughry, J. D., and Gaylord, D. R., 2005. Middle Eocene sedimentary and volcanic infilling of an evolving supradetachment basin: White Lake Basin, south-central British Columbia. Canadian Journal of Earth Sciences, 42(1), 49-66.

Mehl, C., Jolivet, L., and Lacombe, O., 2005. From ductile to brittle: Evolution and localization of deformation below a crustal detachment (Tinos, Cyclades, Greece). Tectonics, 24(4), DOI: 10.1029/2004TC001767

Menant, A., Jolivet, L., Augier, R., Skarpelis, N., 2013. The North Cycladic Detachment System and associated mineralization, Mykonos, Greece: Insights on the evolution of the Aegean domain. Tectonics, DOI: 10.1002/tect.20037

Monger, J.W.H., Price, R.A., Tempelman-Kluit, D.J., 1982. Tectonic accretion and the origin of the two major metamorphic and plutonic welts in the Canadian Cordillera. Geology, 10, 70-75.

Morrison, J., and Anderson, J. L., 1998. Footwall refrigeration along a detachment fault: implications for thermal evolution of core complexes. Science, v. 279, p. 63-66

Mulch, A., Teyssier, C., Cosca, M. A., Vanderhaeghe, O., Vennemann, T. W., 2004. Reconstructing paleoelevation in eroded orogens. Geology, v. 32, p. 525-528.

Mulch, A., Teyssier, C., Cosca, M. A., Vennemann, T. W., 2006. Thermomechanical analysis of strain localization in a ductile detachment zone. Journal of Geophysical Research: Solid Earth, (1978–2012), 111(B12).

Mulch, A., Teyssier, C., Cosca, M. A., Chamberlain, C. P., 2007. Stable isotope paleoaltimetry of Eocene core complexes in the North American Cordillera. Tectonics, v. 26., TC4001, doi:10.1029/2006TC001995.

Norlander, B.H., Whitney, D.L., Teyssier, C., Vanderhaeghe, O., Wiebe, R.A., 2002. Partial melting and decompression of the Thor-Odin Dome, Shuswap metamorphic core complex, Canadian Cordillera. Lithos, v. 61, p. 103-125.

Nyman, M.W., Pattison, D.R.M., Ghent, E.D., 1995. Melt extraction during formation of K-feldspar-sillimanite migmatites, west of Revelstoke, British Columbia. Journal of Petrology, 36, 351-372.

Parkinson, D., 1985. Geochronology of the western side of the Okanogan metamorphic core complex, southern B.C. Geological Society of America Abstracts with Programs, 17, 399.

Parrish, R.R., Carr, S.D., Parkinson, D.L., 1988. Eocene extensional tectonics and geochronology of the southern Omineca belt, British Colombia and Washington. Tectonics, v. 7, p. 181-212.

Person, M. P., Mulch, A., Teyssier, C., Gao, Y., 2007. Isotope Transport and Exchange During Detachment Tectonics, Shuswap Metamorphic Core Complex, British Columbia. American Journal of Science, v. 307, p. 555-589.

Regenauer-Lieb, K., and Yuen, D., 2004. Positive feedback of interacting ductile faults from coupling of equation of state, rheology and thermal-mechanics. Physics of the Earth and Planetary Interiors, 142(1), 113-135.

Rey, P., Teyssier, C., Whitney, D.L., 2009a. Extension rates, crustal melting and core complex dynamics. Geology, 37, 391– 394.

Rey, P.F., Teyssier, C., Whitney, D.L., 2009b. The Role of Partial Melting and Extensional Strain Rates in the Development of Metamorphic Core Complexes. Tectonophysics, v. 477, p. 135–144.

Rey, P.F., Teyssier, C., Kruckenberg, S.C., Whitney, D.L., 2011. Viscous collision in channel explains double domes in metamorphic core complexes. Geology, 39, 4, 387-390

Ring, U., Will, T., Glodny, J., Kumerics, C., Gessner, K., Thomson, S., Güngör, T., Monie, P., Okrusch, M., Drüppel, K., 2007. Early exhumation of high-pressure rocks in extrusion wedges: Cycladic blueschist unit in the eastern Aegean, Greece, and Turkey. Tectonics, 26, TC2001, doi:10.1029/2005TC001872.

Ring, U., Glodny, J., Will, T., Thomson, S., 2010. The Hellenic subduction system: High-pressure metamorphism, exhumation,normal faulting, and large-scale extension. Annu. Rev. Earth Planet. Sci., 38, 45–76 doi:10.1146/annurev.earth.050708.170910.

Robinson, A. C., Yin, A., Lovera, O.M., 2007. The role of footwall deformation and denudation in controlling cooling age patterns of detachment systems: An application to the Kongur Shan extensional system in the Eastern Pamir. Tectonophysics, 496, 28-43.

Sánchez-Gómez, M., Avigad, D., Heimann, A., 2002. Geochronology of clasts in allochthonous Miocene sedimentary sequence on Mykonos and Paros Islands: implications for backarc extension in the Aegean Sea. Journal of the Geological Society of London 159, 45–60.

Schenker, F. L., Gerya, T., Burg, J. P., 2012. Bimodal behavior of extended continental lithosphere: Modeling insight and application to thermal history of migmatitic core complexes. Tectonophysics, 579, 88-103.

Seward, D., Vanderhaeghe, O., Siebenaller, L., Thomson, S., Hibsch, C., Zingg, A., Duchêne, S. (2009). Cenozoic tectonic evolution of Naxos Island through a multi-faceted approach of fission-track analysis. Geological Society, London, Special Publications, 321(1), 179-196.

Siebenaller, L., Boiron, M. C., Vanderhaeghe, O., Hibsch, C., Jessell, M. W., Andre-Mayer, A.S., France-Lanord, C., and Photiades, A., 2012. Fluid record of rock exhumation across the brittle–ductile transition during formation of a Metamorphic Core Complex (Naxos Island, Cyclades, Greece). Journal of Metamorphic Geology, 31, 313-338

Spalla, M. I., Zanoni, D., Williams, P. F., Gosso, G., 2011. Deciphering cryptic P–Td–t histories in the western Thor-Odin dome, Monashee Mountains, Canadian Cordillera: A key to unravelling pre-Cordilleran tectonic signatures, Journal of Structural Geology, 33(3), 399-421.

Stoffel, K.L., Joseph, N.L., Waggoner, S.Z., Gulick, C.W., Korosec, M.A., Bunning, B.B., 1991. Geologic map of Washington Northeast Quadrant. Washington Division of Geology and Earth Resources, Geologic Map GM-39, 1:250 000, 1 sheet, 44 p.

Stübner, K., Ratschbacher, L., Weise, C., Chow, J., Hoffman, J., Khan, J., Rutte, D., Sperner, B., Pfander, J.A., Hacker, B.R., Dunkl, I., Tichomirowa, M., Stearns, M.A., Bahram, I., Gadoev, M., Gloaguen, R., Jonckheere, R., Kanaev, E., Minaev, V., Oimahmadoc, I., Rajabov, N., Stanek, K.P., 2013. The giant Shakhdara migmatitic gneiss dome, Pamir, India–Asia collision zone, II: Timing of dome formation. Tectonics, 32(5), 1404-1431.

Suydam, J.D., and Gaylord, D.R., 1997. Toroda Creek half graben, northeast Washington: Late-stage sedimentary infilling of a syn-extensional basin. Geological Society of America Bulletin, 109, 1333-1348.

Teyssier, C., and Whitney, D.L., 2002. Gneiss domes and orogeny. Geology,v. 30, p. 1139- 1142.

Teyssier, C., Ferré, E.C., Whitney, D.L., Norlander, B., Vanderhaeghe, O., Parkinson, D., 2005. Flow of partially molten crust and origin of detachments during collapse of the Cordilleran orogen, in Bruhn, D., Burlini, L., eds., High-strain zones: Structure and physical properties: London. Geological Society of London Special Publications, vol. 245pp. 39-64,.

Tirel, C., Brun, J.P., and Burov, E., 2004. Thermomechanical modeling of extensional gneiss domes, in Whitney, D.W., Teyssier, C., Siddoway, C.S., eds., Gneiss domes in orogeny: Boulder, Colorado. Geological Society of America Special Paper, 380, p. 67–78.

Toraman, E., Whitney, D.L., Teyssier, C., Fayon, A.K., Thomson, S.K., Reiners, P.W., 2012. Low-temperature thermochronology record of tectonic and erosional exhumation of gneiss domes in the northern North American Cordillera. Geological Society of America Abstract with Programs, vol. 44, no. 7, p.128

Vanderhaeghe, O., Teyssier, C., Wysoczanski, R., 1999. Structural and geochronological constraints on the role of partial melting during the formation of the Shuswap metamorphic core complex at the latitude of the Thor-Odin Dome, British Columbia. Canadian Journal of Earth Sciences, v. 36, p. 917-943.

Vanderhaeghe, O., and Teyssier C., 2001. Crustal scale rheological transitions during late-orogenic collapse. Tectonophysics, 335, 211-228.

Vanderhaeghe, O., Teyssier, C., McDougall, I., Dunlap, W.J, 2003. Cooling and exhumation of the Shuswap metamorphic core complex constrained by Ar/Ar thermochronology. Geological Society of America Bulletin, v 115, p. 200-216.

Vanderhaeghe, O., 2004. Structural development of the Naxos migmatite dome, in Gneiss Domes in Orogeny, edited by D. L. Whitney et al.. Spec. Pap. Geol. Soc. Am., 380, 211–227, doi:10.1130/0-8137-2380-9.211.

Whitney, D.L., Paterson, S.R., Schmidt, K.L., Glazner, A.F., Kopf, C.F., 2004. Growth and demise of continental arcs and orogenic plateaux in the North American Cordillera: from Baja to British Columbia, in Grocott, J., McCaffrey, K.J.W., Taylor, G. and Tikoff, B., eds., Vertical Coupling and Decoupling in the Lithosphere. Geological Society of London Special Publications, vol. 227, pp. 167-176.

Whitney, D. L., Teyssier, C., Rey, P., Buck, W. R., 2013. Continental and oceanic core complexes. Geological Society of America Bulletin, 125(3-4), 273-298.

Wijbrans, J. R., and McDougall, I., 1986. 40Ar/39Ar dating of white micas from an Alpine high-pressure metamorphic belt on Naxos (Greece): the resetting of the argon isotopic system. Contributions to Mineralogy and Petrology, 93(2), 187-194.

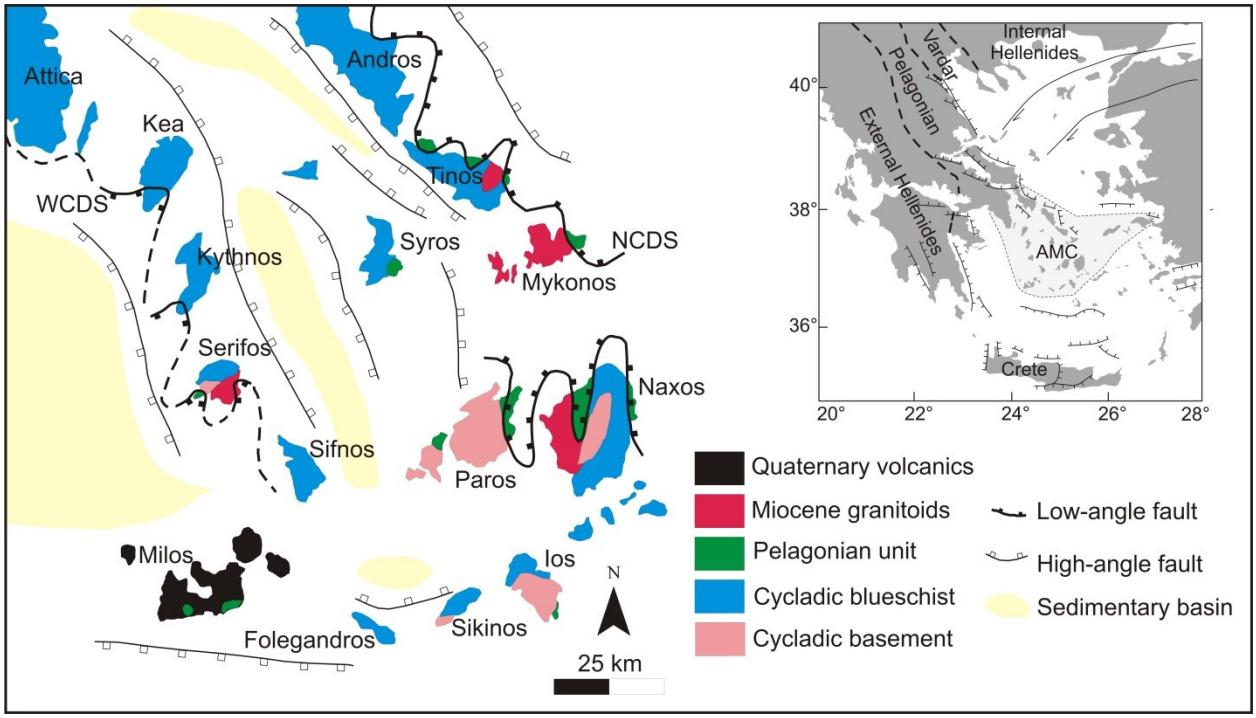

Figure 4.1. Simplified geologic map of the Cycladic islands (after Grasemann et al., 2012). Inset shows tectonic belts of the Aegean domain. WCDS- West Cycladic detachment system; NCDS- North Cycladic detachment system

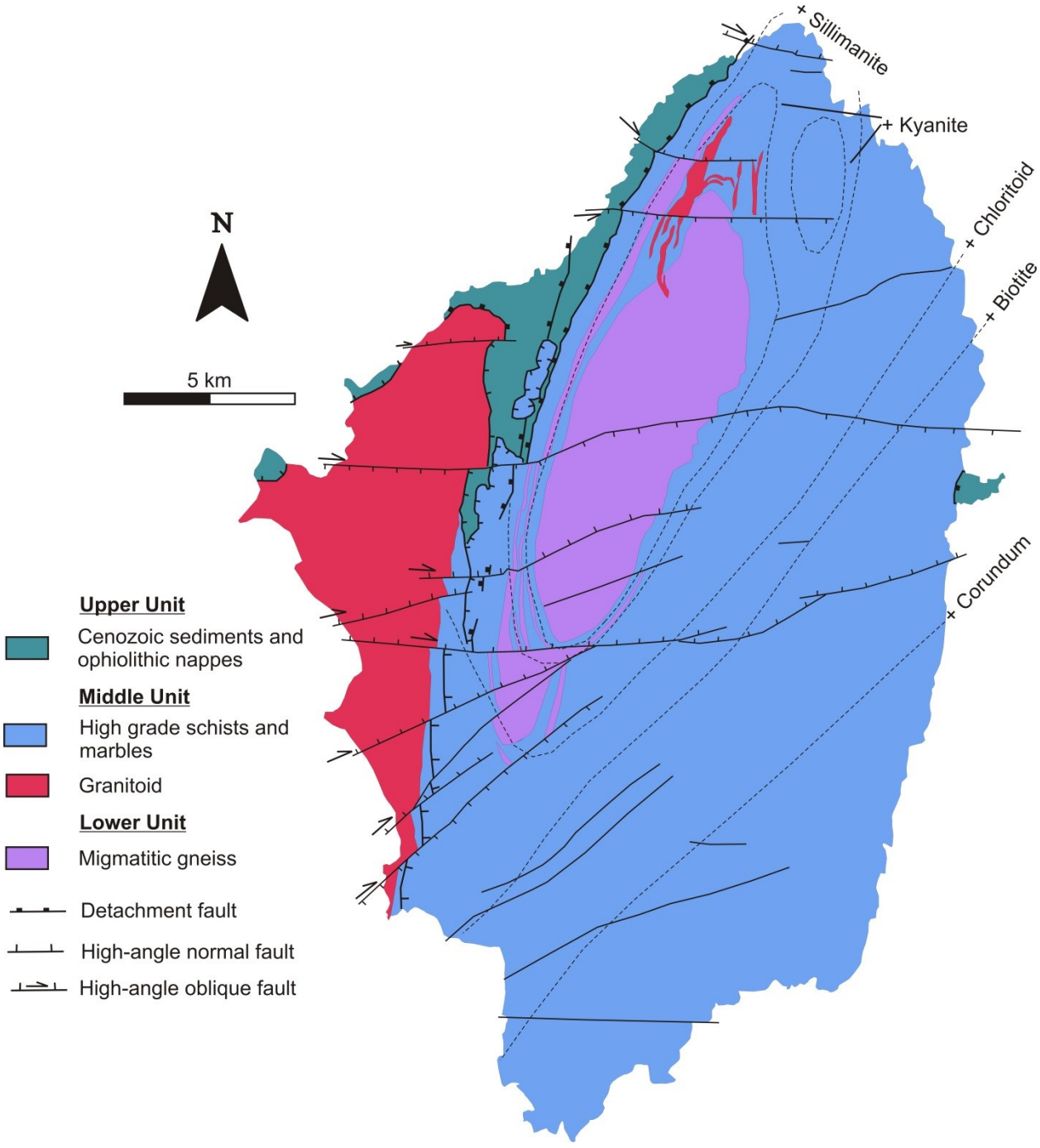

Figure 4.2. Simplified geologic map of Naxos (after Siebenaller et al., 2013).

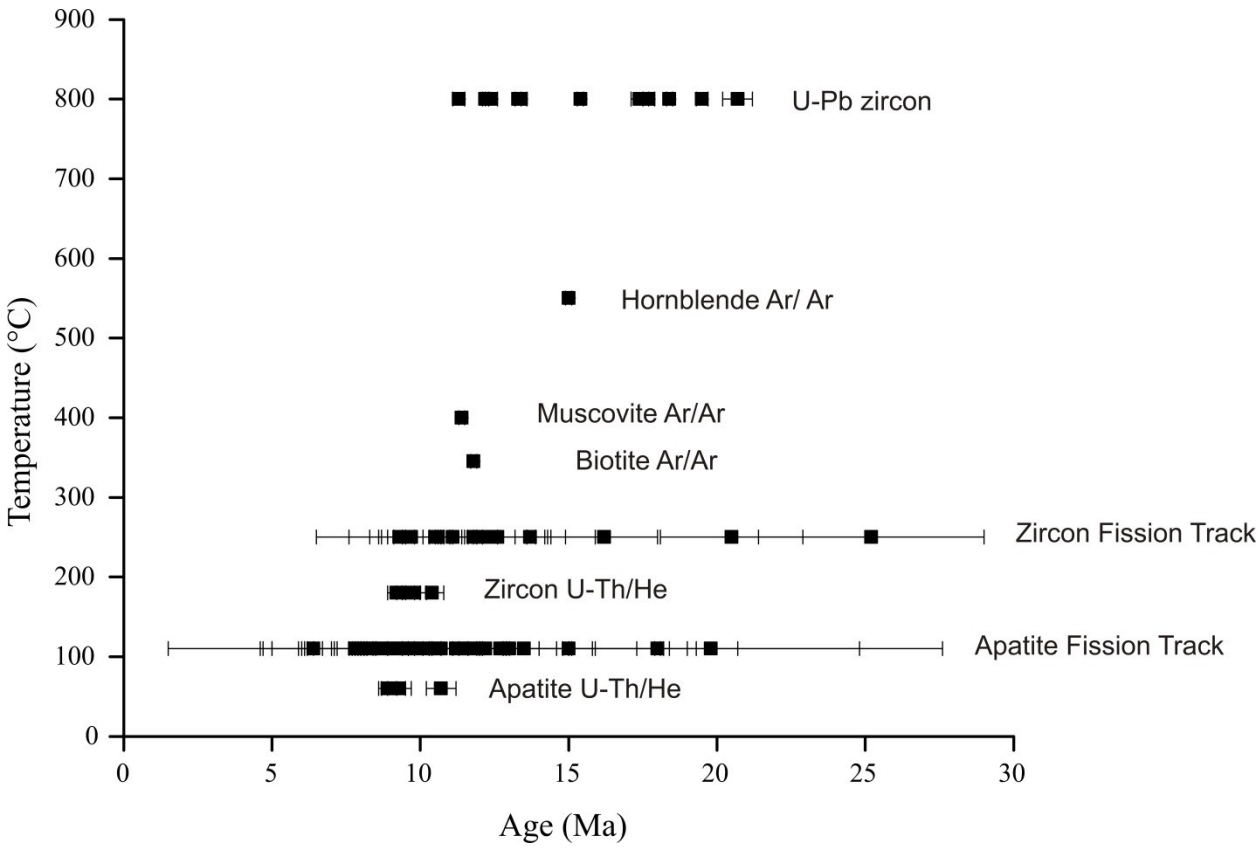

Figure 4.3. Temperature-time plot of geo/thermochronological data from the Naxos dome (Wijbrans and McDougall, 1988; Keay et al., 2001; Martin et al., 2006, 2008; Duchêne et al., 2006; Brichau et al., 2006; Seward et al., 2009)..

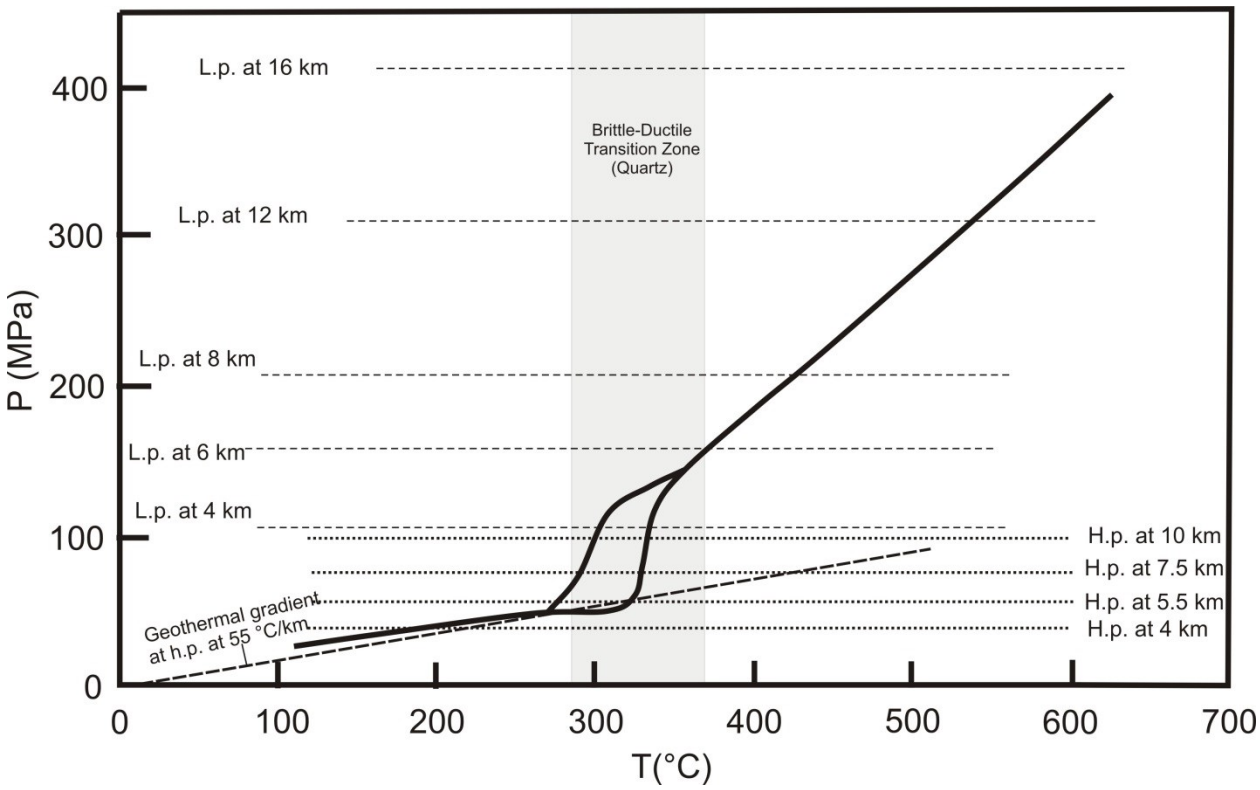

Figure 4.4. P-T-t diagram for Naxos from Seibenaller et al. (2013). H.p.- hydrostatic pressure; L.p. – lithostatic pressure.

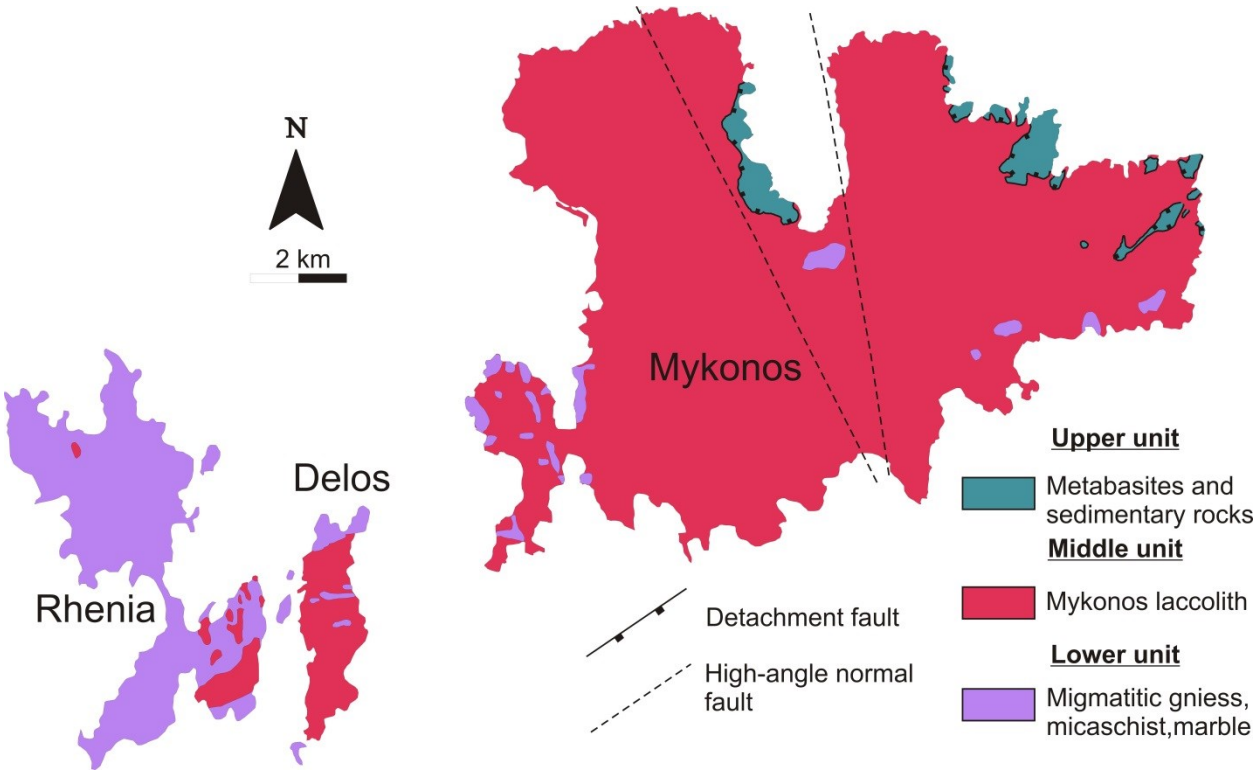

Figure 4.5. Simplified geologic map of Mykonos (modified after Menant et al., 2013)

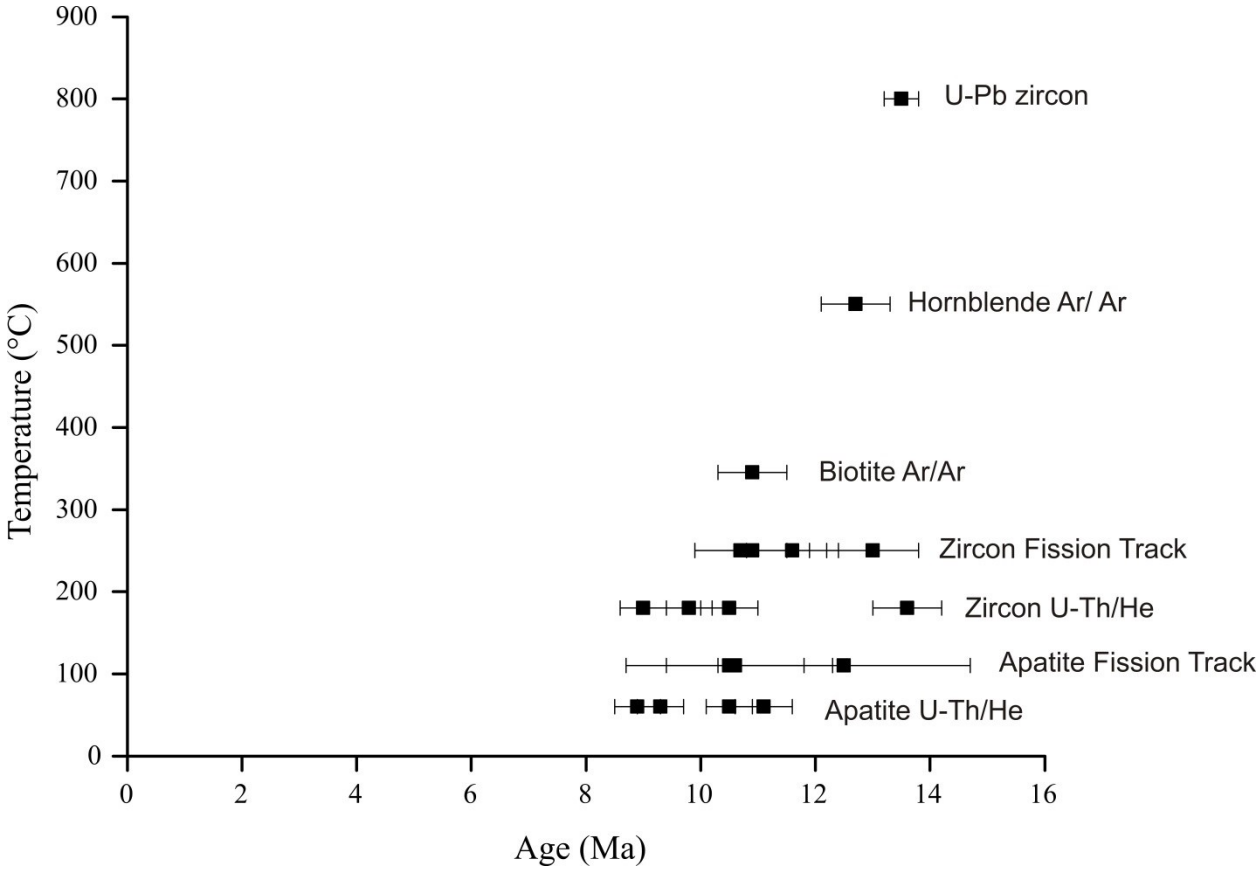

Figure 4.6. Temperature-time plot of geo/thermochronological data from Mykonos island (Brichau et al., 2008).

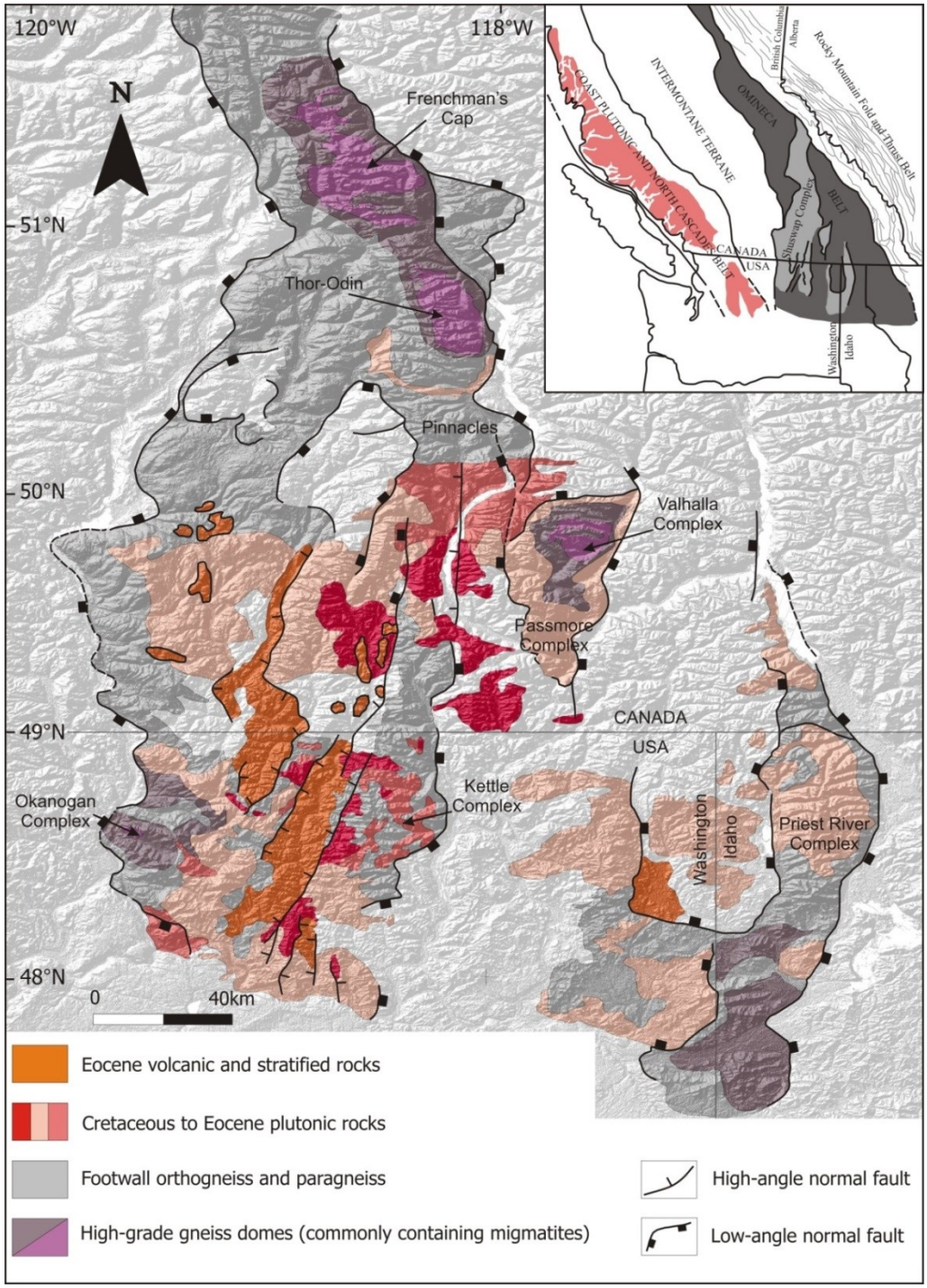

Figure 4.7. Simplified geologic map of the Omineca Belt (after Kruckenberg et al., 2008). Inset shows the location of the Omineca Belt and tectonic belts of the northern Cordillera.

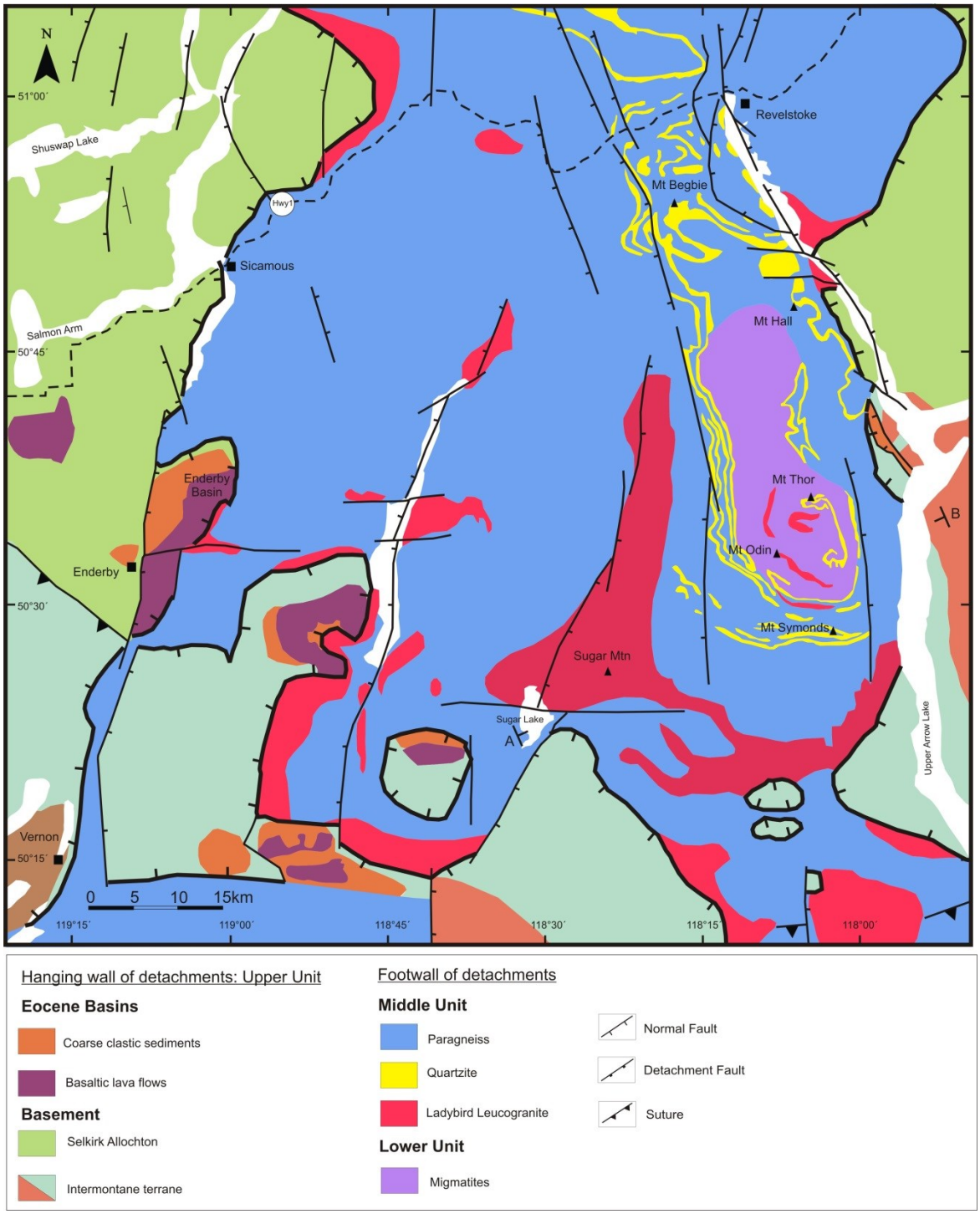

Figure 4.8. Simplified geologic map of the Thor-Odin dome (modified after Vanderhaeghe et al., 2003)

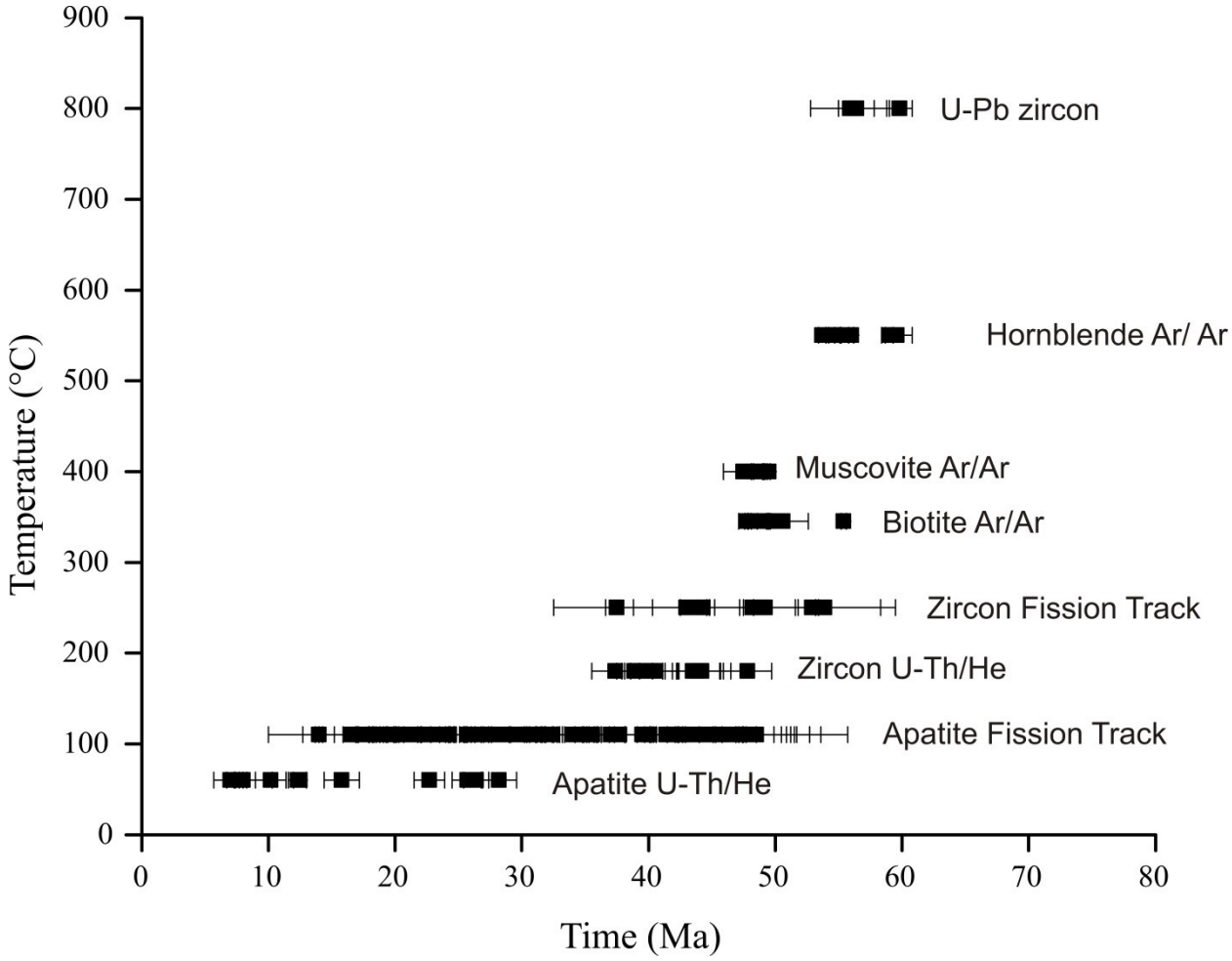

Figure 4.9. Temperature-time plot of geo/thermochronological data from the Thor-Odin dome (Lorencak et al., 2001; Vanderhaeghe et al., 2003; Teyssier et al., 2005; Hinchey et al., 2006; Mulch et al., 2006; Toraman et al, 2012)

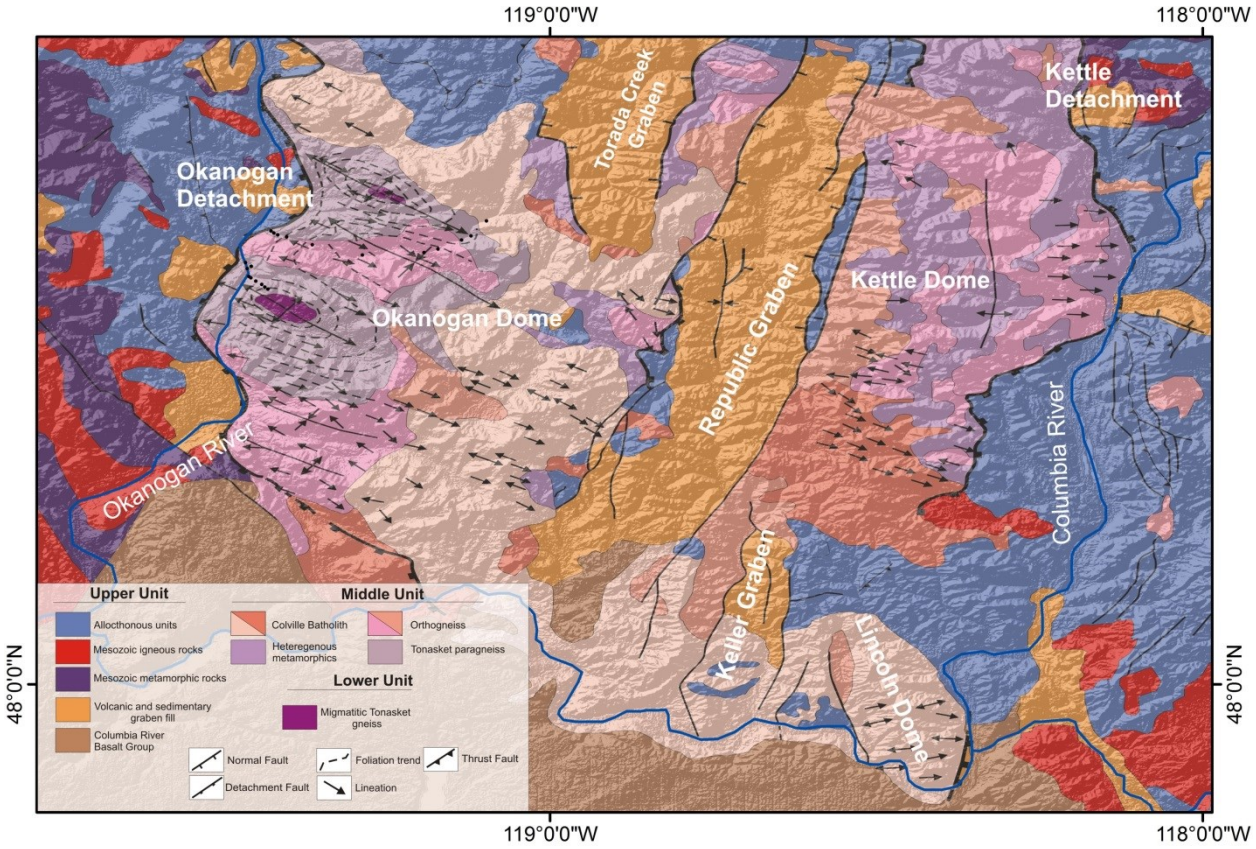

Figure 4.10. Simplified geological map of the Okanogan Dome (after Stoffel et al., 1991 and Kruckenberg et al., 2008).

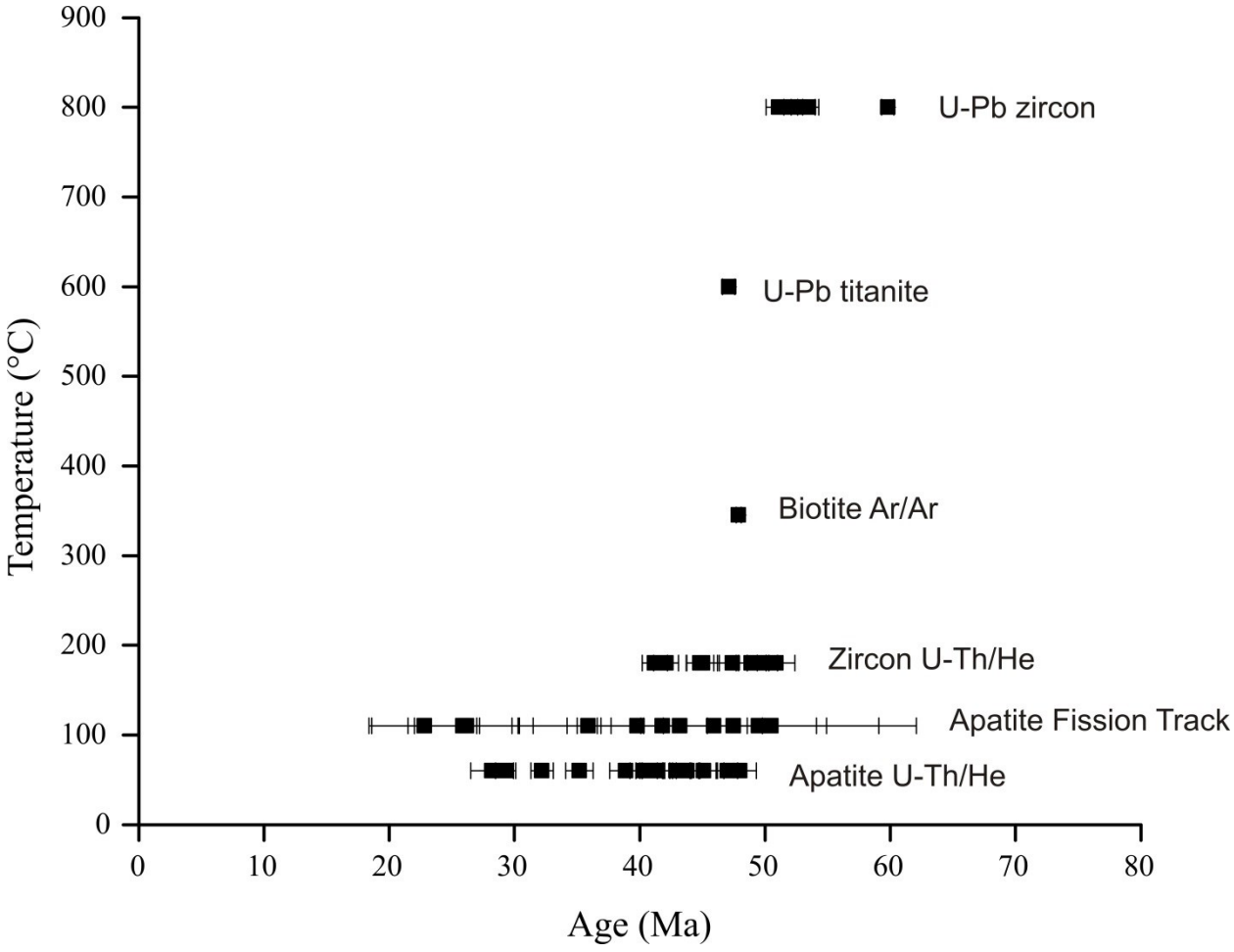

Figure 4.11. Temperature-time plot of geo/thermochronological data from the Okanogan dome. High-to-medium temperature age data (U-Pb and Ar/Ar) are from Kruckenberg et al. (2008).

Conclusions

The results of this dissertation provide insights into the interaction among deep and surface processes during exhumation of partially molten mid-to-lower crustal rocks in the hinterland of the North American Cordillera. This study focuses on the Thor-Odin, Frenchman's Cap, and Okanogan domes that are exposed in the Shuswap metamorphic core complex and were developed during orogenic collapse of previously thickened crust. Both domes record similar conditions of metamorphism, timing of melt formation and crystallization, and cooling through ~350 °C (Norlander et al., 2002; Vanderhaeghe et al., 2003; Kruckenberg et al., 2008; Kruckenberg and Whitney, 2011). The present day topography is drastically different between two domes: the local topographic relief is up to 2 km at the Thor-Odin dome whereas the Okanogan dome has more subdued topography with ≤ 1km of relief. How these rocks continued to cool below ~350°C to surface temperature, therefore, is critical to understand the complete exhumation history of the partially molten crust, including the roles of detachment tectonics and erosional processes, as well as topographic evolution.

The results of multiple low-temperature thermochronology data from different structural levels and elevations document the timing and rates of Cenozoic cooling and exhumation of the Thor-Odin and Frenchman's Cap domes (Chapter 2 of this thesis). Zircon U-Th/He (ZHe) samples are restricted to low elevations (~500 m) and ages range from 45 to 37 Ma. Apatite fission track (AFT) ages range from 48 to 14 Ma, and generally increase with elevation with a break in slope at ~1800 m and ca. 45 Ma in age-

elevation profiles. Combined with tack-length modeling, these AFT ages reveal the presence of the top of a fossil apatite partial annealing zone at ~1800 m, indicating that the dome rocks reached near-surface depths (1-2 km) during the initial exhumation that was largely controlled by detachment tectonics. AFT age and track length data further indicate a second cooling event younger than the middle-Miocene. Apatite U-Th/He (AHe) ages range from 26 to 5 Ma and some low-elevation samples (~500 m) reveal significant intra-sample age variations. Thermal modeling of these low-elevation samples and AHe age variations in single grain ages indicate that the second cooling event is linked to continental glaciation event ca 3 Ma, which lead to accelerated erosion and localized incision in valleys (Chapter 2 of this thesis).

In the Okanogan dome, low-T history is documented in along two transects. ZHe ages from the transect parallel to the shear direction range from 51 to 41 Ma and decrease toward the detachment fault, indicating a slip rate of 3.7 km/myr during faulting. AFT ages range from 51 to 23 Ma and are spatially invariant across the dome. Similar to AFT ages, AHe ages vary between 48 to 28 Ma (Chapter 3 of this thesis). Therefore, AFT and AHe chronometers record ~2 km of erosional unroofing after the cessation of detachment faulting. The results of thermal modeling also document spatial differences in cooling patterns; rocks closer to the detachment zone display rapid cooling rates (≥ 100 °C/myr) whereas deeper structural levels record lower cooling rates (10-30 °C/myr) (Chapter 3 of this thesis).

Results from this thesis work and previous research from the domes exposed in the central Aegean domain indicate the first-order similarities in thermo-mechanical evolution of these migmatite-cored metamorphic core complexes. In both locations

dome rocks experience decompression at high-temperature that facilitates the advection of heat to shallow crustal depths. This heat advection results in elevated geothermal gradients and displacement of the brittle-ductile transition zone to shallow depths, and therefore modifies the crustal rheology and hydrology. The results indicate that percolation of meteoric-fluids through faults and fractures assists rapid cooling of rocks and enhances brittle rheology (Chapter 4 of this thesis).

References

Kruckenberg, S.C., D.L. Whitney, C. Teyssier, M. Fanning, and W.J. Dunlap (2008), Paleocene-Eocene migmatite crystallization, extension, and exhumation in the hinterland of the northern Cordillera: Okanogan dome, Washington USA, Geological Society of America Bulletin, 120(7-8), 912-929.

Kruckenberg, S. C., and D.L. Whitney (2011), Metamorphic evolution of sapphirine-and orthoamphibole-cordierite-bearing gneiss, Okanogan dome, Washington, USA, Journal of Metamorphic Geology, 29(4), 425-449.

Norlander, B.H., D.L. Whitney, C. Teyssier, O. Vanderhaeghe, and R.A. Wiebe (2002), Partial melting and decompression of the Thor-Odin Dome, Shuswap metamorphic core complex, Canadian Cordillera, Lithos, v. 61, p. 103-125.

Vanderhaeghe, O., C. Teyssier, I. McDougall and W.J Dunlap (2003), Cooling and exhumation of the Shuswap metamorphic core complex constrained by Ar/Ar thermochronology, Geological Society of America Bulletin, v 115, p. 200-216

Complete Bibliography

Altherr, R., H. Kreuzer, I. Wendt, H. Lenz, G. A. Wagner, J. Keller, W. Harre, Hohndorf, A., 1982. A Late Oligocene/Early Miocene high temperature belt in the anti-cycladic crystalline complex (SE Pelagonian, Greece), Geol. Jb. 23, 97–164.

Andersen, T. B., Jamtveit, B., Dewey, J. F., Swensson, E., 1991. Subduction and eduction of continental crust: major mechanisms during continent-continent collision and orogenic extensional collapse, a model based on the south Norwegian Caledonides, Terra Nova, 3(3), 303-310.

Armstrong, R.L., 1982. Cordilleran metamorphic core complexes; from Arizona to southern Canada, Annual Review of Earth and Planetary Sciences, v. 10, p. 129-154.

Armstrong, R.L., and Ward, P.L., 1991. Evolving geographic patterns of Cenozoic magmatism in the North American Cordillera; the temporal and spatial association of magmatism and metamorphic core complexes, J. Geophys. Res., 96(B8), 13201–13224, doi:10.1029/91JB00412 .

Avigad, D., Baer, G., Heimann, A., 1998. Block rotations and continental extension in the central Aegean Sea: palaeomagnetic and structural evidence from Tinos and Mykonos (Cyclades, Greece), Earth and Planetary Science Letters, 157(1), 23-40.

Axen, G. J., Lam, P. S., Grove, M., Stockli, D. F., & Hassanzadeh, J., 2001. Exhumation of the west-central Alborz Mountains, Iran, Caspian subsidence, and collision-related tectonics, Geology, 29(6), 559-562.

Bargnesi, E. A., Stockli, D. F., Mancktelow, N., Soukis, K., 2012. Miocene core complex development and coeval supradetachment basin evolution of Paros, Greece, insights from (U-Th)/He thermochronometry, Tectonophysics, 595–596 (2013) 165–182

Beaumont, C., Jamieson, R.A., Nguyen, M.H., and Lee, B., 2001. Himalayan tectonics explained by extrusion of a low-viscosity crustal channel coupled to focused surface denudation, Nature (London), v. 414, p. 738-742.

Bird, P., 1991. Lateral extrusion of lower crust from under high topography, in the isostatic limit, Journal of Geophysical Research, 96, 10275-10286.

Block, L., and Royden, L. H., 1990. Core complex geometries and regional scale flow in the lower crust, Tectonics, 9(4), 557-567.

Brandon, M. T., Roden-Tice, M. K., & Garver, J. I., 1998. Late Cenozoic exhumation of the Cascadia accretionary wedge in the Olympic Mountains, northwest Washington State, Geological Society of America Bulletin, 110(8), 985-1009.

Brichau, S., Ring, U., Ketcham, R. A., Carter, A., Stockli, D., Brunel, M., 2006. Constraining the long-term evolution of the slip rate for a major extensional fault system in the central Aegean, Greece, using thermochronology. Earth and Planetary Science Letters, 241(1), 293-306.

Brichau, S., Ring, U., Carter, A., Monié, P., Bolhar, R., Stockli, D., Brunel, M., 2007. Extensional faulting on Tinos island, Aegean sea, Greece: How many detachments?, Tectonics, 26 (4), doi: 10.1029/2006TC001969

Brichau, S., Ring, U., Carter, A., Bolhar, R., Monié, P., Stockli, D., & Brunel, M., 2008. Timing, slip rate, displacement and cooling history of the Mykonos detachment footwall, Cyclades, Greece, and implications for the opening of the Aegean Sea basin, Journal of the Geological Society, 165(1), 263-277.

Brown, R.L., 1980. Frenchman Cap dome, Shuswap complex, British Columbia: a progress report. *Current Research*, Part A, Geological Survey of Canada, Paper 80-1A, 47–51.

Brown, R.L., Journeay, J.M., Lane, L.S., Murphy, D.C., Rees, C.J., 1986. Obduction, backfolding and piggyback thrusting in the metamorphic hinterland of the southeastern Canadian Cordillera, J. Struct. Geol., 8, 255-268.

Brown, S.R., Gibson, H.D., Andrews, G.D.M., Thorkelson, D.J., Marshall, D.D., Vervoot, J.D., and Rayner, N., 2012. New constrains on Eocene extension within the Canadian Cordillera and identification of Phanerozoic protoliths for footwall gneisses of the Okanagan Valley shear zone, Lithosphere, 4, 4, 354-377.

Brun, J. P., Faccenna, C., 2008. Exhumation of high-pressure rocks driven by slab rollback, Earth Planetary Science Letters, 272, 1–7, doi:10.1016/ j.epsl.2008. 1002.1038

Buick, I. S., and Holland, T. J. B., 1989. The PTt path associated with crustal extension, Naxos, Cyclades, Greece, Geological Society London Special Publications, 43(1), 365-369.

Burg, J. P., Van Den Driessche, J., Brun, J. P., 1994. Syn-to post-thickening extension in theVariscan Belt of Western Europe: modes and structural consequences, Géologie de la France, 3, 33-51.

Callahan, O.A., 2007. Exhumation and topographic development of the Okanogan Range, northeast North Cascades [Master Thesis], Bellingham, Western Washington University, 207 p.

Carlson, D.H., and Moye, F.J., 1990. The Colville igneous complex: Paleogene volcanism, plutonism, and extension in northeastern Washington, *in* Anderson, J.L., ed., The nature and origin of Cordilleran magmatism, Geological Society of America Memoir, v. 174, p. 375–394.

Carlson, W.D., Donelick, R.A., and Ketcham, R.A., 1999. Variability of apatite fission-track annealing kinetics I: Experimental results, American Mineralogist, 9, 1213–1223.

Carr, S.D., 1991. U-Pb zircon and titanite ages of three Mesozoic igneous rocks south of the Thor-Odin-Pinnacles area, southern Omineca Belt, British Columbia, Can. J. Earth Sci., 28, 1877-1882.

Carr, S.D, 1992. Tectonic setting and U-Pb geochronology of the early Tertiary Ladybird leucogranite suite, Thor-Odin-Pinnacles area, southern Omineca belt, British Colombia, Tectonics, 11, 258-278.

Carter, T.J., Kohn, B.P., Foster, D.A., Gleadow, A.J.W., 2004. How the Harcuvar Mountains metamorphic core complex became cool: Evidence from apatite (U-Th)/He thermochronometry, Geology, v. 32, p. 985–988, doi: 10.1130/G20936.1.

Carter, T.J., Kohn, B.P., Foster, D.A., Gleadow, A.J.W., Woodhead, J.D., 2006. Late-stage evolution of the Chemehuevi and Sacramento detachment faults from apatite (U-Th)/He thermochronometry-Evidence for mid-Miocene accelerated slip, Geological Society of America Bulletin, v. 118, p. 689–709.

Chamberlain, C. P., Mix, H. T., Mulch, A., Hren, M. T., Kent-Corson, M. L., Davis, S. J., Horton, T.W., & Graham, S. A., 2012. The Cenozoic climatic and topographic evolution of the western North American Cordillera, American Journal of Science, 312(2), 213-262.

Cheney, E.S., 1980. Kettle dome and related structures of northeastern Washington, in Crittenden, M.D., Coney, P.J., Davis, G.H., eds., Cordilleran Metamorphic Complexes. Geological Society of America Memoir, v. 153, p. 463-483.

Church, N. B., 1973. Geology of the White Lake basin, British Columbia Dept. of Mines Petroleum Resources Bull., v. 61, p. 120

Clark, M.K. & Royden, L.H., 2000. Topographic ooze: Building the eastern margin of Tibet by lower crustal flow, Geology, 28, 703-706.

Colpron, M., Price, R.A., Archibald, D.A., Carmichael D.M., 1996. Middle Jurassic exhumation along the western flank of the Selkirk fan structure: thermobarometric and thermochronometric constrains from the Illecillewaet synclinorium, Southeastern British Columbia, Geological Society of America Bulletin, 108, 1372–1392.

Coney, P.J., 1980. Cordilleran metamorphic core complexes; an overview, *in* Crittenden, M.D., Coney, P.J., Davis, G.H., eds., Cordilleran metamorphic core complexes: Boulder, Colorado, Geological Society of America Memoir, p. 7-31.

Coney, P.J., Harms, T.A., 1984. Cordilleran metamorphic core complexes: Cenozoic extensional relics of Mesozoic compression, Geology, v. 12, p. 550-554.

Crittenden, M.D., Coney, P.J., and Davis, G.H., 1980. Cordilleran metamorphic core complexes, Geological Society of America Memoir, v. 153, 490 p.

Crowley, J., 1997. U-Pb geochronologic constraints on the cover sequence of the Monashee Complex, Canadian Cordillera: Paleoproterozoic deposition on basement, Can. J. Earth Sci., 34, 1008-1022.

Crowley, J.L., and Parrish, R.R., 1999. U-Pb isotopic constraints on diachronous metamorphism in the northern Monashee complex, southern Canadian Cordillera, Journal of Metamorphic Geology, 17, 483-502.

Crowley, J.L., Brown, R.L., and Parrish, R.R., 2001. Diachronous deformation and a strain gradient beneath the Selkirk allochthon, northern Monashee complex, southeastern Canadian Cordillera, Journal of Structural Geology 23, 1103-1121.

Crowley, J.L., Brown, R.L., Gervais, F., and Gibson, H.D., 2008. Assessing inheritance of zircon and monazite in granitic rocks: an example from the Monashee Complex, Canadian Cordillera, Journal of Petrology, 49, 1915-1929.

Cubley, J. F., Pattison, D. R. M., Tinkham, D. K., & Fanning, C. M., 2012. U-Pb geochronological constraints on the timing of episodic regional metamorphism and rapid high-T exhumation of the Grand Forks complex, British Columbia, Lithos, v. 156, p. 241-267

Cubley, J. F., Pattison, D. R. M., Archibald, D. A., & Jolivet, M., 2013. Thermochronological constraints on the Eocene exhumation of the Grand Forks complex, British Columbia, based on 40Ar/39Ar and apatite fission track geochronology, Canadian Journal of Earth Sciences, 50(5), 576-598.

DeCelles, P.G., 2004. Late Jurassic to Eocene evolution of the Cordilleran thrust belt and foreland basin system, western U.S.A., American Journal of Science, 304, 105–168.

Denèle, Y., Olivier, P., Gleizes, G., Barbey, P., 2007. The Hospitalet gneiss dome (Pyrenees) revèisited, Lateral flow during Variscan transpression in the middle crust, Terra Nova, v. 19, p. 419–453, doi:10.1111/j.1365-3121 .2007.00770.x.

Densmore, M. S., Ehlers, T. A., Woodsworth, G.J., 2007. Effect of Alpine glaciation on thermochronometer age-elevation profiles. Geophysical Research Letters, 34, L02502, doi:10.1029/2006GL028371.

Dewey, J. F., Şengör, A.M.C., 1979. Aegean and surrounding regions: Complex multiplate and continuous tectonics in a convergent zone, Geological Society of America Bulletin, 90, 84–92, doi:10.1130/0016-7606(1979) 90<84:AASRCM> 2.0.CO;2.

Dewey, J. F., 1998. Extensional collapse of orogens, Tectonics, 7(6), 1123-1139.

Donelick, R. A., & Miller, D. S., 1991. Enhanced tint fission track densities in low spontaneous track density apatites using ^{252}Cf-derived fission fragment tracks: A model and experimental observations, International Journal of Radiation Applications and Instrumentation. Part D. Nuclear Tracks and Radiation Measurements, 18(3), 301-307.

Donelick, R. A., Ketcham, R. A., and Carlson, W. D., 1999. Variability of apatite fission-track annealing kinetics: II. Crystallographic orientation effects, American Mineralogist, 84, 1224-1234.

Donelick, R.A., O'Sullivan, P.B., and Ketcham, R.A., 2005. Apatite fission track analysis, Reviews in Mineralogy and Geochemistry, vol. 58, 49-94.

Duchêne, S., Aïssa, R., Vanderhaeghe, O., 2006. Pressure-temperaturetime evolution of metamorphic rocks from Naxos (Cyclades, Greece), Constraints from

thermobarometry and Rb/Sr dating. Geodin. Acta, 19, 301–321 doi: 10.3166 /ga.19.301-321.

Duncan, I.J., 1984. Structural evolution of the Thor-Odin gneiss dome, Tectonophysics, 101, 87-130.

Dunkl, I., 2002. TRACKKEY: a Windows program for calculation and graphical presentation of fission track data, Computers & Geosciences, 28(1), 3-12.

Ehlers, T. A., Farley, K. A., Rusmore, M. E., Woodsworth, G. J., 2006. Apatite (U-Th)/He signal of large-magnitude accelerated glacial erosion, southwest British Columbia, Geology, 34(9), 765-768.

Endrun, B., Lebedev, S., Meier, T., Tirel, C., Friederich, W., 2011. Complex layered deformation within the Aegean crust and mantle revealed by seismic anisotropy, Nature Geoscience, 4(3), 203-207.

Eyal, Y., Osadetz, K. G., & Feinstein, S., 2006. Evidence for reactivation of Eocene joints and pre-Eocene foliation planes in the Okanagan core-complex, British Columbia, Canada, Journal of Structural Geology, 28(11), 2109-2120.

Famin, V., Philippot, P., Jolivet, L., Agard, P., 2004. Evolution of hydrothermal regime along a crustal shear zone, Tinos Island, Greece, Tectonics, 23(5), doi:10.1029 /2003TC001509.

Famin, V., Hébert, R., Philippot, P., Jolivet, L., 2005. Ion probe and fluid inclusion evidence for co-seismic fluid infiltration in a crustal detachment, Contributions to Mineralogy and Petrology, 150(3), 354-367.

Farley, K. A., Wolf, L. T., and Silver, L. T., 1996. The effects of long alpha-stopping distances on (U-Th)/He ages, Geochimica et Cosmochimica Acta, *60*, 4223-4229.

Farley, K.A., 2000, Helium diffusion in apatite: General behavior as illustrated by Durango fluorapatite, Journal of Geophysical Research, 105, 2903-2914.

Farley, K.A., Rushmore, M.E., Bouge, S.W., 2001. Post-10 Ma uplift and exhumation of the northern Coast Mountains, British Columbia, Geology, 29, 99-102.

Farley, K.A., 2002. (U-Th)/He dating: Techniques, calibrations, and applications, Reviews in Mineralogy and Geochemistry, vol. 47, 819-844.

Faure, M., Bonneau, M., Pons, J., 1991. Ductile deformation and syntectonic granite emplacement during the late Miocene extension of the Aegean (Greece), Bulletin de la Société Géologique de France, 162, 3-12.

Fayon, A. K., Peacock, S. M., Stump, E., & Reynolds, S. J., 2000. Fission track analysis of the footwall of the Catalina detachment fault, Arizona: Tectonic denudation, magmatism, and erosion, Journal of Geophysical Research Solid Earth, 105(B5), 11047-11062.

Fayon, A.K., A. Mulch, C. Teyssier, M. Person, and O. Vanderhaeghe, 2004a. Fluid flow and heat transfer during exhumation of metamorphic core complexes, GSA Annual meeting, paper no 237-13.

Fayon, A.K., Whitney, D.L., Teyssier, C., 2004b. Exhumation of orogenic crust: diapiric ascent vs. low-angle normal faulting, in Gneiss Domes and Orogeny, edited by D.L.Whitney, C. Teyssier, and C.S. Siddoway, pp. 129-139, Geological Society of America Special Paper, 380.

Fleischer, R. L., Price, P. B., Walker, R. M., 1975. Nuclear Tracks in Solids: Berkeley, California, University of California Press, 605 p.

Flowers, R. M., Shuster, D. L., Wernicke, B. P., Farley, K. A., 2007. Radiation damage control on apatite (U-Th)/He dates from the Grand Canyon region, Colorado Plateau, Geology, *35*(5), 447-450.

Flowers, R. M., Ketcham, R. A., Shuster, D. L., Farley, K. A., 2009. Apatite (U-Th)/He thermochronometry using a radiation damage accumulation and annealing model, Geochimica et. Cosmochimica Acta, 73(8), 2347–2365, doi:10.1016/j.gca. 2009.01.015.

Foster, D. A., and John, B. E., 1999. Quantifying tectonic exhumation in an extensional orogen with thermochronology: Examples from the southern Basin and Range province escape, *in* Ring, U., Brandon, M.T., Lister, G., S., Willett, S.D., eds., Exhumation Processes: Normal Faulting, Ductile Flow and Erosion: London, Geological Society of London Special Publications 154, pp. 87-107.

Foster, D.A., Grice, W.C.Jr., and Kalakay, T.J., 2010. Extension of the Anaconda metamorphic core complex: 40Ar/39Ar thermochronology and implications for Eocene tectonics of the northern Rocky Mountains and the Boulder batholith, Lithosphere, v. 2, p. 232–246,doi:10.1130/L94.1.

Foster, G., Parrish, R.R., Horstwood, M.S.A., Chenery, S., Pyle, J., Gibson, H.D., 2004. The generation of prograde *P-T-t* points and paths; a textural, compositional, and chronological study of metamorphic monazite, Earth and Planetary Science Letters, v. 228, p. 125–142, doi:10.1016/j.epsl.2004.09.024.

Fox, K.F., Jr., Rinehart, C.D., Engels, J.C., and Stern, T.W., 1976. Age of emplacement of the Okanogan gneiss dome, North-central Washington, Geological Society of America Bulletin, v. 87, p. 1217-1224.

Fox, K.F., Jr., Rinehart, C.D., and Engels, J.C., 1977. Plutonism and orogeny in North-central Washington; timing and regional context: Alexandria, Virginia, U.S. Geological Survey Professional Paper 989, 32 p.

Galbraith, R. F., & Laslett, G. M., 1993. Statistical models for mixed fission track ages, Nuclear Tracks and Radiation Measurements, 21(4), 459-470.

Gallagher, K., Brown, R., Johnson, C., 1998. Fission track analysis and its applications to geological problems, Annual Review of Earth and Planetary Sciences, 26(1), 519-572.

Gallagher, K., 1995. Evolving temperature histories from apatite fission-track data, Earth and Planetary Science Letters, 136(3), 421-435.

Gautheron, C., Tassan-Got, L., Barbarand, J., Pagel, M., 2009. Effect of alpha-damage annealing on apatite (U–Th)/He thermochronology, Chemical Geology, 266(3), 157-170.

Gébelin, A., Mulch, A., Teyssier, C., Heizler, M., Vennemann, T., Seaton, N. C. A., 2011. Oligo-Miocene extensional tectonics and fluid flow across the Northern Snake Range detachment system, Nevada, Tectonics, 30, TC5010, doi:10.1029/2010TC002797.

Gervais, F., Brown, R. L., and Crowley, J. L., 2010. Tectonic implications for a Cordilleran orogenic base in the Frenchman Cap dome, southeastern Canadian Cordillera, Journal of Structural Geology, 32(7), 941-959.

Gervais, F., and Brown, R. L., 2011. Testing modes of exhumation in collisional orogens: Synconvergent channel flow in the southeastern Canadian Cordillera, Lithosphere, 3(1), 55-75.

Ghent, E.D., J. Nicholls, M.Z. Stout, Rottenfusser, B., 1977. Clinopyroxene amphibolite boudins from Three Valley Gap, British Columbia, The Canadian Mineralogist, 15, 269– 282.

Gleadow, A. J. W., & Duddy, I. R., 1981. A natural long-term track annealing experiment for apatite, Nuclear Tracks, 5(1), 169-174.

Gleadow, A. J. W., Duddy, I. R., Green, P. F., and Lovering, J. F., 1986. Confined track lengths in apatite: A diagnostic tool for thermal history analysis, Contributions to Mineralogy and Petrology, 94 (4), 405-415.

Gleadow, A. J. W., and Fitzgerald, P.G., 1987. Uplift history and structure of the Transantarctic Mountains: New evidence from fission track dating of basement apatites in the Dry Valleys area, southern Victoria Land, Earth and Planetary Science Letters, 82(1), 1-14.

Glombick, P., R.I. Thompson, P. Erdmer, L. Heaman, R.M. Friedman, M. Villeneuve, and Daughtry, K.L., 2006a. U-Pb constraints on the thermotectonic evolution of the Vernon antiform and the age of the Aberdeen gneiss complex, southeastern Canadian Cordillera, Canadian Journal of Earth Science, 43, 213-244.

Glombick, P., Thompson, R. I., Erdmer, P., & Daughtry, K. L., 2006b. A reappraisal of the tectonic significance of early Tertiary low-angle shear zones exposed in the Vernon map area (82 L), Shuswap metamorphic complex, southeastern Canadian Cordillera, Canadian Journal of Earth Sciences, 43(2), 245-268.

Goergen, E. T., and Whitney, D. L., 2012a. Long length scales of element transport during reaction texture development in orthoamphibole-cordierite gneiss: Thor-Odin dome, British Columbia, Canada, Contributions to Mineralogy and Petrology, 163(2), 337-352.

Goergen, E. T., and Whitney, D.L., 2012b. Corona networks as three-dimensional records of transport scale and pathways during metamorphism, Geology, 40(2), 183-186.

Goodge, J.W., and Hansen, V.L., 1983. Petrology and structure of rocks in the southwest portion of Okanogan Dome, north-central Washington, Northwest Geology, 12, 13-24.

Gordon, S. M., D. L. Whitney, C. Teyssier, M. Grove, and Dunlap, W. J., 2008. Timescales of migmatization, melt crystallization, and cooling in a Cordilleran gneiss dome, Valhalla complex, southeastern British Columbia, *Tectonics*, 27, TC4010, doi:10.1029/2007TC002103.

Gordon, S. M., Little, T. A., Hacker, B. R., Bowring, S. A., Korchinski, M., Baldwin, S. L., Kylander-Clark, A. R. C., and Millet, M.-A., 2012. Multi-stage exhumation of young UHP–HP rocks: timescales of melt crystallization in the D'Entrecasteaux Islands, southeastern Papua New Guinea, Earth and Planetary Science Letters, 351–352, 237–246.

Gottardi, R., Teyssier, C., Mulch, A., Vennemann, T.W., Wells, M.L., 2011. Preservation of an extreme transient geotherm in the Raft River detachment shear zone, Geology, 39, 8, 759-762

Gottardi, R., Kao, P. H., Saar, M. O., & Teyssier, C., 2013. Effects of permeability fields on fluid, heat, and oxygen isotope transport in extensional detachment systems, Geochemistry, Geophysics, Geosystems, p. 1-30.

Grasemann, B., Schneider, D. A., Stöckli, D. F., Iglseder, C., 2012. Miocene bivergent crustal extension in the Aegean: Evidence from the western Cyclades (Greece), Lithosphere, 4(1), 23-39.

Green, P. F., 1981. A new look at statistics in fission-track dating, Nuclear tracks, *5*(1), 77-86.

Guenthner, W. R., Reiners, P. W., Ketcham, R. A., Nasdala, L., Giester, G., 2013. Helium diffusion in natural zircon: Radiation damage, anisotropy, and the interpretation of zircon (U-Th)/He thermochronology, American Journal of Science, 313(3), 145–198. doi:10.2475/03.2013.01.

Hansen, K., and Reiners, P. W., 2006. Low temperature thermochronology of the southern East Greenland continental margin: evidence from apatite (U–Th)/He and fission track analysis and implications for intermethod calibratios, Lithos, 92(1), 117-136.

Hansen, V. L., & Goodge, J. W., 1988. Metamorphism, structural petrology, and regional evolution of the Okanogan complex, northeastern Washington, *in* Ernst, W.G., ed., Metamorphism and Crustal Evolution of the Western United States, Rubey Colloq. Series vol. 7: Englewood Cliffs, N.J., Prentice-Hall, pp. 233-270.

Haug, G. H., Ganopolski, A., Sigman, D. M., Rosell-Mele, A., Swann, G. E., Tiedemann, R., Jaccard, S.L., Bollmann, J., Maslin, M.A., Leng, M.J., Eglinton,

G., 2005. North Pacific seasonality and the glaciation of North America 2.7 million years ago, Nature, 433(7028), 821-825.

Hinchey, A.M., Carr, S.D., McNeill, P.D., and Rayner, N., 2006. Paleocene-Eocene high-grade metamorphism, anatexis, and deformation in the Thor-Odin dome, Monashee complex, southeastern British Columbia, Canadian Journal of Earth Sciences, 43, 1341-1365.

Hinchey, A. M., and Carr, S.D., 2007. Protolith composition of cordierite-gedrite basement rocks and garnet amphibolite of the Bearpaw lake area of the Thor-Odin dome, Monashee Complex, British Columbia, Canada, The Canadian Mineralogist, 45(3), 607-629.

Holder, G. A. M., Holder, R. W., & Carlson, D. H., 1990. Middle Eocene dike swarms and their relation to contemporaneous plutonism, volcanism, core-complex mylonitization, and graben subsidence, Okanogan Highlands, Washington, Geology, 18(11), 1082-1085.

Holder, R.W., and Holder, G.A., 1988. The Colville Batholith; Tertiary plutonism in Northeast Washington associated with graben and core-complex (gneiss dome) formation, Geological Society of America Bulletin, 100, 1971-1980.

Hurford, A. J., and Green, P. F., 1983. The zeta age calibration of fission-track dating, Chemical Geology, 41, 285-317.

Jansen, J. B. H., 1973. Geological Map of Greece, Island of Naxos, 341 pp., Inst. for Geol. and Min. Resour., Athens

Jansen, J. B. H., and Schuiling, R. D., 1976. Metamorphism on Naxos; petrology and geothermal gradients. American Journal of Science, 276(10), 1225-1253.

Johnson, B.J., and Brown, R.L., 1996. Crustal structure and early Tertiary extensional tectonics of the Omineca belt at 518N latitude, southern Canadian Cordillera, Canadian Journal of Earth Sciences, v. 33, p. 1596–1611.

Johnston, D.H., Williams, P.F., Brown, R.L., Crowley, J.L., Carr, S.D., 2000. Northeastward extrusion and extensional exhumation of crystalline rocks of the Monashee Complex, southeastern Canadian Cordillera, Journal of Structural Geology, 22, 603–625.

Jolivet, L., Brun, J.P., Gautier, P., Lallemant, S., Patriat, M., 1994. 3D kinematics of extension in the Aegean region from the early Miocene to the present: Insights from the ductile crust, Bull. Soc. Geol. Fr., 165(3), 195–209

Jolivet, L., Faccenna, C., Goffé, B., Burov, E., Agard, P., 2003. Subduction tectonics and exhumation of high-pressure metamorphic rocks in the Mediterranean orogens, Am. J. Sci., 303, 353–409.

Jolivet, L., Lecomte, E., Huet, B., Denèle, Y., Lacombe, O., Labrousse, L., Le Pourhiet, L., Mehl, C., 2010. The North Cycladic detachment system, Earth and Planetary Science Letters, v. 289, p. 87–104, doi:10.1016/j .epsl.2009.10.032.

Jolivet, L., and Brun, J.P., 2010. Cenozoic geodynamic evolution of the Aegean region, Int. J. Earth Sci., 99, 109–138, doi:10.1007/s00531- 00008-00366-00534.

Keay, S., G. Lister, Buick, I., 2001. The timing of partial melting, Barrovian metamorphism and granite intrusion in the Naxos metamorphic core complex,

Cyclades, Aegean Sea, Greece, Tectonophysics, 342, 275–312, doi:10.1016/ S0040-1951(01)00168-8.

Ketcham, R. A., Donelick, R. A., Carlson, W. D., 1999. Variability of apatite fission-track annealing kinetics: III. Extrapolation to geological time scales, American Mineralogist, 84, 1235-1255.

Ketcham, R. A., 1996. Thermal models of core-complex evolution in Arizona and New Guinea: Implications for ancient cooling paths and present-day heat flow, Tectonics, 15(5), 933-951

Ketcham, R. A., 2003. Observations on the relationship between crystallographic orientation and biasing in apatite fission-track measurements, American Mineralogist, 88 (5-6), 817-829.

Ketcham, R. A., 2005. Forward and inverse modeling of low-temperature thermochronometry data, Reviews in Mineralogy and Geochemistry, 58 (1), 275-314.

Ketcham, R. A., Carter, A., Donelick, R. A., Barbarand, J., Hurford, A. J., 2007a. Improved measurement of fission-track annealing in apatite using c-axis projection, American Mineralogist, 92 (5-6), 789-798.

Ketcham, R. A., Carter, A., Donelick, R. A., Barbarand, J., Hurford, A. J., 2007b. Improved modeling of fission-track annealing in apatite, American Mineralogist, 92(5-6), 799-810.

Kruckenberg, S.C., Whitney, D.L., Teyssier, C., Fanning, M., and Dunlap, W.J., 2008. Paleocene-Eocene migmatite crystallization, extension, and exhumation in the

hinterland of the northern Cordillera: Okanogan dome, Washington USA, Geological Society of America Bulletin, 120(7-8), 912-929.

Kruckenberg, S. C., and Whitney, D.L., 2011. Metamorphic evolution of sapphirine-and orthoamphibole-cordierite-bearing gneiss, Okanogan dome, Washington, USA, Journal of Metamorphic Geology, 29(4), 425-449.

Kruckenberg, S. C., Vanderhaeghe, O., Ferré, E., Teyssier, C., Whitney, D. L., 2011. Flow of partially molten crust and the internal dynamics of a migmatite dome, Naxos, Greece, Tectonics, 30 (3).

Kruse, S., and Williams, P. F., 2005. Brittle faulting in the Thor Odin culmination, Monashee complex, southern Canadian Cordillera: constraints on geometry and kinematics, Canadian Journal of Earth Sciences, 42(12), 2141-2160.

Laslett, G. M., Kendall, W. S., Gleadow, A. J. W., & Duddy, I. R., 1982. Bias in measurement of fission-track length distributions, Nuclear Tracks and Radiation Measurements, 6(2), 79-85.

Lecomte, E., Jolivet, L., Lacombe, O., Denèle, Y., Labrousse, L., Le Pourhiet, L., 2010. Geometry and kinematics of Mykonos detachment, Cyclades, Greece: Evidence for slip at shallow dip, Tectonics, 29 (5). DOI: 10.1029/2009TC002564

Lisiecki, L. E., and Raymo, M. E., 2005. A Pliocene-Pleistocene stack of 57 globally distributed benthic d18O records, Paleoceanography, 20, PA1003, doi:10.1029/ 2004PA001071.

Lister, G.S., Banga, G., and Feenstra, A., 1984. Metamorphic core complexes of Cordilleran type in the Cyclades, Aegean Sea, Greece, Geology, 12, 221-225.

Little, T. A., Hacker, B. R., Gordon, S. M., Baldwin, S. L., Fitzgerald, P. G., Ellis, S., Korchinski, M., 2011. Diapiric exhumation of Earth's youngest (UHP) eclogites in the gneiss domes of the D'Entrecasteaux Islands, Papua New Guinea, Tectonophysics, 510(1), 39-68.

Lorencak, M., Seward, D., Vanderhaeghe, O., Teyssier, C., and Burg, J.P., 2001. Low-temperature cooling history of the Shuswap metamorphic core complex, British Columbia, Constraints from apatite and zircon fission-track ages: Canadian Journal of Earth Sciences, 38, 1615-1625.

Marshall, D., and Simandl, G., 2006. Phase relations and metamorphism in the sapphirine bearing granulites of the Valhalla complex, Slocan Valley, BC, GAC/MAC Annual Meeting, 31, 96.

Martin, L., Duchêne, S., Deloule, E., Vanderhaeghe, O., 2006. The isotopic composition of zircon and garnet, A record of the metamorphic history of Naxos, Greece. Lithos, 87, 174–192, doi:10.1016/j. lithos.2005.06.016.

Martin, L. A. J., S. Duchêne, E. Deloule, Vanderhaeghe, O., 2008. Mobility of trace elements and oxygen in zircon during metamorphism: Consequences for geochemical tracing, Earth Planet. Sci. Lett., 267, 161–174, doi:10.1016/j.epsl. 2007.11.029.

Mathews, W.H., 1981. Early Cenozoic resetting of potassium-argon dates and geothermal history of north Okanagan area, British Columbia, Canadian Journal of Earth Sciences, v. 18, p. 1310–1319.

McClaughry, J. D., & Gaylord, D. R., 2005. Middle Eocene sedimentary and volcanic infilling of an evolving supradetachment basin: White Lake Basin, south-central British Columbia, Canadian Journal of Earth Sciences, 42(1), 49-66.

McFadden, R. R., Teyssier, C., Siddoway, C. S., Whitney, D. L., Fanning, C. M., 2010. Oblique dilation, melt transfer, and gneiss dome emplacement, Geology, 38(4), 375-378.

McKenzie, D., Nimmo, F., Jackson, J.A., Gans, P.B., and Miller, E.L., 2000. Characteristics and consequences of flow in the lower crust, Journal of Geophysical Research, B, Solid Earth and Planets, v. 105, p. 11029-11046.

Meesters, A. G. C. A., and Dunai, T. J., 2002. Solving the production–diffusion equation for finite diffusion domains of various shapes: Part I. Implications for low-temperature (U-Th)/He thermochronology, Chemical Geology, 186(3), 333-344.

Mehl, C., Jolivet, L., Lacombe, O., 2005. From ductile to brittle: Evolution and localization of deformation below a crustal detachment (Tinos, Cyclades, Greece), Tectonics, 24(4), DOI: 10.1029/2004TC001767

Menant, A., Jolivet, L., Augier, R., Skarpelis, N., 2013. The North Cycladic Detachment System and associated mineralization, Mykonos, Greece: Insights on the evolution of the Aegean domain, Tectonics, DOI: 10.1002/tect.20037

Monger, J.W.H., Price, R.A., and Tempelman-Kluit, D.J., 1982. Tectonic accretion and the origin of the two major metamorphic and plutonic welts in the Canadian Cordillera, Geology, 10, 70-75.

Morrison, J., and Anderson, J. L., 1998. Footwall refrigeration along a detachment fault: implications for thermal evolution of core complexes, Science, v. 279, p. 63-66

Mudelsee, M., and Raymo, M. E., 2005. Slow dynamics of the Northern Hemisphere glaciation, Paleoceanography, 20(4).

Mulch, A., Teyssier, C., Cosca, M. A., Vanderhaeghe, O., and Vennemann, T. W., 2004, Reconstructing paleoelevation in eroded orogens, Geology, v. 32, p. 525-528.

Mulch, A., Teyssier, C., Cosca, M. A., Vennemann, T. W., 2006. Thermomechanical analysis of strain localization in a ductile detachment zone, Journal of Geophysical Research: Solid Earth, (1978–2012), 111(B12).

Mulch, A., Teyssier, C., Cosca, M. A., and Chamberlain, C. P., 2007. Stable isotope paleoaltimetry of Eocene core complexes in the North American Cordillera, Tectonics, v. 26., TC4001, doi:10.1029/2006TC001995.

Naeser C. W., Engels J. C. & Dodge F. C. W., 1970, Fission track annealing and age determinations of epidote minerals, Journal of Geophysical Research, 75, 1579 1584.

Norlander, B.H., Whitney, D.L., Teyssier, C., Vanderhaeghe, O., and Wiebe, R.A., 2002. Partial melting and decompression of the Thor-Odin Dome, Shuswap metamorphic core complex, Canadian Cordillera. Lithos, v. 61, p. 103-125.

Nyman, M.W., Pattison, D.R.M., Ghent, E.D., 1995. Melt extraction during formation of K-feldspar-sillimanite migmatites, west of Revelstoke, British Columbia, Journal of Petrology, 36, 351-372.

Okulitch, A.V., 1984. The role of the Shuswap metamorphic complex in Cordilleran tectonism; a review, Canadian Journal of Earth Sciences, 21, 1171-1193.

Olen, S. M., Ehlers, T. A., Densmore, M. S., 2012. Limits to reconstructing paleotopography from thermochronometer data, Journal of Geophysical Research: Earth Surface, (2003–2012), 117(F1).

O'Sullivan, P. B., & Parrish, R. R., 1995. The importance of apatite composition and single-grain ages when interpreting fission track data from plutonic rocks: a case study from the Coast Ranges, British Columbia, Earth and Planetary Science Letters, 132(1), 213-224.

Parkinson, D., 1985. Geochronology of the western side of the Okanogan metamorphic core complex, southern B.C., Geological Society of America Abstracts with Programs, 17, 399.

Parkinson, D.L., 1991. Age and isotopic character of Early Proterozoic basement gneisses in the southern Monashee Complex, southeastern British Columbia, Canadian Journal of Earth Sciences, 28, 1159-1168.

Parkinson, D.L., 1992. Age and tectonic evolution of the southern Monashee complex, southeastern British Columbia: A window into the deep crust, Ph.D. thesis, Univ. of California, Santa Barbara.

Parrish, R.R., and Wheeler, J.O., 1983. An U-Pb zircon age for the Kuskanax batholith, southeast British Columbia, Canadian Journal of Earth Sciences, 20, 1751-1756.

Parrish, R.R., S.D. Carr, and Parkinson, D.L., 1988. Eocene extensional tectonics and geochronology of the southern Omineca belt, British Colombia and Washington, Tectonics, v. 7, p. 181-212.

Parrish, R.R., 1995. Thermal evolution of the southeastern Canadian Cordillera, Canadian Journal of Earth Sciences, 32, 1618-1642.

Pearson, R.C., and Obradovich, J.D., 1977. Eocene rocks in Northeast Washington; radiometric ages and correlation, Washington, U.S. Geological Survey Bulletin, 50 p.

Person, M. P., Mulch, A., Teyssier, C., Gao, Y., 2007. Isotope Transport and Exchange During Detachment Tectonics, Shuswap Metamorphic Core Complex, British Columbia, American Journal of Science, v. 307, p. 555-589.

Regenauer-Lieb, K., and Yuen, D., 2004. Positive feedback of interacting ductile faults from coupling of equation of state, rheology and thermal-mechanics, Physics of the Earth and Planetary Interiors, 142(1), 113-135.

Reiners, P. W., and Farley, K. A., 2001. Influence of crystal size on apatite (U–Th)/He thermochronology: an example from the Bighorn Mountains, Wyoming, Earth and Planetary Science Letters, 188(3), 413-420.

Reiners, P. W., Zhou, Z., Ehlers, T. A., Xu, C., Brandon, M. T., Donelick, R. A., and Nicolescu, S., 2003. Post-orogenic evolution of the Dabie Shan, eastern China, from (U-Th)/He and fission-track dating, American Journal of Science, 303, 489 – 518.

Reiners, P.W., Spell, T.L., Nicolescu, S., Zanetti, K.A., 2004. Zircon (U-Th)/He thermochronometry: He diffusion and comparison with Ar/Ar dating, Geochimica et Cosmochimica Acta, 68, 1857-1887.

Reiners, P.W., 2005. Zircon (U-Th)/He thermochronometry, Reviews in Mineralogy and Geochemistry, v. 58, 151-179.

Rey, P., Vanderhaeghe, O., Teyssier, C., 2001. Gravitational collapse of the continental crust: definition, regimes and modes, Tectonophysics, 342, 435-449.

Rey, P., Teyssier, C., Whitney, D.L., 2009a. Extension rates, crustal melting and core complex dynamics, Geology, 37, 391– 394.

Rey, P.F., Teyssier, C., Whitney, D.L., 2009b, The Role of Partial Melting and Extensional Strain Rates in the Development of Metamorphic Core Complexes, Tectonophysics, v. 477, p. 135–144.

Rey, P. F., Teyssier, C., Whitney, D. L., 2010. Limit of channel flow in orogenic plateau, Lithosphere, 2(5), 328-332.

Rey, P.F., Teyssier, C., Kruckenberg, S.C., and Whitney, D.L., 2011. Viscous collision in channel explains double domes in metamorphic core complexes, Geology, 39, 4, 387-390

Ring, U., Will, T., Glodny, J., Kumerics, C., Gessner, K., Thomson, S., Güngör, T., Monie, P., Okrusch, M., Drüppel, K., 2007. Early exhumation of high-pressure rocks in extrusion wedges: Cycladic blueschist unit in the eastern Aegean, Greece, and Turkey, Tectonics, 26, TC2001, doi:10.1029/2005TC001872.

Ring, U., Glodny, J., Will, T., Thomson, S., 2010. The Hellenic subduction system: High-pressure metamorphism, exhumation,normal faulting, and large-scale extension, Annu. Rev. Earth Planet. Sci., 38, 45–76 doi:10.1146/annurev.earth. 050708.170910.

Robinson, A. C., Yin, A., Lovera, O.M., 2007. The role of footwall deformation and denudation in controlling cooling age patterns of detachment systems: An application to the Kongur Shan extensional system in the Eastern Pamir, Tectonophysics, 496, 28-43.

Sánchez-Gómez, M., Avigad, D., Heimann, A., 2002. Geochronology of clasts in allochthonous Miocene sedimentary sequence on Mykonos and Paros Islands: implications for backarc extension in the Aegean Sea, Journal of the Geological Society of London 159, 45–60.

Schenker, F. L., Gerya, T., Burg, J. P., 2012. Bimodal behavior of extended continental lithosphere: Modeling insight and application to thermal history of migmatitic core complexes, Tectonophysics, 579, 88-103.

Sevigny, J.H., Parrish, R.R., Ghent, E.D., 1989. Petrogenesis of peraluminous granites, Monashee Mountains, southeastern Canadian Cordillera, Journal of Petrology, 30, 557- 581.

Seward, D., Vanderhaeghe, O., Siebenaller, L., Thomson, S., Hibsch, C., Zingg, A., Duchêne, S., 2009. Cenozoic tectonic evolution of Naxos Island through a multi-faceted approach of fission-track analysis, Geological Society, London, Special Publications, 321(1), 179-196.

Shuster, D. L., Flowers, R. M., Farley, K. A., 2006. The influence of natural radiation damage on helium diffusion kinetics in apatite, Earth and Planetary Science Letters, 249(3), 148-161.

Siebenaller, L., Boiron, M. C., Vanderhaeghe, O., Hibsch, C., Jessell, M. W., Andre-Mayer, A.S., France-Lanord, C., and Photiades, A., 2012. Fluid record of rock exhumation across the brittle–ductile transition during formation of a Metamorphic Core Complex (Naxos Island, Cyclades, Greece), Journal of Metamorphic Geology, 31, 313-338.

Snook, J.R., 1965. Metamorphic and structural history of “Colville batholith” gneisses, north central Washington, Geological Society of America Bulletin, 76, 759-776.

Spalla, M. I., Zanoni, D., Williams, P. F., Gosso, G., 2011. Deciphering cryptic P–Td–t histories in the western Thor-Odin dome, Monashee Mountains, Canadian Cordillera: A key to unravelling pre-Cordilleran tectonic signatures, Journal of Structural Geology, 33(3), 399-421.

Spiegel, C., Kohn, B., Belton, D., Berner, Z., Gleadow, A., 2009. Apatite (U–Th–Sm)/He thermochronology of rapidly cooled samples: the effect of He implantation, Earth and Planetary Science Letters, 285(1), 105-114.

Stockli, D. F., Farley, K. A., & Dumitru, T. A., 2000. Calibration of the apatite (U-Th)/He thermochronometer on an exhumed fault block, White Mountains, California, Geology, 28(11), 983-986.

Stockli, D.F., 2005. Application of low-temperature thermochronometry to extensional tectonic settings, Reviews in Mineralogy and Geochemistry, vol. 58, p. 420-461.

Stoffel, K.L., Joseph, N.L., Waggoner, S.Z., Gulick, C.W., Korosec, M.A., and Bunning, B.B., 1991. Geologic map of Washington Northeast Quadrant, Washington Division of Geology and Earth Resources, Geologic Map GM-39, 1:250 000, 1 sheet, 44 p. text.

Stübner, K., Ratschbacher, L., Weise, C., Chow, J., Hoffman, J., Khan, J., Rutte, D., Sperner, B., Pfander, J.A., Hacker, B.R., Dunkl, I., Tichomirowa, M., Stearns, M.A., Bahram, I., Gadoev, M., Gloaguen, R., Jonckheere, R., Kanaev, E., Minaev, V., Oimahmadoc, I., Rajabov, N., Stanek, K.P., 2013. The giant

Shakhdara migmatitic gneiss dome, Pamir, India–Asia collision zone, II: Timing of dome formation. Tectonics, 32(5), 1404-1431. DOI: 10.1002/tect.20059

Stüwe, K., L. White & R. Brown, 1994. The influence of eroding topography on steady-state isotherms. Application to fission track analysis, Earth and Planetary Science Letters, 124(1), 63-74.

Suydam, J.D., and Gaylord, D.R., 1997. Toroda Creek half graben, northeast Washington: Late-stage sedimentary infilling of a syn-extensional basin, Geological Society of America Bulletin, 109, 1333-1348.

Teyssier, C., and Whitney, D.L., 2002. Gneiss domes and orogeny, Geology,v. 30, p. 1139- 1142.

Teyssier, C., Ferré, E.C., Whitney, D.L., Norlander, B., Vanderhaeghe, O., Parkinson, D., 2005. Flow of partially molten crust and origin of detachments during collapse of the Cordilleran orogen, in Bruhn, D., Burlini, L., eds., High-strain zones: Structure and physical properties: London. Geological Society of London Special Publications, vol. 245pp. 39-64,.

Thiede, R. C., Arrowsmith, J. R., Bookhagen, B., McWilliams, M., Sobel, E. R., Strecker, M. R., 2006. Dome formation and extension in the Tethyan Himalaya, Leo Pargil, northwest India, Geological Society of America Bulletin, 118(5-6), 635-650.

Thomson, S.N., and Ring, U., 2006. Thermochronologic evaluation of post-collision extension in the Anatolide orogen, western Turkey, Tectonics, 25, TC3005, doi:10.1029/2005TC001833

Thomson, S.N., Ring, U., Brichau, S., Glodny, J., Will, T.M., 2009. Timing and nature of formation of the Ios metamorphic core complex, southern Cyclades, Greece, in Extending a Continent: Architecture, Rheology and Heat Budget, edited by U. Ring, and B. Wernicke, p. 139–167, Geological Society of London Special Publication, 321.

Tirel, C., Brun, J.P., and Burov, E., 2004. Thermomechanical modeling of extensional gneiss domes, *in* Whitney, D.W., Teyssier, C., Siddoway, C.S., eds., Gneiss domes in orogeny, Geological Society of America Special Paper, 380, p. 67–78.

Toraman, E., Whitney, D.L., Teyssier, C., Fayon, A.K., Thomson, S.K., Reiners, P.W., 2012. Low-temperature thermochronology record of tectonic and erosional exhumation of gneiss domes in the northern North American Cordillera, Geological Society of America Abstract with Programs, vol. 44, no. 7, p.128

Vanderhaeghe, O., and Teyssier, C., 1997. Formation of the Shuswap metamorphic complex during late-orogenic collapse of the Canadian Cordillera: role of ductile thinning and partial melting of the mid- to lower crust, Geodinamica Acta, 10, 41-58.

Vanderhaeghe, O., Teyssier, C., Wysoczanski, R., 1999. Structural and geochronological constraints on the role of partial melting during the formation of the Shuswap metamorphic core complex at the latitude of the Thor-Odin Dome, British Columbia, Canadian Journal of Earth Sciences, v. 36, p. 917-943.

Vanderhaeghe, O., and Teyssier C., 2001. Crustal scale rheological transitions during late-orogenic collapse, Tectonophysics, 335, 211-228.

Vanderhaeghe, O., Teyssier, C., McDougall, I., and Dunlap, W.J, 2003, Cooling and exhumation of the Shuswap metamorphic core complex constrained by Ar/Ar thermochronology, Geological Society of America Bulletin, v 115, p. 200-216.

Vanderhaeghe, O., 2004. Structural development of the Naxos migmatite dome, in Gneiss Domes in Orogeny, edited by D. L. Whitney et al.. Spec. Pap. Geol. Soc. Am., 380, 211–227, doi:10.1130/0-8137-2380-9.211.

Wagner, G., and Van den Haute, P., 1992. Fission track dating: Dordrecht, Kluwer Academic Publishers, 285 p.

Wdowinski, S., and Axen, G.J., 1992. Isostatic rebound due to tectonic denudation: A viscous flow model of a layered lithosphere, Tectonics, 11, 303-315.

Wells, M.L., Snee, L.W., and Blythe, A.E., 2000. Dating of major normal fault systems using thermochronology: An example from the Raft River detachment, Basin and Range, western United States, Journal of Geophysical Research, 105, 16303-16327.

Whitney, D.L., Paterson, S.R., Schmidt, K.L., Glazner, A.F., and Kopf, C.F., 2004. Growth and demise of continental arcs and orogenic plateaux in the North American Cordillera: from Baja to British Columbia, *in* Grocott, J., McCaffrey, K.J.W., Taylor, G. and Tikoff, B., eds., Vertical Coupling and Decoupling in the Lithosphere, Geological Society of London Special Publications, vol. 227, pp. 167-176

Whitney, D. L., Teyssier, C., Rey, P., and Buck, W. R., 2013. Continental and oceanic core complexes, Geological Society of America Bulletin, 125(3-4), 273-298.

Wijbrans, J. R., and McDougall, I., 1986. 40Ar/39Ar dating of white micas from an Alpine high-pressure metamorphic belt on Naxos (Greece): the resetting of the argon isotopic system, Contributions to Mineralogy and Petrology, 93(2), 187-194.

Wolf, R. A., Farley, K. A., Kass, D. M., 1998. Modeling of the temperature sensitivity of the apatite (U–Th)/He thermochronometer, Chemical Geology, 148(1), 105-114.

Wolfe, J. A., Forest, C. E., and Molnar, P., 1998. Paleobotanical evidence of Eocene and Oligocene paleoaltitudes in midlatitude western North America, Geological Society of America Bulletin, v. 110, n. 5, p. 664–678.

Zeitler, P. K., Herczeg, A. L., McDougall, I., Honda, M., 1987. U-Th-He dating of apatite, A potential thermochronometer: Geochimica et Cosmochimica Acta, 51(10), 2865-2868.

Appendix: Apatite fission track data tables

Sample No: 03-OK-80
Irradiation No: FT-018-10

Rock type:	Migmatite	Elevation [m]:	886
Lat/Lon:	48.596/ -119.419	Zeta [ζ]:	289 ± 11
U conc. SRM612:	37 ppm	Area of basic unit:	$63.5*10^{-5}$
N_d:	3314	ρ_d:	$1.08*10^{-6}$
Analyst:	Erkan Toraman		

No	N_s	N_i	Area	Age [Ma] ± 1σ
1	9	55	100	25.5 ± 9.2
2	14	67	100	32.5 ± 9.6
3	3	39	100	12.0 ± 7.2
4	9	62	100	22.6 ± 8.1
5	2	34	100	9.2 ± 6.7
6	6	50	100	18.7 ± 8.1
7	6	41	100	22.8 ± 10
8	10	79	100	19.7 ± 6.7
9	9	61	100	23.0 ± 8.3
10	7	54	100	20.2 ± 8.2
11	8	54	100	23.1 ± 8.8
12	6	60	100	15.6 ± 6.7
13	6	36	100	26.0 ± 11.5
14	11	43	100	39.8 ± 13.5
15	8	39	100	31.9 ± 12.5
16	9	65	100	21.6 ± 7.7
17	5	37	100	21.1 ± 10.1
18	7	60	100	18.2 ± 7.3
19	8	42	100	29.7 ± 11.5

Length [μm]	#
0-1	0
1-2	0
2-3	0
3-4	0
4-5	0
5-6	1
6-7	1
7-8	4
8-9	2
9-10	5
10-11	5
11-12	15
12-13	21
13-14	21
14-15	21
15-16	3
16-17	1
17-18	0
18-19	0
19-20	0

$\chi^2 = 10.25$
P [χ^2] = 92.3%
U [ppm] = 26.5

MTL = 12.43
SE = 0.21
SD = 2.09
# = 100
DPAR= 0

Pooled Age ± 1σ [Ma] = 22.8 ± 2.2
Mean Age ± 1σ [Ma] = 22.8 ± 1.7
Central Age ± 1σ [Ma] = 22.8 ± 2.2

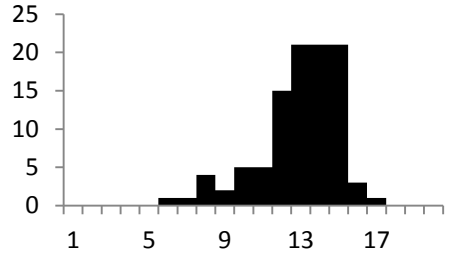

Sample No:	OK-305
Irradiation No:	FT-015-22

Rock type:	Q-feld gneiss	Elevation [m]:	1001
Lat/Lon:	48.605/-119.431	Zeta [ζ]:	289 ± 11
U conc. SRM612:	37 ppm	Area of basic unit:	$63.5*10^{-5}$
N_d:	1917	ρ_d:	$1.728*10^{-6}$
Analyst:	Erkan Toraman		

No	N_s	N_i	Area	Age [Ma] ± 1σ
1	10	178	100	14.0 ± 4.6
2	12	146	100	20.5± 6.2
3	7	82	100	21.3 ± 8.4
4	1	13	16	19.2 ± 19.9
5	17	181	100	23.4 ± 6.0
6	10	134	100	18.6 ± 6.2
7	18	134	100	33.5 ± 8.5
8	19	224	100	21.1 ± 5.1
9	15	186	100	20.1 ± 5.5
10	23	312	100	18.4 ± 4.1
11	10	71	28	35.1 ± 11.9
12	7	52	16	33.5 ± 13.6
13	17	110	100	38.5 ± 10.2

Length [μm]	#
0-1	0
1-2	0
2-3	0
3-4	0
4-5	0
5-6	0
6-7	0
7-8	0
8-9	0
9-10	0
10-11	0
11-12	0
12-13	0
13-14	0
14-15	0
15-16	0
16-17	0
17-18	0
18-19	0
19-20	0

χ^2 = 13.35
P [χ^2] = 34.4%
U [ppm] = 58.1

MTL = 0
SE = 0
SD = 0
# = 0
DPAR= 0

Pooled Age ± 1σ [Ma] = 22.7 ± 2.1
Mean Age ± 1σ [Ma] = 24.4 ± 2.2
Central Age ± 1σ [Ma] = 22.8 ± 2.1

Sample No: OK-307
Irradiation No: FT-015-20

Rock type:	Migmatite	Elevation [m]:	750
Lat/Lon:	48.612/-119.450	Zeta [ζ]:	289 ± 11
U conc. SRM612:	37 ppm	Area of basic unit:	$63.5*10^{-5}$
N_d:	1917	ρ_d:	$1.665*10^{-6}$
Analyst:	Erkan Toraman		

No	N_s	N_i	Area	Age [Ma] ± 1σ
1	17	110	100	37.1 ± 9.8
2	6	113	100	12.8 ± 5.4
3	4	70	46	13.7 ± 7.1
4	16	105	64	36.6 ± 9.9
5	18	149	100	29.0 ± 7.4
6	26	184	80	33.9 ± 7.3
7	7	115	100	14.6 ± 5.7
8	9	126	100	17.2 ± 6.0
9	22	232	100	22.8 ± 5.2
10	18	173	100	25.0 ± 6.3
11	22	156	100	33.9 ± 7.9
12	28	265	100	25.4 ± 5.2
13	14	119	60	28.2 ± 8.1

Length [μm]	#
0-1	0
1-2	0
2-3	0
3-4	0
4-5	0
5-6	0
6-7	0
7-8	2
8-9	1
9-10	1
10-11	7
11-12	9
12-13	22
13-14	30
14-15	22
15-16	5
16-17	1
17-18	0
18-19	0
19-20	0

$\chi^2 = 15.55$
P [χ^2] = 21.3%
U [ppm] = 56.1

MTL= 13.03
SE= 0.16
SD = 1.58
#= 100
DPAR= 3.19

Pooled Age ± 1σ [Ma] = 25.9 ± 2.2
Mean Age ± 1σ [Ma] = 25.4 ± 2.4
Central Age ± 1σ [Ma] = 25.9 ± 2.2

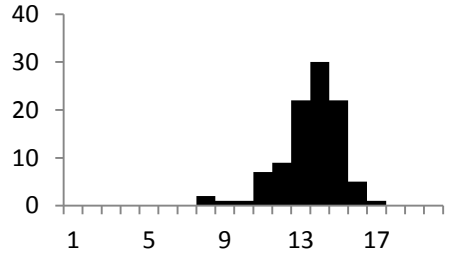

Sample No: OK-311
Irradiation No: FT-015-19

Rock type:	Migmatite	Elevation [m]:	616
Lat/Lon:	48.617/-119.450	Zeta [ζ]:	289 ± 11
U conc. SRM612:	37 ppm	Area of basic unit:	$63.5*10^{-5}$
N_d:	1917	ρ_d:	$1.634*10^{-6}$
Analyst:	Erkan Toraman		

No	N_s	N_i	Area	Age [Ma] ± 1σ
1	7	33	100	49.9 ± 20.9
2	21	75	100	65.8 ± 16.5
3	13	102	100	30.0 ± 8.9
4	56	276	100	47.7 ± 7.3
5	32	176	100	42.8 ± 8.4
6	35	93	100	88.3 ± 17.9
7	20	98	100	48.0 ± 12.0
8	27	165	100	38.5 ± 8.2
9	18	99	100	42.8 ± 11.1
10	28	129	100	51.1 ± 10.9
11	15	80	100	44.1 ± 12.6
12	23	67	100	80.6 ± 19.8
13	21	102	100	48.4± 11.8
14	19	75	100	59.5 ± 15.5
15	9	104	100	20.4 ± 7.2
16	25	145	100	40.6 ± 8.9
17	15	84	100	42.0 ± 11.9
18	18	129	100	32.9 ± 8.4
19	23	106	100	51.0 ± 12.0
20	20	85	100	55.3 ± 14.0

Length [μm]	#
0-1	0
1-2	0
2-3	0
3-4	0
4-5	0
5-6	0
6-7	0
7-8	0
8-9	0
9-10	0
10-11	0
11-12	1
12-13	4
13-14	10
14-15	23
15-16	16
16-17	1
17-18	0
18-19	0
19-20	0

$\chi^2 = 31.71$
P [χ^2] = 3.4%
U [ppm] = 37.8

MTL = 14.48
SE = 0.13
SD = 0.94
# = 55
DPAR= 2.38

Pooled Age ± 1σ [Ma] = 47.1 ± 3.1
Mean Age ± 1σ [Ma] = 49.0 ± 3.5
Central Age ± 1σ [Ma] = 47.5 ± 3.7

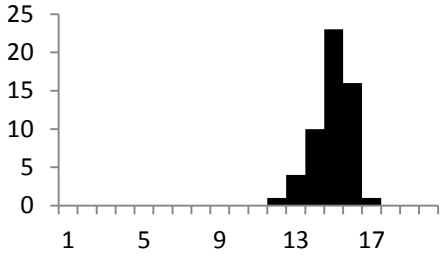

Sample No: OK-315
Irradiation No: FT-015-18

Rock type:	Gneiss	Elevation [m]:	399
Lat/Lon:	48.622/-119.458	Zeta [ζ]:	289 ± 11
U conc. SRM612:	37 ppm	Area of basic unit:	$63.5*10^{-5}$
N_d:	1917	ρ_d:	$1.603*10^{-6}$
Analyst:	Erkan Toraman		

No	N_s	N_i	Area	Age [Ma] ± 1σ
1	21	165	100	29.4 ± 6.9
2	44	177	100	57.3 ± 10.0
3	38	215	100	40.8 ± 7.4
4	25	191	100	30.3 ± 6.6
5	26	172	100	34.9 ± 7.5
6	25	164	100	35.2 ± 7.7
7	21	140	100	34.7 ± 8.3
8	36	146	100	56.9 ± 10.9
9	14	121	100	26.8 ± 7.6
10	23	200	100	26.6 ± 6.0
11	26	183	100	32.8 ± 7.0
12	22	170	100	29.9 ± 6.9
13	37	116	100	73.5 ± 14.2
14	36	170	100	48.9 ± 9.2
15	21	124	100	39.1 ± 9.4
16	34	199	100	39.5 ± 7.5
17	32	196	100	37.7 ± 7.4
18	17	127	100	30.9 ± 8.1
19	40	191	100	48.3 ± 8.7
20	27	150	100	41.6 ± 8.9
21	30	138	100	50.2 ± 10.3

Length [μm]	#
0-1	0
1-2	0
2-3	0
3-4	0
4-5	0
5-6	0
6-7	0
7-8	0
8-9	4
9-10	3
10-11	12
11-12	6
12-13	18
13-14	21
14-15	25
15-16	11
16-17	0
17-18	0
18-19	0
19-20	0

$\chi^2 = 36.87$
P [χ^2] = 1.2%
U [ppm] = 57.09

MTL = 12.98
SE = 0.18
SD = 1.85
# = 100
DPAR= 2.46

Pooled Age ± 1σ [Ma] = 39.8 ± 2.4
Mean Age ± 1σ [Ma] = 40.3 ± 2.6
Central Age ± 1σ [Ma] = 39.8 ± 2.8

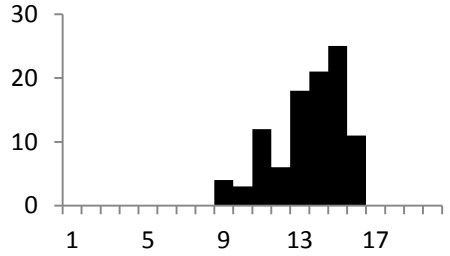

Sample No: OK-317
Irradiation No: FT-015-17

Rock type:	Q-feld gneiss	Elevation [m]:	343
Lat/Lon:	48.624/-119.461	Zeta [ζ]:	289 ± 11
U conc. SRM612:	37 ppm	Area of basic unit:	$63.5*10^{-5}$
N_d:	1917	ρ_d:	$1.571*10^{-6}$
Analyst:	Erkan Toraman		

No	N_s	N_i	Area	Age [Ma] ± 1σ
1	5	45	100	25.2 ± 11.9
2	2	39	100	11.6 ± 8.5
3	31	227	100	31.0 ± 6.1
4	47	245	100	43.4 ± 7.2
5	34	226	100	34.1 ± 6.5
6	50	277	100	40.9 ± 6.5
7	16	89	100	40.7 ± 11.2
8	49	261	100	42.5 ± 6.9
9	14	125	100	25.4 ± 7.3
10	26	132	100	44.6 ± 9.7
11	31	257	100	27.3 ± 5.3
12	10	55	100	41.1 ± 14.3
13	24	122	100	44.5 ± 10.1
14	18	98	100	41.6 ± 10.8
15	18	150	100	27.2 ± 6.9
16	43	276	100	35.3 ± 6.0
17	21	201	100	23.7 ± 5.5
18	36	225	100	36.2 ± 6.7
19	38	182	100	47.2 ± 8.7
20	48	303	100	35.9 ± 5.8

Length [μm]	#
0-1	0
1-2	0
2-3	0
3-4	0
4-5	0
5-6	0
6-7	1
7-8	0
8-9	1
9-10	0
10-11	2
11-12	10
12-13	19
13-14	26
14-15	20
15-16	4
16-17	1
17-18	0
18-19	0
19-20	0

$\chi^2 = 20.58$
P [χ^2] = 36.1%
U [ppm] = 62.6

MTL = 13.20
SE = 0.20
SD = 1.46
# = 84
DPAR= 2.01

Pooled Age ± 1σ [Ma] = 35.9 ± 2.2
Mean Age ± 1σ [Ma] = 35.0 ± 2.1
Central Age ± 1σ [Ma] = 35.9 ± 2.2

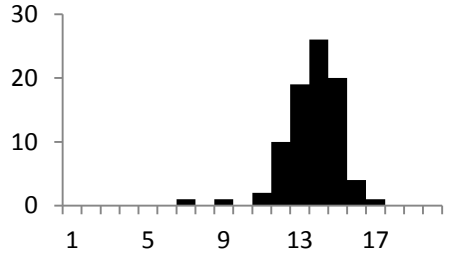

Sample No: OK-319
Irradiation No: FT-015-08

Rock type:	Granodioritic gneiss	Elevation [m]:	988
Lat/Lon:	48.709/-119.097	Zeta [ζ]:	289 ± 11
U conc. SRM612:	37 ppm	Area of basic unit:	$63.5*10^{-5}$
N_d:	1917	ρ_d:	$1.259*10^{-6}$
Analyst:	Erkan Toraman		

No	N_s	N_i	Area	Age [Ma] ± 1σ
1	17	42	100	73.2 ± 21.3
2	10	42	100	43.2 ± 15.3
3	12	84	100	25.9 ± 8.1
4	9	23	36	70.8 ± 28.0
5	14	42	100	60.4 ± 18.8
6	21	69	100	55.1 ± 14.0
7	10	27	100	67.0 ± 25.0
8	12	23	70	94.2 ± 33.8
9	12	27	42	80.4 ± 28.1
10	11	46	90	43.4 ± 14.7
11	21	90	100	42.3 ± 10.4
12	11	44	100	45.3 ± 15.4
13	6	10	100	108.2 ± 56.1
14	11	64	100	31.2 ± 10.3
15	8	34	80	42.7 ± 16.9
16	18	56	100	58.2± 16.0
17	7	19	100	66.7 ± 29.6
18	4	30	89	24.2 ± 12.9
19	12	37	100	58.7 ± 19.7
20	15	48	100	56.6 ± 16.9
21	12	69	100	31.6 ± 9.9
22	9	25	80	65.2 ± 25.5

Length [μm]	#
0-1	0
1-2	0
2-3	0
3-4	0
4-5	0
5-6	0
6-7	0
7-8	0
8-9	0
9-10	0
10-11	0
11-12	0
12-13	0
13-14	0
14-15	0
15-16	0
16-17	0
17-18	0
18-19	0
19-20	0

$\chi^2 = 25.15$
P [χ^2] = 24.1%
U [ppm] = 21.34

MTL = 0
SE = 0
SD = 0
# = 0
DPAR= 0

Pooled Age ± 1σ [Ma] = 49.9 ± 4.0
Mean Age ± 1σ [Ma] = 56.6 ± 4.6
Central Age ± 1σ [Ma] = 50.5 ± 4.3

Sample No: OK-320
Irradiation No: FT-015-16

Rock type:	Migmatitic gneiss	Elevation [m]:	962
Lat/Lon:	48.686/-119.120	Zeta [ζ]:	289 ± 11
U conc. SRM612:	37 ppm	Area of basic unit:	$63.5*10^{-5}$
N_d:	1917	ρ_d:	$1.54*10^{-6}$
Analyst:	Erkan Toraman		

No	N_s	N_i	Area	Age [Ma] ± 1σ
1	27	135	100	44.4 ± 9.6
2	16	110	60	32.3 ± 8.8
3	16	123	100	28.9 ± 7.8
4	24	117	100	45.5 ± 10.4
5	10	151	100	14.7 ± 4.8
6	59	269	100	48.6 ± 7.3
7	20	98	80	45.3 ± 11.3
8	22	92	100	53.0 ± 12.8
9	60	273	100	48.7 ±7.3
10	28	95	100	65.3 ± 14.3
11	71	203	100	77.4 ± 11.2
12	13	62	70	46.5 ± 14.3
13	71	251	100	62.6 ± 8.9
14	15	73	100	45.6 ± 13.1
15	20	178	100	24.9 ± 6.0
16	20	103	90	43.1± 10.7
17	46	250	100	40.8 ± 6.8
18	13	64	46	45.0 ± 13.8
19	45	151	100	65.9 ± 11.6

Length [μm]	#
0-1	0
1-2	0
2-3	0
3-4	0
4-5	0
5-6	0
6-7	0
7-8	0
8-9	0
9-10	0
10-11	0
11-12	0
12-13	0
13-14	0
14-15	0
15-16	0
16-17	0
17-18	0
18-19	0
19-20	0

χ^2 = 52.94
P [χ^2] = 0%
U [ppm] = 57.2

MTL = 0
SE = 0
SD = 0
# = 0
DPAR= 0

Pooled Age ± 1σ [Ma] = 47.2 ± 2.9
Mean Age ± 1σ [Ma] = 46.3 ± 3.4
Central Age ± 1σ **[Ma] = 45.9 ± 4.1**

Sample No: OK-323
Irradiation No: FT-015-15

Rock type:	Migmatitic augen gneiss	Elevation [m]:	725
Lat/Lon:	48.661/-119.193	Zeta [ζ]:	289 ± 11
U conc. SRM612:	37 ppm	Area of basic unit:	$63.5*10^{-5}$
N_d:	1917	ρ_d:	$1.509*10^{-6}$
Analyst:	Erkan Toraman		

No	N_s	N_i	Area	Age [Ma] ± 1σ
1	21	184	100	24.8 ± 5.83
2	17	70	100	52.7 ± 14.5
3	83	445	100	40.5 ± 5.2
4	21	41	50	110.7 ± 30.1
5	36	260	100	30.1 ± 5.5
6	35	99	100	76.6 ± 15.4
7	18	88	100	44.5 ± 11.7
8	15	126	100	25.9 ± 7.2
9	15	78	100	41.8 ± 11.9
10	33	118	100	60.7 ± 12.3
11	5	73	100	14.9 ± 6.9
12	52	449	100	25.2 ± 3.9
13	19	95	100	43.4 ± 11.1
14	14	132	100	23.1 ± 6.6
15	57	255	100	48.6 ± 7.4
16	39	390	100	21.8 ± 3.8

Length [μm]	#
0-1	0
1-2	0
2-3	0
3-4	0
4-5	0
5-6	0
6-7	0
7-8	0
8-9	0
9-10	0
10-11	0
11-12	0
12-13	0
13-14	0
14-15	0
15-16	0
16-17	0
17-18	0
18-19	0
19-20	0

χ^2 = 78.17
P [χ^2] = 0%
U [ppm] = 67.8

MTL = 0
SE = 0
SD = 0
# = 0
DPAR= 0

Pooled Age ± 1σ [Ma] = 36.0 ± 2.3
Mean Age ± 1σ [Ma] = 42.9 ± 6.1
Central Age ± 1σ **[Ma] = 39.8 ± 5.0**

Sample No: OK-324
Irradiation No: FT-015-14

Rock type:	Granodioritic augen gneiss	Elevation [m]:	654
Lat/Lon:	48.657/-119.287	Zeta [ζ]:	289 ± 11
U conc. SRM612:	37 ppm	Area of basic unit:	$63.5*10^{-5}$
N_d:	1917	ρ_d:	$1.478*10^{-6}$
Analyst:	Erkan Toraman		

No	N_s	N_i	Area	Age [Ma] ± 1σ
1	19	115	100	34.6 ± 8.7
2	21	73	100	61.2 ± 15.4
3	11	110	100	21.3 ± 6.8
4	9	131	100	14.7 ± 5.1
5	29	174	100	35.5 ± 7.3
6	26	81	100	68.2 ± 15.7
7	26	118	100	46.9 ± 10.4
8	31	141	100	46.8 ± 9.5
9	52	269	100	41.2 ± 6.5
10	49	165	100	63.1 ± 10.6
11	18	107	100	35.8 ± 9.3
12	52	220	100	50.3 ± 8.1
13	31	179	100	36.9 ± 7.4
14	43	183	100	49.9 ± 8.8
15	39	215	100	38.6 ± 7.0
16	58	354	75	34.9 ± 5.2
17	56	210	100	56.7 ± 8.9
18	30	166	100	38.5 ± 7.8
19	52	197	100	56.1 ± 9.1

Length [μm]	#
0-1	0
1-2	0
2-3	0
3-4	0
4-5	0
5-6	0
6-7	0
7-8	0
8-9	1
9-10	2
10-11	2
11-12	3
12-13	14
13-14	33
14-15	32
15-16	12
16-17	2
17-18	1
18-19	0
19-20	0

$\chi^2 = 42.6$
P [χ^2] = 0.1%
U [ppm] = 65.9

MTL = 13.75
SE = 0.14
SD = 1.39
# = 102
DPAR= 2.47

Pooled Age ± 1σ [Ma] = 43.3 ± 2.6
Mean Age ± 1σ [Ma] = 43.8 ± 3.2
Central Age ± 1σ **[Ma] = 43.2 ± 3.3**

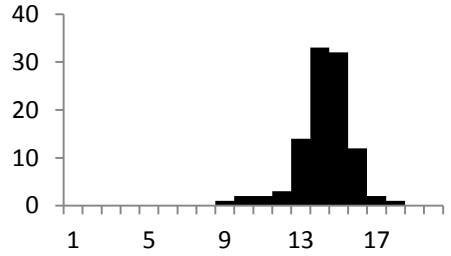

Sample No: OK-325
Irradiation No: FT-015-06

Rock type:	Q-feld gneiss	Elevation [m]:	585
Lat/Lon:	48.673/-119.364	Zeta [ζ]:	289 ± 11
U conc. SRM612:	37 ppm	Area of basic unit:	$63.5*10^{-5}$
N_d:	1917	ρ_d:	$1.228*10^{-6}$
Analyst:	Erkan Toraman		

No	N_s	N_i	Area	Age [Ma] ± 1σ
1	15	84	100	31.6 ± 8.9
2	10	41	82	43.1 ± 15.3
3	36	166	100	38.4 ± 7.3
4	13	65	100	35.4 ± 10.9
5	7	12	100	102.7 ± 49.1
6	19	56	100	59.9 ± 16.1
7	14	46	100	53.8 ± 16.6
8	7	40	100	30.9 ± 12.8
9	5	23	100	38.5 ± 19.1
10	7	22	100	56.2 ± 24.5
11	7	31	100	39.9 ± 16.8
12	13	27	100	84.9 ± 28.9
13	6	31	100	34.3 ± 15.4
14	17	80	49	37.6 ± 10.2
15	11	59	93	33.0 ± 10.9
16	8	51	100	27.8 ± 10.6
17	9	37	90	43.0 ± 16.1
18	14	52	95	47.6 ± 14.5
19	5	15	90	58.9 ± 30.5
20	10	59	100	30.0 ± 10.3

Length [μm]	#
0-1	0
1-2	0
2-3	0
3-4	0
4-5	0
5-6	0
6-7	0
7-8	0
8-9	0
9-10	0
10-11	0
11-12	0
12-13	0
13-14	0
14-15	0
15-16	0
16-17	0
17-18	0
18-19	0
19-20	0

χ^2 = 17.65
P [χ^2] = 61.0%
U [ppm] = 26.3

MTL = 0
SE = 0
SD = 0
# = 0
DPAR= 0

Pooled Age ± 1σ [Ma] = 41.8 ± 3.4
Mean Age ± 1σ [Ma] = 46.5 ± 4.1
Central Age ± 1σ **[Ma] = 41.8 ± 3.4**

Sample No: OK-327
Irradiation No: FT-015-12

Rock type:	Q-feld gneiss	Elevation [m]:	585
Lat/Lon:	48.673/-119.364	Zeta [ζ]:	289 ± 11
U conc. SRM612:	37 ppm	Area of basic unit:	$63.5*10^{-5}$
N_d:	1917	ρ_d:	$1.415*10^{-6}$
Analyst:	Erkan Toraman		

No	N_s	N_i	Area	Age [Ma] ± 1σ
1	17	42	100	73.2 ± 21.3
2	10	42	100	43.2 ± 15.3
3	12	84	100	25.9 ± 8.1
4	9	23	36	70.8 ± 28.0
5	14	42	100	60.4 ± 18.8
6	21	69	100	55.1 ± 14.0
7	10	27	100	67.0 ± 25.0
8	12	23	70	94.3 ± 33.8
9	12	27	42	80.4 ± 28.1
10	11	46	90	43.4 ± 14.7
11	21	90	100	42.3 ± 10.4
12	11	44	100	45.3 ± 15.4
13	6	10	100	108.2 ± 56.1
14	11	64	100	31.2 ± 10.3
15	8	34	80	42.7 ± 16.9
16	18	56	100	58.2 ± 16.0
17	7	19	100	66.7 ± 29.6
18	4	30	89	24.2 ± 12.9
19	12	37	100	58.7 ± 19.7
20	15	48	100	56.6 ± 16.9
21	12	69	100	31.6 ± 9.9
22	9	25	80	65.2 ± 25.5

Length [μm]	#
0-1	0
1-2	0
2-3	0
3-4	0
4-5	0
5-6	0
6-7	0
7-8	1
8-9	0
9-10	0
10-11	2
11-12	6
12-13	13
13-14	27
14-15	32
15-16	17
16-17	1
17-18	1
18-19	0
19-20	0

χ^2 = 25.15
P [χ^2] = 24.1%
U [ppm] = 21.3

MTL = 13.84
SE = 0.14
SD = 1.37
# = 100
DPAR= 3.18

Pooled Age ± 1σ [Ma] = 49.9 ± 4.0
Mean Age ± 1σ [Ma] = 56.6 ± 4.6
Central Age ± 1σ **[Ma] = 50.5 ± 4.3**

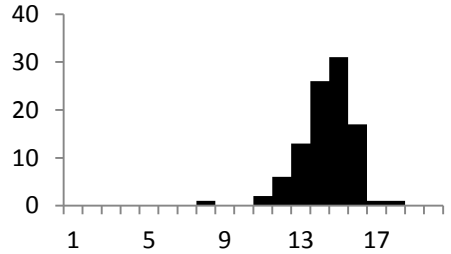

Sample No:	OK-338
Irradiation No:	FT-015-05

Rock type:	Mylonitic gneiss	Elevation [m]:	273
Lat/Lon:	48.636/-119.463	Zeta [ζ]:	289 ± 11
U conc. SRM612:	37 ppm	Area of basic unit:	$63.5*10^{-5}$
N_d:	1917	ρ_d:	$1.196*10^{-6}$
Analyst:	Erkan Toraman		

No	N_s	N_i	Area	Age [Ma] ± 1σ
1	1	5	100	34.5 ± 37.8
2	3	16	100	32.3 ± 20.4
3	3	25	100	20.7 ± 12.7
4	13	41	100	54.6 ± 17.5
5	2	5	100	68.8 ± 57.6
6	7	27	100	44.6 ± 19.0
7	3	21	100	24.6 ± 15.2
8	4	8	60	85.8 ± 52.7
9	5	20	100	43.1 ± 21.6
10	2	7	100	49.2 ± 39.5
11	4	9	100	76.4 ± 46.0
12	3	10	100	51.6 ± 34.1
13	8	13	100	105.5 ± 47.6
14	1	6	100	28.7 ± 31.1
15	3	16	100	32.3 ± 20.4
16	6	11	100	93.6 ± 47.7
17	9	43	100	36.1 ± 13.3
18	2	10	100	34.5 ± 26.7
19	8	11	100	124.5 ± 58.1
20	2	6	100	57.4 ± 46.9

Length [μm]	#
0-1	0
1-2	0
2-3	0
3-4	0
4-5	0
5-6	0
6-7	0
7-8	0
8-9	0
9-10	0
10-11	0
11-12	0
12-13	0
13-14	0
14-15	0
15-16	0
16-17	0
17-18	0
18-19	0
19-20	0

χ^2 = 16.55
P [χ^2] = 62.0%
U [ppm] = 7.3

MTL = 0
SE = 0
SD = 0
# = 0
DPAR= 0

Pooled Age ± 1σ [Ma] = 49.4 ± 6.3
Mean Age ± 1σ [Ma] = 55.0 ± 6.4
Central Age ± 1σ [Ma] = 49.5 ± 6.3

Sample No: OK-339
Irradiation No: FT-015-09

Rock type:	Gneiss	Elevation [m]:	275
Lat/Lon:	48.645/-119.466	Zeta [ζ]:	289 ± 11
U conc. SRM612:	37 ppm	Area of basic unit:	$63.5*10^{-5}$
N_d:	1917	ρ_d:	$1.321*10^{-6}$
Analyst:	Erkan Toraman		

No	N_s	N_i	Area	Age [Ma] ± 1σ
1	16	107	100	28.5 ± 7.74
2	12	124	100	18.5 ± 5.6
3	10	63	100	30.2 ± 10.4
4	8	119	100	12.8 ± 4.7
5	32	208	100	29.3 ± 5.7
6	11	38	60	55.0 ± 19.0
7	23	143	100	30.6 ± 7.0
8	10	58	100	32.8 ± 11.3
9	5	22	46	43.2 ± 21.5
10	5	22	46	43.2 ± 21.5
11	19	92	100	39.3 ± 10.1
12	4	56	46	13.6 ± 7.1
13	13	93	100	26.6 ± 7.9
14	4	23	100	33.1 ± 18.0
15	5	96	46	9.9 ± 4.6
16	5	41	100	23.2 ± 11.1
17	12	92	100	24.9 ± 7.7
18	10	72	100	26.5 ± 9.0
19	28	204	100	26.2 ± 5.4
20	21	173	100	23.1 ± 5.4

Length [μm]	#
0-1	0
1-2	0
2-3	0
3-4	0
4-5	0
5-6	0
6-7	0
7-8	0
8-9	1
9-10	3
10-11	2
11-12	12
12-13	22
13-14	40
14-15	19
15-16	1
16-17	0
17-18	0
18-19	0
19-20	0

χ^2 = 23.75
P [χ^2] = 20.6%
U [ppm] = 44.2

MTL = 13.02
SE = 0.13
SD = 1.31
# = 100
DPAR= 3.04

Pooled Age ± 1σ [Ma] = 26.1 ± 2.0
Mean Age ± 1σ [Ma] = 28.5 ± 2.5
Central Age ± 1σ **[Ma] = 26.2 ± 2.1**

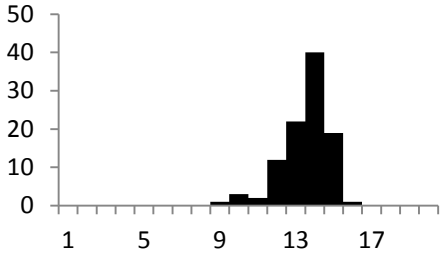

Sample No: BC-08-01
Irradiation No: FT-016-12

Rock type:	Quartzite	Elevation [m]:	611
Lat/Lon:	51°13.245'/-118°13.583	Zeta [ζ]:	289 ± 11
U conc. SRM612:	37 ppm	Area of basic unit:	$63.5*10^{-5}$
N_d:	8145	ρ_d:	$1.260*10^{-6}$
Analyst:	Erkan Toraman		

No	N_s	N_i	Area	Age [Ma] ± 1σ
1	5	93	100	9.8 ± 4.5
2	3	37	100	14.8 ± 8.9
3	3	65	100	8.4 ± 5.0
4	2	23	36	15.8 ± 11.7
5	2	16	36	22.7 ± 17.1
6	2	17	36	21.4 ± 16.0
7	2	15	36	24.2 ± 18.3
8	3	57	100	9.6 ± 5.7
9	2	14	25	26.0 ± 19.6
10	2	17	16	21.4 ± 16.0
11	4	50	100	14.6 ± 7.6
12	5	32	100	28.4 ± 13.7
13	1	28	100	6.5 ± 6.6
14	6	49	100	22.3 ± 9.7
15	3	55	100	9.9 ± 5.9
16	6	70	100	15.6 ± 6.7
17	1	16	36	11.4 ± 11.7
18	2	10	36	36.3 ± 28.2
19	2	79	80	4.6 ± 3.3
20	5	47	100	19.3 ± 9.1

Length [μm]	#
0-1	0
1-2	0
2-3	0
3-4	0
4-5	0
5-6	0
6-7	0
7-8	0
8-9	0
9-10	0
10-11	0
11-12	0
12-13	0
13-14	0
14-15	0
15-16	0
16-17	0
17-18	0
18-19	0
19-20	0

χ^2 = 13.39
P [χ^2] = 81.8%
U [ppm] = 24.6

MTL = 0
SE = 0
SD = 0
# = 0
DPAR= 0

Pooled Age ± 1σ [Ma] = 14.0 ± 2.0
Mean Age ± 1σ [Ma] = 17.1 ± 1.8
Central Age ± 1σ **[Ma] = 14.0 ± 2.0**

Sample No:	BC-08-29
Irradiation No:	FT-016-10

Rock type:	Quartzite	Elevation [m]:	575
Lat/Lon:	50°50.771'/-118°06.762'	Zeta [ζ]:	289 ± 11
U conc. SRM612:	37 ppm	Area of basic unit:	$63.5*10^{-5}$
N_d:	8145	ρ_d:	$1.220*10^{-6}$
Analyst:	Erkan Toraman		

No	N_s	N_i	Area	Age [Ma] ± 1σ
1	16	221	100	12.8 ± 3.3
2	13	214	100	10.7 ± 3.1
3	13	191	100	12.0 ± 3.5
4	14	173	100	14.3 ± 4.0
5	9	47	100	33.7 ± 12.3
6	11	163	100	11.9 ± 3.7
7	7	113	100	10.9 ± 4.3
8	4	22	100	32.0 ± 17.4
9	12	101	100	20.9 ± 6.4
10	14	152	100	16.2 ± 4.6
11	4	28	100	25.1 ± 13.5
12	14	87	100	28.3 ± 8.2
13	6	62	100	10.6 ± 4.9
14	7	86	100	17.0 ± 7.3
15	4	35	100	14.3 ± 5.7
16	3	43	100	20.1 ± 10.6
17	7	54	100	22.8 ± 9.2
19	3	21	100	25.1 ± 15.5
20	13	83	100	27.6 ± 8.3
21	4	21	100	33.5 ± 18.3

Length [μm]	#
0-1	0
1-2	0
2-3	0
3-4	0
4-5	0
5-6	0
6-7	0
7-8	0
8-9	0
9-10	0
10-11	0
11-12	0
12-13	0
13-14	0
14-15	0
15-16	0
16-17	0
18-19	0
19-20	0

χ^2 = 25.35
P [χ^2] = 18.9%
U [ppm] = 77.1

MTL = 0
SE = 0
SD = 0
# = 0
DPAR= 0

Pooled Age ± 1σ [Ma] = 16.1 ± 1.4
Mean Age ± 1σ [Ma] = 19.6 ± 1.7
Central Age ± 1σ **[Ma] = 16.5 ± 1.5**

Sample No: BC-08-24
Irradiation No: FT-016-23

Rock type:	Metasandstone	Elevation [m]:	966
Lat/Lon:	51°01.166'/-118°16.193'	Zeta [ζ]:	289 ± 11
U conc. SRM612:	37 ppm	Area of basic unit:	$63.5*10^{-5}$
N_d:	8145	ρ_d:	$1.500*10^{-6}$
Analyst:	Erkan Toraman		

No	N_s	N_i	Area	Age [Ma] ± 1σ
1	11	145	100	16.4 ± 5.2
2	7	46	36	32.9 ± 13.4
3	2	23	36	18.8 ± 13.9
4	6	57	100	22.8 ± 9.8
5	6	126	100	10.3 ± 4.3
6	6	59	100	22.0 ± 9.5
7	7	53	36	28.6 ± 11.5
8	11	98	100	24.3 ± 7.8
9	6	31	36	41.8 ± 18.7
10	8	128	100	13.5 ± 5.0
11	2	43	36	10.1 ± 7.3
12	6	106	100	12.3 ± 5.2
13	5	71	100	15.3 ± 7.1
14	1	5	16	43.2 ± 47.4
15	7	82	36	18.5 ± 7.3
16	5	61	100	17.7 ± 8.3
17	2	14	16	30.9 ± 23.4
18	7	91	100	16.7 ± 6.6
19	2	25	36	17.3 ± 12.7
20	15	127	100	25.6 ± 7.1

Length [μm]	#
0-1	0
1-2	0
2-3	0
3-4	0
4-5	0
5-6	0
6-7	1
7-8	1
8-9	15
9-10	17
10-11	13
11-12	10
12-13	19
13-14	15
14-15	7
15-16	1
16-17	1
17-18	0
18-19	0
19-20	0

χ^2 = 14.96
P [χ^2] = 72.5%
U [ppm] = 37.6

MTL = 11.44
SE = 0.21
SD = 2.05
# = 100
DPAR= 3.8

Pooled Age ± 1σ [Ma] = 19.0 ± 1.9
Mean Age ± 1σ [Ma] = 21.9 ± 2.1
Central Age ± 1σ **[Ma] = 19.0 ± 1.9**

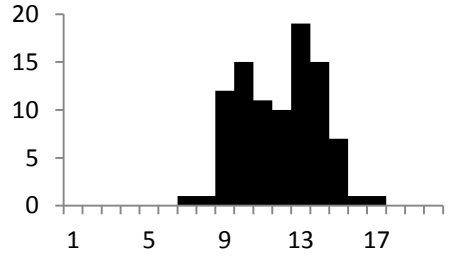

Sample No:	BC-08-29
Irradiation No:	FT-016-10

Rock type:	Quartzite	Elevation [m]:	575
Lat/Lon:	50°50.771'/-118°06.762'	Zeta [ζ]:	289 ± 11
U conc. SRM612:	37 ppm	Area of basic unit:	$63.5*10^{-5}$
N_d:	8145	ρ_d:	$1.220*10^{-6}$
Analyst:	Erkan Toraman		

No	N_s	N_i	Area	Age [Ma] ± 1σ
1	16	221	100	12.8 ± 3.3
2	13	214	100	10.7 ± 3.1
3	13	191	100	12.0 ± 3.5
4	14	173	100	14.3 ± 4.0
5	9	47	100	33.7 ± 12.3
6	11	163	100	11.9 ± 3.7
7	7	113	100	10.9 ± 4.3
8	4	22	16	32.0 ± 17.4
9	12	101	100	20.9 ± 6.4
10	14	152	100	16.2 ± 4.6
11	4	28	16	25.1 ± 13.5
12	14	87	36	28.3 ± 8.2
13	5	83	36	10.6 ± 4.9
14	6	62	36	17.0 ± 7.3
15	7	86	36	14.3 ± 5.7
16	4	35	16	20.1 ± 10.6
17	3	43	36	12.3 ± 7.4
18	7	54	36	22.8 ± 9.2
19	3	21	16	25.1 ± 15.5
20	13	83	36	27.6 ± 8.3
21	4	21	16	33.5 ± 18.3

Length [μm]	#
0-1	0
1-2	0
2-3	0
3-4	0
4-5	0
5-6	0
6-7	0
7-8	0
8-9	0
9-10	0
10-11	0
11-12	0
12-13	0
13-14	0
14-15	0
15-16	0
16-17	0
17-18	0
18-19	0
19-20	0

χ^2 = 25.35
P [χ^2] = 18.9%
U [ppm] = 77.1

MTL = 0
SE = 0
SD = 0
# = 0
DPAR= 0

Pooled Age ± 1σ [Ma] = 16.1 ± 1.4
Mean Age ± 1σ [Ma] = 19.6 ± 1.7
Central Age ± 1σ **[Ma] = 16.5 ± 1.5**

Sample No:	BC-08-33
Irradiation No:	FT-016-17

Rock type:	Quartzite	Elevation [m]:	1678
Lat/Lon:	51°24.887'/-118°34.624'	Zeta [ζ]:	289 ± 11
U conc. SRM612:	37 ppm	Area of basic unit:	$63.5*10^{-5}$
N_d:	8145	ρ_d:	$1.370*10^{-6}$
Analyst:	Erkan Toraman		

No	N_s	N_i	Area	Age [Ma] ± 1σ
1	45	468	100	19.0 ± 3.1
2	8	39	36	40.5 ± 15.8
3	11	81	36	26.8 ± 8.7
4	5	98	36	10.1 ± 4.6
5	16	150	100	21.1 ± 5.6
6	23	196	36	23.2 ± 5.2
7	8	70	100	22.6 ± 8.5
8	22	194	100	22.4 ± 5.1
9	15	123	100	24.1 ± 6.7
10	11	171	100	12.7 ± 4.0
11	9	67	100	26.5 ± 9.5
12	12	75	100	31.6 ± 9.9
13	13	130	100	19.8 ± 5.8
14	7	72	36	19.2 ± 7.7
15	11	86	36	25.3 ± 8.2
16	5	47	36	21.0 ± 9.9
17	4	34	100	23.3 ± 12.3
18	18	125	100	28.4 ± 7.3
19	11	110	36	19.8 ± 6.3
20	16	188	36	16.8 ± 4.4
21	9	88	36	20.2 ± 7.1

Length [μm]	#
0-1	0
1-2	0
2-3	0
3-4	0
4-5	0
5-6	0
6-7	0
7-8	0
8-9	0
9-10	0
10-11	0
11-12	0
12-13	0
13-14	0
14-15	0
15-16	0
16-17	0
17-18	0
18-19	0
19-20	0

χ^2 = 14.72
P [χ^2] = 79.2%
U [ppm] = 85.1

MTL = 0
SE = 0
SD = 0
# = 0
DPAR= 0

Pooled Age ± 1σ [Ma] = 21.1 ± 1.6
Mean Age ± 1σ [Ma] = 22.6 ± 1.4
Central Age ± 1σ **[Ma] = 21.1 ± 1.6**

Sample No:	BC-08-34
Irradiation No:	FT-016-16

Rock type:	Quartzite	Elevation [m]:	1678
Lat/Lon:	51°24.887'/-118°34.625'	Zeta [ζ]:	289 ± 11
U conc. SRM612:	37 ppm	Area of basic unit:	$63.5*10^{-5}$
N_d:	8145	ρ_d:	$1.350*10^{-6}$
Analyst:	Erkan Toraman		

No	N_s	N_i	Area	Age [Ma] ± 1σ
1	16	54	100	57.5 ± 16.5
2	8	20	100	77.6 ± 32.6
3	5	15	36	64.7 ± 33.5
4	4	6	36	128.8 ± 83.3
5	6	26	100	44.9 ± 20.4
6	4	36	100	21.6 ± 11.4
7	2	13	36	29.9 ± 22.8
8	4	9	16	86.1 ± 51.9
9	1	29	100	6.7 ± 6.8
10	5	29	100	33.6 ± 16.3
11	11	82	100	26.1 ± 8.5
12	2	7	36	55.5 ± 44.6
13	1	2	16	96.8 ± 119.0

Length [μm]	#
0-1	0
1-2	0
2-3	0
3-4	0
4-5	0
5-6	0
6-7	0
7-8	0
8-9	0
9-10	0
10-11	0
11-12	0
12-13	0
13-14	0
14-15	0
15-16	0
16-17	0
17-18	0
18-19	0
19-20	0

χ^2 = 18.6
P [χ^2] = 9.9%
U [ppm] = 14.5

MTL = 0
SE = 0
SD = 0
# = 0
DPAR= 0

Pooled Age ± 1σ [Ma] = 21.1 ± 1.6
Mean Age ± 1σ [Ma] = 22.6 ± 1.4
Central Age ± 1σ **[Ma] = 21.1 ± 1.6**

Sample No: BC-08-40
Irradiation No: FT-016-13

Rock type:	Quartzite	Elevation [m]:	1382
Lat/Lon:	51°01.166'/-118°16.193'	Zeta [ζ]:	289 ± 11
U conc. SRM612:	37 ppm	Area of basic unit:	$63.5*10^{-5}$
N_d:	8145	ρ_d:	$1.280*10^{-6}$
Analyst:	Erkan Toraman		

No	N_s	N_i	Area	Age [Ma] ± 1σ
1	5	52	100	17.8 ± 8.4
2	3	30	36	18.5 ± 11.2
3	5	59	36	15.7 ± 7.3
4	10	104	100	17.8 ± 5.9
5	2	21	36	17.6 ± 13.0
6	2	12	16	30.8 ± 23.5
7	1	7	16	26.4 ± 28.2
8	3	14	36	39.5 ± 25.2
9	15	84	100	32.9 ± 9.3
10	2	22	36	16.8 ± 12.4
11	5	18	36	51.2 ± 25.9
12	5	42	36	22.0 ± 10.4
13	2	17	16	21.7 ± 16.3
14	3	26	36	21.3 ± 13.0
15	7	51	100	25.3 ± 10.3
16	2	23	36	16.1 ± 11.9
17	10	42	36	43.9 ± 15.5
18	5	22	16	41.9 ± 20.8
19	10	60	100	30.8 ± 10.6
20	2	11	16	33.5 ± 25.8

Length [μm]	#
0-1	0
1-2	0
2-3	0
3-4	0
4-5	0
5-6	0
6-7	0
7-8	0
8-9	3
9-10	3
10-11	4
11-12	17
12-13	18
13-14	24
14-15	19
15-16	10
16-17	2
17-18	0
18-19	0
19-20	0

$\chi^2 = 11.25$
P [χ^2] = 91.5%
U [ppm] = 34.9

MTL = 13.03
SE = 0.18
SD = 1.81
# = 100
DPAR= 2.61

Pooled Age ± 1σ [Ma] = 25.7 ± 2.9
Mean Age ± 1σ [Ma] = 27.5 ± 2.3
Central Age ± 1σ **[Ma] = 25.7 ± 2.9**

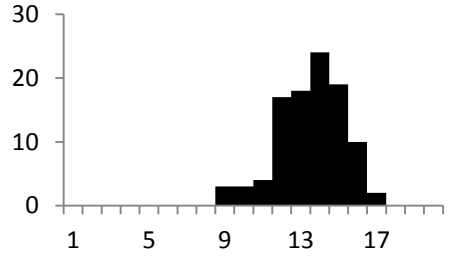

Sample No:	BC-08-41
Irradiation No:	FT-016-4

Rock type:	Pegmatite	Elevation [m]:	1193
Lat/Lon:	51°23.645'/-118°40.291'	Zeta [ζ]:	289 ± 11
U conc. SRM612:	37 ppm	Area of basic unit:	$63.5*10^{-5}$
N_d:	8145	ρ_d:	$1.090*10^{-6}$
Analyst:	Erkan Toraman		

No	N_s	N_i	Area	Age [Ma] ± 1σ
1	10	71	100	22.2 ± 7.5
2	11	68	100	25.4 ± 8.3
3	4	22	36	28.6 ± 15.6
4	15	74	100	31.9 ± 9.1
5	10	67	100	23.5 ± 8.0
6	8	51	100	24.7 ± 9.4
7	18	80	100	35.3 ± 9.3
8	11	100	100	17.3 ± 5.5
9	9	61	100	23.2 ± 8.3
10	13	76	100	26.9 ± 8.1
11	4	14	16	44.9 ± 25.5
12	11	64	100	27.0 ± 8.9
13	11	66	100	26.2 ± 8.6
14	7	34	36	32.4 ± 13.5
15	14	68	100	32.4 ± 9.6
16	10	62	100	25.4 ± 8.7
17	13	78	100	26.2 ± 7.9
18	6	24	36	39.3 ± 18.0
19	5	31	36	25.4 ± 12.3
20	12	84	100	22.5 ± 7.0

Length [μm]	#
0-1	0
1-2	0
2-3	0
3-4	0
4-5	0
5-6	0
6-7	0
7-8	0
8-9	0
9-10	0
10-11	0
11-12	0
12-13	0
13-14	0
14-15	0
15-16	0
16-17	0
17-18	0
18-19	0
19-20	0

$\chi^2 = 6.76$
P [χ^2] = 99.5%
U [ppm] = 37.4

MTL = 0
SE = 0
SD = 0
# = 0
DPAR= 0

Pooled Age ± 1σ [Ma] = 26.6 ± 2.3
Mean Age ± 1σ [Ma] = 28.0 ± 1.4
Central Age ± 1σ [Ma] = 26.6 ± 2.3

Sample No:	BC-08-44
Irradiation No:	FT-016-15

Rock type:	Gneiss	Elevation [m]:	865
Lat/Lon:	51°23.448'/-118°40.916'	Zeta [ζ]:	289 ± 11
U conc. SRM612:	37 ppm	Area of basic unit:	$63.5*10^{-5}$
N_d:	8145	ρ_d:	$1.330*10^{-6}$
Analyst:	Erkan Toraman		

No	N_s	N_i	Area	Age [Ma] ± 1σ
1	15	113	100	25.5 ± 7.1
2	10	52	36	36.9 ± 12.8
3	7	24	36	55.8 ± 24.1
4	3	19	100	30.3 ± 18.8
5	3	21	36	27.4 ± 16.9
6	13	121	100	20.6 ± 6.1
7	8	55	100	27.9 ± 10.6
8	6	40	100	28.8 ± 12.6
9	22	111	100	38.0 ± 9.0
10	3	39	36	14.8 ± 8.9
11	8	46	16	33.3 ± 12.8
12	14	77	36	34.9 ± 10.2
13	6	32	100	35.9 ± 16.0
14	6	27	100	42.6 ± 19.3
15	9	56	36	30.8 ± 11.1
16	1	5	16	38.3 ± 42.0
17	1	11	36	17.5 ± 18.2
18	4	18	100	42.6 ± 23.6
19	5	20	36	47.9 ± 24.0
20	2	9	36	42.6 ± 33.3

Length [μm]	#
0-1	0
1-2	0
2-3	0
3-4	0
4-5	0
5-6	1
6-7	2
7-8	4
8-9	12
9-10	15
10-11	13
11-12	16
12-13	14
13-14	13
14-15	6
15-16	2
16-17	1
17-18	0
18-19	0
19-20	0

$\chi^2 = 6.76$
P [χ^2] = 99.5%
U [ppm] = 37.4

MTL = 11.04
SE = 0.22
SD = 2.25
# = 100
DPAR= 1.93

Pooled Age ± 1σ [Ma] = 31.2 ± 3.1
Mean Age ± 1σ [Ma] = 33.6 ± 2.3
Central Age ± 1σ [Ma] = 31.2 ± 3.1

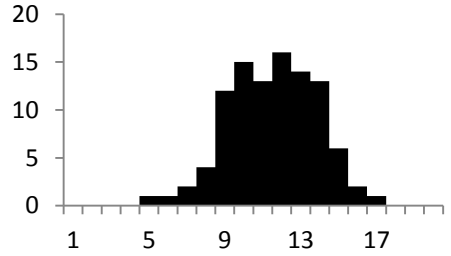

Sample No: BC-08-45
Irradiation No: FT-016-14

Rock type:	Garnetschist	Elevation [m]:	788
Lat/Lon:	51°22.181'/-118°42.407'	Zeta [ζ]:	289 ± 11
U conc. SRM612:	37 ppm	Area of basic unit:	$63.5*10^{-5}$
N_d:	8145	ρ_d:	$1.300*10^{-6}$
Analyst:	Erkan Toraman		

No	N_s	N_i	Area	Age [Ma] ± 1σ
1	16	164	100	18.3 ± 4.9
2	12	132	100	17.1 ± 5.2
3	5	37	36	25.3 ± 12.1
4	30	257	100	21.9 ± 4.3
5	9	115	100	14.7 ± 5.1
6	14	121	36	21.7 ± 6.2
7	22	191	100	21.6 ± 4.9
8	30	240	100	23.4 ± 4.6
9	10	61	36	30.7 ± 10.6
10	14	126	100	20.8 ± 5.9
11	6	83	36	13.6 ± 5.8
12	21	257	100	15.3 ± 3.5
13	11	131	100	15.8 ± 5.0
14	11	60	36	34.4 ± 11.3
15	17	178	100	17.9 ± 4.6
16	12	86	36	26.2 ± 8.1
17	7	47	36	27.9 ± 11.4
18	17	140	36	22.8 ± 5.9
19	22	144	36	28.6 ± 6.7
20	19	126	36	28.3 ± 7.1

Length [μm]	#
0-1	0
1-2	0
2-3	0
3-4	0
4-5	0
5-6	1
6-7	6
7-8	6
8-9	12
9-10	18
10-11	25
11-12	16
12-13	9
13-14	4
14-15	2
15-16	1
16-17	0
17-18	0
18-19	0
19-20	0

$\chi^2 = 14.53$
P [χ^2] = 75.2%
U [ppm] = 92.1

MTL = 10.30
SE = 0.19
SD = 1.95
# = 100
DPAR= 2.75

Pooled Age ± 1σ [Ma] = 21.2 ± 1.5
Mean Age ± 1σ [Ma] = 22.3 ± 1.3
Central Age ± 1σ [Ma] = 21.2 ± 1.5

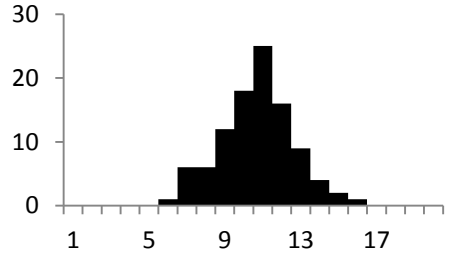

Sample No:	BC-08-50
Irradiation No:	FT-016-6

Rock type:	Granitic gneiss boulder	Elevation [m]:	1169
Lat/Lon:	50°38.248'/-119°02.378'	Zeta [ζ]:	289 ± 11
U conc. SRM612:	37 ppm	Area of basic unit:	$63.5*10^{-5}$
N_d:	8145	ρ_d:	$1.130*10^{-6}$
Analyst:	Erkan Toraman		

No	N_s	N_i	Area	Age [Ma] ± 1σ
1	5	40	36	20.4 ± 9.7
2	15	104	100	23.5 ± 6.6
3	10	67	100	24.3 ± 8.3
4	7	46	100	24.8 ± 10.1
5	7	90	100	12.7 ± 5.0
6	9	100	100	14.7 ± 5.1
7	14	65	100	35.1 ± 10.4
8	10	37	100	44.0 ± 15.8
9	5	35	36	23.3 ± 11.2
10	8	112	100	11.7 ± 4.3
11	4	29	36	22.5 ± 12.0
12	15	106	100	23.1± 6.4
13	19	95	100	32.6 ± 8.3
14	9	63	100	23.3 ± 8.4
15	10	40	100	40.7 ± 14.5
16	12	148	100	13.2 ± 4.0
17	8	61	100	21.4 ± 8.1
18	21	169	100	20.3 ± 4.8
19	8	32	100	40.7 ± 16.2
20	6	35	36	27.9 ± 12.4
21	16	146	100	17.9 ± 4.8

Length [μm]	#
0-1	0
1-2	0
2-3	0
3-4	0
4-5	0
5-6	0
6-7	0
7-8	0
8-9	0
9-10	0
10-11	0
11-12	0
12-13	0
13-14	0
14-15	0
15-16	0
16-17	0
17-18	0
18-19	0
19-20	0

$\chi^2 = 25.55$
P [χ^2] = 18.1%
U [ppm] = 43.7

MTL = 0
SE = 0
SD = 0
# = 0
DPAR= 0

Pooled Age ± 1σ [Ma] = 21.9 ± 1.8
Mean Age ± 1σ [Ma] = 24.7 ± 2.0
Central Age ± 1σ [Ma] = 22.3 ± 2.0

Sample No:	BC-10-07
Irradiation No:	FT-019-02

Rock type:	Quartzite	Elevation [m]:	1326
Lat/Lon:	50°27.722'/-118°01.829'	Zeta [ζ]:	289 ± 11
U conc. SRM612:	37 ppm	Area of basic unit:	$63.5*10^{-5}$
N_d:	4383	ρ_d:	$1.230*10^{-6}$
Analyst:	Erkan Toraman		

No	N_s	N_i	Area	Age [Ma] ± 1σ
1	27	170	100	28.2 ± 6.0
2	10	82	100	21.6 ± 7.3
3	8	62	64	22.9 ± 8.7
4	5	46	28	19.3 ± 9.1
5	7	37	100	33.5 ± 13.9
6	10	75	100	23.7 ± 8.0
7	4	36	100	19.7 ± 10.4
8	11	117	36	16.7 ± 5.3
9	9	56	36	28.5 ± 10.3
10	10	45	36	39.4 ± 13.9
11	19	78	40	43.2 ± 11.2
12	35	216	100	28.7 ± 5.4
13	3	13	25	40.9 ± 26.2
14	11	92	60	21.2 ± 6.8
15	6	49	100	21.7 ± 49.4
16	16	135	100	21.0 ± 5.6
17	7	56	60	22.2 ± 8.9
18	13	59	100	39.0 ± 12.1
19	3	15	36	35.5 ± 22.5
20	17	135	100	22.3 ± 5.8

Length [μm]	#
0-1	0
1-2	0
2-3	0
3-4	0
4-5	2
5-6	2
6-7	1
7-8	9
8-9	7
9-10	15
10-11	14
11-12	17
12-13	18
13-14	7
14-15	5
15-16	3
16-17	0
17-18	0
18-19	0
19-20	0

χ^2 = 13.84
P [χ^2] = 79.3%
U [ppm] = 54.2

MTL = 10.81
SE = 0.24
SD = 2.36
# = 100
DPAR= 3.22

Pooled Age ± 1σ [Ma] = 26.0 ± 2.1
Mean Age ± 1σ [Ma] = 27.5 ± 1.8
Central Age ± 1σ [Ma] = 26.0 ± 2.1

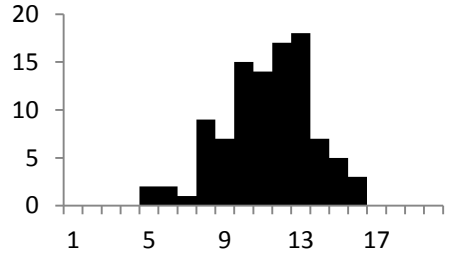

Sample No:	BC-10-08
Irradiation No:	FT-019-03

Rock type:	Gneiss	Elevation [m]:	2143
Lat/Lon:	50°27.803'/-118°05.543'	Zeta [ζ]:	289 ± 11
U conc. SRM612:	37 ppm	Area of basic unit:	$63.5*10^{-5}$
N_d:	4383	ρ_d:	$1.250*10^{-6}$
Analyst:	Erkan Toraman		

No	N_s	N_i	Area	Age [Ma] ± 1σ
1	4	21	16	34.3 ± 18.8
2	7	38	16	33.2 ± 13.7
3	7	15	16	48.0 ± 27.1
4	10	40	36	45.0 ± 16.0
5	6	15	16	71.9 ± 34.8
6	23	104	36	39.8 ± 9.3
7	4	13	16	53.3 ± 31.7
8	4	11	16	65.4 ± 38.2
9	6	26	36	41.6 ± 18.9
10	3	9	16	59.9 ± 40.0
11	4	22	16	32.8 ± 17.9
12	5	28	36	32.2 ± 15.7
13	12	64	36	33.8 ± 10.7
14	16	75	100	38.4 ± 10.7
15	9	28	36	57.8 ± 22.3
16	15	84	100	32.2 ± 9.1
17	9	23	16	70.3 ± 27.8
18	17	55	36	55.6 ± 15.6
19	4	8	16	89.7 ± 55.0
20	5	13	16	69.1 ± 36.5

Length [μm]	#
0-1	0
1-2	0
2-3	0
3-4	0
4-5	0
5-6	0
6-7	0
7-8	1
8-9	1
9-10	0
10-11	0
11-12	3
12-13	12
13-14	39
14-15	33
15-16	10
16-17	1
17-18	0
18-19	0
19-20	0

$\chi^2 = 10.71$
P [χ^2] = 93.3%
U [ppm] = 51.0

MTL = 13.75
SE = 0.12
SD = 1.24
# = 100
DPAR= 2.38

Pooled Age ± 1σ [Ma] = 43.3 ± 4.1
Mean Age ± 1σ [Ma] = 50.3 ± 3.8
Central Age ± 1σ [Ma] = 43.4 ± 4.1

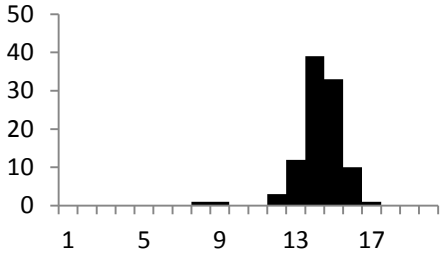

Sample No: BC-10-09
Irradiation No: FT-019-04

Rock type:	Gneiss	Elevation [m]:	2034
Lat/Lon:	50°27.781'/-118°05.377'	Zeta [ζ]:	289 ± 11
U conc. SRM612:	37 ppm	Area of basic unit:	$63.5*10^{-5}$
N_d:	4383	ρ_d:	$1.270*10^{-6}$
Analyst:	Erkan Toraman		

No	N_s	N_i	Area	Age [Ma] ± 1σ
1	26	74	16	64.2 ± 14.9
2	65	337	100	35.3 ± 5.0
3	19	88	36	39.5 ± 10.1
4	25	129	36	35.5 ± 7.9
5	31	137	36	41.4 ± 8.4
6	15	58	16	47.3 ± 13.8
7	35	126	36	50.8 ± 9.9
8	13	62	16	38.4 ± 11.8
9	15	62	16	44.3 ± 12.9
10	24	88	16	49.9 ± 11.7
11	20	68	16	53.8 ± 13.8
12	28	109	16	47.0 ± 10.1
13	14	65	36	39.4 ± 11.7
14	17	90	16	34.6 ± 9.3
15	23	98	16	42.9 ± 10.1
16	16	94	16	31.2 ± 8.5
17	18	80	16	41.2 ± 10.9
18	12	52	36	42.2 ± 13.6
19	7	52	16	24.7 ± 10.0
20	17	69	16	45.1 ± 12.3

Length [μm]	#
0-1	0
1-2	0
2-3	0
3-4	0
4-5	0
5-6	0
6-7	0
7-8	0
8-9	0
9-10	0
10-11	0
11-12	2
12-13	7
13-14	28
14-15	36
15-16	24
16-17	3
17-18	0
18-19	0
19-20	0

χ^2 = 12.7
P [χ^2] = 85.4%
U [ppm] = 181.1

MTL = 14.28
SE = 0.10
SD = 1.04
# = 100
DPAR= 3.46

Pooled Age ± 1σ [Ma] = 41.5 ± 2.8
Mean Age ± 1σ [Ma] = 42.4 ± 1.9
Central Age ± 1σ [Ma] = 41.5 ± 2.8

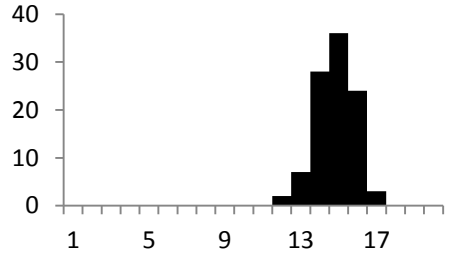

Sample No: BC-10-11
Irradiation No: FT-019-06

Rock type:	Gneiss	Elevation [m]:	1800
Lat/Lon:	50°27.715'/-118°03.518'	Zeta [ζ]:	289 ± 11
U conc. SRM612:	37 ppm	Area of basic unit:	$63.5*10^{-5}$
N_d:	4383	ρ_d:	$1.310*10^{-6}$
Analyst:	Erkan Toraman		

No	N_s	N_i	Area	Age [Ma] ± 1σ
1	20	91	16	41.5 ± 10.4
2	6	55	16	20.6 ± 8.9
3	19	142	36	25.3 ± 6.3
4	44	340	100	24.5 ± 4.0
5	18	76	16	44.7 ± 11.9
6	12	98	16	23.1 ± 7.1
7	14	72	16	36.7 ± 10.8
8	12	82	36	27.6 ± 8.6
9	8	79	16	19.1 ± 7.1
10	7	38	16	34.8 ± 14.4
11	74	478	100	29.2 ± 3.8
12	14	94	36	28.1 ± 8.1
13	24	134	36	33.8 ± 7.6
14	14	159	36	16.7 ± 4.7
15	18	103	36	33.0 ± 8.5
16	13	87	16	28.2 ± 8.5
17	20	100	16	37.8 ± 9.4
18	13	60	36	40.9 ± 12.6
19	7	62	16	21.3 ± 8.6
20	28	174	36	30.4 ± 6.3

Length [μm]	#
0-1	0
1-2	0
2-3	0
3-4	0
4-5	0
5-6	0
6-7	1
7-8	3
8-9	2
9-10	10
10-11	13
11-12	7
12-13	25
13-14	22
14-15	15
15-16	2
16-17	0
17-18	0
18-19	0
19-20	0

χ^2 = 17.73
P [χ^2] = 54.0%
U [ppm] = 178.3

MTL = 12.25
SE = 0.19
SD = 1.99
# = 100
DPAR= 1.90

Pooled Age ± 1σ [Ma] = 28.8 ± 2.0
Mean Age ± 1σ [Ma] = 29.9 ± 1.8
Central Age ± 1σ [Ma] = 28.8 ± 2.0

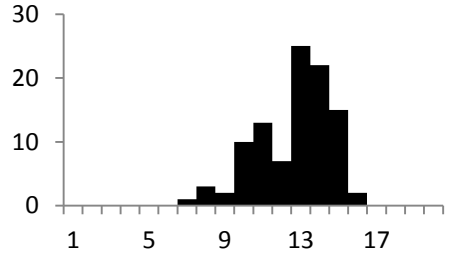

Sample No: BC-10-12
Irradiation No: FT-019-07

Rock type:	Mafic gneiss	Elevation [m]:	1688
Lat/Lon:	50°27.750'/-118°03.076'	Zeta [ζ]:	289 ± 11
U conc. SRM612:	37 ppm	Area of basic unit:	$63.5*10^{-5}$
N_d:	4383	ρ_d:	$1.340*10^{-6}$
Analyst:	Erkan Toraman		

No	N_s	N_i	Area	Age [Ma] ± 1σ
1	35	232	100	29.2 ± 5.4
2	11	60	16	35.4 ± 11.7
3	10	27	16	71.3 ± 26.6
4	15	72	36	40.2 ± 11.5
5	11	50	16	42.5 ± 14.2
6	17	95	100	34.6 ± 9.2
7	20	105	100	36.8 ± 9.1
8	8	59	100	26.2 ± 9.9
9	20	115	36	33.6 ± 8.3
10	3	18	16	32.2 ± 20.1
11	15	90	100	32.2 ± 9.1
12	22	141	100	30.1 ± 7.0
13	7	28	16	48.2 ± 20.5
14	33	172	100	37.0 ± 7.2
15	44	267	100	31.8 ± 5.3
16	9	42	16	41.4 ± 15.3
17	10	72	36	26.8 ± 9.1
18	9	50	16	34.8 ± 12.7
19	11	77	36	27.6 ± 9.0
20	11	44	100	48.2 ± 16.4

Length [μm]	#
0-1	0
1-2	0
2-3	0
3-4	0
4-5	0
5-6	0
6-7	0
7-8	1
8-9	1
9-10	4
10-11	9
11-12	8
12-13	21
13-14	27
14-15	19
15-16	9
16-17	1
17-18	0
18-19	0
19-20	0

χ^2 = 10.0
P [χ^2] = 95.2%
U [ppm] = 80.1

MTL = 12.93
SE = 0.17
SD = 1.72
# = 100
DPAR= 2.81

Pooled Age ± 1σ [Ma] = 34.1 ± 2.5
Mean Age ± 1σ [Ma] = 37.0 ± 2.3
Central Age ± 1σ **[Ma] = 34.1 ± 2.5**

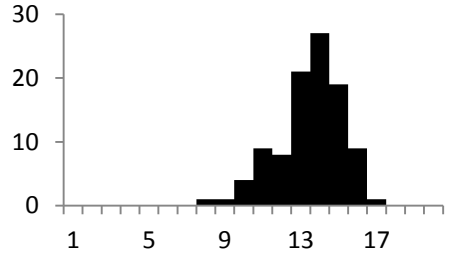

Sample No: BC-10-14
Irradiation No: FT-019-08

Rock type:	Gneiss	Elevation [m]:	1427
Lat/Lon:	50°27.052'/-118°02.014'	Zeta [ζ]:	289 ± 11
U conc. SRM612:	37 ppm	Area of basic unit:	$63.5*10^{-5}$
N_d:	4383	ρ_d:	$1.360*10^{-6}$
Analyst:	Erkan Toraman		

No	N_s	N_i	Area	Age [Ma] ± 1σ
1	9	63	36	28.0 ± 10.0
2	30	202	100	29.1 ± 15.8
3	9	36	16	48.9 ± 18.4
4	16	93	100	33.7 ± 9.2
5	4	16	16	48.9 ± 27.4
6	9	101	100	17.5 ± 6.1
7	6	33	36	35.6 ± 15.9
8	5	50	36	19.6 ± 9.2
9	7	71	70	19.4 ± 7.7
10	6	75	36	15.7 ± 6.7
11	6	37	16	31.8 ± 14.1
12	13	134	100	19.0 ± 5.6
13	9	48	36	36.7 ± 13.4
14	7	64	36	21.5 ± 8.6
15	7	79	36	17.4 ± 6.9
16	26	133	100	38.3 ± 8.4

Length [μm]	#
0-1	0
1-2	0
2-3	0
3-4	0
4-5	0
5-6	0
6-7	0
7-8	4
8-9	2
9-10	4
10-11	12
11-12	13
12-13	18
13-14	25
14-15	17
15-16	5
16-17	0
17-18	0
18-19	0
19-20	0

$\chi^2 = 16.21$
P [χ^2] = 36.8%
U [ppm] = 63.0

MTL = 12.45
SE = 0.18
SD = 1.89
# = 100
DPAR= 2.20

Pooled Age ± 1σ [Ma] = 26.8 ± 2.4
Mean Age ± 1σ [Ma] = 28.8 ± 2.7
Central Age ± 1σ [Ma] = 26.8 ± 2.5

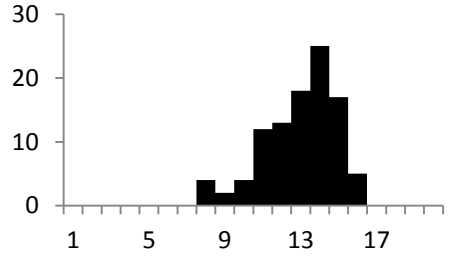

Sample No: BC-10-18
Irradiation No: FT-018-03

Rock type:	Migmatite	Elevation [m]:	1161
Lat/Lon:	50°34.656'/-118°01.927'	Zeta [ζ]:	289 ± 11
U conc. SRM612:	37 ppm	Area of basic unit:	$63.5*10^{-5}$
N_d:	3314	ρ_d:	$0.913*10^{-6}$
Analyst:	Erkan Toraman		

No	N_s	N_i	Area	Age [Ma] ± 1σ
1	26	225	100	15.2 ± 3.2
2	7	55	36	16.8 ± 6.8
3	11	46	36	31.5 ± 10.6
4	10	59	36	22.3 ± 7.7
5	8	47	36	22.4 ± 8.6
6	25	152	100	21.7 ± 4.8
7	8	66	100	16.0 ± 6.0
8	12	69	36	22.9 ± 7.2
9	20	157	100	16.8 ± 4.1
10	27	115	100	30.9 ± 6.7
11	7	17	16	54.1 ± 24.4
12	12	63	36	25.1 ± 8.0
13	16	61	36	34.5 ± 9.8
14	13	96	100	17.8 ± 5.3
15	11	51	36	28.4 ± 9.5
16	39	205	100	25.1 ± 4.5
17	9	45	36	26.3 ± 9.7
18	4	36	16	14.6 ± 7.7
19	8	28	16	37.6 ± 15.1
20	9	28	36	42.3 ± 16.3

Length [μm]	#
0-1	0
1-2	0
2-3	0
3-4	0
4-5	0
5-6	0
6-7	0
7-8	1
8-9	1
9-10	5
10-11	10
11-12	8
12-13	19
13-14	28
14-15	15
15-16	11
16-17	2
17-18	0
18-19	0
19-20	0

$\chi^2 = 22.87$
P [χ^2] = 24.31%
U [ppm] = 90.7

MTL = 12.89
SE = 0.18
SD = 1.83
# = 100
DPAR= 2.74

Pooled Age ± 1σ [Ma] = 22.9 ± 1.7
Mean Age ± 1σ [Ma] = 26.1 ± 2.3
Central Age ± 1σ [Ma] = 23.2 ± 1.9

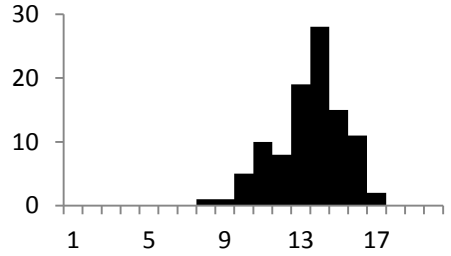

Sample No: BC-10-33
Irradiation No: FT-019-10

Rock type:	Amphibolite	Elevation [m]:	535
Lat/Lon:	50°57.432'/-118°24.027'	Zeta [ζ]:	289 ± 11
U conc. SRM612:	37 ppm	Area of basic unit:	$63.5*10^{-5}$
N_d:	4383	ρ_d:	$1.400*10^{-6}$
Analyst:	Erkan Toraman		

No	N_s	N_i	Area	Age [Ma] ± 1σ
1	29	227	100	25.8 ± 5.2
2	12	190	100	12.8 ± 3.8
3	5	67	36	15.1 ± 7.0
4	10	191	100	10.6 ± 3.5
5	36	303	100	24.0 ± 4.3
6	15	96	36	31.5 ± 8.9
7	18	259	100	14.0 ± 3.5
8	32	246	100	26.3 ± 5.1
9	15	125	36	24.2 ± 6.7
10	20	270	100	15.0 ± 3.5
11	5	71	16	14.2 ± 6.6
12	12	103	36	23.5 ± 7.2
13	23	228	100	20.4 ± 4.5
14	39	386	100	20.4 ± 3.5
15	8	91	36	17.8 ± 6.6
16	20	236	100	17.1 ± 4.1
17	13	128	36	20.5 ± 6.0
18	19	225	100	17.1 ± 4.1
19	15	93	36	32.6 ± 9.2
20	19	116	36	33.1 ± 8.3

Length [μm]	#
0-1	0
1-2	0
2-3	0
3-4	0
4-5	0
5-6	0
6-7	0
7-8	1
8-9	3
9-10	6
10-11	11
11-12	21
12-13	19
13-14	27
14-15	8
15-16	4
16-17	0
17-18	0
18-19	0
19-20	0

χ^2 = 27.48
P [χ^2] = 9.39%
U [ppm] = 108.9

MTL = 12.28
SE = 0.17
SD = 1.72
# = 100
DPAR= 2.42

Pooled Age ± 1σ [Ma] = 20.2 ± 1.4
Mean Age ± 1σ [Ma] = 20.8 ± 1.5
Central Age ± 1σ [Ma] = 20.3 ± 1.6

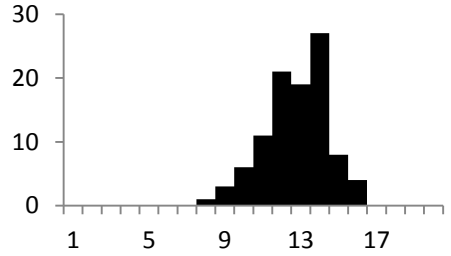

Sample No: BC-10-35
Irradiation No: FT-019-10

Rock type:	Quartzite	Elevation [m]:	599
Lat/Lon:	50°59.739'/-118°21.031'	Zeta [ζ]:	289 ± 11
U conc. SRM612:	37 ppm	Area of basic unit:	$63.5*10^{-5}$
N_d:	4383	ρ_d:	$1.420*10^{-6}$
Analyst:	Erkan Toraman		

No	N_s	N_i	Area	Age [Ma] ± 1σ
1	15	235	100	13.1 ± 3.5
2	17	158	100	22.0 ± 5.7
3	8	240	100	6.8 ± 2.5
4	25	164	100	31.2 ± 6.8
5	6	83	36	14.8 ± 6.3
6	13	177	100	15.1 ± 4.4
7	7	34	36	42.1 ± 17.6
8	7	63	36	22.8 ± 9.1
9	10	229	100	9.0 ± 2.9
10	11	176	100	12.8 ± 4.0
11	10	137	100	15.0 ± 4.9
12	5	92	100	11.1± 5.1
13	17	87	36	40.0 ± 10.7
14	4	87	36	9.4 ± 4.8
15	9	83	36	22.2 ± 7.9
16	18	146	100	25.3 ± 6.4
17	7	95	100	15.1 ± 6.0
18	6	95	36	13.0 ± 5.5
19	4	141	100	5.8 ± 3.0
20	10	173	100	11.9 ± 3.9

Length [μm]	#
0-1	0
1-2	0
2-3	0
3-4	0
4-5	1
5-6	1
6-7	2
7-8	4
8-9	14
9-10	10
10-11	12
11-12	29
12-13	16
13-14	8
14-15	1
15-16	2
16-17	0
17-18	0
18-19	0
19-20	0

$\chi^2 = 53.48$
P [χ^2] = 0.00%
U [ppm] = 71.31

MTL = 10.78
SE = 0.21
SD = 2.07
# = 100
DPAR= 2.34

Pooled Age ± 1σ [Ma] = 15.9 ± 1.3
Mean Age ± 1σ [Ma] = 17.9 ± 2.3
Central Age ± 1σ [Ma] = 16.7 ± 2.0

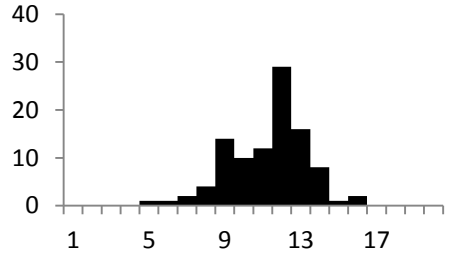

Sample No: BC-10-40
Irradiation No: FT-019-12

Rock type:	Gneiss	Elevation [m]:	690
Lat/Lon:	50°38.128'/-118°50.577'	Zeta [ζ]:	289 ± 11
U conc. SRM612:	37 ppm	Area of basic unit:	$63.5*10^{-5}$
N_d:	4383	ρ_d:	$1.440*10^{-6}$
Analyst:	Erkan Toraman		

No	N_s	N_i	Area	Age [Ma] ± 1σ
1	4	19	36	43.7 ± 24.1
2	13	100	75	27.0 ± 8.0
3	12	78	36	31.9 ± 10.0
4	8	62	36	26.8 ± 10.1
5	4	69	100	12.1 ± 6.2
6	6	49	36	25.4 ± 11.0
7	2	15	36	27.7 ± 20.9
8	12	74	62	33.7 ± 10.6
9	15	164	100	19.0 ± 5.2
10	13	74	100	36.5 ± 11.1
11	6	36	16	34.6 ± 15.3
12	3	61	100	10.2 ± 6.1
13	5	43	36	24.2 ± 11.5
14	7	63	36	23.1 ± 9.2
15	5	118	100	8.8 ± 4.0
16	3	55	100	11.3 ± 6.7
17	2	50	36	8.3 ± 6.0
18	4	40	36	20.8 ± 10.9
19	13	121	100	22.3 ± 6.6
20	6	83	100	15.0 ± 6.4

Length [μm]	#
0-1	0
1-2	0
2-3	0
3-4	0
4-5	0
5-6	0
6-7	0
7-8	1
8-9	3
9-10	4
10-11	7
11-12	24
12-13	27
13-14	14
14-15	16
15-16	2
16-17	1
17-18	0
18-19	0
19-20	1

$\chi^2 = 22.16$
P [χ^2] = 27.7%
U [ppm] = 46.1

MTL = 12.47
SE = 0.18
SD = 1.85
# = 100
DPAR= 3.34

Pooled Age ± 1σ [Ma] = 21.6 ± 2.1
Mean Age ± 1σ [Ma] = 23.1 ± 2.2
Central Age ± 1σ [Ma] = 21.7 ± 2.3

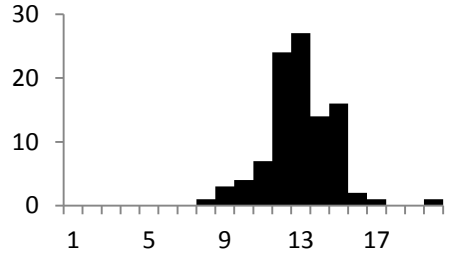

Sample No: BC-10-41
Irradiation No: FT-019-12

Rock type:	Granodiorite	Elevation [m]:	1681
Lat/Lon:	50°26.564'/-118°26.130'	Zeta [ζ]:	289 ± 11
U conc. SRM612:	37 ppm	Area of basic unit:	$63.5*10^{-5}$
N_d:	4383	ρ_d:	$1.470*10^{-6}$
Analyst:	Erkan Toraman		

No	N_s	N_i	Area	Age [Ma] ± 1σ
1	17	142	100	25.4 ± 6.6
2	25	150	100	35.3 ± 7.8
3	19	148	100	27.2 ± 6.7
4	19	141	100	28.6 ± 7.1
5	9	55	36	34.7 ± 12.5
6	22	117	100	39.8 ± 9.4
7	2	18	16	23.6 ± 17.6
8	23	126	100	38.7 ± 8.9
9	6	47	36	27.1 ± 11.8
10	11	83	36	28.1 ± 9.1
11	26	112	100	49.1 ± 10.9
12	26	120	100	45.9 ± 10.1
13	10	42	36	50.4 ± 17.8
14	8	42	36	40.3 ± 15.6
15	17	122	100	29.5 ± 7.7
16	13	104	100	26.5 ± 7.9
17	24	108	100	47.0 ± 10.8
18	17	94	100	38.3 ± 10.2
19	28	176	100	33.7 ± 7.0
20	23	107	100	45.5 ± 10.6

Length [μm]	#
0-1	0
1-2	0
2-3	0
3-4	0
4-5	0
5-6	0
6-7	0
7-8	0
8-9	0
9-10	1
10-11	3
11-12	5
12-13	25
13-14	28
14-15	32
15-16	6
16-17	1
17-18	0
18-19	0
19-20	0

χ^2 = 14.55
P [χ^2] = 75.1%
U [ppm] = 49.7

MTL = 13.47
SE = 0.11
SD = 1.18
# = 100
DPAR= 2.41

Pooled Age ± 1σ [Ma] = 35.6 ± 2.5
Mean Age ± 1σ [Ma] = 35.7 ± 1.9
Central Age ± 1σ [Ma] = 35.6 ± 2.5

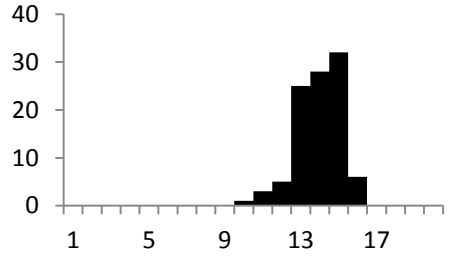

Sample No: BC-10-42
Irradiation No: FT-019-14

Rock type:	Granite	Elevation [m]:	1369
Lat/Lon:	50°26.386'/-118°27.600'	Zeta [ζ]:	289 ± 11
U conc. SRM612:	37 ppm	Area of basic unit:	$63.5*10^{-5}$
N_d:	4383	ρ_d:	$1.490*10^{-6}$
Analyst:	Erkan Toraman		

No	N_s	N_i	Area	Age [Ma] ± 1σ
1	34	153	100	47.7 ± 9.3
2	27	227	100	25.6 ± 5.3
3	14	55	100	54.6 ± 16.5
4	11	41	16	57.5 ± 19.7
5	1	4	16	53.6 ± 60.0
6	7	49	100	30.7 ± 12.5
7	11	93	100	25.4 ± 8.2
8	15	66	36	48.8 ± 14.1
9	11	72	100	32.8 ± 10.7
10	10	91	100	23.6 ± 7.9
11	10	60	36	35.8 ± 12.3
12	10	77	100	27.9 ± 9.5
13	10	40	100	53.6 ± 19.1
14	10	86	100	25.0 ± 8.4
15	22	137	100	34.5 ± 8.0
16	13	73	16	38.2 ± 11.6
17	18	129	100	30.0 ± 7.6
18	11	115	100	20.6 ± 6.5
19	9	46	36	42.0 ± 15.4
20	23	115	100	42.9 ± 10.0

Length [μm]	#
0-1	0
1-2	0
2-3	0
3-4	0
4-5	0
5-6	1
6-7	2
7-8	4
8-9	5
9-10	5
10-11	15
11-12	12
12-13	16
13-14	24
14-15	15
15-16	1
16-17	0
17-18	0
18-19	0
19-20	0

$\chi^2 = 21.28$
P [χ^2] = 32.1%
U [ppm] = 49.6

MTL = 11.90
SE = 0.22
SD = 2.17
# = 100
DPAR= 1.87

Pooled Age ± 1σ [Ma] = 34.4 ± 2.6
Mean Age ± 1σ [Ma] = 37.5 ± 2.6
Central Age ± 1σ [Ma] = 34.6 ± 2.8

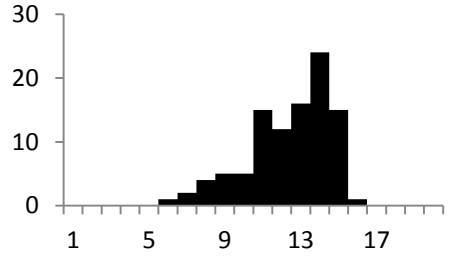

Sample No: BC-10-46
Irradiation No: FT-019-15

Rock type:	Granite	Elevation [m]:	2080
Lat/Lon:	50°26.640'/-118°23.372'	Zeta [ζ]:	289 ± 11
U conc. SRM612:	37 ppm	Area of basic unit:	$63.5*10^{-5}$
N_d:	4383	ρ_d:	$1.510*10^{-6}$
Analyst:	Erkan Toraman		

No	N_s	N_i	Area	Age [Ma] ± 1σ
1	4	54	16	16.1 ± 8.4
2	16	83	36	41.9 ± 11.6
3	16	122	36	28.6 ± 7.7
4	44	336	100	28.5 ± 4.7
5	37	247	100	32.6 ± 5.9
6	49	278	100	38.3 ± 6.1
7	5	38	16	28.7 ± 13.7
8	10	86	32	25.3 ± 8.5
9	6	53	16	24.7 ± 10.7
10	11	47	16	50.9 ± 17.2
11	27	108	36	54.3 ± 11.9
12	24	133	36	39.3 ± 8.9
13	56	326	100	37.4 ± 5.6
14	15	101	36	32.3 ± 9.0
15	26	139	36	40.7 ± 8.9
16	8	36	16	48.3 ± 19.0
17	24	102	40	51.1 ± 11.8
18	22	97	36	49.3 ± 11.8
19	19	110	36	37.6 ± 9.5
20	41	168	60	53.0 ± 9.5

Length [μm]	#
0-1	0
1-2	0
2-3	0
3-4	0
4-5	0
5-6	0
6-7	0
7-8	0
8-9	0
9-10	0
10-11	0
11-12	0
12-13	0
13-14	0
14-15	0
15-16	0
16-17	0
17-18	0
18-19	0
19-20	0

χ^2 = 22.83
P [χ^2] = 26.6%
U [ppm] = 108.6

MTL = 0
SE = 0
SD = 0
# = 0
DPAR= 0

Pooled Age ± 1σ [Ma] = 37.6 ± 2.4
Mean Age ± 1σ [Ma] = 38.0 ± 2.4
Central Age ± 1σ **[Ma] = 37.7 ± 2.6**

Sample No: BC-10-48
Irradiation No: FT-019-16

Rock type:	Granite	Elevation [m]:	2182
Lat/Lon:	50°26.553'/-118°23.374'	Zeta [ζ]:	289 ± 11
U conc. SRM612:	37 ppm	Area of basic unit:	$63.5*10^{-5}$
N_d:	4383	ρ_d:	$1.530*10^{-6}$
Analyst:	Erkan Toraman		

No	N_s	N_i	Area	Age [Ma] ± 1σ
1	5	17	16	64.7 ± 33.0
2	14	50	36	61.6 ± 18.8
3	21	86	60	53.8 ± 13.3
4	8	26	16	67.7 ± 27.5
5	24	140	100	37.8 ± 8.5
6	11	69	36	35.2 ± 11.5
7	16	84	64	42.0 ± 11.6
8	21	63	36	73.3 ± 18.7
9	6	27	16	48.9 ± 22.2
10	7	34	16	45.4 ± 18.9
11	17	61	36	61.3 ± 17.0
12	9	37	16	53.6 ± 20.0
13	20	53	36	82.9 ± 22.0
14	8	40	36	44.1 ± 17.2
15	17	110	64	34.1 ± 9.0
16	8	50	16	44.1 ± 17.2
17	7	51	36	30.3 ± 12.3
18	5	25	16	44.1 ± 21.7
19	9	60	36	33.1 ± 11.9
20	14	21	16	42.0 ± 23.0
21	12	56	36	47.2 ± 15.1
22	6	25	16	52.8 ± 24.1

Length [μm]	#
0-1	0
1-2	0
2-3	0
3-4	0
4-5	0
5-6	0
6-7	0
7-8	0
8-9	0
9-10	0
10-11	0
11-12	0
12-13	0
13-14	0
14-15	0
15-16	0
16-17	0
17-18	0
18-19	0
19-20	0

χ^2 = 17.13
P [χ^2] = 70.3%
U [ppm] = 58.8

MTL = 0
SE = 0
SD = 0
# = 0
DPAR= 0

Pooled Age ± 1σ [Ma] = 47.8 ± 3.8
Mean Age ± 1σ [Ma] = 50.0 ± 2.9
Central Age ± 1σ **[Ma] = 47.9 ± 3.9**

Sample No: BC-10-51
Irradiation No: FT-018-04

Rock type:	Granite	Elevation [m]:	655
Lat/Lon:	50°35.562'/-118°24.062'	Zeta [ζ]:	289 ± 11
U conc. SRM612:	37 ppm	Area of basic unit:	$63.5*10^{-5}$
N_d:	3314	ρ_d:	$0.937*10^{-6}$
Analyst:	Erkan Toraman		

No	N_s	N_i	Area	Age [Ma] ± 1σ
1	6	76	100	10.7 ± 4.6
2	13	71	100	24.7 ± 7.5
3	2	25	36	10.8 ± 8.0
4	9	88	100	13.8 ± 4.9
5	5	19	36	35.5 ± 17.9
6	10	63	100	21.5 ± 7.4
7	4	21	16	25.7 ± 14.1
8	16	152	100	14.2 ± 3.8
9	12	132	100	12.3 ± 3.7
10	8	70	100	15.5 ± 5.8
11	25	159	100	21.3 ± 4.7
12	7	80	100	11.8 ± 4.7
13	5	23	36	29.4 ± 14.5
14	12	81	100	20.0 ± 6.3
15	6	47	100	17.3 ± 7.5
16	14	72	100	26.3 ± 7.8
17	6	51	36	15.9 ± 6.9
18	5	58	100	11.7 ± 5.5
19	6	39	36	20.8 ± 9.2
20	16	134	100	16.2 ± 4.3

Length [μm]	#
0-1	0
1-2	0
2-3	0
3-4	0
4-5	0
5-6	0
6-7	1
7-8	1
8-9	1
9-10	3
10-11	7
11-12	15
12-13	34
13-14	23
14-15	13
15-16	2
16-17	0
17-18	0
18-19	0
19-20	0

χ^2 = 14.97
P [χ^2] = 72.5%
U [ppm] = 54.9

MTL = 12.54
SE = 0.15
SD = 1.55
# = 100
DPAR= 2.23

Pooled Age ± 1σ [Ma] = 17.3 ± 1.5
Mean Age ± 1σ [Ma] = 18.8 ± 1.5
Central Age ± 1σ [Ma] = 17.3 ± 1.5

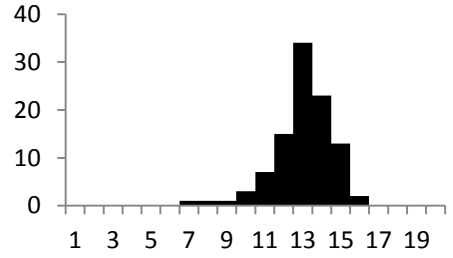

Sample No: 99-141
Irradiation No: FT-016-22

Rock type:	Gneiss	Elevation [m]:	1719
Lat/Lon:	50°31.417'/-118°09.249'	Zeta [ζ]:	289 ± 11
U conc. SRM612:	37 ppm	Area of basic unit:	$63.5*10^{-5}$
N_d:	8145	ρ_d:	$1.480*10^{-6}$
Analyst:	Erkan Toraman		

No	N_s	N_i	Area	Age [Ma] ± 1σ
1	24	144	36	35.6 ± 8.0
2	26	170	36	32.6 ± 7.0
3	65	367	100	37.8 ± 5.3
4	22	94	16	49.9 ± 12.0
5	39	135	36	61.5 ± 11.4
6	5	10	15	106.1± 58.2
7	4	14	16	60.8 ± 34.6
8	21	110	36	40.7 ± 9.8
9	22	120	36	39.1 ± 9.2
10	20	120	36	35.6 ± 8.7
11	12	60	16	42.6 ± 13.6
12	27	146	36	39.4 ± 8.4
13	18	81	36	47.4 ± 12.5

Length [μm]	#
0-1	0
1-2	0
2-3	0
3-4	0
4-5	0
5-6	0
6-7	0
7-8	0
8-9	1
9-10	0
10-11	3
11-12	7
12-13	16
13-14	24
14-15	30
15-16	13
16-17	4
17-18	1
18-19	1
19-20	0

χ^2 = 12.18
P [χ^2] = 43.1%
U [ppm] = 125.3

MTL = 13.84
SE = 0.15
SD = 1.52
# = 100
DPAR= 2.60

Pooled Age ± 1σ [Ma] = 41.4 ± 3.1
Mean Age ± 1σ [Ma] = 48.4 ± 5.4
Central Age ± 1σ [Ma] = 41.4 ± 3.1

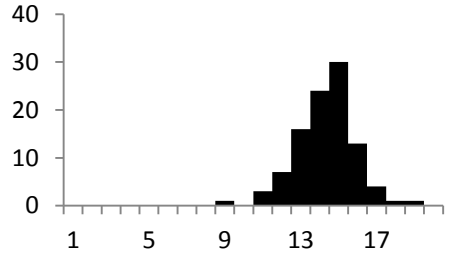

Sample No: 99-142
Irradiation No: FT-017-03

Rock type:	Gedrite-cordierite rock	Elevation [m]:	2611
Lat/Lon:	50°32.640'/-118°09.250'	Zeta [ζ]:	289 ± 11
U conc. SRM612:	37 ppm	Area of basic unit:	$63.5*10^{-5}$
N_d:	4061	ρ_d:	$1.510*10^{-6}$
Analyst:	Erkan Toraman		

No	N_s	N_i	Area	Age [Ma] ± 1σ
1	35	94	100	80.7 ± 16.3
2	15	70	36	46.6 ± 13.4
3	11	52	36	46.0 ± 15.4
4	21	73	36	62.5 ± 15.7
5	21	127	36	36.0 ± 8.6
6	26	99	100	57.1 ± 12.8
7	12	104	36	25.1 ± 7.7
8	11	60	36	39.9 ± 13.2
9	10	63	36	34.5 ± 11.8
10	15	41	36	79.3 ± 24.2
11	15	41	36	79.3 ± 24.2
12	34	157	100	47.1 ± 9.1
13	7	69	36	22.1 ± 8.8
14	12	86	36	30.4 ± 9.4
15	12	41	36	63.6 ± 21.0
16	8	56	36	31.1 ± 11.8
17	12	34	36	76.6 ± 25.9
18	11	99	36	24.2 ± 7.8
19	11	88	36	27.2 ± 8.8
20	17	101	36	36.6 ± 9.7

Length [μm]	#
0-1	0
1-2	0
2-3	0
3-4	0
4-5	0
5-6	0
6-7	0
7-8	0
8-9	0
9-10	0
10-11	0
11-12	4
12-13	10
13-14	21
14-15	36
15-16	20
16-17	6
17-18	3
18-19	0
19-20	0

χ^2 = 42.1
P [χ^2] = 0.2%
U [ppm] = 68.1

MTL = 14.35
SE = 0.12
SD = 1.23
# = 100
DPAR= 3.50

Pooled Age ± 1σ [Ma] = 44.2 ± 3.3
Mean Age ± 1σ [Ma] = 47.3 ± 4.5
Central Age ± 1σ [Ma] = 44.8 ± 4.4

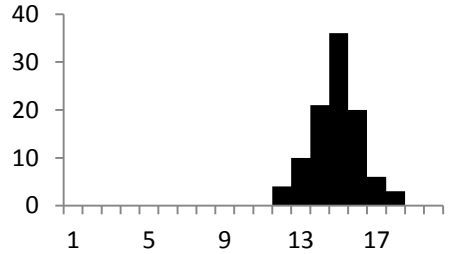

Sample No: 99-83
Irradiation No: FT-016-21

Rock type:	Metapelite	Elevation [m]:	1251
Lat/Lon:	50°42.996'/-118°18.001'	Zeta [ζ]:	289 ± 11
U conc. SRM612:	37 ppm	Area of basic unit:	$63.5*10^{-5}$
N_d:	4061	ρ_d:	$1.460*10^{-6}$
Analyst:	Erkan Toraman		

No	N_s	N_i	Area	Age [Ma] ± 1σ
1	23	213	100	22.7 ± 5.1
2	12	89	36	28.4 ± 8.8
3	6	63	36	20.1 ± 8.6
4	13	88	36	31.1 ± 9.3
5	16	69	36	48.7 ± 13.7
6	10	67	36	31.4 ± 10.7
7	16	129	100	26.1 ± 7.0
8	5	37	36	28.5 ± 13.6
9	12	51	36	49.5 ± 16.0
10	9	73	36	26.0 ± 9.2
11	12	86	36	29.4 ± 9.1
12	10	78	36	27.0 ± 9.1
13	28	161	36	36.6 ± 7.6
14	7	74	36	19.9 ± 7.9
15	13	90	36	30.4 ± 9.1
16	8	72	36	23.4 ± 8.8
17	14	68	36	43.3 ± 12.8
18	19	191	100	21.0 ± 5.1
19	12	107	36	23.6 ± 7.3
20	9	51	36	37.1 ± 13.5

Length [μm]	#
0-1	0
1-2	0
2-3	0
3-4	0
4-5	0
5-6	0
6-7	0
7-8	1
8-9	0
9-10	2
10-11	5
11-12	17
12-13	21
13-14	31
14-15	14
15-16	8
16-17	0
17-18	3
18-19	1
19-20	0

χ^2 = 16.2
P [χ^2] = 64.42%
U [ppm] = 80.2

MTL = 13.03
SE = 0.15
SD = 1.50
# = 100
DPAR= 2.70

Pooled Age ± 1σ [Ma] = 28.8 ± 2.2
Mean Age ± 1σ [Ma] = 30.2 ± 2.0
Central Age ± 1σ **[Ma] = 28.8 ± 2.2**

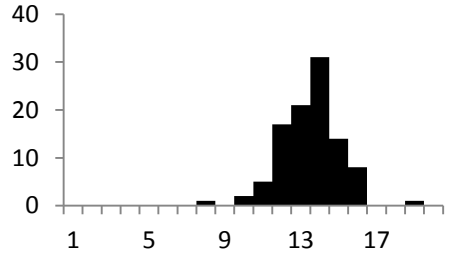

Sample No: 531
Irradiation No: FT-017-01

Rock type:	Metapelitic gneiss	Elevation [m]:	1916
Lat/Lon:	50°28.998'/-118°05.832'	Zeta [ζ]:	289 ± 11
U conc. SRM612:	37 ppm	Area of basic unit:	$63.5*10^{-5}$
N_d:	4061	ρ_d:	$1.570*10^{-6}$
Analyst:	Erkan Toraman		

No	N_s	N_i	Area	Age [Ma] ± 1σ
1	25	108	100	58.6 ± 12.6
2	14	83	36	38.2 ± 11.1
3	26	113	100	52.0 ± 11.5
4	28	176	100	36.0 ± 7.5
5	6	35	36	38.8 ± 17.2
6	23	106	36	49.0 ± 11.5
7	10	59	36	38.3 ± 13.2
8	14	71	36	44.6 ± 13.2
9	18	101	36	40.3 ± 10.4
10	12	85	36	32.0 ± 9.9
11	7	33	36	47.9 ± 20.0

Length [μm]	#
0-1	0
1-2	0
2-3	0
3-4	0
4-5	0
5-6	0
6-7	0
7-8	0
8-9	0
9-10	0
10-11	0
11-12	0
12-13	0
13-14	0
14-15	0
15-16	0
16-17	0
17-18	0
18-19	0
19-20	0

$\chi^2 = 4.1$
P [χ^2] = 94.3%
U [ppm] = 64.06

MTL = 0
SE = 0
SD = 0
# = 0
DPAR= 0

Pooled Age ± 1σ [Ma] = 42.7 ± 3.9
Mean Age ± 1σ [Ma] = 42.7 ± 2.1
Central Age ± 1σ [Ma] = 42.7 ± 3.9

Sample No: E-2F
Irradiation No: FT-016-18

Rock type:	Migmatite	Elevation [m]:	2181
Lat/Lon:	50°33.563'/-118°09.618'	Zeta [ζ]:	289 ± 11
U conc. SRM612:	37 ppm	Area of basic unit:	$63.5*10^{-5}$
N_d:	8145	ρ_d:	$1.390*10^{-6}$
Analyst:	Erkan Toraman		

No	N_s	N_i	Area	Age [Ma] ± 1σ
1	16	105	16	30.5 ± 8.3
2	29	165	36	35.2 ± 7.2
3	51	251	36	40.7 ± 6.5
4	48	263	36	36.6 ± 5.9
5	56	270	36	41.5 ± 6.3
6	45	230	36	39.2 ± 6.6
7	41	143	16	57.3 ± 10.4
8	23	93	16	49.5 ± 11.7
9	20	100	16	40.1 ± 9.9
10	55	223	36	49.4 ± 7.7
11	46	237	36	38.9 ± 6.5
12	20	62	16	64.5 ± 16.8
13	25	146	16	34.3 ± 7.6
14	35	154	16	45.5 ± 8.7
15	25	97	16	51.6 ± 11.7
16	32	134	16	41.6 ± 8.3
17	21	129	16	32.6 ± 7.8
18	24	141	16	34.1 ± 7.7
19	40	173	36	46.3 ± 8.3
20	12	60	16	40.1 ± 12.8

Length [μm]	#
0-1	0
1-2	0
2-3	0
3-4	0
4-5	0
5-6	0
6-7	0
7-8	0
8-9	0
9-10	0
10-11	1
11-12	1
12-13	6
13-14	27
14-15	38
15-16	18
16-17	8
17-18	1
18-19	0
19-20	0

χ^2 = 15.91
P [χ^2] = 66.4%
U [ppm] = 271.31

MTL = 14.45
SE = 0.11
SD = 1.11
# = 100
DPAR= 2.74

Pooled Age ± 1σ [Ma] = 41.9 ± 2.5
Mean Age ± 1σ [Ma] = 42.8 ± 1.9
Central Age ± 1σ [Ma] = 41.9 ± 2.5

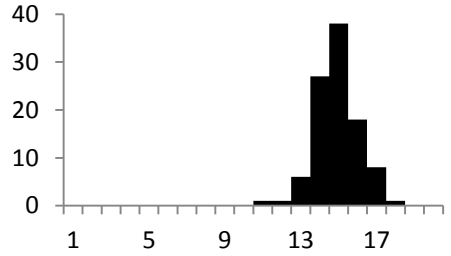

Sample No: LC-10
Irradiation No: FT-016-19

Rock type:	Gneiss	Elevation [m]:	1594
Lat/Lon:	50°27.663'/-118°02.635'	Zeta [ζ]:	289 ± 11
U conc. SRM612:	37 ppm	Area of basic unit:	$63.5*10^{-5}$
N_d:	8145	ρ_d:	$1.410*10^{-6}$
Analyst:	Erkan Toraman		

No	N_s	N_i	Area	Age [Ma] ± 1σ
1	17	112	100	30.9 ± 8.1
2	8	48	36	33.9 ± 13.0
3	20	245	100	16.6 ± 3.9
4	19	176	36	22.0 ± 5.4
5	28	258	36	22.1 ± 4.5
6	24	165	100	29.6 ± 6.6
7	3	58	36	10.5 ± 6.3
8	11	106	36	21.1 ± 6.7
9	4	19	16	42.8 ± 23.6
10	18	150	100	24.4 ± 6.2
11	4	24	16	33.9 ± 18.3
12	10	63	36	32.3 ± 11.1
13	19	126	100	30.7 ± 7.6
14	16	155	100	21.0 ± 5.6
15	5	69	36	14.8 ± 6.9
16	3	16	16	38.1 ± 24.0
17	9	84	36	21.8 ± 7.7
18	9	67	36	27.3 ± 9.8
19	4	63	36	12.9 ± 6.7
20	17	117	36	29.5 ± 7.8

Length [μm]	#
0-1	0
1-2	0
2-3	0
3-4	0
4-5	0
5-6	0
6-7	0
7-8	0
8-9	0
9-10	0
10-11	0
11-12	0
12-13	0
13-14	0
14-15	0
15-16	0
16-17	0
17-18	0
18-19	0
19-20	0

χ^2 = 15.45
P [χ^2] = 69.3%
U [ppm] = 86.84

MTL = 0
SE = 0
SD = 0
# = 0
DPAR= 0

Pooled Age ± 1σ [Ma] = 23.8 ± 1.9
Mean Age ± 1σ [Ma] = 25.8 ± 1.9
Central Age ± 1σ **[Ma] = 23.8 ± 1.9**

Sample No: LC-12
Irradiation No: FT-016-20

Rock type:	Amphibolite	Elevation [m]:	1264
Lat/Lon:	50°00.663'/-118°02.328'	Zeta [ζ]:	289 ± 11
U conc. SRM612:	37 ppm	Area of basic unit:	$63.5*10^{-5}$
N_d:	8145	ρ_d:	$1.430*10^{-6}$
Analyst:	Erkan Toraman		

No	N_s	N_i	Area	Age [Ma] ± 1σ
1	2	13	36	31.7 ± 24.1
2	4	11	36	74.7 ± 43.7
3	5	16	100	64.3 ± 33.0
4	7	76	60	19.0 ± 7.5
5	1	5	16	41.2 ± 45.2
6	1	9	16	22.9 ± 24.2
7	4	20	36	41.2 ± 22.6
8	2	3	16	136.3 ± 125.0
9	2	3	36	136.3 ± 125.0
10	6	57	100	21.7 ± 9.4
11	3	14	100	44.1 ± 28.1
12	2	44	100	9.4 ± 6.8
13	4	31	100	26.6 ± 14.2
14	5	51	100	20.2 ± 9.5
15	3	8	36	77.0 ± 52.2
16	6	27	100	45.8 ± 20.7
17	2	5	36	82.1 ± 68.8
18	4	8	38	102.5 ± 62.9
19	3	20	36	30.9 ± 19.2
20	1	3	16	68.5 ± 79.2
21	5	60	100	17.2 ± 8.0
22	5	19	100	54.2 ± 27.3

Length [μm]	#
0-1	0
1-2	0
2-3	0
3-4	0
4-5	0
5-6	0
6-7	0
7-8	3
8-9	1
9-10	8
10-11	11
11-12	13
12-13	16
13-14	25
14-15	16
15-16	6
16-17	1
17-18	0
18-19	0
19-20	0

$\chi^2 = 29.51$
P [χ^2] = 10.2%
U [ppm] = 14.39

MTL = 12.49
SE = 0.19
SD = 1.98
# = 100
DPAR= 1.80

Pooled Age ± 1σ [Ma] = 31.6 ± 4.1
Mean Age ± 1σ [Ma] = 53.2 ± 7.8
Central Age ± 1σ [Ma] = 34.4 ± 5.0

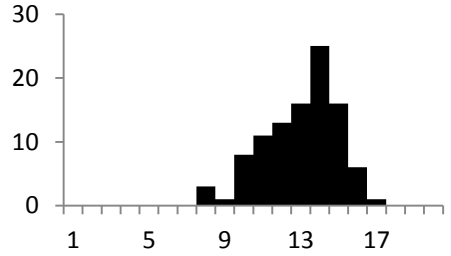

Sample No: LC-15
Irradiation No: FT-017-04

Rock type:	Gneiss	Elevation [m]:	519
Lat/Lon:	50°47.196'/-118°34.362'	Zeta [ζ]:	289 ± 11
U conc. SRM612:	37 ppm	Area of basic unit:	$63.5*10^{-5}$
N_d:	4061	ρ_d:	$1.480*10^{-6}$
Analyst:	Erkan Toraman		

No	N_s	N_i	Area	Age [Ma] ± 1σ
1	25	92	100	57.9 ± 13.3
2	41	249	100	35.1 ± 6.1
3	19	110	100	36.8 ± 9.3
4	24	99	36	51.6 ± 11.9
5	15	100	36	32.0 ± 9.0
6	10	58	36	36.8 ± 12.7
7	18	123	36	31.2 ± 8.0
8	11	92	36	25.5 ± 8.2
9	15	87	36	36.8 ± 10.4
10	17	96	36	37.8 ± 10.1
11	25	108	36	49.3 ± 11.1
12	10	73	36	29.2 ± 9.9
13	7	68	36	22.0 ± 8.8
14	17	106	36	34.2 ± 9.1
15	11	65	36	36.1 ± 11.9
16	13	64	36	43.3 ± 13.3
17	16	78	36	43.7 ± 12.1
18	10	90	36	23.7± 8.0
19	18	88	36	43.6 ± 11.4
20	10	69	36	30.9 ± 10.5

Length [μm]	#
0-1	0
1-2	0
2-3	0
3-4	0
4-5	0
5-6	0
6-7	0
7-8	2
8-9	2
9-10	5
10-11	12
11-12	13
12-13	22
13-14	21
14-15	13
15-16	8
16-17	2
17-18	0
18-19	0
19-20	0

χ^2 = 15.64
P [χ^2] = 68.1%
U [ppm] = 84.9

MTL = 12.65
SE = 0.19
SD = 1.91
# = 100
DPAR= 2.03

Pooled Age ± 1σ [Ma] = 37.0 ± 2.7
Mean Age ± 1σ [Ma] = 36.9 ± 2.1
Central Age ± 1σ [Ma] = 37.0 ± 2.7

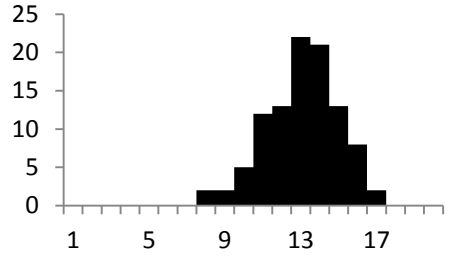

Sample No: LC-8
Irradiation No: FT-016-09

Rock type:	Gneiss	Elevation [m]:	1711
Lat/Lon:	50°28.165'/-118°03.360'	Zeta [ζ]:	289 ± 11
U conc. SRM612:	37 ppm	Area of basic unit:	$63.5*10^{-5}$
N_d:	8145	ρ_d:	$1.200*10^{-6}$
Analyst:	Erkan Toraman		

No	N_s	N_i	Area	Age [Ma] ± 1σ
1	5	41	36	21.1 ± 10.0
2	6	45	36	23.1 ± 10.1
3	9	83	100	18.8 ± 6.6
4	9	103	100	15.1 ± 5.3
5	17	131	100	22.5 ± 5.9
6	13	139	100	16.2 ± 4.7
7	14	81	100	29.9 ± 8.7
8	11	71	100	26.8 ± 8.8
9	7	84	100	14.4 ± 5.7
10	4	36	36	19.2 ± 10.2
11	6	89	100	11.7 ± 5.0
12	7	53	36	22.9 ± 9.2
13	7	34	36	35.6 ± 14.8
14	4	74	100	9.4 ± 4.8
15	11	79	100	24.1 ± 7.8
16	11	78	100	24.4 ± 7.9
17	20	127	100	27.3 ± 6.6
18	3	38	16	13.7 ± 8.2
19	12	77	100	27.0 ± 8.4

Length [μm]	#
0-1	0
1-2	0
2-3	0
3-4	0
4-5	0
5-6	0
6-7	0
7-8	0
8-9	0
9-10	0
10-11	0
11-12	0
12-13	0
13-14	0
14-15	0
15-16	0
16-17	0
17-18	0
18-19	0
19-20	0

χ^2 = 15.45
P [χ^2] = 69.3%
U [ppm] = 86.84

MTL = 0
SE = 0
SD = 0
# = 0
DPAR= 0

Pooled Age ± 1σ [Ma] = 23.8 ± 1.9
Mean Age ± 1σ [Ma] = 25.8 ± 1.9
Central Age ± 1σ **[Ma] = 23.8 ± 1.9**

Sample No: 01-12
Irradiation No: FT-08-04

Rock type:	Unknown	Elevation [m]:	572
Lat/Lon:	50°57.360'/-118°24.357'	Zeta [ζ]:	310 ± 5
U conc. SRM612:	37 ppm	Area of basic unit:	$63.5*10^{-5}$
N_d:	13215	ρ_d:	$2.092*10^{-6}$
Analyst:	Annia K. Fayon		

No	N_s	N_i	Area	Age [Ma] ± 1σ
1	7	90	60	25.2 ± 9.9
2	4	72	25	18.0 ± 9.2
3	14	210	100	21.6 ± 6.0
4	15	218	100	22.3 ± 6.0
5	24	236	100	32.9 ± 7.1
6	12	129	50	30.1 ± 9.1
7	17	135	50	40.7 ± 10.5
8	13	215	100	19.6 ± 5.6

Length [μm]	#
0-1	0
1-2	0
2-3	0
3-4	0
4-5	0
5-6	0
6-7	0
7-8	0
8-9	0
9-10	0
10-11	0
11-12	0
12-13	0
13-14	0
14-15	0
15-16	0
16-17	0
17-18	0
18-19	0
19-20	0

$\chi^2 = 6.79$
P [χ^2] = 45.0%
U [ppm] = 16.6

MTL = 0
SE = 0
SD = 0
# = 0
DPAR= 0

Pooled Age ± 1σ [Ma] = 26.3 ± 2.7
Mean Age ± 1σ [Ma] = 26.3 ± 2.8
Central Age ± 1σ [Ma] = 26.3 ± 2.7

Sample No: 01-18
Irradiation No: FT-013-01

Rock type:	Unknown	Elevation [m]:	511
Lat/Lon:	50°56.171'/-118°26.193'	Zeta [ζ]:	301± 11
U conc. SRM612:	37 ppm	Area of basic unit:	$63.5*10^{-5}$
N_d:	8365	ρ_d:	$1.380*10^{-6}$
Analyst:	Erkan Toraman		

No	N_s	N_i	Area	Age [Ma] ± 1σ
1	4	50	100	16.6 ± 8.7
2	5	31	100	33.4 ± 16.2
3	4	52	100	16.0 ± 8.2
4	2	10	16	41.4 ± 32.1
5	2	16	36	26.0 ± 19.5
6	2	13	36	31.9 ± 24.2
7	13	87	100	31.0 ± 9.3
8	4	14	36	59.1 ± 33.6
9	6	48	100	26.0 ± 11.3
10	9	37	100	50.3 ± 18.8
11	6	58	100	21.5 ± 9.2
12	4	60	100	13.8 ± 7.2
13	8	83	100	20.0 ± 7.4
14	4	38	100	21.8 ± 11.5
15	3	50	100	12.4 ± 7.4
16	2	19	36	21.8 ± 16.2

Length [μm]	#
0-1	0
1-2	0
2-3	0
3-4	0
4-5	0
5-6	5
6-7	3
7-8	3
8-9	11
9-10	8
10-11	17
11-12	15
12-13	16
13-14	13
14-15	7
15-16	2
16-17	0
17-18	0
18-19	0
19-20	0

$\chi^2 = 12.62$
P [χ^2] = 63.13%
U [ppm] = 20.88

MTL = 10.95
SE = 0.24
SD = 2.43
# = 100
DPAR= 2.20

Pooled Age ± 1σ [Ma] = 24.3 ± 3.1
Mean Age ± 1σ [Ma] = 227.7 ± 3.3
Central Age ± 1σ [Ma] = 24.3 ± 3.1

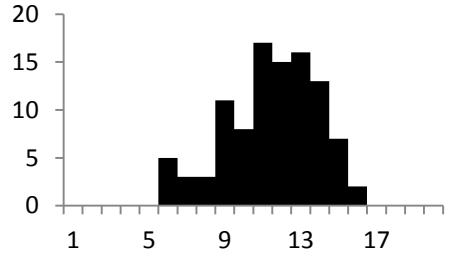

Sample No: 01-19
Irradiation No: FT-11-02

Rock type:	Unknown	Elevation [m]:	510
Lat/Lon:	50°56.522'/-118°26.280'	Zeta [ζ]:	294± 0
U conc. SRM612:	37 ppm	Area of basic unit:	$63.5*10^{-5}$
N_d:	12003	ρ_d:	$1.800*10^{-6}$
Analyst:	Annia K. Fayon (age), Erkan Toraman (length)		

No	N_s	N_i	Area	Age [Ma] ± 1σ
1	13	143	25	24.0 ± 7.0
2	33	275	25	31.7 ± 5.8
3	28	334	25	22.1 ± 4.4
4	54	685	100	20.8 ± 2.9
5	19	178	25	28.2 ± 6.8
6	16	237	25	17.8 ± 4.6
7	14	142	25	26.0 ± 7.3
8	10	118	25	22.4 ± 7.4
9	11	122	25	23.8 ± 7.5
10	20	337	100	15.7 ± 3.6

Length [μm]	#
0-1	0
1-2	0
2-3	0
3-4	0
4-5	0
5-6	2
6-7	1
7-8	8
8-9	10
9-10	16
10-11	17
11-12	17
12-13	19
13-14	5
14-15	5
15-16	0
16-17	0
17-18	0
18-19	0
19-20	0

$\chi^2 = 8.37$
P [χ^2] = 49.7%
U [ppm] = 52.4

MTL = 10.69
SE = 0.20
SD = 2.04
# = 100
DPAR= 0

Pooled Age ± 1σ [Ma] = 22.4 ± 1.6
Mean Age ± 1σ [Ma] = 23.3 ± 1.5
Central Age ± 1σ [Ma] = 22.4 ± 1.6

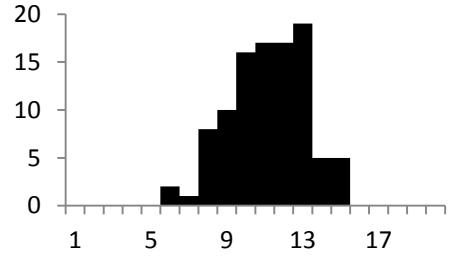

Sample No: 01-20
Irradiation No: FT-08-07

Rock type:	Unknown	Elevation [m]:	515
Lat/Lon:	50°56.490'/-118°27.359'	Zeta [ζ]:	294± 5
U conc. SRM612:	37 ppm	Area of basic unit:	$63.5*10^{-5}$
N_d:	13215	ρ_d:	$2.074*10^{-6}$
Analyst:	Annia K. Fayon (age), Erkan Toraman (length)		

No	N_s	N_i	Area	Age [Ma] ± 1σ
1	15	148	25	30.8 ± 8.4
2	17	127	25	40.7 ± 10.5
3	20	154	50	39.5 ± 9.4
4	24	247	25	29.6 ± 6.3
5	14	200	25	21.3 ± 5.9
6	22	280	25	23.9 ± 5.3
7	33	404	100	24.9 ± 4.5
8	22	261	25	25.7 ± 5.7
9	13	150	25	26.4 ± 7.6
10	29	286	25	30.8 ± 6.0

Length [μm]	#
0-1	0
1-2	0
2-3	0
3-4	0
4-5	1
5-6	1
6-7	4
7-8	2
8-9	10
9-10	12
10-11	22
11-12	20
12-13	20
13-14	4
14-15	2
15-16	1
16-17	0
17-18	1
18-19	0
19-20	0

$\chi^2 = 6.77$
P [χ^2] = 66.0%
U [ppm] = 48.4

MTL = 10.74
SE = 0.20
SD = 2.05
# = 100
DPAR= 0

Pooled Age ± 1σ [Ma] = 28.2 ± 2.1
Mean Age ± 1σ [Ma] = 29.4 ± 2.1
Central Age ± 1σ [Ma] = 28.2 ± 2.1

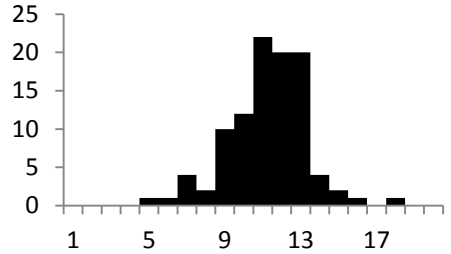

Sample No: 01-26
Irradiation No: FT-11-04

Rock type:	Unknown	Elevation [m]:	518
Lat/Lon:	50°56.345'/-118°27.660'	Zeta [ζ]:	310± 5
U conc. SRM612:	37 ppm	Area of basic unit:	$63.5*10^{-5}$
N_d:	12003	ρ_d:	$1.846*10^{-6}$
Analyst:	Annia K. Fayon (age), Erkan Toraman (length)		

No	N_s	N_i	Area	Age [Ma] ± 1σ
1	67	714	100	26.8 ± 3.5
2	22	468	50	13.4 ± 2.9
3	16	270	50	16.9 ± 4.4
4	53	714	100	21.2 ± 3.0
5	40	646	100	17.7 ± 2.9
6	13	243	25	15.3 ± 4.4
7	13	191	25	19.4 ± 5.6
8	9	143	25	18.0 ± 6.2
9	23	368	25	17.9 ± 3.9
10	9	125	25	20.6 ± 7.1

Length [μm]	#
0-1	0
1-2	0
2-3	0
3-4	0
4-5	0
5-6	1
6-7	3
7-8	5
8-9	6
9-10	7
10-11	17
11-12	29
12-13	12
13-14	14
14-15	4
15-16	2
16-17	0
17-18	0
18-19	0
19-20	0

χ^2 = 11.20
P [χ^2] = 26.2%
U [ppm] = 62.4

MTL = 11.24
SE = 0.20
SD = 2.00
# = 100
DPAR= 0

Pooled Age ± 1σ [Ma] = 19.5 ± 1.3
Mean Age ± 1σ [Ma] = 18.7 ± 1.2
Central Age ± 1σ [Ma] = 19.5 ± 1.3

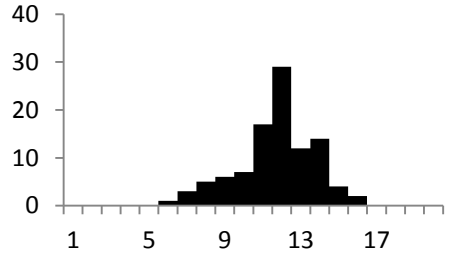

Sample No: 01-28
Irradiation No: FT-11-05

Rock type:	Unknown	Elevation [m]:	533
Lat/Lon:	50°56.171'/-118°26.193'	Zeta [ζ]:	310± 5
U conc. SRM612:	37 ppm	Area of basic unit:	$63.5*10^{-5}$
N_d:	12003	ρ_d:	$1.869*10^{-6}$
Analyst:	Annia K. Fayon (age), Erkan Toraman (length)		

No	N_s	N_i	Area	Age [Ma] ± 1σ
1	37	584	100	18.3 ± 3.1
2	10	99	50	29.2 ± 9.7
3	12	135	25	25.7 ± 7.8
4	7	101	25	20.0 ± 7.8
5	6	43	25	40.3 ± 17.6
6	42	359	25	33.8 ± 5.5
7	14	239	25	16.9 ± 4.7
8	12	209	100	16.6 ± 4.9
9	25	362	100	20.0 ± 4.1
10	8	106	25	21.8 ± 8.0

Length [μm]	#
0-1	0
1-2	0
2-3	0
3-4	0
4-5	0
5-6	1
6-7	1
7-8	2
8-9	6
9-10	17
10-11	11
11-12	24
12-13	17
13-14	12
14-15	9
15-16	0
16-17	0
17-18	0
18-19	0
19-20	0

χ^2 = 13.10
P [χ^2] = 15.8%
U [ppm] = 37.3

MTL = 11.34
SE = 0.19
SD = 1.89
# = 100
DPAR= 0

Pooled Age ± 1σ [Ma] = 22.4 ± 1.8
Mean Age ± 1σ [Ma] = 24.3 ± 2.5
Central Age ± 1σ [Ma] = 22.4 ± 1.8

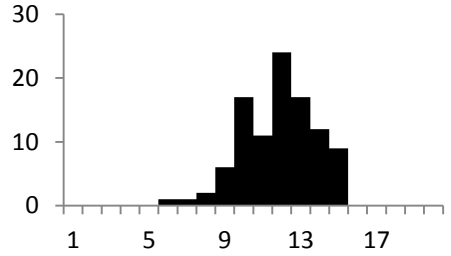

Sample No: 01-63
Irradiation No: FT-013-05

Rock type:	Unknown	Elevation [m]:	798
Lat/Lon:	50°55.798'/-118°27.959'	Zeta [ζ]:	301 ± 11
U conc. SRM612:	37 ppm	Area of basic unit:	$63.5*10^{-5}$
N_d:	8365	ρ_d:	$1.320*10^{-6}$
Analyst:	Erkan Toraman		

No	N_s	N_i	Area	Age [Ma] ± 1σ
1	4	24	36	33.0 ± 17.9
2	9	39	36	45.7 ± 17.0
3	3	9	16	65.9 ± 44.0
4	9	85	100	21.0 ± 7.4
5	3	41	36	14.5 ± 8.7
6	6	27	36	44.0 ± 19.9
7	7	23	36	60.2 ± 26.1
8	17	107	100	31.5 ± 8.3
9	11	48	36	45.4 ± 15.3
10	10	97	36	20.5 ± 6.8
11	6	34	36	34.9 ± 15.5
12	11	41	36	53.1 ± 18.1
13	5	22	36	45.0 ± 22.4
14	4	19	16	41.7 ± 23.0
15	9	93	100	19.2 ± 6.7
16	4	34	36	23.3 ± 12.4
17	7	33	36	42.0 ± 17.6
18	5	38	36	26.1 ± 12.4
19	4	13	16	60.9 ± 34.9
20	4	26	36	30.5 ± 16.4

Length [μm]	#
0-1	0
1-2	0
2-3	0
3-4	0
4-5	2
5-6	1
6-7	4
7-8	2
8-9	2
9-10	7
10-11	9
11-12	9
12-13	11
13-14	16
14-15	8
15-16	0
16-17	1
17-18	0
18-19	0
19-20	0

$\chi^2 = 18.71$
P [χ^2] = 47.5%
U [ppm] = 42.3

MTL = 11.51
SE = 0.31
SD = 2.63
# = 100
DPAR= 2.3

Pooled Age ± 1σ [Ma] = 32.1 ± 3.2
Mean Age ± 1σ [Ma] = 37.9 ± 3.3
Central Age ± 1σ [Ma] = 32.4 ± 3.3

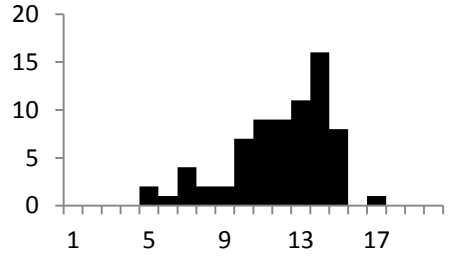

Sample No: 01-72
Irradiation No: FT-013-07

Rock type:	Unknown	Elevation [m]:	553
Lat/Lon:	50°43.225'/-118°00.475'	Zeta [ζ]:	301 ± 11
U conc. SRM612:	37 ppm	Area of basic unit:	$63.5*10^{-5}$
N_d:	8365	ρ_d:	$1.290*10^{-6}$
Analyst:	Erkan Toraman		

No	N_s	N_i	Area	Age [Ma] ± 1σ
1	5	37	100	26.2 ± 12.5
2	6	54	100	21.5 ± 9.3
3	3	48	100	12.1 ± 7.2
4	3	16	16	36.3 ± 22.9
5	3	127	100	10.7 ± 4.2
6	7	37	36	21.0 ± 11.1
7	4	53	100	21.9 ± 9.5
8	6	58	100	16.7 ± 7.8
9	5	64	100	15.2 ± 7.1
10	5	74	100	7.9 ± 4.6
11	3	26	36	14.9 ± 11.0
12	2	46	36	21.1 ± 9.9
13	5	59	100	16.4 ± 7.7
14	5	72	100	26.9 ± 9.1
15	10	82	100	11.8 ± 5.5
16	3	72	100	8.1 ± 4.8
17	6	57	100	20.4 ± 8.8
18	2	5	36	77.2 ± 64.7
19	11	62	100	34.4 ± 11.3
20	4	30	100	25.8 ± 13.8

Length [μm]	#
0-1	0
1-2	0
2-3	0
3-4	0
4-5	0
5-6	0
6-7	0
7-8	0
8-9	0
9-10	0
10-11	0
11-12	0
12-13	0
13-14	0
14-15	0
15-16	0
16-17	0
17-18	0
18-19	0
19-20	0

$\chi^2 = 19.68$
P [χ^2] = 41.4%
U [ppm] = 29.5

MTL = 0
SE = 0
SD = 0
# = 0
DPAR= 0

Pooled Age ± 1σ [Ma] = 18.0 ± 2.0
Mean Age ± 1σ [Ma] = 22.3 ± 3.4
Central Age ± 1σ **[Ma] = 18.0 ± 2.1**

Sample No: 01-78
Irradiation No: FT-11-06

Rock type:	Unknown	Elevation [m]:	441
Lat/Lon:	50°34.558'/-118°56.990'	Zeta [ζ]:	310± 5
U conc. SRM612:	37 ppm	Area of basic unit:	$63.5*10^{-5}$
N_d:	12003	ρ_d:	$1.892*10^{-6}$
Analyst:	Annia K. Fayon (age), Erkan Toraman (length)		

No	N_s	N_i	Area	Age [Ma] ± 1σ
1	20	362	100	16.2 ± 3.7
2	10	115	50	25.4 ± 8.4
3	8	110	25	21.3 ± 7.8
4	9	106	25	24.9 ± 8.6
5	5	41	25	35.7 ± 16.9
6	16	277	100	16.9 ± 4.4
7	12	121	50	29.0 ± 8.8

Length [μm]	#
0-1	0
1-2	0
2-3	0
3-4	0
4-5	3
5-6	5
6-7	7
7-8	8
8-9	11
9-10	17
10-11	10
11-12	19
12-13	7
13-14	6
14-15	4
15-16	3
16-17	0
17-18	0
18-19	0
19-20	0

$\chi^2 = 5.08$
P [χ^2] = 53.4%
U [ppm] = 24.9

MTL = 9.97
SE = 0.26
SD = 2.62
# = 100
DPAR= 0

Pooled Age ± 1σ [Ma] = 20.7 ± 2.4
Mean Age ± 1σ [Ma] = 24.2 ± 2.6
Central Age ± 1σ [Ma] = 20.7 ± 2.4

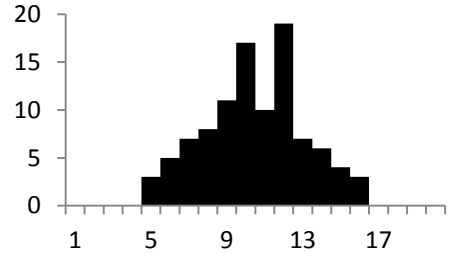

Sample No: 01-79
Irradiation No: FT-11-11

Rock type:	Unknown	Elevation [m]:	574
Lat/Lon:	50°36.539'/-118°57.183'	Zeta [ζ]:	310± 5
U conc. SRM612:	37 ppm	Area of basic unit:	$63.5*10^{-5}$
N_d:	12003	ρ_d:	$2.007*10^{-6}$
Analyst:	Annia K. Fayon (age), Erkan Toraman (length)		

No	N_s	N_i	Area	Age [Ma] ± 1σ
1	4	46	100	27.0 ± 14.1
2	5	102	100	15.2 ± 7.0
3	5	22	50	70.3 ± 34.9
4	2	33	50	18.8 ± 13.7
5	7	65	100	33.4 ± 13.3
6	5	46	70	33.7 ± 15.9
7	4	28	25	44.3 ± 23.7
8	5	27	70	57.4 ± 28.0

Length [μm]	#
0-1	0
1-2	0
2-3	0
3-4	0
4-5	4
5-6	4
6-7	2
7-8	9
8-9	7
9-10	13
10-11	7
11-12	16
12-13	13
13-14	15
14-15	4
15-16	5
16-17	1
17-18	0
18-19	0
19-20	0

$\chi^2 = 8.14$
P [χ^2] = 32.1%
U [ppm] = 5.1

MTL = 10.76
SE = 0.29
SD = 2.85
# = 100
DPAR= 0

Pooled Age ± 1σ [Ma] = 31.1 ± 5.5
Mean Age ± 1σ [Ma] = 37.5 ± 6.8
Central Age ± 1σ [Ma] = 31.1 ± 5.5

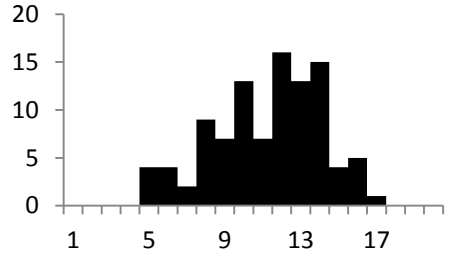

Sample No: 01-80
Irradiation No: FT-09-06

Rock type:	Unknown	Elevation [m]:	441
Lat/Lon:	50°38.586'/-118°56.384'	Zeta [ζ]:	310± 5
U conc. SRM612:	37 ppm	Area of basic unit:	$63.5*10^{-5}$
N_d:	9278	ρ_d:	$2.115*10^{-6}$
Analyst:	Annia K. Fayon (age), Erkan Toraman (length)		

No	N_s	N_i	Area	Age [Ma] ± 1σ
1	3	48	25	20.5 ± 12.2
2	4	36	25	36.3 ± 19.2
3	2	27	50	24.2 ± 17.8
4	2	40	50	16.4 ± 11.9
5	3	47	50	20.9 ± 12.4
6	3	45	50	21.8 ± 13.0

Length [μm]	#
0-1	0
1-2	0
2-3	0
3-4	0
4-5	1
5-6	1
6-7	1
7-8	10
8-9	10
9-10	15
10-11	19
11-12	12
12-13	13
13-14	6
14-15	9
15-16	3
16-17	0
17-18	0
18-19	0
19-20	0

$\chi^2 = 1.07$
P [χ^2] = 95.6%
U [ppm] = 7.2

MTL = 10.80
SE = 0.23
SD = 2.32
# = 100
DPAR= 0

Pooled Age ± 1σ [Ma] = 22.9 ± 5.8
Mean Age ± 1σ [Ma] = 23.4 ± 2.8
Central Age ± 1σ [Ma] = 22.9 ± 5.8